

**The Sweet Side of the Extracellular Matrix –  
Glycosaminoglycans in Matrix Remodeling, Endothelial  
Cell Activation and Functional Biomaterials**

**DISSERTATION**

zur Erlangung des akademischen Grades

Doctor rerum naturalium

(Dr. rer. nat.)

vorgelegt

der Fakultät Mathematik und Naturwissenschaften  
der Technischen Universität Dresden

von

**staatl. gepr. Diplom-Lebensmittelchemikerin Sandra Rother**

geboren am 14.09.1987 in Lutherstadt Wittenberg

Eingereicht am 18.07.2017

Verteidigt am 19.10.2017

Die Dissertation wurde in der Zeit von Juli 2013 bis Juli 2017 in der Gruppe Biomaterial-Entwicklung am Max-Bergmann-Zentrum für Biomaterialien Dresden in Kooperation mit der Professur für Lebensmittelchemie angefertigt.



Gutachter: Prof. Dr. rer. nat. Dr.-Ing. habil. Thomas Henle  
Professur für Lebensmittelchemie  
Fakultät Chemie und Lebensmittelchemie  
Technische Universität Dresden

Prof. Dr. rer. nat. Dr.-Ing. habil. Dieter Scharnweber  
Gruppe Biomaterial-Entwicklung  
Max-Bergmann-Zentrum für Biomaterialien  
Fakultät Maschinenwesen  
Technische Universität Dresden



**TABLE OF CONTENT**

TABLE OF CONTENT .....	I
LIST OF FIGURES.....	VI
LIST OF TABLES .....	IX
LIST OF ABBREVIATIONS .....	X
1 INTRODUCTION AND AIMS .....	1
2 BACKGROUND AND STATE OF KNOWLEDGE.....	3
2.1 Extracellular matrix (ECM) .....	3
2.1.1 Structural proteins .....	3
2.1.2 Proteoglycans (PGs) and glycosaminoglycans (GAGs).....	6
2.1.2.1 Chondroitin sulfate (CS) .....	7
2.1.2.2 Dermatan sulfate (DS).....	7
2.1.2.3 Keratan sulfate (KS).....	8
2.1.2.4 Heparan sulfate/heparin (HS/HEP) .....	9
2.1.2.5 Hyaluronan (HA).....	10
2.1.2.6 Enzymatic degradation of GAGs .....	11
2.1.3 ECM of skin .....	13
2.1.4 ECM of bone .....	14
2.2 Wound healing .....	15
2.2.1 Cutaneous wound healing .....	15
2.2.2 Bone regeneration .....	17
2.2.3 Factors influencing wound healing .....	18
2.3 Matrix metalloproteinases (MMPs) .....	19
2.4 Tissue inhibitors of metalloproteinases (TIMPs).....	24
2.5 Regulation of ECM remodeling .....	26
2.6 Low-density lipoprotein receptor-related protein-1 (LRP-1).....	28
2.7 Angiogenesis .....	31
2.7.1 Vascular endothelial growth factor (VEGF) signaling .....	32
2.7.2 TIMP-3 as regulator of VEGF-A activity .....	33
2.7.3 Role of GAGs in VEGF-A signaling .....	34

2.8 Biomaterials for bone and skin regeneration.....	35
2.8.1 Design criteria for biomaterials.....	35
2.8.2 Artificial extracellular matrices (aECMs).....	37
2.8.3 GAG derivatives.....	37
2.8.3.1 Methods to adjust the molecular weight of GAGs.....	39
2.8.3.2 Synthesis strategies for sulfated GAG derivatives.....	40
2.8.3.3 Strategies for cross-linkable GAGs and GAG-based hydrogels.....	41
3 MATERIALS AND METHODS.....	43
3.1 Chemicals, materials and devices.....	43
3.1.1 Chemicals.....	43
3.1.2 Mediator proteins, enzymes and antibodies.....	47
3.1.3 Glycosaminoglycans.....	48
3.1.4 Consumables.....	49
3.1.5 Devices and software.....	51
3.1.6 Cell culture reagents.....	52
3.2 Preparation and characterization of GAG derivatives.....	53
3.2.1 Preparation of low molecular weight HA.....	54
3.2.2 Synthesis of low-sulfated HA derivatives.....	54
3.2.3 Synthesis of regio-selectively sulfated HA derivatives.....	55
3.2.4 Synthesis of high-sulfated GAG derivatives.....	55
3.2.5 Synthesis of acrylated GAG derivatives.....	55
3.2.6 Fluorescence-labelling of sulfated HA derivatives.....	56
3.2.7 Biotin-labelling of HA derivatives.....	56
3.2.8 Synthesis of sulfated HA oligosaccharides.....	57
3.3 Preparation of biomaterials.....	59
3.3.1 aECM coatings composed of collagen type I and GAGs (coll/GAG).....	59
3.3.2 Hyaluronan/collagen hydrogels (HA-AC/coll).....	59
3.4 Analytical and further methods.....	61
3.4.1 Immobilization of GAGs on polystyrene surfaces.....	61
3.4.2 Binding of mediator proteins to GAG-coated surfaces.....	62

3.4.3 Binding of lysozyme or VEGF-A to hydrogels .....	63
3.4.4 Quantification of TIMP-3 and VEGF-A via ELISA .....	64
3.4.5 HA degradation via Hyal in the presence of GAGs .....	65
3.4.6 Enzyme kinetic analysis .....	66
3.4.7 Surface plasmon resonance (SPR) .....	68
3.4.8 Enzymatic degradation of aECMs via collagenase .....	73
3.4.9 Qualitative analysis of collagen - Sirius red staining .....	73
3.4.10 Qualitative analysis of sulfated glycosaminoglycans - Toluidine blue staining ...	74
3.4.11 Quantification of collagen - Lowry assay .....	74
3.4.12 Quantification of sulfated glycosaminoglycans - Dimethylmethylene blue assay	74
3.4.13 Quantification of glycosaminoglycans - Hexosamine assay .....	75
3.4.14 Agarose gel electrophoresis of GAGs .....	76
3.4.15 Determination of the elastic modulus of hydrogels .....	77
3.4.16 Analysis of hydrogel swelling properties and characteristics .....	78
3.4.17 Degradation of hydrogels via Hyal .....	78
3.4.18 Scanning electron microscopy (SEM).....	78
3.4.19 Atomic force microscopy (AFM).....	78
3.5 Cell culture .....	79
3.5.1 Cultivation of endothelial cells (PAE/KDR cells) .....	79
3.5.2 Stimulation of VEGFR-2 phosphorylation on PAE/KDR cells .....	80
3.5.3 Quantification of VEGFR-2 and phosphorylated VEGFR-2 via ELISA .....	81
3.5.4 Migration of PAE/KDR cells .....	82
3.5.5 Influence of solute GAGs and VEGF-A on the proliferation and tube formation of PAE/KDR cells cultivated on collagen coatings .....	83
3.5.6 Quantification of the protein content in cell lysates - Nanodrop .....	84
3.5.7 Cultivation of PAE/KDR cells on hydrogels .....	84
3.5.7.1 Cell proliferation on hydrogels in the presence of serum .....	84
3.5.7.2 Effects of VEGF-A-loaded gels on PAE/KDR cells.....	85
3.5.8 Determination of the LDH activity and DNA amount .....	85
3.5.9 Immunofluorescence staining.....	86
3.6 Statistics .....	88

4	RESULTS AND DISCUSSION .....	89
4.1	Selection of GAGs and GAG derivatives.....	89
4.2	Interaction of GAGs with mediator proteins and enzymes .....	90
4.2.1	Influence of GAGs on MMP-1/-2 activity .....	90
4.2.2	Interaction of TIMP-3 with GAGs .....	92
4.2.3	Interaction of acrylated GAGs with lysozyme .....	95
4.2.4	Interaction of acrylated GAGs with VEGF-A.....	96
4.3	Consequences of GAG/protein interactions on protein functions, receptor binding and intracellular signaling .....	98
4.3.1	Influence of GAGs on the TIMP-3 induced MMP inhibition.....	98
4.3.2	Interaction of TIMP-3 with LRP-1 cluster II and IV .....	99
4.3.3	Influence of GAGs on the TIMP-3/LRP-1 interplay .....	101
4.3.4	Interaction of TIMP-3 and VEGF-A with VEGFR-2 .....	104
4.3.5	Influence of GAGs on the TIMP-3/VEGFR-2 interaction.....	105
4.3.6	Influence of GAGs on the VEGF-A/VEGFR-2 interaction .....	107
4.3.7	Influence of GAGs on the TIMP-3/VEGF-A/VEGFR-2 interaction .....	109
4.3.8	Biological consequences on the VEGFR-2 signaling .....	113
4.4	Biomaterial coatings functionalized with HA derivatives (2.5D aECMs).....	117
4.4.1	Development and characterization of aECMs with one or two GAGs .....	117
4.4.2	Morphology of aECMs.....	120
4.4.3	Enzymatic aECM degradation via collagenases .....	122
4.5	Hydrogels as 3D aECMs for mediator protein binding and cell cultivation .....	123
4.5.1	Hydrogel characteristics, composition and structure .....	123
4.5.2	HA and hydrogel degradation via Hyal.....	127
4.5.3	Interaction of lysozyme with hydrogels .....	129
4.5.4	Interaction of VEGF-A with hydrogels.....	131
4.5.5	Endothelial cell growth within hydrogels in the presence of serum .....	133
4.5.6	Influence of solute GAGs on VEGF-A stimulated endothelial cells .....	135
4.5.7	Effects of VEGF-A-loaded hydrogels on endothelial cells.....	138
4.6	Potential limitations.....	141
5	SUMMARY .....	142



---

6	OUTLOOK.....	150
7	APPENDIX.....	151
	LITERATURE .....	157
	PERMISSIONS TO REUSE DATA FOR THESIS/DISSERTATION.....	179
	LIST OF PUBLICATIONS .....	180
	ACKNOWLEDGEMENT .....	184
	DECLARATION .....	186

**LIST OF FIGURES**

Fig. 2.1 Schematic overview of the ECM. ....	3
Fig. 2.2 Schematic overview on the axial structure of triple-helical collagen type I, III or V monomers in a fibril with associated collagen type XII or XIV as present in skin. ....	5
Fig. 2.3 Schematic overview on the location of GAGs and their biological functions. ....	7
Fig. 2.4 Structural characteristics of native GAGs. ....	8
Fig. 2.5 ECM of skin. ....	13
Fig. 2.6 Simplified scheme of the matrix compartments of bone. ....	14
Fig. 2.7 Phases of cutaneous wound healing. ....	15
Fig. 2.8 Mechanisms of MMP activity regulation. ....	21
Fig. 2.9 Multidomain structure of MMP-1 and MMP-2. ....	22
Fig. 2.10 Interaction of the catalytic domain of MMPs with the propeptide domain and substrates. ....	22
Fig. 2.11 Interaction of the catalytic domain of MMPs with their inhibitor TIMP-1. ....	25
Fig. 2.12 Physiologic and pathologic ECM remodeling of skin and bone tissue. ....	27
Fig. 2.13 Structure of LRP-1 and overview of LRP-1 ligands. ....	29
Fig. 2.14 Activities of endothelial cells during angiogenesis. ....	31
Fig. 2.15 Overview on the VEGF-VEGFR system. ....	33
Fig. 2.16 Structures of the pentasaccharide fondaparinux. ....	38
Fig. 2.17 Structures of cross-linkable HA derivatives. ....	41
Fig. 3.1 Structures of sulfated HA and CS derivatives. ....	54
Fig. 3.2 Structure of fluorescence-labeled HA derivatives. ....	56
Fig. 3.3 Structure of biotin-labeled HA derivatives. ....	57
Fig. 4.1 Activity of MMP-1 and -2 in the presence of GAG polysaccharides. ....	91
Fig. 4.2 Interaction of GAG polysaccharides with TIMP-3. ....	93
Fig. 4.3 Binding of GAG oligosaccharides to TIMP-3. ....	94
Fig. 4.4 Binding of lysozyme to immobilized GAGs. ....	96
Fig. 4.5 Interaction of VEGF-A with immobilized GAG derivatives. ....	97
Fig. 4.6 Interaction of solute GAG derivatives with immobilized VEGF-A. ....	98
Fig. 4.7 MMP activity in the presence of TIMP-3 and GAGs. ....	99
Fig. 4.8 Kinetic analyses of the TIMP-3/LRP-1 cluster II and IV interaction. ....	100
Fig. 4.9 Influence of GAG polysaccharides on the interaction of TIMP-3 with LRP-1 cluster II and IV. ....	101
Fig. 4.10 Influence of HA tetrasaccharides on the TIMP-3/LRP-1 cluster II and IV interaction. ....	103
Fig. 4.11 Kinetic analyses of TIMP-3/VEGFR-2 and VEGF-A/VEGFR-2 interactions. ....	105
Fig. 4.12 Influence of GAG polysaccharides on the binding of TIMP-3 to VEGFR-2. ....	106
Fig. 4.13 Effects of GAG oligosaccharides on the TIMP-3/VEGFR-2 interaction. ....	107

Fig. 4.14 Interference of GAG polysaccharides with the VEGF-A/VEGFR-2 binding. ....	108
Fig. 4.15 Effects of GAG oligosaccharides on the VEGF-A/VEGFR-2 interplay. ....	109
Fig. 4.16 Interference of GAG polysaccharides with the TIMP-3/VEGF-A competition for VEGFR-2. ....	110
Fig. 4.17 Interference of GAG oligosaccharides with the TIMP-3/VEGF-A competition for VEGFR-2. ....	111
Fig. 4.18 Sequential interaction analysis of TIMP-3, sHA3 and VEGF-A binding to VEGFR- 2. ....	112
Fig. 4.19 Binding of VEGF-A or TIMP-3 to GAG surfaces. ....	113
Fig. 4.20 Effects of sHA3 on the VEGF-A/TIMP-3 controlled phosphorylation of VEGFR-2 and on endothelial cell migration. ....	114
Fig. 4.21 Simplified scheme of VEGF-A/VEGFR-2 signaling in the presence of TIMP-3 and GAGs. ....	116
Fig. 4.22 Composition of aECMs. ....	118
Fig. 4.23 Quantification and separation of sHA derivatives from the multi-GAG aECM. ....	119
Fig. 4.24 Fibril morphology of aECMs. ....	121
Fig. 4.25 Enzymatic degradation of aECMs. ....	122
Fig. 4.26 Characterization of HA/collagen hydrogels. ....	124
Fig. 4.27 Composition of HA/collagen hydrogels. ....	126
Fig. 4.28 Morphology of hydrogels. ....	127
Fig. 4.29 Enzymatic degradation of HA coatings and HA/collagen hydrogels via Hyal. ....	128
Fig. 4.30 Binding and release of lysozyme after incubation with hydrogels. ....	130
Fig. 4.31 Binding and release of VEGF-A after incubation with hydrogels. ....	132
Fig. 4.32 Effects of hydrogel composition on endothelial cells. ....	134
Fig. 4.33 Influence of VEGF-A and solute GAGs on PAE/KDR cells. ....	136
Fig. 4.34 Endothelial cell stimulatory activity of VEGF-A in the presence of GAGs. ....	137
Fig. 4.35 Influence of VEGF-A on PAE/KDR cells cultivated on HA-AC/collagen hydrogels. .....	139
Fig. 4.36 Influence of VEGF-A on the morphology of PAE/KDR cells cultivated on HA-AC/collagen hydrogels. ....	140
Fig. 7.1 Influence of solute GAGs on the TIMP-3/LRP-1 complex formation. ....	151
Fig. 7.2 Interaction of HA tetrasaccharides with LRP-1. ....	151
Fig. 7.3 Effects of a psHA tetrasaccharide on the TIMP-3/LRP-1 cluster II and IV binding. ....	152
Fig. 7.4 Interaction of solute GAGs with VEGFR-2. ....	152
Fig. 7.5 Influence of sHA3 polysaccharide concentrations on the TIMP-3/VEGFR-2 and VEGF-A/VEGFR-2 interaction. ....	153
Fig. 7.6 Effects of GAG oligosaccharides on the TIMP-3/VEGFR-2 interplay. ....	153
Fig. 7.7 Effects of GAG oligosaccharides on the VEGF-A/VEGFR-2 interaction. ....	154
Fig. 7.8 Effect of sHA3 on the VEGF-A and TIMP-3 competition for VEGFR-2 binding. .	154

---

Fig. 7.9 Visualization of sulfated GAGs and collagen in hydrogels.....	155
Fig. 7.10 Influence of VEGF-A and solute GAGs on the tube formation of PAE/KDR cells. .....	155
Fig. 7.11 Solute VEGF-A after incubation of hydrogels with VEGF-A in cell culture media. .....	156

**LIST OF TABLES**

Tab. 2.1 Overview on GAG degrading enzymes. ....	12
Tab. 2.2 Local and systemic factors influencing wound healing. ....	18
Tab. 2.3 Overview of matrix substrates and GAG interaction of MMPs.....	20
Tab. 2.4 Characteristics and functions of TIMPs. ....	25
Tab. 2.5 Selected LRP-1 ligands known to interaction with GAGs. ....	30
Tab. 2.6 Binding affinities of selected VEGF-A isoforms for HEP and HS.....	34
Tab. 2.7 Selected findings of the Transregio 67 obtained with solute or aECM-bound GAG derivatives. ....	39
Tab. 3.1 Overview of used chemicals. ....	43
Tab. 3.2 Overview of used mediator proteins, enzymes and antibodies. ....	47
Tab. 3.3 Overview of used commercially available glycosaminoglycans. ....	48
Tab. 3.4 Overview of used consumables.....	49
Tab. 3.5 Overview of used devices and software.....	51
Tab. 3.6 Overview of used cell culture reagents. ....	52
Tab. 3.7 Characteristics of GAG oligo- and polysaccharides used for interaction analyses. ..	58
Tab. 3.8 Characteristics of polymeric GAG derivatives used for aECM preparation. ....	58
Tab. 3.9 Characteristics of polymeric GAG derivatives used for hydrogel preparation.....	58
Tab. 3.10 Preparation of HA-AC/collagen hydrogels.....	60
Tab. 3.11 Composition of 1 ml aqueous acrylated polymer mixture. ....	61
Tab. 3.12 Activation of proMMP-1 and proMMP-2 via APMA. ....	67
Tab. 3.13 Scheme for the performance of MMP kinetic analysis.....	67
Tab. 3.14 Immobilization conditions used for the different SPR measurements.....	70
Tab. 3.15 Analysis and regeneration conditions of the different SPR measurements. ....	71
Tab. 3.16 Sample preparation and performance of the hexosamine assay.....	76
Tab. 3.17 Sample preparation and performance of the agarose gel electrophoresis.....	77
Tab. 3.18 Procedure to stimulate VEGFR-2 phosphorylation on PAE/KDR cells.....	81
Tab. 3.19 Migration assay procedure. ....	83
Tab. 3.20 Immunofluorescence staining procedure. ....	87
Tab. 4.1 Kinetic parameters characterizing the TIMP-3 interaction with LRP-1.....	100
Tab. 4.2 Kinetic parameters of the TIMP-3/VEGFR-2 and VEGF-A/VEGFR-2 interplay...	105
Tab. 4.3 GAG to collagen mass ratios of HA-AC/collagen hydrogels. ....	126

## LIST OF ABBREVIATIONS

<b>Abbreviation</b>	<b>Meaning</b>
AC	Acrylated
ADAM	A disintegrin and metalloprotease
ADAMTS	A disintegrin and metalloproteinase with thrombospondin type I motifs
aECM	Artificial extracellular matrix
AFM	Atomic force microscopy
AGEs	Advanced glycation end-products
APMA	4-Aminophenylmercuric acetate
Apo E	Apolipoprotein E
AT-III	Antithrombin-III
bFGF	Basic fibroblast growth factor
BMP	Bone morphogenetic protein
BMU	Basic multicellular unit
BSA	Bovine serum albumin
C	Chondroitin
Calcein AM	Calcein acetoxymethyl ester
CD44	Cluster of differentiation-44
ChC	Clostridium histolyticum collagenase
Coll/GAG	Collagen-based matrix containing the respective GAG
CR	Complement-like domain
CS	Chondroitin sulfate
CS-A	Chondroitin-4-sulfate
CS-C	Chondroitin-6-sulfate
CS-E	Chondroitin-4,6-sulfate
CSPG	Chondroitin sulfate proteoglycan
D	Dimensional
D.S.	Degree of substitution
D.S. <sub>AC</sub>	Degree of acrylation
D.S. <sub>S</sub>	Degree of sulfation
D.U.	Disaccharide unit
DAMPs	Damage of associated molecular patterns
DAPI	4',6-Diamidino-2-phenylindol
DMAB	4-(Dimethylamino)benzaldehyde
DMEM	Dulbecco's modified eagle's medium
DMF	<i>N,N</i> -dimethylformamide

<b>Abbreviation</b>	<b>Meaning</b>
DMMB	1,9-Dimethylmethylene blue
DMSO	Dimethylsulfoxide
DNA	Desoxyribonucleic acid
DPBS	Dulbecco's phosphate buffered saline
DS	Dermatan sulfate
DSPG	Dermatan sulfate proteoglycan
ECM	Extracellular matrix
EDC	1-Ethyl-3-(3-dimethylaminopropyl)carbodiimide hydrochlorid
EDTA	Ethylenediaminetetraacetic acid
EGF	Epidermal growth factor
ELISA	Enzyme linked immunosorbent assay
ER	Endoplasmic reticulum
FACIT	Fibril associated collagens with interrupted triple helices
FBS	Fetal bovine serum
FGF	Fibroblast growth factor
Fn	Fibronectin
FT-IR	Fourier transform-infrared
GAG	Glycosaminoglycan
GFOGER	Gly-Phe-Hyp-Gly-Glu-Arg
GMP	Good manufacturing practice
HA	Hyaluronan
HBS-EP	HEPES buffered saline containing EDTA and P20
HEP	Heparin
HEPES	<i>N</i> -2-Hydroxyethylpiperazine- <i>N'</i> -2-ethanesulfonic acid
hMSC	human mesenchymal stromal cell
HMW	High molecular weight
HPLC	High pressure liquid chromatography
HPX	Hemopexin
HRP	Horseradish peroxidase
HS	Heparan sulfate
HSPG	Heparan sulfate proteoglycan
HUVEC	Human umbilical vein endothelial cell
Hyal	Hyaluronidase
IL	Interleukin
init	Initial time point
K <sub>D</sub>	Equilibrium dissociation constant
KDR	Kinase insert domain receptor

<b>Abbreviation</b>	<b>Meaning</b>
KGF	Keratinocyte growth factor
KS	Keratan sulfate
KSPG	Keratan sulfate proteoglycan
LAP	Lithium phenyl-2,4,6-trimethyl-benzoylphosphinate
LDH	Lactate dehydrogenase
LDL	Low-density lipoprotein
LMW	Low molecular weight
LRP-1	Low-density lipoprotein receptor-related protein-1
M-CSF	Monocyte/macrophage colony-stimulating factor
MMP	Matrix metalloproteinase
MT-MMP	Membrane-type matrix metalloproteinase
MTT	Thiazolyl blue tetrazolium bromide
Mw	Molecular weight
NHS	<i>N</i> -Hydroxy succinimide
NMR	Nuclear magnetic resonance
NNGH	<i>N</i> -Isobutyl- <i>N</i> -(4-methoxyphenylsulfonyl)glycyl hydroxamic acid
Nrp	Neuropilin
OPG	Osteoprotegerin
P/S	Penicillin/Streptomycin
PAE	Porcine aortic endothelial cells
PBS	Phosphate buffered saline
PDGF	Platelet-derived growth factor
PEG	Poly(ethylene glycol)
PF	Platelet factor
PG	Proteoglycan
pI	Isoelectric point
PLA	Poly(lactic acid)
PLGA	Poly(lactic-co-glycolic acid)
PIGF	Placenta growth factor
PS	Polystyrene
psHA	Per-sulfated hyaluronan
RANK	Receptor activator of NF- $\kappa$ B
RANKL	Receptor activator of NF- $\kappa$ B ligand
RAP	Receptor associated protein
RGD	Arg-Gly-Asp
RHAMM	Receptor for hyaluronan-mediated motility
RT	Room temperature



<b>Abbreviation</b>	<b>Meaning</b>
RU	Resonance units
sCS	Over-sulfated chondroitin sulfate
SD	Standard deviation
SDS	Sodium dodecyl sulfate
SE	Standard error
SEM	Scanning electron microscopy
sGAG	Sulfated glycosaminoglycan
sHA	Sulfated hyaluronan derivative
SLRP	Small leucine-rich proteoglycan
SO <sub>3</sub>	Sulfur trioxide
SO <sub>3</sub> -DMF	Sulfur trioxide- <i>N,N</i> -dimethylformamide complex
SO <sub>3</sub> -pyridine	Sulfur trioxide-pyridine complex
SPR	Surface plasmon resonance
TBAF	Tetra- <i>n</i> -butyl ammonium fluoride hydrate
TBS	Tris-buffered saline
TeBA-HA	Tetrabutylammonium salt of hyaluronan
TES	<i>N</i> -[Tris(hydroxymethyl)methyl]-2-aminoethanesulfonic acid
TFA	Trifluoroacetic acid
TGF- $\beta$	Transforming growth factor- $\beta$
TIMP	Tissue inhibitor of metalloproteases
TNF	Tumor necrotic factor
Tris	Tris(hydroxymethyl)aminomethane
TS	Thrombospondin
UDP	Uridine-diphosphate
UV	Ultraviolet
VEGF	Vascular endothelial growth factor
VEGFR	Vascular endothelial growth factor receptor



## 1 INTRODUCTION AND AIMS

The demographic changes in industrial countries lead to rising numbers of elderly and multi-morbid patients with an accompanying increase in poorly healing bone fractures, implant failures and chronic wounds such as skin ulcers. All of this can not only strongly reduce the quality of life of these patients, but also leads to a significant increase in health care costs [1–3]. Thus, innovative functional materials that promote healing processes in health-compromised patients are a step towards both improving quality of life and reducing costs. In this context, the development of novel adaptive biomaterials and coatings as well as their characterization in terms of their impact on matrix remodeling and angiogenesis are essential.

One promising approach for the development of, for example, novel implant coatings or wound dressings is the use of functional components of the extracellular matrix (ECM) as this will provide an environment favorable for the regeneration of vascularized tissues such as bone and skin. The organic ECM of skin and bone is characterized by a complex, tissue-specific composition of collagen and several non-collagenous components like glycosaminoglycans (GAGs). Besides cell-cell interactions, cell-matrix interactions represent key factors that influence fundamental biological processes like cell adhesion, proliferation and differentiation [4,5]. GAGs like heparin (HEP), chondroitin sulfate (CS) and hyaluronan (HA) are negatively charged linear unbranched polysaccharides. Native sulfated GAGs (sGAGs) interact with biological mediator proteins like vascular endothelial growth factor-A (VEGF-A), matrix metalloproteinases (MMPs) and tissue inhibitor of metalloproteinase-3 (TIMP-3), which are crucial for angiogenesis and tissue remodeling during wound healing [6–8], and can modify their effects. However, the limited availability as well as the batch-to-batch variability of native GAGs are detrimental for clinical translation and the analysis of structure-function relationships in their interaction with biological mediators and cells. To overcome these limitations, non-sulfated HA can be chemically modified with e.g. sulfate groups in a more defined manner. HA sulfation has been shown to promote the interaction with several mediator proteins such as growth factors and to have direct positive effects on cells relevant to wound healing [9R]. Hence, specifically modified GAGs are promising functional compounds for biomaterials improving tissue regeneration in bone and skin.

For the design of functional biomaterials aiming to improve wound healing by directing the cellular behavior towards patient-specific needs and to closer mimic the *in vivo* situation, it is necessary to evaluate the impact of GAGs on ECM remodeling and angiogenesis and to develop novel, multi-component 2.5-dimensional (2.5D) and 3D artificial ECMs (aECMs) based on polymeric GAG derivatives and collagen type I. However, even though native sGAGs are known for their protein binding properties, studies on the interplay of GAGs with VEGF-A and TIMP-3 as well as their potential consequences on the mediator protein activity and the biological consequences of these GAG-protein binding for example on the inhibition of MMPs, TIMP-3 endocytosis and VEGF-A signaling are sparse and often restricted to HEP [10,11].

Thus, only little is known about the structure-function relationship of GAGs in this regard at present. This leads to the following aims of this PhD thesis: <sup>1</sup>

- (i) Analyze the interaction of native and chemically modified GAGs with TIMP-3 and VEGF-A as important mediator proteins involved in tissue remodeling and angiogenesis,
- (ii) Determine the impact of the TIMP-3/GAG interplay on the inhibition of matrix metalloproteinase-1 and -2, the TIMP-3 complex formation with its endocytic receptor low-density lipoprotein receptor-related protein-1 (LRP-1) and on the competition of TIMP-3 with VEGF-A for VEGF receptor-2 (VEGFR-2),
- (iii) Study the biological consequences of the GAG interaction with TIMP-3 and VEGF-A on the signal transduction via VEGFR-2 and the migration of endothelial cells,
- (iv) Engineer and characterize functional multi-component biomaterials based on aECMs as 2.5D and 3D biomimetic cellular microenvironments,
- (v) Analyze the impact of GAG derivatives on the enzymatic degradation of native HA and HA/collagen-based hydrogels via hyaluronidase (Hyal) and of collagen-based aECM coatings via collagenases,
- (vi) Reveal the binding and release profiles of 3D HA/collagen-based hydrogels for lysozyme and VEGF-A,
- (vii) Evaluate the potential influence of solute or hydrogel-bound GAG derivatives on the proliferation and functional morphology of endothelial cells in the absence or presence of VEGF-A.

---

<sup>1</sup> This work was embedded in the DFG-funded SFB Transregio 67 “Functional biomaterials for controlling healing processes in bone and skin - from material science to clinical application” as part of the subproject A3 “Development and characterization of artificial extracellular matrices based on collagen and glycosaminoglycan derivatives”. Parts of this thesis have been already published (compare list of publications, first authorships are indicated by a “R” before the number of the cited publications (e.g. R316), while co-authorships are highlighted by a “R” after the respective number of the cited publication (e.g. 9R).

## 2 BACKGROUND AND STATE OF KNOWLEDGE

### 2.1 Extracellular matrix (ECM)

The space between cells is filled with the ECM that provides the structural surrounding and mechanical support for cells as well as multiple biomechanical and biochemical cues. All this has the ability to direct and influence various fundamental biological processes like cell differentiation, angiogenesis and tissue homeostasis [5]. Matrix composition and architecture is tissue specific and depends on the physiological state, resulting in a strong heterogeneity. For example the ECM composition is altered in cancerous tissue compared to healthy ones [12]. However, in general each ECM is composed of water, fibrous proteins, glycoproteins, proteoglycans (PGs) and GAGs. A schematic overview of the ECM is given in Fig. 2.1. Due to the interaction of GAGs with mediator proteins such as growth factors, the ECM also functions as reservoir for these proteins. This binding of proteins to the ECM can alter their function in a stimulatory or inhibitory way. Cells adhere to the ECM via specific ECM-sensing cell-surface receptors, e.g. integrins [13,14], syndecans [15] and discoidin domain receptors [16], which influence signal transduction and thus cellular processes such as the cytoskeletal arrangement and cell migration [17]. The ECM as a whole is a highly dynamic structure being continuously enzymatically or non-enzymatically remodeled and post-translationally modified.

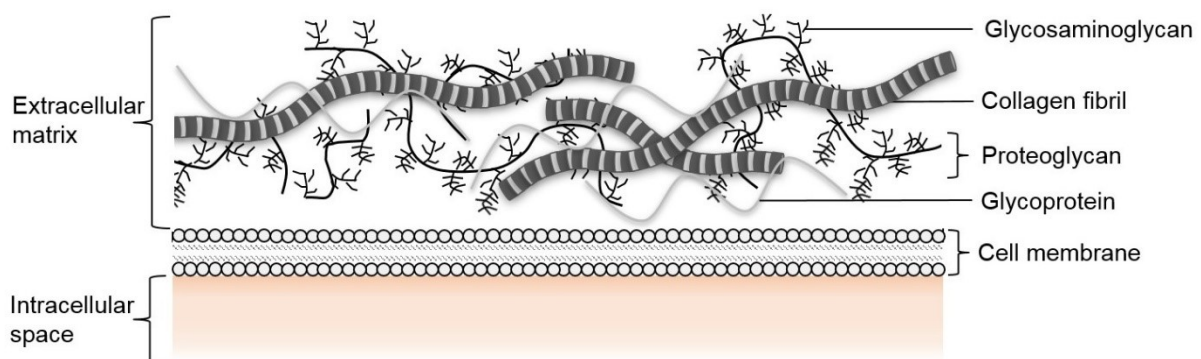


**Fig. 2.1 Schematic overview of the ECM.**

#### 2.1.1 Structural proteins

Different collagen types and non-collagenous glycoproteins such as elastin, fibronectins (Fns) and laminins represent the structural proteins of the ECM [18].

##### Collagens

Collagens are a family with at least 29 different members [19]. They are the major structural proteins in the ECM (about 25% of total tissue protein) and essential for tissue stability, integrity and structure [20]. The peptide composition of all collagens is special due to the high amounts of glycine (every third amino acid) and proline residues, leading to the repeating sequence Gly-X-Y in which X and Y are often proline and its post-translational modification hydroxyproline. Several lysine and proline residues of collagen are hydroxylated and are

important for the formation of the characteristic coiled-coil right-handed triple helices composed of three polypeptide  $\alpha$  chains. Based on their structural characteristics, three types can be distinguished: i) fibril forming collagens, ii) non-fibril forming collagens, and iii) fibril associated collagens with interrupted triple helices (FACIT) [19]. Collagens type I, II, III, V, XI, XXIV and XXVII are fibril forming collagens.

The biosynthesis of fibrillar collagen involves several intra- and extracellular steps, which determine the properties of the resulting fibrils. The transcription of the respective genes in the nucleus induces that procollagen  $\alpha$  chains are synthesized on the ribosome. After entering the lumen of the rough endoplasmatic reticulum (ER), the respective signal peptide is removed and post-translational modifications take place. Hydroxylases modify proline to 4- and 3-hydroxyproline as well as lysine residues to hydroxylysines. Furthermore, some hydroxylysine residues are glycosylated to galactosylhydroxylysine and glucosylgalactosylhydroxylysine [21]. Ascorbate, ferrous ions, 2-oxoglutarate and molecular oxygen serve as co-factors of these reactions. Three collagen chains then associate via their C-propeptides and are stabilized by the formation of intra- and interchain disulfide bonds. This process initiates the assembly of the triple helix in the direction of the N-terminus. Afterwards, the procollagen triple helices are transferred into secretory vesicles within the Golgi apparatus and secreted into the extracellular environment, where the propeptides located at the C- and N-termini of procollagen are cleaved by proteases [22].

The supramolecular spontaneous assembly of collagen monomers to fibrils termed fibrillogenesis is a complex, entropy driven-process [23]. During the initial lag period the monomers form a nucleus and in the following growth phase the fibrils grow in diameter and length, a process that can be followed by measuring the increase in turbidity over time [24,25]. Electrostatic and hydrophobic interactions between the collagen monomers lead to the formation of quarter-staggered complexes that form five-stranded micro-fibrils which then assemble into fibrils which are further stabilized by covalent cross-links. This staggered arrangement results in the characteristic banding pattern (D-periodicity with  $D \approx 67$  nm) (Fig. 2.2) [23]. Several factors such as the collagen type or the presence of further collagen types and proteoglycans (e.g. decorin, biglycan) influence the fibrillogenesis and thereby the resulting fibril morphology *in vivo* [25–27], though different models exist that explain the effects of for instance decorin on the collagen organization. Some suggest that the formation of interfibrillar GAG bridges may control the interfibrillar distance in collagen [28].

The most abundant protein in skin and bone tissue is collagen type I, while collagen type II is the main type found in cartilage [29,30]. Type III collagen is known to increase the strength of hollow constructs such as the intestine, arteries and the uterus, and type IV collagen builds the basal lamina. Collagen type I is important for the mechanical properties of bone as it represents the primary matrix component and provides nucleation sites for mineralization. Additionally, it influences the osteoblastogenesis by for example promoting the bone morphogenic

protein (BMP) induced osteogenesis as well as the osteoclastogenesis by functioning as degradable substrate for osteoclasts. Collagen type III is reported to promote bone formation in general [31]. An overview on further collagen types and their functions is given by Gelse et al. and will not be discussed here in detail [22].

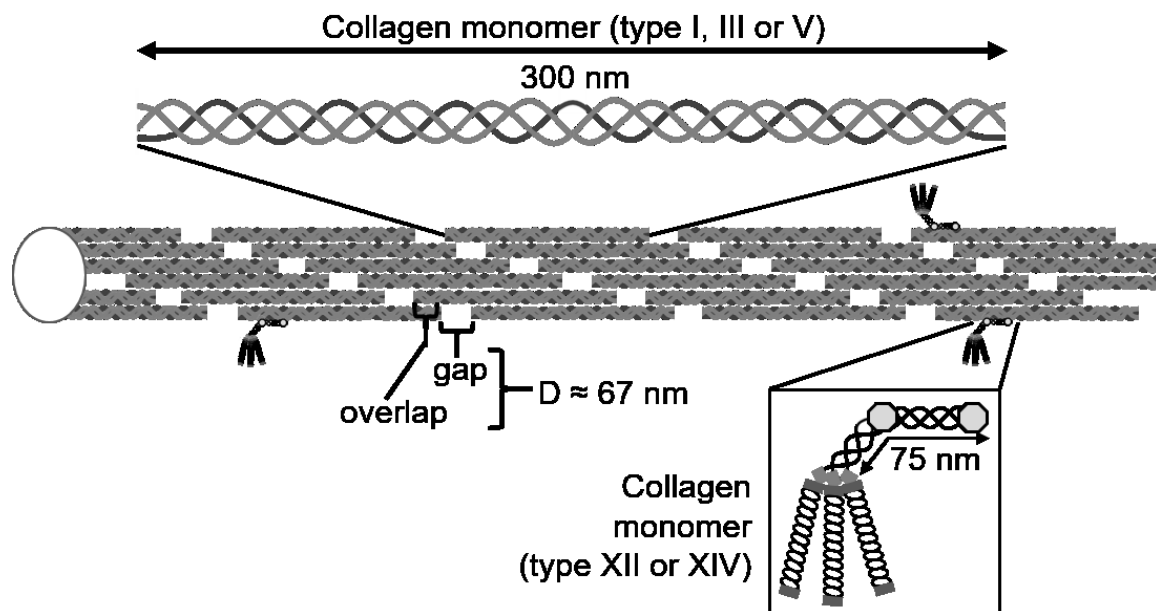


**Fig. 2.2** Schematic overview on the axial structure of triple-helical collagen type I, III or V monomers in a fibril with associated collagen type XII or XIV as present in skin. Adapted from [23,32] with modifications according to [33,34]).

Collagen type I contains two  $\alpha_1$  (I) chains and one  $\alpha_2$  (I) chain, while collagen type II and collagen type III are homotrimers consisting of three  $\alpha_1$  (II) chains or three  $\alpha_1$  (III) chains, respectively. Tropocollagen is composed of three polypeptide chains with about 1000 amino acids each that form a triple helix with a diameter of about 1.4 nm and a length of about 300 nm. Each turn of the triple helix consists of 3.3 residues with a translational distance between them of 0.286 nm, resulting in an extended pitch of the helix of about 0.95 nm [35].

Beside their functions in biomechanics, collagens contain binding sites for further ECM components such as GAGs [20]. For example, HEP has a high affinity for collagen type I ( $K_D \approx 150$  nM) [36] and collagen type V binds CS-E and HEP with  $K_D$  values of 5 - 40 nM [37]. Due to their direct or indirect interplay with cytokines and growth factors, they also contribute to the sequestering of mediator proteins within the ECM. Furthermore, cells are able to directly interact with collagens via several specific receptor types like glycoprotein VI and integrins that recognize the Arg-Gly-Asp (RGD) sequence. These interactions influence fundamental processes such as cell adhesion, growth, differentiation, survival and activity [22].

### **Fibronectin (Fn)**

Fn is a ubiquitous homodimeric glycoprotein composed of two 220 - 250 kDa subunits connected by two disulfide bonds. Each Fn subunit contains three domains (type I, II and III)

[38]. There are two forms of Fn with different functions. The plasma form of Fn is part of the fibrin clot, which is formed as provisional matrix after an injury [39]. Cells such as keratinocytes, myofibroblasts and endothelial cells secrete cellular Fn, which assembles into a fibrillary network for instance in the dermis, the dermal-epidermal basement membrane region as well as the bone marrow niche [40]. This network influences several processes such as cell adhesion, proliferation and polarization [41], for example through integrin-mediated cell-binding via a RGD sequence or through interaction with collagen, syndecans, perlecan or HEP via specific binding sites [42,43]. Especially the interaction with GAGs and PGs is reported to alter the Fn matrix assembly [44].

### 2.1.2 Proteoglycans (PGs) and glycosaminoglycans (GAGs)

PGs are glycosylated proteins that bind high quantities of water thereby forming a hydrogel that fills the space in the extracellular environment [45]. Beside their buffering functions and importance for water retention and resistance against compressive forces within the ECM, PG are known to bind mediator proteins such as growth factors and cytokines and to influence the ECM structure. They are composed of one or more GAG chains covalently bound to a core protein and have a high variability in their protein sequence as well as their GAG chains, resulting in a multitude of different structures and functions [46]. There are three main PG families: i) modular PG, ii) small leucine-rich PGs (SLRPs) and iii) cell-surface PGs [47].

GAGs are linear negatively charged polysaccharides characterized by repeating disaccharide units composed of an acetylated amino sugar (*N*-acetyl-glucosamine or *N*-acetyl-galactosamine) and most commonly uronic acid (L-iduronic acid or D-glucuronic acid). The variety of GAG structures is a result of polymer modifications like acetylation, isomerization and sulfation. These variations of the disaccharide sequences may direct the wide range of interactions with different proteins, which led to the suggestion of a sulfation code of GAGs. However, the term code in this context does not refer to a template driven process comparable to transcription and translation but should be interpreted as influence of the GAG structure on the specificity of GAG-protein interactions [48].

GAGs have multiple biological functions and participate in the regulation of e.g. angiogenesis (section 2.7.3), development, tissue homeostasis (sections 2.3, 2.4) and cancer progression (an overview on different GAG functions is given in Fig. 2.3). Further, they are involved in microbial pathogenesis since several pathogens such as viruses (e.g. herpes simplex virus), parasites and bacteria are reported to target their host cells via their interaction with cell surface-bound GAGs [49,51].

GAGs function as polyelectrolytes and trigger cellular response in different ways: i) indirectly by binding and accumulating mediator proteins such as growth factors and ii) directly due to their interaction with cells. They are able the binding of signaling proteins to cell receptors and thus cell signaling. As shown in Fig. 2.4, two classes of GAGs exist: i) the non-sulfated GAG



HA and ii) the sulfated GAGs CS, dermatan sulfate (DS), keratan sulfate (KS), HEP and heparan sulfate (HS), with only class ii) members bound to core proteins via a serine containing tetrasaccharide linker (GlcA- $\beta$ 1,3-Gal- $\beta$ 1,3-Gal- $\beta$ 1,4-Xyl- $\beta$ 1-O-Ser) [53].

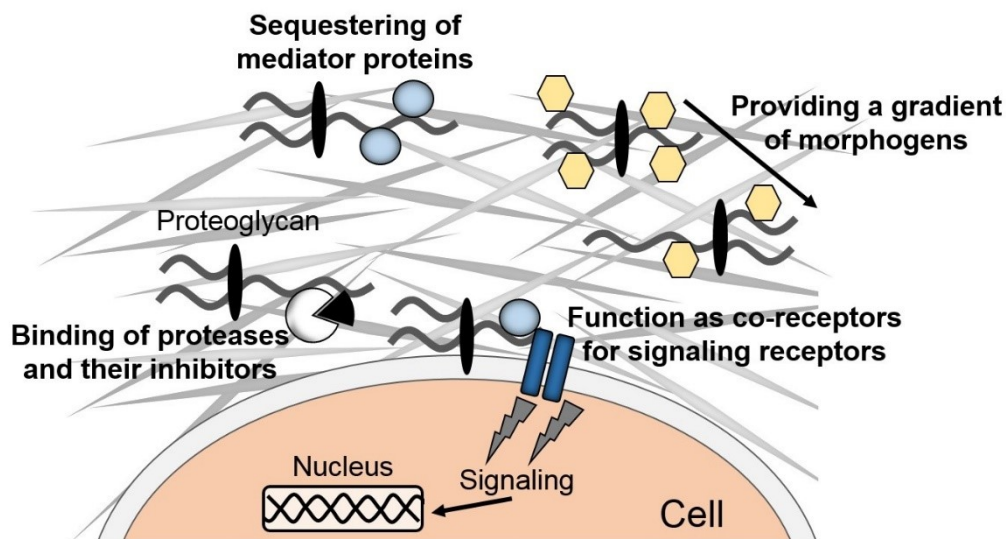


**Fig. 2.3 Schematic overview on the location of GAGs and their biological functions.** Adapted from [49,50] with modifications).

### 2.1.2.1 Chondroitin sulfate (CS)

CS consists of repeating disaccharide units (D.U.) of D-glucuronic acid  $\beta$ -1,3-linked to N-acetylgalactosamine residues that are assembled in the ER/Golgi apparatus. The activity of sulfotransferases results in different sulfation patterns of CS that are termed CS-A (sulfate residues at the C4 position of N-acetylgalactosamine), -C (sulfation of the C6 position of N-acetylgalactosamine), -D (sulfate groups at the C2 of glucuronic acid and the C4 of N-acetylgalactosamine) or -E (sulfation of the C4 and C6 position of N-acetylgalactosamine), while the non-sulfated derivative is named chondroitin (C) [54]. CS is a major component of arterial walls and the dominant GAG in the bone ECM [55,56]. It is ubiquitous on cell surfaces and within the ECM in the form of PGs (CSPGs) like versican or aggrecan where CS chains are covalently bound to serine residues of the core proteins. These CSPGs strongly vary in the number of CS chains as well as in their size from 80 - 3500 kDa [57]. CSPGs are involved in a number of different biological events such as morphogenesis and neural development [54,58] and CS interacts with several mediator proteins and ECM components such as BMP-4 and Fn [59,60].

Commercially available CS is in most cases extracted from shark cartilage or from bovine trachea [61]. It is currently used as nutraceutical product for self-medicating patients against osteoarthritis even though its effects are discussed controversially and the bioavailability of CS after oral up-take is unclear [62].

### 2.1.2.2 Dermatan sulfate (DS)

DS (formerly called CS-B) is a stereoisomer of CS present in skin, blood vessels and heart valves and composed of L-iduronic acid bound to D-galactosamine via a  $\beta$ -1,3 linkage. The

iduronic acid is sulfated at the C2 position, while the galactosamine residue can be sulfated at the C4 or the C6 position. The intracellular epimerization of glucuronic acid to iduronic acid leads to the formation of dermatan sulfate from CS. DS is present in DSPG where DS is covalently bound to a serine residue of the core protein via an *O*-xylose linkage. Decorin, biglycan, thrombomodulin and versican are examples for DS chain containing PGs [63].

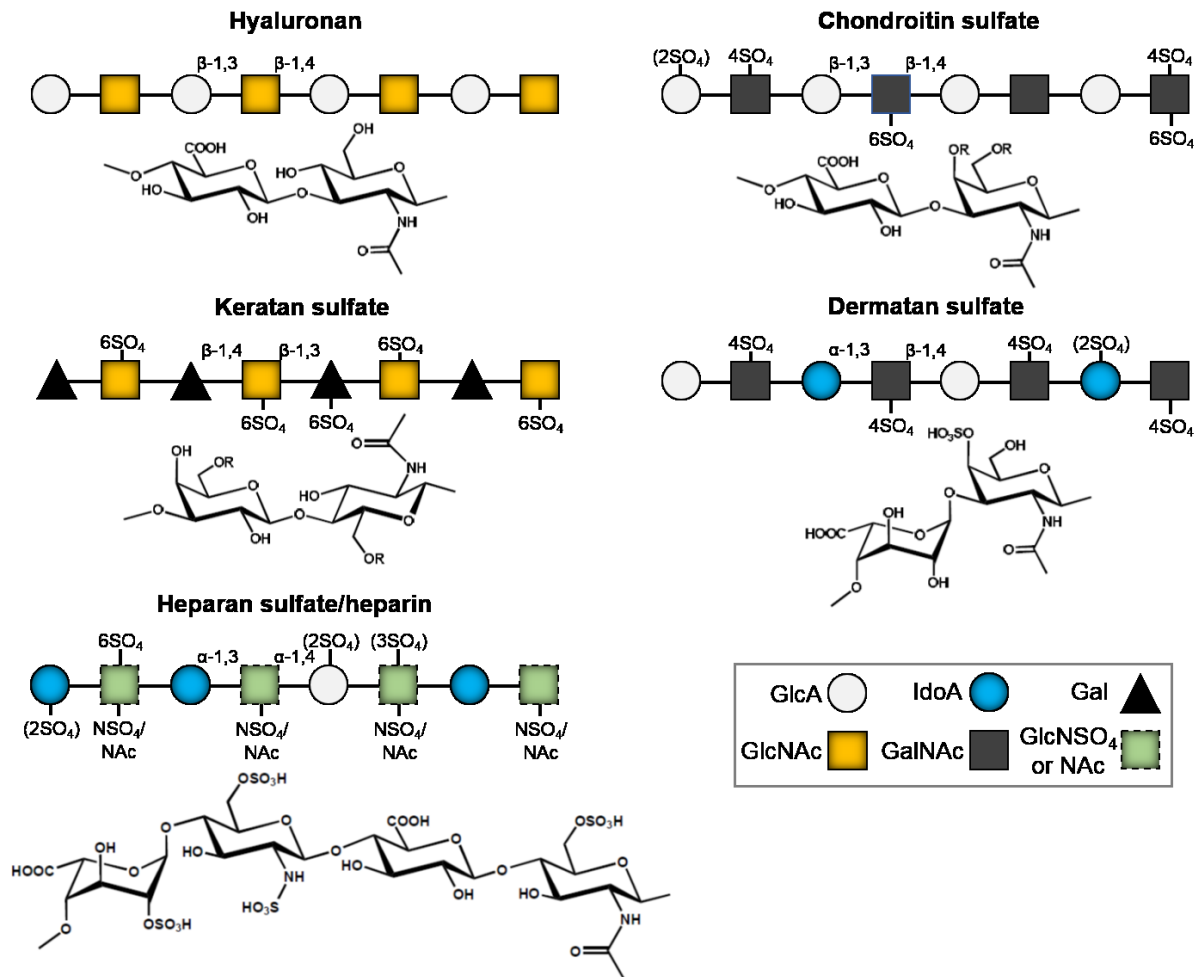


**Fig. 2.4 Structural characteristics of native GAGs.** Adapted from [46,52]. HA, CS, KS, DS, HS and HEP are polysaccharides composed of repeating D.U., which are displayed as cartoon representatives showing the diversity of possible modifications within one polymer chain (upper panels) as well as structural formulas representing the most abundant saccharide compositions with R = H or SO<sub>3</sub>H (lower panels).

### 2.1.2.3 Keratan sulfate (KS)

KS is composed of *N*-acetyl-glucosamine  $\beta$ -1,3 linked to *D*-galactose and is present in the ECM of for instance cartilage, bone and cornea [64]. It is mostly 6-*O*-sulfated at the *N*-acetyl-glucosamine residue but can be modified at the *D*-galactose residue as well [65]. Due to its structural characteristics, KS is the only GAG without acidic residues and thus less acidic in solution compared to the other GAG types. KS can be differentiated in KS I, which is *N*-linked to asparagine residues of a core protein and is the predominant GAG in cornea, and KS II, which is *O*-linked to threonine or serine residues and is for example present in cartilage [66].

Examples for PGs with KS (KSPG) are keratocan, fibromodulin, lumican and osteoadherin, which belong to the SLRPs.

KSPGs in cornea are required to maintain the hydration level and thereby tissue transparency [67]. Because of this KS is often used as an eye drop ingredient. KS is also present in aggrecan and contributes to the typical hydration properties of cartilage. In bone, osteoadherin expressed by osteoblasts binds to hydroxyapatite and promotes an integrin-mediated cell binding [68].

#### **2.1.2.4 Heparan sulfate/heparin (HS/HEP)**

HS is synthesized by all cells and widely distributed within the matrix and on cell surfaces, while HEP is solely produced by connective-tissue-type mast cells and present as PG serglycin in their cytoplasmic granules [69,70]. HEP plays a critical role in the intracellular storage of granule-localized proteases, serotonin and histamine, in mast cells [71]. HEP is more sulfated and epimerized than HS. A typical HS chain has a multidomain structure and contains about 50 - 250 D.U. resulting in a molecular weight ( $M_w$ ) of 20 - 100 kDa and 0.6 - 1.8 sulfate groups per repeating D.U. In contrast, HEP has an average  $M_w$  of 7 - 20 kDa and about 1.8 - 2.6 sulfate residues per disaccharide [48]. Because of this, HEP is the GAG with the highest negative charge density [72]. Syndecans with a transmembrane domain and glypicans characterized by a glycosyl-phosphatidylinositol anchor represent the main families of cell surface-bound PGs with HS (HSPGs), while perlecan, agrin and collagen type XVIII are the major types of HSPGs that are located in the ECM [70].

The biological functions of HSPGs mainly base on the interaction of sulfated chain regions with proteins (e.g. morphogens, growth factors) and can affect their localization, biological activity or signaling processes. Since the interaction of proteins and HS are crucial for development and tissue homeostasis, an in-depth understanding of the structure-function relationship is required to clarify for instance their role in several pathophysiologic conditions [70].

To qualify as a HS-binding protein (HSBP) several criteria have to be met. They have to show a significant interaction with HS under physiological conditions regarding pH and ionic strength. In general, there should be a detectable protein binding to HEP, e.g. to HEP/sepharose columns, which is not disrupted in the presence of isotonic saline concentrations. The same criterion must be fulfilled for their interplay with HS. The third criterion for a HSBP is that it must be attendant in a relevant biological context such as at the ECM or cell surface [48].

Up to now, about 300 human proteins are known for their HEP-binding properties and most of them are HSBPs [73]. A HS-protein interaction is defined as specific when only a specific sequence within the polymer directs the interplay and as non-specific if several sequences participate equally [74]. One example for a specific interaction is the pentasaccharide  $\text{Glc}_{\text{NAc}/\text{NS6S}}\text{-GlcA-Glc}_{\text{NS3S,6S}}\text{-IdoA}_{2\text{S}}\text{-Glc}_{\text{NS6S}}$  that provides the binding site for the serine protease inhibitor antithrombin-III (AT-III), which causes the anticoagulant activity of HEP [75,76].

HEP is widely used in the clinics as intravenous anticoagulant ( $K_D$  of 3 nM for AT-III) [48], and the HEP crisis in 2007 - 2008 highlighted the consequences of HEP contamination with a semi-synthetic over-sulfated CS as this led to anaphylactic responses causing hypotension and nearly 100 deaths [77]. Furthermore, the availability of animal-derived HEP (mainly from porcine intestinal mucosa) is limited, highlighted by the fact that one pig is required to isolate one dose of low  $M_w$  (LMW)-HEP or three doses of unfractionated HEP. This also results in high cost for pharmaceutical grade HEP [78].

#### **2.1.2.5 Hyaluronan (HA)**

HA is unique since it is non-sulfated and not epimerized or covalently linked to any protein core. Furthermore, it is the only GAG that is synthesized at the inner surface of the plasma membrane catalyzed by HA synthases and not in the Golgi apparatus. There, it is elongated at its reducing end by the continuous addition of uridine-diphosphate (UDP)-activated-*N*-acetylglucosamine and UDP-glucuronic acid, while the chain elongation of sGAGs occurs at the non-reducing end [79].

HA is found in the ECM of skin, eye, and cartilage, in synovial fluid and to a lower extent also in the ECM of bone and other tissues. It is composed of repeating D.U. of *N*-acetylglucosamine bound via a  $\beta$ -1,3 linkage to glucuronic acid. The respective disaccharides in turn are linked via a  $\beta$ -1,4 linkage, resulting in polymers of high  $M_w$  (HMW) (up to 20000 kDa) [80]. One D.U. has a length of about 1 nm resulting in a total length of 10  $\mu$ m for a HA molecule with 10000 D.U. [81]. Even though it is known that extracted HA has a random coil conformation, the actual conformation of HA in the tissue is not fully elucidated today [82].

HA is nowadays mainly obtained by bacterial fermentation (*Streptococcus* groups A or C) since this is much easier and more cost efficient than extraction from tissues like rooster comb [61]. It became popular due to its wide use for intradermal injections in cosmetics to treat for instance wrinkles. However, HA has much more important functions than just serving as filling material [83]. For example, the clinical efficiency of intra-articular HA injections to reduce pain associated with osteoarthritis in the knee [84,85].

The size of HA mainly dictates its function as signaling molecule. HMW-HA acts as space-filler within the ECM by incorporating large amounts of water and has anti-angiogenic, anti-inflammatory and immunosuppressive effects, while smaller HA fragments of 25 - 50 D.U. that result from degradation of HMW-HA stimulate the immune response, promote angiogenesis and inflammation [82]. Furthermore, both high- and LMW-HA (36000 kDa, 300 kDa) was reported to function as antioxidant *in vitro* by scavenging reactive oxygen species and free radicals [86]. In addition, HA tetrasaccharides can protect cells from apoptosis and HA oligosaccharides are crucial for chondrogenesis [82].

Further factors determining the function of HA are its concentration and localization as well as its interaction with specific HA-binding proteins, the so-called hyaladherins [87]. Examples for

such HA-binding proteins are the members of the link module family (e.g. aggrecan, versican, brevican, neurocan, cluster of differentiation-44 (CD44)) and non-link module hyaladherins such as RHAMM (receptor for hyaluronan-mediated motility, also known as CD168). CD44 as the main HA receptor is ubiquitously expressed by cells and responsible for the internalization of HA. Furthermore, it can interact with other ligands like Fn, collagen, serglycin, osteopontin and laminin. There are different splicing variants of CD44 that are involved in several processes like cell signaling and ECM organization by supporting cell-matrix adhesion [88]. RHAMM is present in multiple cell compartments like the cell membrane, mitochondria, cell nucleus and the cytoskeleton. It contributes for example to the arrangement of the actin cytoskeleton through association with actin, functions as an adapter molecule connecting signaling complexes with the cytoskeleton and activates several tyrosine and serine/threonine kinases (e.g. focal adhesion kinase) by its interaction with HA. Overall it is important for the migration and proliferation of cells during physiologic and pathologic conditions [89]. Moreover, HA can be chemically modified to tune its properties and functionality, which will be discussed in section 2.8.3.

#### **2.1.2.6 Enzymatic degradation of GAGs**

An ordered enzymatic degradation of glycosaminoglycans is mandatory to maintain tissue properties and functions. Since native sGAGs always occur bound to a protein core, free GAGs, except HA, represent degradation products of PGs from the ECM. ADAMTS (a disintegrin and metalloproteinase with thrombospondin type I motifs) family members are PG degrading proteinases [52]. For example, ADAMTS-5 has the highest activity to degrade aggrecan and cleaves the Glu<sup>373</sup> - Ala<sup>374</sup> bond of the core protein [90].

The intracellular GAG digestion takes place in two steps with specific pathway for each GAG type. PGs are initially depolymerized in the endosome through endolytic GAG cleavage by heparanase, Hyal and endo-galactosidase. The resulting oligosaccharides are desulfated and exolytically cleaved into monosaccharides in the lysosome by sulfatases, glycosidases and a transferase. Enzyme deficiencies result in the manifestation of seven mucopolysaccharidoses, which are reviewed by Coutinho et al. [91]. In contrast to the biosynthesis of GAGs, their catabolism is not fully understood today [54].

Hydrolases depolymerize GAGs *in vivo*, while the heparinases, chondroitinases and hyaluronidases often used for analytical and preparative purpose are lyases of mainly bacterial origin [92]. Lyases cleave the glycosidic linkage by  $\beta$ -elimination at the non-reducing end of uronic acids resulting in unsaturated C4-C5 bonds. In contrast, hydrolases can specifically cleave either of the two bonds existing in the GAG polymer and leave all carbons saturated. An overview of different GAG degrading enzymes is given in Tab. 2.1.

Two hydrolase types of Hyal can be distinguished based on their mechanisms of substrate cleavage. Hyal-I or testicular Hyal randomly cleaves HA and CS by hydrolyzing the  $\beta$ -1,4 glycosidic bond between the *N*-acetylglucosamine or *N*-galactosamine and the glucuronic acid

residues, while Hyal-II or leech Hyal catalyze the cleavage of the  $\beta$ -1,3 glycosidic linkage [93]. *In vivo*, HMW-HA is first cleaved by Hyal-II on the cell membrane to generate fragments of about 20 kDa [94]. These products are internalized into endosomes and cleaved after their transport to lysosomes by Hyal-I into smaller oligosaccharides, which are afterwards degraded by the activity of  $\beta$ -N-acetyl-hexosaminidase and  $\beta$ -D-glucuronidase that remove non-reducing sugars [81]. These enzymes are present in serum and inside the cells; for example, Hyal-I concentrations in the human serum are reported to be about 60 ng/ml [95].

**Tab. 2.1 Overview on GAG degrading enzymes.** Adapted from [50].

	Enzyme	Substrate	Cleaved linkage <sup>1</sup>
Lyases (EC 4.2.2.X)	Heparinase I (X = 7)	HEP	H <sub>NS,6Z</sub> -( $\alpha$ -1,4)-I <sub>2S</sub> (endo, exo)
	Heparinase II	HEP, HS	H <sub>NY,6Z</sub> -( $\alpha$ -1,4)-U <sub>2Z</sub> (endo)
	Heparinase III (X = 8)	HS	H <sub>NAc</sub> -( $\alpha$ -1,4)-I, H <sub>NY,6Z</sub> -( $\alpha$ -1,4)-G (endo)
	Chondroitinase ABC (X = 4)	CS-A/-C, C, DS, HA	H <sub>NAc,4Z,6Z</sub> -( $\beta$ -1,4)-U <sub>2Z</sub> <sup>2</sup> (exo)
	Chondroitinase AC (X = 5)	CS-A, CS- C, C, HA	H <sub>NAc,4Z,6Z</sub> -( $\beta$ -1,4)-G (endo or mixed)
	Chondroitinase B (X = 19)	DS	H <sub>NAc,4Z,6Z</sub> -( $\beta$ -1,4)-I <sub>2Z</sub>
	Chondroitinase C	CS-C, HA, CS-A	H <sub>NAc,6S</sub> -( $\beta$ -1,4)-I <sub>2Z</sub>
	Hyaluronidase (X = 1)	HA, DS, CS, C	H <sub>NAc</sub> -( $\beta$ -1,4)-G
Hydrolases (EC 3.2.1.X)	Heparanase (X = 166)	HEP, HS	I <sub>2Z</sub> -H <sub>NY,6Z</sub> -G-( $\beta$ -1,4)-H <sub>NY,6Z,3Z</sub> (endo)
	Keratanase I (X = 103)	KS	H <sub>NAc,6Z</sub> -Gal-( $\beta$ -1,4)-H <sub>NAc,6Z</sub> (endo)
	Keratanase II	KS	H <sub>NAc,6S</sub> -( $\beta$ -1,3)-Gal <sub>6Z</sub> -H <sub>NAc,6S</sub> (endo)
	Hyal I (X = 35)	HA, CS, DS	H <sub>NAc</sub> -( $\beta$ -1,4)-G (endo)
	Hyal II (X = 36)	HA	G-( $\beta$ -1,3)-H <sub>NAc</sub> (endo)
	$\beta$ -D-glucuronidase (X = 31)	HS, CS	G-( $\beta$ -1,4)/( $\beta$ -1,3)-H <sub>NY,6S</sub> or <sub>4S</sub> (exo)
	$\alpha$ -L-iduronidase (X = 76)	HS, DS	I-( $\alpha$ -1,4)/( $\alpha$ -1,3)-H <sub>NY,4Z,6Z</sub> (exo)
	$\beta$ -galactosidase (X = 23)	KS	Gal-( $\beta$ -1,4)/( $\beta$ -1,3)-H <sub>NAc,6Z</sub> (exo)
	$\alpha$ -N-acetyl-glucosaminidase (X = 50)	HEP, HS	H <sub>NAc</sub> -( $\alpha$ -1,4)-G <sub>2Z</sub> (exo)
	$\beta$ -N-acetyl-hexosaminidase (X = 52)	HA, KS, CS, DS	H <sub>NAc</sub> -( $\beta$ -1,4)/( $\beta$ -1,3)-G <sub>2Z</sub> (exo)

<sup>1</sup>G = glucuronic acid, H = hexosamine, I = iduronic acid, U = uronic acid, Y = sulfated or acetylated, Z = unsubstituted or sulfated

<sup>2</sup>At least one sulfate residue at the galactosamine moiety required

### 2.1.3 ECM of skin

Skin consists of an outer layer, the epidermis, the dermis as an underlying connective tissue connected to the epidermis via a basement membrane (Fig. 2.5), and the subcutis. The epidermis comprises the multilayered epithelium and the interfollicular epidermis with sebaceous glands and hair follicles [96]. 80% of the total collagen in skin is collagen type I and 15% is collagen type III, which is located in the dermis and required to maintain the structure and integrity of the tissue. Collagen type III is also important for the flexibility, softness and tensility of the dermis and modulates the diameter of collagen fibrils [29]. The basement membrane ECM mainly contains a network of collagen type IV, which is connected via perlecan and nidogens to laminins [97]. Especially laminin 332 is crucial to link the epidermis to the dermis [32].

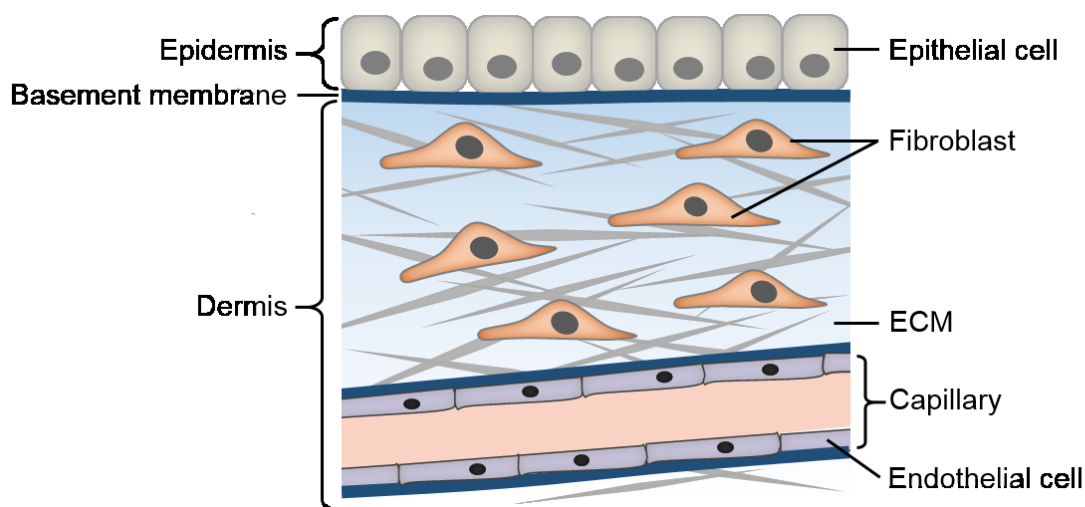


**Fig. 2.5 ECM of skin.** Simplified overview of the layered structure of skin including characteristic cell types. Adapted from [98] with modifications.

The papillary dermis, which is closest to the epidermis as outer skin layer, contains mainly thin collagen fibers, while a highly cross-linked, dense collagen network present above the layer of subcutaneous fat characterizes the underlying reticular dermis. Beside fibroblasts, mast cells, T and B cells and macrophages, blood vessels, nerves and lymphatics are present in the dermis [96].

The major PGs in skin are decorin and versican. With increasing age, the amount of versican as a large CS-containing PG decreases, while the amount of decorin as a DS-containing PG rises [99]. GAGs make up about 0.1 - 0.3% of the dry weight of skin [100]. HA, DS and CS are the main GAGs in skin with approximately 58%, 20% and 21% of the total GAGs, respectively [101]. It is of note that about 50% of the total body HA is present in the skin ECM. The HA content is higher in the dermis compared to the epidermis [102,103].

### 2.1.4 ECM of bone

The mechanical properties of bone are determined by both the hard and rigid inorganic part of the ECM that contains mainly hydroxyapatite [ $\text{Ca}_{10}(\text{PO}_4)_6(\text{OH})_2$ ] and constitutes about 70% of the bone ECM, and the more flexible organic part. This is made up of 90% collagen type I and over 100 further ECM proteins like other collagen types, PGs, Fn, osteopontin and osteocalcin [104,105].

Examples of PGs in bone are decorin, biglycan and osteoadherin [68,106]. GAGs constitute 4 - 5% of the collagen dry weight in the bone ECM [107]. CS-A represents 90% of the GAGs present, while HA, DS and CS-C are the remaining parts [56]. It is known that the ECM is an important modulator of matrix mineralization, cell function as well as tissue morphogenesis. CS-E for example is reported to be critical for the intramembranous ossification and it is suggested to function as ligand for the potential CS receptors cadherin-11 and N-cadherin, thereby promoting osteogenic differentiation *in vitro* [108].

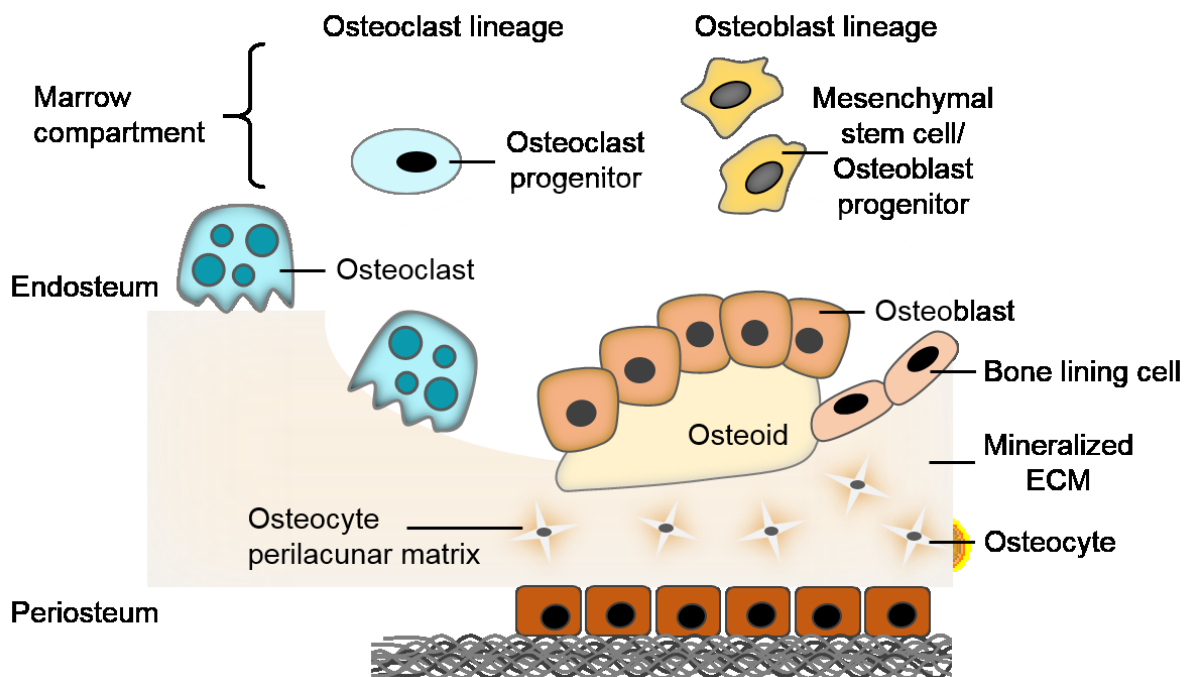


**Fig. 2.6 Simplified scheme of the matrix compartments of bone.** Adapted from [31] with modifications.

Bone is composed of the following matrix compartments: i) the mineralized bone ECM, ii) marrow, iii) endosteum, iv) periosteum and v) osteocyte perilucanar matrix (Fig. 2.6). The irregular and loose marrow ECM is required for the support of hematopoietic stem cell differentiation, human mesenchymal stromal cells (hMSCs) as well as osteoclast precursor cells. In contrast, the endosteum contains bone lining cells with their insufficiently characterized ECM and the osteoid that is a non-mineralized ECM produced by osteoblasts. During bone maturation, this osteoid will transform into mineralized bone [31]. The periosteum



is composed of two histological layers, a fibrous, collagen rich layer and a cell rich cambium layer [109].

The osteocyte non-mineralized perilacunar matrix is embedded in the mineralized bone matrix and surrounds the osteocytes. It connects these cells with each other as well as with the vasculature and further bone cells located on the bone surface. This matrix is characterized by fluid-like mechanical properties due to the matrix proteins such as small integrin-binding ligand-linked glycoproteins and matrix extracellular phosphoglycoprotein secreted by osteocytes [110].

## 2.2 Wound healing

Wound healing is a well-orchestrated dynamic process which requires the interaction of several cell types with the ECM, growth factors and cytokines and can be affected via a variety of different factors [111].

### 2.2.1 Cutaneous wound healing

The skin represents the largest organ of the human body and is composed of the three layers: epidermis, dermis and subcutis (compare section 2.1.3). It functions as a barrier against the environment including microorganisms, provides mechanical protection against traumata, protects against physical stress (ultraviolet (UV) light, heat, cold) and loss of water, regulates the body temperature, contributes to the immunological protection and is a sensory organ for tactile and pain stimulus. Multiple biological processes, which will be described in the following section, are required to restore the integrity of the skin after an injury. Disruption of these sequential processes can cause several pathologic conditions and diseases [29].

#### Phases of wound healing

The complex process of dermal wound healing can be divided into five partially overlapping phases: hemostasis, inflammation, proliferation/granulation, epithelization and remodeling (Fig. 2.7).

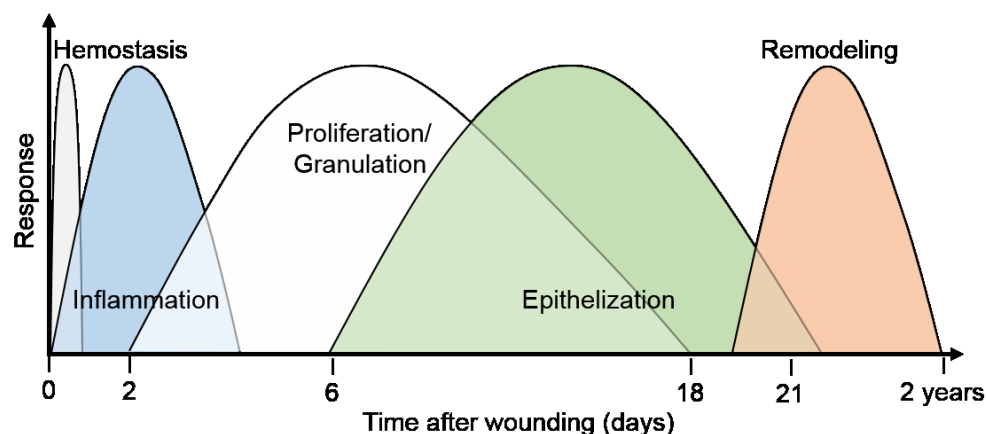


**Fig. 2.7 Phases of cutaneous wound healing.** The displayed times are approximate values, which can differ strongly due to patient specific factors. Adapted from [112] with modifications according to [113].

The hemostasis starts immediately after wounding. Vasoconstrictors (thromboxane A<sub>2</sub>, prostaglandin 2- $\alpha$ ) are released and a coagulate consisting of fibrin, collagen, blood platelets, thrombin and Fn forms. The damage of associated molecular patterns (DAMPs) such as nucleic acids, intracellular proteins from dying cells and fragments of the ECM (e.g. LMW-HA) initiates inflammation [114]. Pro-inflammatory cytokines and growth factors like TGF- $\beta$  (transforming growth factor- $\beta$ ), PDGF (platelet-derived growth factor), FGF (fibroblast growth factor) and EGF (epidermal growth factor) are released by the platelets from the coagulate and the surrounding wound area to initiate the inflammatory phase [111]. After the bleeding is stopped, inflammatory cells such as neutrophils, monocytes and lymphocytes start to migrate into the wound [115] where the fibrin network functions as scaffold for the arriving cells (inflammatory cells, fibroblasts and endothelial cells) and accumulates cytokines and growth factors.

Due to this several hundred genes are activated within one hour after injury. Mechanical signals and/or bacterial toxins stimulate mast cells, T-cells and Langerhans cells to produce IL-1 (interleukin 1), TNF- $\alpha$  (tumor necrotic factor- $\alpha$ ), TGF- $\beta$  and PF-4 (platelet factor-4) which attract neutrophils. M1- and M2-macrophages as well as neutrophils degrade and remove the detritus and bacteria via the release of proteolytic enzymes like MMPs and the up-take by phagocytosis, while also producing reactive oxygen species and nitrogen monoxide. The released interleukins and growth factors stimulate angiogenesis and keratinocytes and induces fibroblasts to produce collagen during the next phase [116].

During the following granulation phase new tissue is formed to fill the wound. PDGF and EGF stimulate proliferation and migration of activated fibroblasts. The stimulation of fibroblast with TGF- $\beta$ 1 induces their differentiation into myofibroblasts, which produce collagen and stress fibers to contract the wound. The provisional ECM mainly consists of collagen type III, PGs and Fn. Angiogenesis is further activated during this phase by VEGF-A [117].

Activated thrombocytes and macrophages release EGF and TGF- $\alpha$  to induce the following epithelization phase, which is characterized by the wound closure due to wound contraction and formation of scar tissue. Collagen fibrils are produced and crosslinked. Fibroblasts release KGF-1 (keratinocyte growth factor-1) and IL-6 to stimulate the migration and proliferation of keratinocytes, which leads to the formation of a closed epidermis starting either from the wound edges or from an intact basement membrane [118].

The final remodeling phase can last weeks until months and completely re-establishes the skin properties and functions. Inflammatory cells are removed from the wound and the provisional matrix is transformed into a regular skin ECM for example by replacing collagen type III by the more stable collagen type I. New cells of skin tissue are produced only in a few isolated cases and the formation of new vascular structures is reduced for instance by the activity of anti-angiogenic factors like TIMP-3 [119] to maintain a physiological vascular density [120].

### 2.2.2 Bone regeneration

Bone tissue is continuously remodeled to adapt the loading capacity under mechanical load, to maintain its mechanical properties, to repair micro fractures and to regulate the serum calcium ion concentration [121]. Locally and systemically released cytokines and growth factors such as BMPs together with mechanical and electrical signals control the processes of bone remodeling, resorption and formation [122].

Four cell types mainly characterize bone tissue: the bone-building osteoblasts, the bone-resorbing osteoclasts, osteocytes and the bone lining cells, with the latter two belonging to the osteoblast lineage (Fig. 2.6). Osteoclasts derive from haemopoietic stem cells and are related to monocytes and macrophages, while osteoblasts originate from mesenchymal stem cells [31]. The communication between osteoblasts and osteoclasts is especially important during bone remodeling and is coordinated by several key molecules.

90% of all bone cells are osteocytes embedded in the mineralized matrix. They have long dendritic extensions that form a sensory network able to recognize and communicate mechanical stress within the bone. Bone remodeling takes several weeks after bone damage and is conducted by clusters of osteoclasts and osteoblasts building basic multicellular units (BMUs). 1 - 2 million of such active BMUs are present in the human skeleton [123].

The process of bone remodeling is characterized by five sequential phases: activation, resorption, reversal, formation and termination [124]. During the activation phase, initial signals of bone damage (mechanical stress or other signals) are detected by osteocytes and initiate the recruitment of osteoclast precursor cells. Osteoclast precursors require the monocyte/macrophage colony-stimulating factor (M-CSF) and receptor activator of NF- $\kappa$ B ligand (RANKL)-induced stimulation of receptor activator of NF- $\kappa$ B (RANK) to differentiate into active multinucleated osteoclasts. RANKL can be expressed by osteoblasts, stromal cells from the bone marrow and T and B lymphocytes. The natural antagonist of RANKL is osteoprotegerin (OPG), which can be also produced by osteoblasts.

The second phase is characterized by mature osteoclasts that resorb bone by creating a sealing zone with an acidic pH after attachment to the bone. The release of the proteinase cathepsin K leads to collagen degradation, which is mediated by collagen-associated GAGs that are suggested to first bind cathepsin K and thereby facilitate the subsequent hydrolysis of collagen fibers [125]. During the reversal phase, hMSCs and osteoprogenitor cells are recruited to the specific bone site and differentiate into osteoblasts. The remaining undigested demineralized collagen matrix is removed by monocytes and other phagocytic cells, the so-called reversal cells that originated from the osteoblast lineage. Especially the Wnt/ $\beta$ -catenin pathway is crucial for the differentiation into osteoblasts. [124].

During the formation phase osteoblasts secrete an ECM composed of collagen type I and non-collagenous proteins (e.g. osteocalcin, osteonectin and osteopontin), the osteoid, to re-fill the

resorption lacuna. Vitamin D and parathyroid hormone can enhance these processes. During the termination phase, the osteoid is mineralized and the bone remodeling is completed [123]. Some osteoblasts undergo apoptosis, while others terminally differentiate into osteocytes. These cells express factors regulating the phosphate metabolism and are the producers of the Wnt-pathway inhibitor sclerostin. Secretion of sclerostin inhibits osteoblast differentiation and thereby bone formation [126]. At the end of normal bone remodeling, the bone mass and quality prior to damage should be completely restored [123].

### 2.2.3 Factors influencing wound healing

Inflammation, changes and/or aging of fibroblasts in case of chronic wounds, local ischemia, bacterial load as well as the age of the patient and the wound location direct the course of biological processes during wound healing. The influencing factors can be divided into local and systemic ones [111]. An overview of these factors, which can also occur simultaneously, is given in Tab. 2.2, and selected examples will be discussed in the following section.

**Tab. 2.2 Local and systemic factors influencing wound healing.** Adapted from [111,127].

Local factors	Systemic factors
	Age, gender
	Sex hormones
	Psychological stress
Oxygenation, ischemia	Obesity
Infection	Diseases (e.g. diabetes mellitus, hypothyroidism)
Foreign body	Genetic syndromes (e.g. osteogenesis imperfecta)
Edema, raised tissue pressure	Medication
Venous sufficiency	Alcoholism, smoking
	Immunosuppression (e.g. AIDS, cancer, radiation therapy)
	Nutrition

#### Oxygenation

A tissue has to be supplied with oxygen for wound healing and cell metabolism [128]. Sustained hypoxia can reduce the ability of fibroblasts to produce collagen, lower the activity of neutrophils and leukocytes and promote endothelial cell apoptosis, thereby disturbing the ordered wound healing process [127,129].

#### Infection

An ongoing inflammatory reaction caused by a chronic bacterial colonization is another local factor. Both bacteria and their endotoxins can prolong the inflammation phase by stimulating the release of pro-inflammatory cytokines, the cellular phagocytosis and the extensive release of reactive oxygen species and ECM-degrading enzymes like MMPs by activated neutrophils. These proteinases partially degrade both ECM and growth factors and can thereby hinder cell

migration [130,131]. The formation of a bacterial biofilm for example by *Pseudomonas aeruginosa* shields the bacteria from treatment with antibiotics as well as from phagocytosis and alters the natural skin flora. Here especially the type (for example  $\beta$ -hemolytic *streptococci*) and not only the number of pathogens (above  $10^5$  organisms per g tissue defines a high bacterial load) is crucial for the interference with the wound healing progress [127].

### **Age**

Age as systemic factor can influence the course of wound healing. The initial wound healing is temporarily delayed in elderly patients [132]. Experiments with mice show an altered ECM production, inflammatory response, a retarded angiogenesis and epithelization as well as a reduced TGF- $\beta$  and VEGF expression of aged individuals compared to young ones [133,134]. The cutaneous wound healing is disturbed due to the reduced proliferation of aged fibroblasts as well as their decreased sensitivity for growth factors [135]. Furthermore these fibroblasts show a disrupted autophagy decreasing the expression and release of procollagen type I, elastin and HA. Simultaneously MMP-1 expression and activity are increased *in vitro*, which may contribute to an age-dependent rise of skin fragility [136]. In addition the biological and mechanical functions of bone are altered with increasing age due to changes in the bone mineral density, the cross-linking profile of collagen and the bone morphology making it more fragile [137].

### **Diabetes**

Diabetes mellitus is an important systemic factor since according to recent estimates one in eleven adults has diabetes (415 million people worldwide, 56 million people in Europe) [138,139]. Patients with diabetes show often higher levels of ECM-degrading enzymes like MMPs [140]. About 15% of the patients develop diabetic foot ulcers as chronic wounds as consequence of for example a decreased sensitivity of cells for growth factors and reduced local angiogenesis [141]. These wounds are also insufficiently perfused with oxygen, resulting in hypoxia and further delaying wound healing [142]. The function of diabetic fibroblasts is altered, leading to a reduced cell migration and VEGF release, a decreased fibroblast stimulation under hypoxic conditions as well as an increased MMP-9 level [143]. Furthermore, hyperglycemia fosters the development of advanced glycation end-products (AGEs) which may influence the wound healing process as well [111]. Patients with diabetes have a higher risk for fractures often due to a decreased bone quality [144].

## **2.3 Matrix metalloproteinases (MMPs)**

MMPs form a large class of 25 zinc-dependent endopeptidases able to cleave a variety of different substrates (Tab. 2.3) [145]. They are produced by several cell types such as fibroblasts, endothelial cells, neutrophils and macrophages [146]. Besides their action as matrix-degrading enzymes, they are responsible for the release and activation of ECM-bound mediator proteins such as growth factors as well as their activation and for the production of matrix degradation

products that alter the cell response [147]. They are crucial for several biological processes like tissue development, angiogenesis, tissue remodeling and wound healing.

**Tab. 2.3 Overview of matrix substrates and GAG interaction of MMPs.** Adapted from [148,149] with modifications according to [8].

Type	Protease	Matrix substrates	GAG interplay
Collagenases	MMP-1	Native collagen types: III > I > II, VII, X; gelatin; aggrecan; link protein; entactin, tenascin; perlecan	HEP, HS
	MMP-8	Native collagen types: I > II > III, VII, X; gelatin; entactin, tenascin; aggrecan	
	MMP-13	Native collagen types: II > III > I, VII, X; gelatin; entactin; tenascin; aggrecan	
	MMP-18	Native collagen type I, II, III, gelatin	
Gelatinases	MMP-2	Denaturated collagens (gelatin); native collagen types I, IV, V, VII, X, XI; elastin; Fn; laminin-5; aggrecan; brevican; neurocan; decorin; vitronectin	CS, HEP, HS
	MMP-9	Denaturated collagens (gelatin); native collagen types I, IV, V, VII, X, XI; elastin; Fn; laminin; aggrecan; link protein; vitronectin	CS, HS
Membrane-anchored MMPs	MMP-14	Native collagen types I, II, III; gelatin; Fn; vitronectin; aggrecan	
	MMP-15	PG	
	MMP-16	Native collagen type III, Fn	
	MMP-17	Gelatin; fibrin/fibrinogen	
	MMP-24	Fn, PG; gelatin	
	MMP-25	Native collagen type IV; gelatin; Fn; PGs with DS (DSPG); CSPG; laminin-1; fibrin/fibrinogen	
Stromelysins	MMP-3	Aggrecan; laminin; Fn; non-triple helical regions of collagen types II, III, IV, V, IX, X, XI; gelatin; entactin; perlecan; decorin; tenascin; vitronectin; fibrin/fibrinogen; link protein; elastin	
	MMP-10	Gelatin from collagen types I, II, IV, V; Fn, PG	
	MMP-11	Fn; laminin; aggrecan	
Matrilysins	MMP-7	Fn; laminin; non-helical segments of collagen types IV, V, IX, X, XI; gelatin; aggrecan; entactin; tenascin; vitronectin; fibrin/fibrinogen	CS, HS, HEP
	MMP-26	Native collagen type IV; gelatin; Fn; fibrin/fibrinogen	

Type	Protease	Matrix substrates	GAG interplay
Other MMPs	MMP-12	Elastin; Fn; laminin; PG, fibrin/fibrinogen	
	MMP-19	Native collagen type IV; gelatin; laminin; Fn; tenascin; entactin; aggrecan, fibrin/fibrinogen	
	MMP-20	Amelogenin; aggrecan	
	MMP-21	Gelatin	
	MMP-21	No matrix substrate defined	
	MMP-27	No matrix substrate defined	
	MMP-28	No matrix substrate defined; degrades casein	

Depending on their location, they can be distinguished in secreted and membrane-anchored MMPs. Due to their different substrate affinities some of them are designated as collagenases (MMP-1, -8, -13 and -18) and gelatinases (MMP-2 and -9). Collagen type I, II and III degradation is catalyzed by collagenases that cleave the peptide bond between Gly<sup>775</sup> and Leu/Ile<sup>776</sup>, releasing one quarter of the collagen as a fragment [150,151], while the core protein of PGs such as aggrecan can be degraded by ADAMTSs and MMPs [52,152]. The proteolytic activity of MMPs is tightly controlled via their transcription/expression, the activation of zymogens, the inhibition via extracellular inhibitors such as TIMPs or  $\alpha$ 2-macroglobulin as well as via their endocytic up-take and degradation (Fig. 2.8) [153,154]. Furthermore, glycosylation can modulated the enzyme activity as reported for MMP-9 [155].

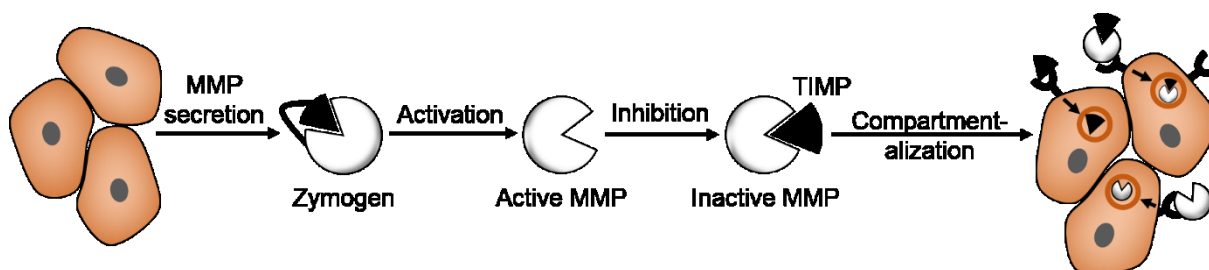


**Fig. 2.8 Mechanisms of MMP activity regulation.**

### Structure

MMPs belong to the metzincins superfamily because they have the characteristic zinc-binding sequence His-Glu-X-X-His-X-X-Gly-X-X-His as well as a methionine forming Met-turn [156]. All MMPs are multidomain enzymes synthesized with a *N*-terminal signal peptide, which is detached in the ER to obtain the zymogen. This contains a propeptide with the conserved sequence Pro-Arg-Cys-Gly-X-Pro-Asp that is responsible for their latency after secretion, the mechanism based on forming a bridge with the catalytic domain containing the respective zinc ion (Fig. 2.9, Fig. 2.10 A). Except MMP-7, -23 and -26, all MMPs have a hemopexin (HPX)-like domain that is connected via a linker (hinge-region) to the catalytic domain. MMP-2 and -9 additionally possess three repeats of a Fn type II like module near the zinc-binding motif in the catalytic domain. The membrane-type MMPs (MT-MMPs) are connected to the cell membrane

either via a type I or type II transmembrane domain or via a glycosylphosphatidylinositol anchor [157].

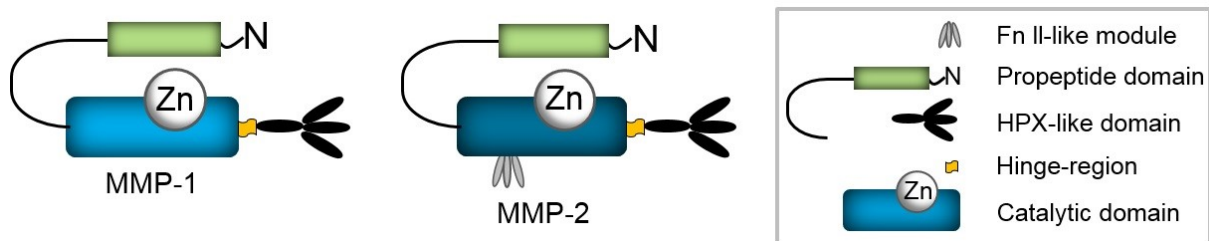


**Fig. 2.9 Multidomain structure of MMP-1 and MMP-2.** Adapted from [157].

### Activation and reaction mechanism

The inactive zymogens are activated stepwise either by the proteolytic removal of the propeptide domain or via chemical agents that disrupt the cysteine-zinc interaction of the cysteine switch. Examples for such chemical activators are thiol-modifying chemicals like 4-aminophenylmercuric acetate (APMA), mercury chloride or sodium dodecyl sulfate (SDS) and reactive oxygen species [158].

For substrate cleavage the carbonyl group of the peptide bond to be cleaved is strongly polarized by its interaction with the zinc ion of the catalytic domain after the formation of an enzyme/substrate complex (Fig. 2.10 B). Afterwards the catalytic glutamate activates the water molecule that is bound to the zinc ion. The activated water molecule reacts with the electrophilic carbonyl carbon leading to the formation of a tetrahedral intermediate complex, which is stabilized by the catalytic zinc. In addition, one proton of the water molecule is transferred by the carboxylate group of the catalytic glutamate to the amino group of the scissile peptide bond. Then the peptide bond is cleaved, a further proton is shuttled to the amino group and both cleavage products are released from the catalytic domain [153].

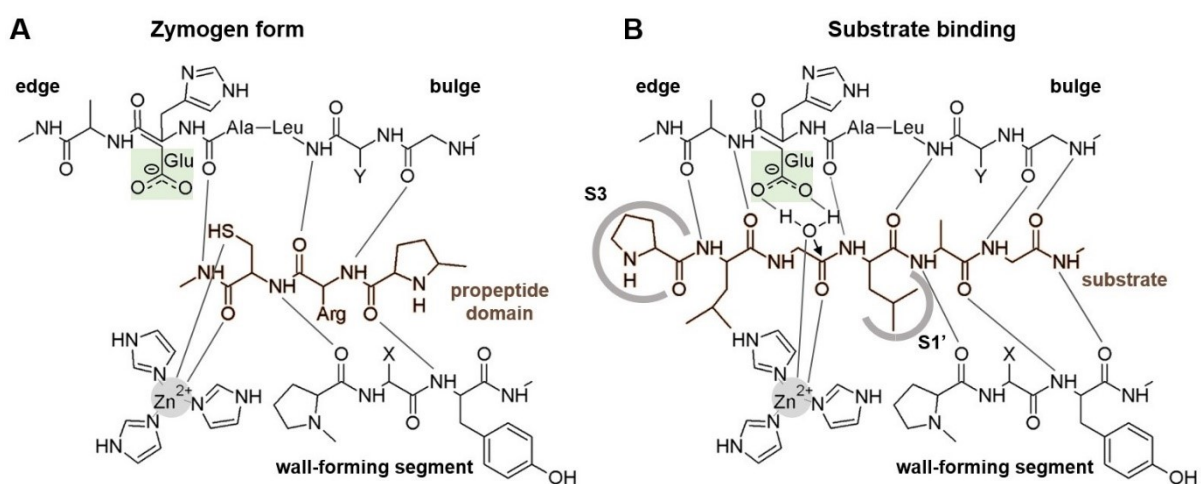


**Fig. 2.10 Interaction of the catalytic domain of MMPs with the propeptide domain and substrates.** Adapted from [153] with modifications. The MMP is displayed in black and the catalytic glutamate is highlighted in green, while the propeptide domain as well as the substrate are shown in brown and substrate binding pockets in gray.



## Functions

MMP activity is crucial for wound healing since it is required for degrading damaged matrix, sloughing out biofilms from bacteria during the inflammation phase and cleaving of the capillary basement membrane to allow vessel sprouting [146,159]. Furthermore, it allows the migration of endothelial cells, epithelial cells and fibroblasts through the matrix during the proliferation phase [160–162]. During the remodeling phase, they contribute to the contraction and remodeling of scar tissue [163,164]. In bone, osteoblasts and osteocytes secrete MMP-2 and -9 to degrade the non-mineralized osteoid for example to facilitate the formation of the osteocyte lacunar-canalicular network [31,165].

MMP-1 is released by a large number of cell types and plays an important role in tissue remodeling [166]. Neutrophil granulocytes are the major producers of MMP-8, explaining its involvement during the inflammation phase of wound healing [167], while MMP-13 is secreted by osteoblasts, osteoclasts as well as hypertrophic chondrocytes [22,168]. The degradation of collagen is an important function of MMPs (MMP-1, -8 and -13). Since the catalytic active site of the MMPs is too small for the triple helical collagen structure, it is assumed that the HPX-like domain contributes to the interaction and facilitates the unwinding and bending of the triple helix, allowing the collagen degradation [169]. Mechanical loading was also reported to influence the enzymatic degradation of collagen tissues by altering the structure of the collagen fibers and thereby their accessibility for proteases [170,171]. The importance of MMPs for tissue homeostasis is highlighted by the fact that an imbalance between MMPs and TIMPs with for instance increased MMP-9 and decreased TIMP-1 levels correlates with a decreased wound healing rate in diabetic foot ulcers [172].

## Interaction of MMPs with GAGs

Several MMPs are reported to bind to HEP columns with different affinities [173,174], however, little is known regarding the interplay of GAGs with MMPs (Tab. 2.3). MMP-1, -2, -7, -9 and -13 are suggested to interact with HS, and proMMP-9 is also known to be covalently bound via disulfide bonds to the core protein of CSPGs [8,175]. This binding of MMPs to GAGs like HS in the ECM may contribute to the localization and regulation of MMP levels by function for example as reservoir for proenzymes [8]. Furthermore, the interaction of GAGs with MMPs can alter the enzyme activity *in vitro* as shown for MMP-1, -7 and -13 by zymography in the presence of HEP [176]. Crabbe et al. measured a relatively weak interaction of HEP with MMP-2 and an increase in MMP-2 activation by APMA in the presence of HEP. According to their proposed model, HEP binding to both the active as well as the latent form of MMP-2 mimics an elevated local enzyme concentration and thereby promotes the initial zymogen activation [177]. In addition, the interaction of GAGs with proMMPs can lead to conformational changes initiating the allosteric activation of the enzyme by disrupting the cysteine-Zn<sup>2+</sup> interaction. The resultant enzyme is transitionally active and can auto-catalyze the cleavage of the propeptide domain [149].

Structurally GAGs are shown to bind to the HEP binding site located at the HPX-like domain of MMP-1, -2 and -9 [178–180]. Since GAGs provide numerous possible interaction sites, they can simultaneously bind an active MMP and its substrate by forming a highly coordinated trimeric complex [181]. For example, Iida et al. demonstrated that CS-A but not HA, HS or CS-C facilitates the proMMP-2 activation by MMP-16, possibly by binding to the C-terminal domain of proMMP-2 and thereby effectively presenting the zymogen to MMP-16 [182]. Further examples of GAG-proteinase interactions are reviewed by Tocchi and Parks and Theocharis et al. [149,181].

## 2.4 Tissue inhibitors of metalloproteinases (TIMPs)

The native counterparts of MMPs are TIMPs, a family with four homologous members (TIMP-1, -2, -3 and -4). TIMP-1, -2 and -3 are widely expressed in many tissues, while TIMP-4 is only present in heart, ovary, kidney, pancreas, colon, testes, adipose and brain tissue [183]. Fibroblasts release TIMP-1 and -3 after stimulation with TGF- $\beta$ 1 [184], osteoblasts and osteocytes express TIMP-1, -2 and -3 during bone formation [165], hMSCs secrete amongst others TIMP-3 [185] and human umbilical vein endothelial cells (HUVECs) produce TIMP-1 [186].

### Structure

TIMPs are wedge-shaped and possess six disulfide bridges. Their *N*-terminal section contains about 120 amino acids and forms a five-stranded  $\beta$ -barrel, while the shorter *C*-terminal section (about 60 amino acids) forms a  $\beta$ -turn [153].

### Functions

An overview on characteristic properties and function of TIMPs is given in Tab. 2.4. As their name indicates, they function as inhibitors of metalloproteinases with a high binding affinity for these proteinases and inhibition constants in the nM range [183]. They form a 1:1 non-covalent complex with the catalytic domain of MMPs via their *N*-terminal part, thereby coordinating the zinc ion of the catalytic site, blocking the substrate access and inhibiting their catalytic activity (Fig. 2.11, compare Fig. 2.10). The first five amino acids of the *N*-terminal TIMP part are essential for the binding to the catalytic site in a quasi-substrate-like fashion [153]. Furthermore, they inhibit ADAM (a disintegrin and metalloprotease) and additionally ADAMTS in case of TIMP-3 [187–189]. All TIMPs are able to bind via hydrophobic/polar interfaces to the HPX-like domain of pro-gelatinases with their *C*-terminal part [190–193].

Their function is strongly controlled by their localization. TIMP-1, -2 and -4 are soluble or bound to cell surface proteins such as MT-MMPs, while TIMP-3 is the only member of the TIMP family that is located in the ECM *in vivo* due to its interaction with native GAGs [7], which will be discussed in the following section. TIMP-1 is further known as a cytokine involved in diseases like cancer [194], while TIMP-3 competes with VEGF-A for the binding to VEGFR-2. This blocks the VEGF-A-mediated activation of endothelial cells required for angiogenesis (section 2.7). Due to its anti-angiogenic effect and the TIMP-3 induced apoptosis in several

cancer cell lines, TIMP-3 functions also as tumor suppressor [119,195]. Furthermore, an enhanced expression of TIMP-3 is beneficial for reducing the late failure of vein grafts *in vivo* [196]. Reduced TIMP-3 tissue concentrations were described for several pathological situations such as diabetic foot ulcerations, atherosclerosis and osteoarthritis [197–199].

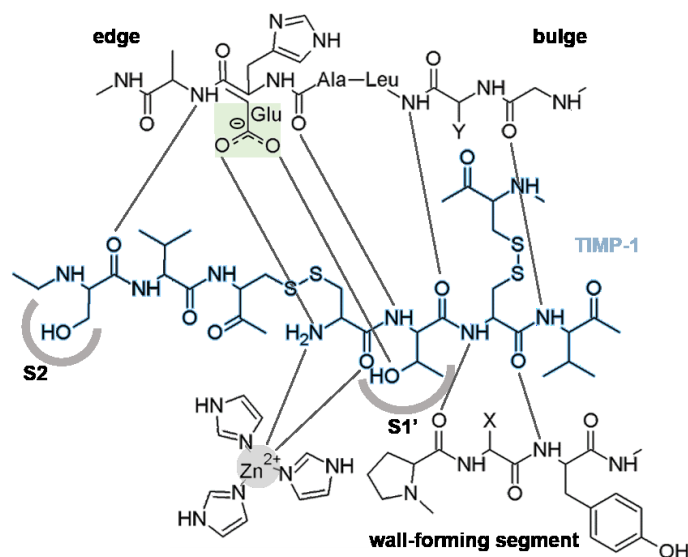


**Fig. 2.11 Interaction of the catalytic domain of MMPs with their inhibitor TIMP-1.** Adapted from [153,183] with modifications. The MMP is shown in black and the catalytic glutamate is highlighted in green, while TIMP-1 is displayed in blue and substrate binding pockets in gray.

**Tab. 2.4 Characteristics and functions of TIMPs.** Adapted from [183,200] with modifications according to [201]. The asterisk (\*) indicates the glycosylated form of TIMP-3.

Property	TIMP-1	TIMP-2	TIMP-3	TIMP-4
Mw (kDa)	28	22	22 or 27*	22
Amino acids	184	194	188	194
Isoelectric point	8.5	6.5	9.1	7.2
Localization	Solute, cell surface-bound	Solute, cell surface-bound	ECM and cell surface-bound	Solute, cell surface-bound
Interaction with cell surface receptors	$\beta$ 1 integrin, CD63, LRP-1	$\alpha$ 3 $\beta$ 1 integrin, LRP-1	VEGFR-2, LRP-1, Angiotensin- IIR, EFEMP1	
ADAM inhibition	ADAM-10	ADAM-12	ADAM-10/-12/ -17/-19/-33	ADAM-17/-28
ADAMTS inhibition			ADAMTS-1/- 2/-4/-5	
proMMP binding	proMMP-9	proMMP-2	proMMP-2/-9	proMMP-2
MMP inhibition	All	All	All	Most
MT-MMP inhibition	Weak	Yes	Yes	Yes

### **Interaction of TIMP-3 with GAGs**

TIMP-3 is unique since it binds to HSPGs and further sulfated PGs within the ECM mainly due to electrostatic interaction of the positively charged regions present in the *N*- and *C*-terminal domain of TIMP-3 with the negatively charged GAG chains [7,202]. Thus TIMP-3 is suggested to be a main modulator of tissue homeostasis. Recently, Troeberg et al. determined  $K_D$  values in the range of 10 - 39 nM for the binding of TIMP-3 to immobilized HS and CS-E. Interestingly, they could show that this TIMP-3 interplay with GAGs is able to reduce the TIMP-3 up-take via the endocytic receptor LRP-1 in HTB94 chondrosarcoma cells *in vitro*. They also showed that GAG stabilize TIMP-3/ADAMTS-5 complexes as indicated by a decreased dissociation rate [10]. Surface plasmon resonance (SPR) analysis demonstrated the direct binding of TIMP-3 to HEP surfaces with an affinity ( $K_D$  of about 59 nM) almost comparable to those of HS and CS-E [203]. However, as native GAGs were used in these studies that are not fully characterized (e.g. regarding their sulfation pattern), an in-depth analysis of the structure-function relationship of GAGs on their interaction with TIMP-3 is still missing.

## **2.5 Regulation of ECM remodeling**

ECM remodeling is required for maintaining and restoring the physiological properties of a tissue. During development and normal wound healing, matrix degradation is required for example for vessel sprouting during angiogenesis and for the release of matrix-bound growth factors [204]. A disruption of this ordered process and a resulting dysregulation of the ECM structure, stiffness, abundance and composition often lead to the manifestation of pathologic conditions such as fibrosis, osteoarthritis and cancer [205]. An overview on different aspects of ECM remodeling in skin and bone is displayed in Fig. 2.12. Since MMPs and TIMPs are crucial regulators of the ECM proteolysis, their activities and tissue levels have to be strictly controlled [206,207].

### **Increased ECM deposition**

Even though the activation of fibroblasts via the response of TGF- $\beta$ 1 is mandatory during wound healing to reconstitute the dermal ECM, an excessive production of collagen by fibroblasts and deposition of further ECM components together with a decreased protease activity leads the formation of fibrosis and scars [96]. Fibrosis is a result of an chronic infection and characterized by a hardened, overgrown and/or scarred tissue [210]. Since excessive levels of growth factors like TGF- $\beta$ 1 can promote the formation of keloids and hypertrophic scars [113], these proteins are major targets in the development of new treatment strategies against fibrosis [211].

### **Excessive ECM breakdown**

The extensive degradation of matrix components plays an important role in the progression of several diseases. The abnormal destruction of cartilage ECM during osteoarthritis is caused to

some extent by an overexpression of ADAMTS-4 and -5, leading to an increased aggrecan degradation [212].

Osteoporosis is a disease that is characterized by decreased bone mass and stability leading to a high risk for fractures [126]. Postmenopausal osteoporosis (or type I osteoporosis) occurs as result of the estrogen deficiency starting at menopause, which increases bone resorption. The age-related type II osteoporosis is present in both men and women and characterized by a reduced bone formation as well as an accelerated bone resorption [123]. Bisphosphonates are established to treat osteoporosis, however, since they not only block the matrix resorption via osteoclasts but also induce their apoptosis, they strongly disrupt the essential paracrine signaling between osteoclasts and osteoblasts. Nowadays novel strategies for the treatment of this disease mainly focus on the development of compounds with anti-resorptive and uncoupling effects [126].

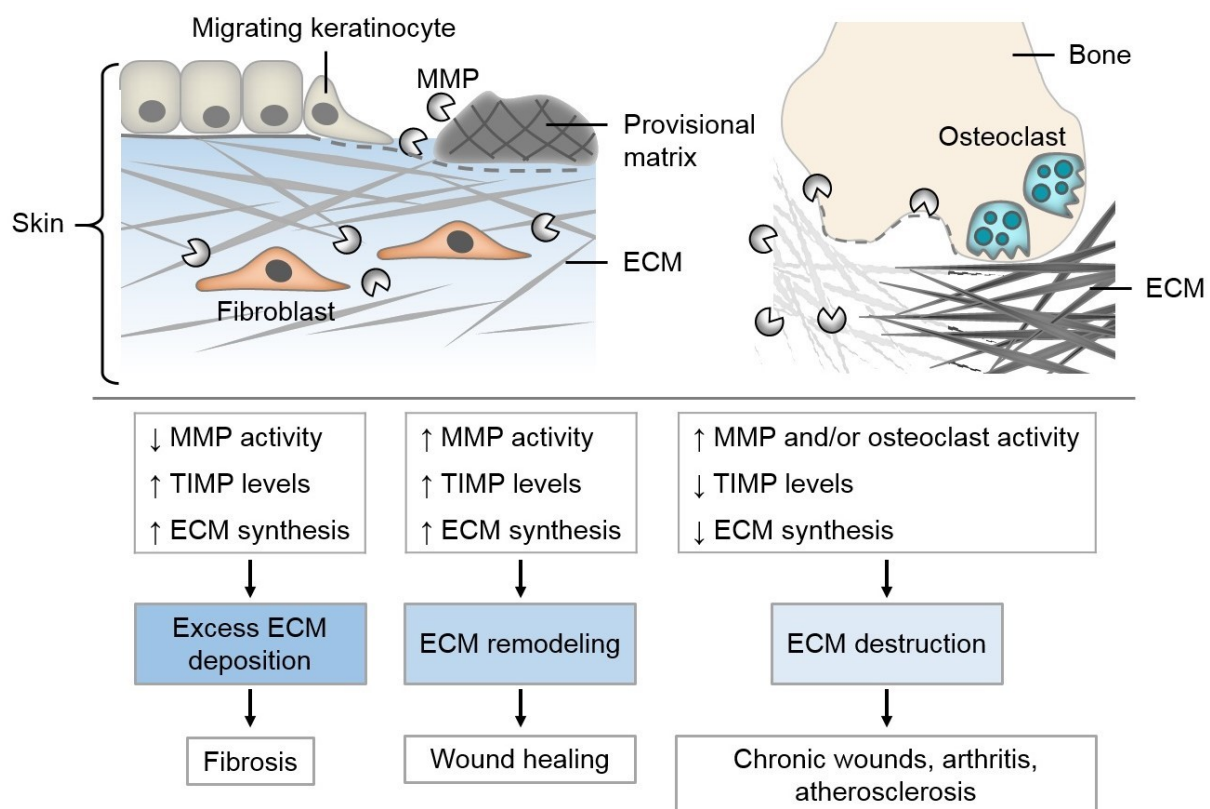


**Fig. 2.12 Physiologic and pathologic ECM remodeling of skin and bone tissue.** Adapted from [208,209] with modifications.

Chronic wounds like vascular ulcers and diabetic ulcers are further examples for pathologic conditions characterized by an altered phenotype and activity of some cells as well as an excessive ECM degradation due to increased MMP expression [213,214]. The wound healing process is disrupted, the inflammation phase is usually extended and the re-epithelization fails as a consequence of for instance the limited migration of keratinocytes and response of fibroblast to TGF- $\beta$ 1 [215–217]. The delayed wound healing is the consequence of an increased inflammatory response due to factors like a high load of bacterial toxins and proteases. They

initiate an increased release of cytokines and free radicals that induce the cells to produce an excess of proteases. This leads to an imbalance between proteinases like MMPs and their inhibitors TIMPs, resulting in the further damage of tissue through degradation of matrix components and mediator proteins such as growth factors, thus fostering a continuous inflammation [146].

## **2.6 Low-density lipoprotein receptor-related protein-1 (LRP-1)**

The low-density lipoprotein (LDL) receptor-related protein-1 (LRP-1) is a multifunctional endocytic receptor expressed by several cell types like osteoblasts, hMSCs, vascular smooth muscle cells, adipocytes, endothelial cells and macrophages [218]. It is reported to be involved in a variety of different biological processes such as the up-take and degradation of proteases and their inhibitors, the lipoprotein metabolism, integrin function as well as the cellular entrance of viruses and bacterial toxins [219]. Up to now more than forty structurally non-related LRP-1 ligands are known, highlighting its fundamental role in physiology. Besides its function as endocytic receptor, recent studies revealed that it also acts as a modulator in signaling pathways as for PDGF [220].

### **Structure**

LRP-1 consists of a 515 kDa alpha-chain with a modular structure containing cysteine-rich  $\text{Ca}^{2+}$ -binding complement-like domains (CR) organized as clusters,  $\beta$ -propeller domains, EGF repeats, and a 85 kDa beta-chain with a transmembrane and a cytoplasmic domain (Fig. 2.13). LRP-1 has four clusters designated as cluster I, II, III and IV. They contain the 2, 8, 10 and 11 CR domains responsible for ligand binding, respectively. Cluster II and IV interact with most of the ligands, while only the chaperone receptor associated protein (RAP) is reported to interact with cluster I and III [218]. By binding tightly to multiple LRP-1 ligand-binding sites, RAP hinders the LRP-1 interaction with other ligands in the ER, thereby facilitating receptor delivery through the intracellular space to the cell membrane. Modeling predicted that Tyr-Trp-Thr-Asp repeats appear as  $\beta$ -propeller domains [221]. These domains are bound to repeats with a homology with the EGF precursor. The EGF and  $\beta$ -propeller domains are required for ligand release under low pH conditions in the endosomal compartments [222,223]. The  $\beta$ -propeller domain can act as a LRP-1 ligand by binding to CR4 and CR5, possibly facilitating the release of other ligands [224]. However, due to the large size of this receptor there is no experimental structure of the entire receptor available up to now.

### **Functions**

LRP-1 is consecutively active and mediates up to 100 ligand internalization steps within 20 hours [225]. The high affinity of LRP-1 for numerous different ligands is due to 31 CR domains. They create a characteristic surface profile and charge distribution. This allows several interplays between the LRP-1 receptor and the ligands, including a sequential binding of the ligand to different combinations of CR domains as well as an interaction with single clusters [218].

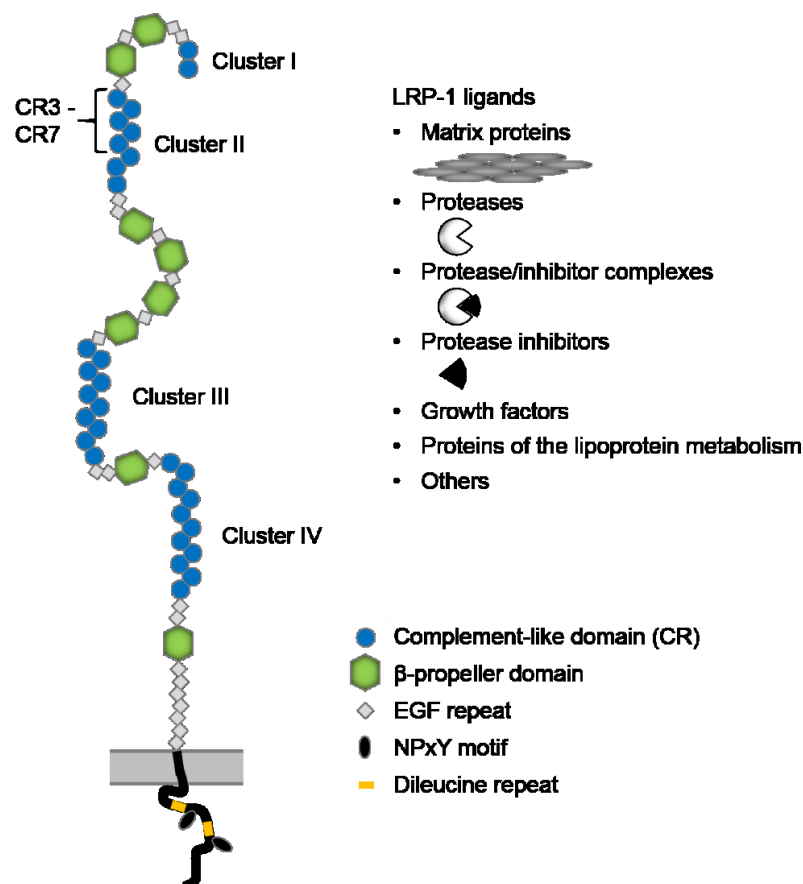


**Fig. 2.13 Structure of LRP-1 and overview of LRP-1 ligands.** Adapted from [219].

Neels et al. described that the regions CR3 to CR7 of cluster II are of special importance for the ligand/receptor interplay [226]. CR7 and CR8 are also required for the binding of RAP to both repeats [227,228]. After ligand binding to the receptor the ligand/receptor complex is internalized. In the endosome, the ligands dissociate from LRP-1, the receptor is recycled and transported to the plasma membrane where a new cycle can start.

The high number of different ligands results in a multitude of LRP-1 functions, which are reviewed in [218,219]. Due to its structural similarity to other LDL receptors, one of the roles identified for LRP-1 was its involvement in the lipoprotein metabolism [229]. The clearance of chylomicron remnants lipoprotein particles that remain after the removal of triglycerides from intestinal chylomicrons by the enzyme lipoprotein lipase is mediated by the binding of apolipoprotein E (apo E) to LRP-1 and other LDL receptors as well as to HSPG [230]. LRP-1 is able to inhibit the canonical Wnt-3a signaling pathway by sequestering the receptor Frizzled-1 and thereby blocking the receptor/coreceptor complex formation between Frizzled-1 and LRP-5/-6, which is required for Wnt induced bone formation and remodeling [231].

Another important function of LRP-1 is the regulation of extracellular proteinase and proteinase inhibitor levels, thereby controlling ECM proteolysis and homeostasis [232,233]. Some proteinases like ADAMTS-4, -5 and MMP-9 bind directly to LRP-1, while others such as MMP-13 require the prior binding to specific co-receptors or the formation of a proteinase/inhibitor complex (e.g. MMP-2) before internalization via LRP-1 [234–237]. Recent

studies revealed that LRP-1 also mediates the up-take and degradation of TIMP-3 [238], however, the distinct protein binding sites involved in this interaction are still unidentified.

### Interplay with GAGs

LRP-1 is responsible for the endocytosis of the PG decorin via its direct binding to the receptor clusters II and IV. Since the protein core or CS alone were less efficient in inhibiting cellular decorin up-take compared to a combination of both, the authors suggested a participation of the GAG chain and the proteoglycan protein core in this process. They proposed that LRP-1 may also be responsible for the up-take of the related PG biglycan [239]. Interestingly, several LRP-1 ligands are known to interact with GAGs, suggesting a potential modulatory function of GAG binding on LRP-1 mediated endocytosis and signaling. Examples of such LRP-1 ligands are displayed in Tab. 2.5.

**Tab. 2.5 Selected LRP-1 ligands known to interaction with GAGs.**

LRP-1 ligand	Interaction with LRP-1	Interaction with GAGs
ADAMTS-4	$K_D$ of 51 nM for the ectodomain, $K_D$ of 98 nM for cluster II, $K_D$ of 73 nM for cluster IV [234]	HEP [240]
ADAMTS-5	$K_D$ of 3.8 nM of ADAMTS-5 w/o TS2 domain for the ectodomain, $K_D$ of 3.5 nM for cluster II, $K_D$ of 9 nM for cluster IV [234]	CS [241], $K_D$ of 10 nM for HEP [10]
ApoE	$K_D$ of 1.1 - 1.6 nM for LRP-1 [242]	HSPG, $K_D$ of 0.022 $\mu$ M for HEP [243]
Fn	Direct or sequential binding to other cell-surface sites and LRP-1 suggested [244]	HEP [37], low-sulfated HA (sHA1) [245]
MMP-13	Endocytosis by LRP-1 together with a MMP-13 specific receptor [236]	$K_D$ of 34 nM for HEP [246]
MMP-2	As MMP-2/thrombospondin-2 complex [237], As proMMP-2/TIMP-2 complex with a $K_D$ of $7 \times 10^{-8}$ M for LRP-1 [232]	$K_D$ of 61.7 nM for HEP [247]
MMP-9	$K_D$ of 53 nM for LRP-1 [235]	CSPG [175], HEP [8]
TGF- $\beta$ 1	$K_D$ of 50 - 400 pM for LRP-1 [248,249]	HS, HEP [250–252], sulfated HA (sHA) derivatives [253]
Thrombospondin-1	$K_D$ of 5 nM for LRP-1 [254]	$K_D$ of 41 nM for HEP, $K_D$ of 487 nM for cartilage CS [255]
TIMP-3	$K_D$ of 28 nM for the ectodomain [10]	$K_D$ of 29 nM for HS, $K_D$ of 10-39 nM for CS-E [10], $K_D$ of 59 nM for HEP [203]



The ability of thrombospondin-1 to interact with HEP and its fibroblast-mediated endocytosis was shown to be strongly reduced for a truncated recombinant protein. The authors suggested that HEP-binding was important for subsequent endocytosis of this protein [256]. However, HEP did not affect the binding of protease inhibitor  $\alpha_2$ -macroglobulin to LRP-1 *in vitro* [249], which correlates with the fact that  $\alpha_2$ -macroglobulin did not interact with HEP [257]. HEP can reduce the binding of ADAMTS-4, ADAMTS-5 and TIMP-3 to LRP-1, and decrease their endocytosis, possibly by masking LRP-1 binding sites of the enzymes [240,241,258]. It still remains to be studied if GAGs altering LRP-1 mediated protein endocytosis is a general mechanism, and what structural requirements GAGs would have to fulfill to interfere with these interactions.

## 2.7 Angiogenesis

Angiogenesis describes the sprouting from pre-existing vessels to form a network that is subsequently remodeled into arteries and veins [259], while vasculogenesis is the assembly and differentiation of angioblasts into endothelial cells to build a vascular system [260]. Only a small number of tissues like cartilage contain no blood vessels; the majority of tissue types is vascularized [261]. Endothelial cells represent one of the main cells of blood vessels and, form a barrier that separates the blood from the surrounding tissue [262]. Matrix degradation, cell migration and proliferation as well as morphogenesis are crucial functions of endothelial cells during angiogenesis as shown in Fig. 2.14 [204]. Endothelial cells must assemble into vessel tubes, then build a new capillary lumen and synthesize a new basement membrane, which is afterwards supported by recruited pericytes and smooth muscle cells [263,264]. The characteristics and functions of endothelial cells differ with respect to the tissue and size of the vessel; for example the expression of growth factor receptors vary between arterial and venous endothelial cells [265–267].

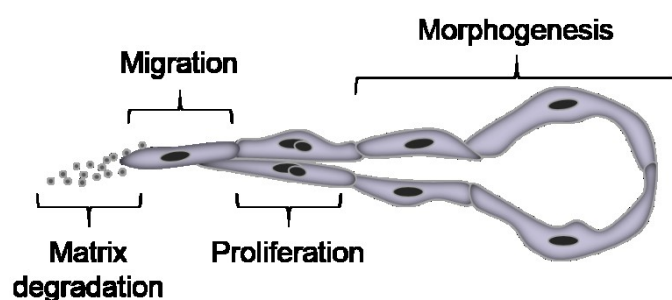


**Fig. 2.14 Activities of endothelial cells during angiogenesis.** Adapted from [204].

The ECM as a 3D cell environment is crucial for angiogenesis since it contains a number of stimulatory and inhibitory angiogenesis factors [268,269]. In particular the spatial localization of angiogenesis regulating signals in the ECM is critical for the formation of new vascular structures [270]. Angiogenesis is also crucial for wound healing; for instance, it delivers the osteogenic precursors as well as osteoblast and osteoclast activity modulating mediator proteins required for bone remodeling. In bone, angiogenesis and osteogenesis are found to be directly

coupled [122,271], and osteoblasts, osteoclasts and osteocytes are reported to release angiogenic factors like EGF and VEGF-A [272]. Abnormal angiogenesis is associated with several diseases and pathological conditions such as chronic wounds and cancer [273]. The role and function of VEGF and their receptors will be discussed in detail in the following section.

### **2.7.1 Vascular endothelial growth factor (VEGF) signaling**

Five genes of the human genome encode the information for the five members of the VEGF family: VEGF-A (often designated as VEGF), -B, -C, -D and placenta growth factor (PlGF). All VEGF family members are homodimers consisting of two subunits with about 120 - 200 amino acids. VEGF-A is the most important molecule controlling endothelial cell activity and thereby blood-vessel morphology [274,275]. It is required for the migration and differentiation of angioblasts, the mesoderm-derived endothelial precursor cells [276]. The alternative splicing of VEGF-A pre-mRNA results in eight different isoforms, which are termed VEGF<sub>111</sub>, VEGF<sub>121</sub>, VEGF<sub>145</sub>, VEGF<sub>148</sub>, VEGF<sub>165</sub>, VEGF<sub>183</sub>, VEGF<sub>189</sub> and VEGF<sub>206</sub> in accordance with their number of amino acids [277,278]. VEGF<sub>165</sub> is the major isoform of VEGF-A and partially bound to the ECM and the cell surface, while VEGF<sub>121</sub> diffuses freely in the extracellular space since it is the only isoform without HEP binding properties [279]. VEGF<sub>189</sub> and VEGF<sub>206</sub> are mainly ECM-bound due to their high affinity for HEP [280].

#### **VEGF receptors**

An overview on the different VEGF forms and their receptors is given in Fig. 2.15. VEGF-A interacts with the two specific receptor tyrosine kinases VEGFR-1 (also termed Flt-1) and VEGFR-2 (or kinase insert domain receptor (KDR)). VEGF-B and PlGF exclusively bind to VEGFR-1, while VEGF-C and VEGF-D have their highest affinity for VEGFR-3 and a lower for VEGFR-2 [281].

The soluble form of VEGFR-1 (sVEGFR-1) can act as VEGF-A inhibitor and plays a role in regulating the placenta [275]. VEGF-B and PlGF influence the function of cardiac vasculature and play only a secondary role for angiogenesis [282,283]. VEGF-C and -D are mainly involved in lymphangiogenesis [284]. The importance of VEGF-A was especially obvious in VEGF-A (+/-) mice lacking one VEGF-A allele, as this resulted in embryonic lethality due to diminished blood-island formation and angiogenesis [285,286]. Hence, the following sections will focus on VEGF-A and its role in angiogenesis.

VEGFR-1 and -2 are mostly expressed on endothelial cells. Both consists of an extracellular domain that binds the ligand and contains seven immunoglobulin-like domains, a transmembrane region, a tyrosine kinase sequence with a kinase-insert domain and a downstream carboxy terminal region [274,287]. The affinity of VEGF-A to VEGFR-1 ( $K_D \approx 10$  pM) is much higher than for VEGFR-2 ( $K_D$  of 75 - 760 pM) [287,288]. However, VEGFR-2 functions as a major signal transducer with a high kinase activity, while VEGFR-1 exhibits only a weak tyrosine kinase activity and acts mainly as a negative regulator of angiogenesis [289].

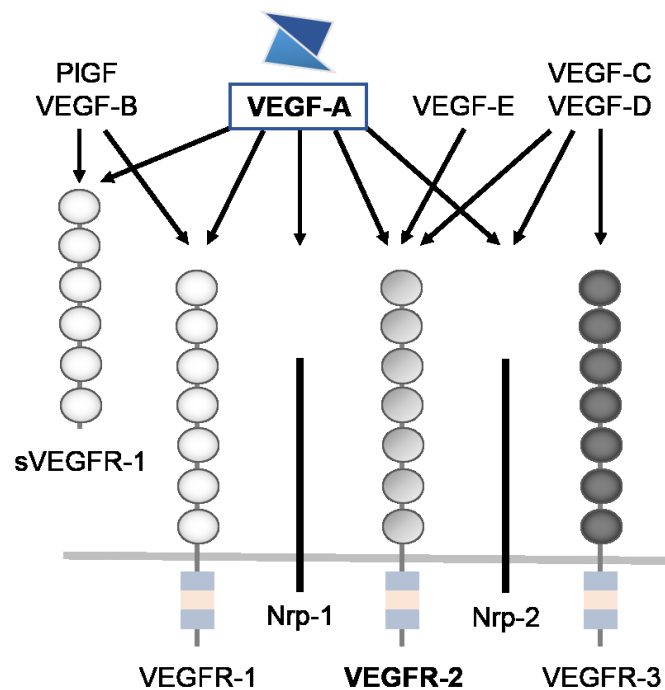


**Fig. 2.15 Overview on the VEGF-VEGFR system.** Adapted from [275,281].

The binding of VEGF-A to VEGFR-1 occurs at the second immunoglobulin-like domain, that to VEGFR-2 at the second and third. The following immunoglobulin-like domains are required for the dimerization and activation of the receptors [290]. VEGFR-2 kinase activation is initiated by the interaction of the VEGF-A dimer with two monomeric receptors that stimulates receptor dimerization. Afterwards, several tyrosines (e.g. residue 951, 1054, 1059, 1175 and 1214) in the kinase-insert domain and the carboxy terminal region of VEGFR-2 are autophosphorylated for signal transduction [291,292].

Neuropilin Nrp-1 and Nrp-2 are co-receptors of VEGF-A (except VEGF<sub>121</sub>). Since Nrp-1 is reported to increase the binding of VEGF<sub>165</sub> to VEGFR-2, it is suggested that the presentation of VEGF<sub>165</sub> to VEGFR-2 by Nrp-1 results in an improved VEGF-A/VEGFR-2 complex formation [293].

Since VEGF, VEGFR-1 and -2 are involved in several diseases such as tumor angiogenesis and chronic inflammation, inhibitors of the VEGF signal like anti-VEGF antibodies (e.g. Bevacizumab, Ranibizumab) have been developed for anti-angiogenic therapies [281,294].

### 2.7.2 TIMP-3 as regulator of VEGF-A activity

Since 2003 it is known that TIMP-3 acts as an inhibitor of angiogenesis. This function is independent of its inhibitory function on proteinases. TIMP-3 binds to VEGFR-2 and blocks the receptor's interaction with VEGF-A and subsequent downstream signaling [119]. Structurally, mainly the C-terminal domain of TIMP-3 is involved in the interaction with VEGFR-2. Furthermore, TIMP-3 inhibits the VEGF-induced actin reorganization in endothelial cells [295]. *In vivo* studies on mice lacking TIMP-3 demonstrated the importance of TIMP-3 as

inhibitor of VEGF-A-mediated signaling since these mice exhibited a pathologic neovascularization e.g. in the cornea [296]. TIMP-3 can also inhibit tumor growth in mice by down-regulating the tumor-induced neovascularization [119].

### 2.7.3 Role of GAGs in VEGF-A signaling

The different isoforms of VEGF-A vary in their affinity for HEP and HSPG (Tab. 2.6). These differences are based on the alternative mRNA splicing, which leads to changes in the amino acids sequences responsible for the HEP binding encoded on exon 6 and 7 [297]. Interestingly, the HS binding site of VEGF-A<sub>165</sub> contains only four basic residues (Arg123, Arg124, Arg156, Arg159), which are sufficient for a high GAG binding affinity [298].

**Tab. 2.6 Binding affinities of selected VEGF-A isoforms for HEP and HS.**

VEGF-A isoform	Affinity for HEP	Affinity for HS
VEGF <sub>145</sub>	-	K <sub>D</sub> of 50 - 94 nM [299]
VEGF <sub>165</sub>	K <sub>D</sub> of 22 - 42 nM [300]	K <sub>D</sub> of 20 μM [300]
VEGF <sub>189</sub>	-	K <sub>D</sub> of 0.1 - 8.8 nM [300]

In this context, it is well established that the balance between HSPG-bound VEGF-A and its freely diffusible form results in the formation of a VEGF-A gradient that is crucial to direct angiogenesis [301]. 50 - 70% of VEGF<sub>165</sub> for example are associated to HSPGs at the cell membrane and within the ECM, while the remaining 30 - 50% are solute. By sequestering VEGF-A, HSPGs may protect the protein from enzymatic degradation, and HEP binding to VEGF<sub>165</sub> can prolong its biological activity by partially protecting the growth factor against e.g. free radicals, which could be present during the inflammation phase of wound healing [280,302]. The binding of VEGF-A to HSPGs in the matrix can also lead to the release of previously HSPG-bound growth factors like basic fibroblast growth factor (bFGF), which can further stimulate angiogenesis [303]. Cell surface-bound HSPGs are reported to function as co-receptors for VEGF-A-mediated signaling [304], meaning HS may have a bridging function between VEGF-A and neuropilin [305]. Glypican-1 as a HSPG present on endothelial cells is reported to exhibit a chaperone-like function that can restore the receptor binding of VEGF-A<sub>165</sub> after damage by oxidation [306].

In general the modulating functions of HEP/HS are receptor type as well as VEGF isoform dependent [307]. However, there are conflicting reports on the effect of GAGs on the activity of VEGF-A. Ashikari-Hada et al. found an enhanced proliferation and increased tube formation of HUVECs in the presence of HEP and VEGF<sub>165</sub> compared to control cells stimulated with only HEP or VEGF<sub>165</sub>. This was not the case in the presence of 2-*O*- or 6-*O*-desulfated HEP [308], which indicates that especially the GAG structure and sulfation determine their modulatory function on the VEGF-A activity. 0.1 - 10 μg/ml HEP was reported to enhance the binding of VEGF<sub>165</sub> to its receptors, while higher concentrations showed the opposite effect

[309]. Furthermore, the interaction of VEGF<sub>121</sub> and VEGF<sub>165</sub> with VEGFR-1 can be inhibited by 1 µg/ml solute HEP [310,311]. As the findings about the effect of GAGs on VEGF-A signaling are partially contradictory, an in-depth analysis of the underlying modes of actions is required to assess whether GAGs and especially GAG derivatives could be used to modulate this growth factor signaling process and thereby potentially the activation of endothelial cells and angiogenesis.

## **2.8 Biomaterials for bone and skin regeneration**

As a consequence of a prolonged life expectancy the incidence of bone fractures in the aging population due to bone defects and osteoporosis increases. This leads to a growing need for biomaterials able to improve bone regeneration, particularly in health-compromised patients with impaired wound healing capacities. According to recent estimates up to 5 - 20% of the four-million operations involving endoprosthetics per year are accompanied by implant failure, delayed healing and complications. Furthermore, malignant diseases and comminuted fractures also lead to bone defects, which often require the treatment with biomaterials [312].

As a further example of vascularized tissue, skin can be damaged and lost as a consequence of acute trauma after burns and chronic wounds. This can even lead to death of the patients, especially in the case of not successfully treated large, deep wounds [313]. It should be noted that all full-thickness skin injuries with a diameter above 1 cm are not able to epithelialize and show an abnormal wound healing with extensive scarring. This often results in cosmetic deformations and a limited flexibility and mobility. That is why, these wounds require skin grafting [314].

Autologous bone or skin (epidermis, dermis) are the gold standard for bone or skin replacement, but its availability is limited and the harvesting causes pain and creates a further wound. As the implant incorporation into bone tissue and the wound healing process in general depend on the patient-specific healing potential of the respective tissue as well as the properties of the biomaterial, new strategies to improve tissue regeneration are required [315,316]. Here especially the field of tissue engineering is promising since it aims to regenerate instead of replace damaged connective tissues or organs. To achieve this, cells and scaffold biomaterials are combined to function as biological substitutes that restore, maintain or improve the functions of the respective tissue [317]. The following sections will focus on functional requirements for biomaterials and will describe selected examples that are of special interest for the design of functional biomimetic materials.

### **2.8.1 Design criteria for biomaterials**

Independent of tissue type several requirements have to be considered when designing biomaterials for regenerative medicine:

- (i) Non-toxicity and biocompatibility: The biomaterial should neither contain nor release toxic compounds (e.g. products of corrosion or degradation, or contaminants of the main constituents of the biomaterial). The ability to perform with an appropriate host response in a specific application is defined as biocompatibility (Consensus Conference of the European Society for Biomaterials, Chester, 1986) [318]. The materials should have a surface chemistry suitable for cell attachment, proliferation and differentiation. In case of porous 3D scaffolds, especially the pore size and their interconnectivity are important to allow cell growth and the transport of nutrients and metabolic waste within the scaffold [319].
- (ii) Mechanical properties: Ideally, the mechanical properties should match those of the respective target tissue [319]. For example, it was shown that by adjusting the matrix elasticity the stem cell differentiation can be directed into specific lineages [320]. In case of bone, however, there is currently no material available that mimics all mechanical properties.
- (iii) Biodegradability or chemical stability: The degradation time should be controllable since it is advantageous to have a material that initially provides support for cells, but is later replaced by the ECM produced by the cells. Since biodegradable scaffolds are not permanent, long-term complications associated with the biomaterial are avoided [321]. In general, the biodegradation should be proportional to the formation of new matrix, matching tissue growth *in vivo* [322]. In contrast, non-degradable materials in bone applications like total joint replacement prostheses should be chemically stable over time since these materials have to stay in the body to provide the required mechanical stability. However, such materials do not allow complete regeneration because they cannot be replaced by newly formed tissue [318].
- (iv) Specific interaction: Materials exhibiting specific interaction profiles depending on their application are desirable. Preferably, a bioactive material should effect the surrounding biological system in a defined manner to promote healing processes. Examples for such possible bioactive compounds, which can be included in biomaterials are growth factors, native GAGs and GAG derivatives [323,324].
- (v) Manufacturing technology: In the end the ability to manufacture the biomaterial with well-defined, reproducible properties is mandatory for a successful translation into clinical practice. The manufacturing process should be scalable and has to fulfill the criteria of good manufacturing practice (GMP) [325].
- (vi) Sterilizability: The material should be sterilizable to avoid contaminations with microorganisms (e.g. with bacteria) as these can lead to infections and/or ultimately implant or biomaterial rejection. Even though the standard is  $\gamma$ -irradiation with 25 kGray, not all materials are resistant against this. If no usual sterilization method (e.g. reduced dose of  $\gamma$ -irradiation, ethylene oxide) is suitable, the whole manufacturing process needs to be aseptic and sterile which increases the costs and investment for production [326].

### 2.8.2 Artificial extracellular matrices (aECMs)

An aECM is defined as matrix that contains isolated major components of the native ECM such as fibrillary collagen or Fn that have been re-formed using *in vitro* techniques. The aim is to obtain a cellular microenvironment that resembles parts of the ECM and is able to induce a specific host response [18]. Numerous strategies are established to mimic distinct properties and/or functions of the native ECM. To develop biomimetic materials the use of synthetic polymers especially in combination with natural ECM components is a promising approach. Collagen, gelatin and HA are examples of classically used biopolymers for wound healing applications [18,327,328]. Although nearly 30 types of collagen exist, the main focus is on the fibrillar collagen types I and III. Collagen-based biomaterials can be used for clotting, hemostasis, platelet aggregation and thrombocyte adhesion and activation. They are usually characterized by a sufficient mechanical strength and the required collagen is commonly extracted from bovine or porcine skin and tendons. Since the protein structure is highly conserved between these species and human, collagen has a low immunogenicity [329]. A composite of porcine collagens type I and III which is already used in the clinics for soft tissue augmentation is Mucograft® [330]. Comparably new is a study of worm and spider silk and resilin as natural polymers for biomaterials [331,332].

Examples for synthetic polymers used alone or in combination with ECM components like collagen and hydroxyapatite are degradable poly( $\alpha$ -hydroxy acids) such as poly(lactic acid) (PLA) and copolymers such as poly(lactic-co-glycolic acid) (PLGA) [333–336]. PLA is of particular interest since it is biodegradable via hydrolysis within months, has good mechanical properties, can be processed using thermoplastic procedures and is eco-friendly. This explains its use in biodegradable surgical implant material and sutures, drug delivery systems and porous scaffolds for the growth of new tissue [337].

### 2.8.3 GAG derivatives

Sulfated GAGs are important functional components of the native bone and skin ECM (section 2.1.2) offering a promising potential to functionalize biomaterials. The usage of isolated GAG chains instead of PGs is advantageous in this respect as it excludes the risk of an immunological response against the protein core of the PG. Even though native GAGs are known for their diverse modulatory function through direct or indirect interaction with cells, their usefulness in analyzing the structure/function relationship of GAGs with mediator proteins such as growth factors is limited. This is due to the often significant batch-to-batch variability and the high structural variations regarding sulfation degree and pattern as well as their carbohydrate backbone. Furthermore, their broad clinical application is restricted because of their high costs and limited availability, which was especially obvious during the HEP crisis [77]. And there are additional drawbacks of animal-derived GAGs: for example, patients sensitive against poultry can show an antigen response against HA from rooster comb. Moreover, animal-derived

GAGs could potentially contain unwanted agents (e.g. viruses in HEP from pigs or prions in CS samples from cattle) and contribute to the endangerment of distinct species like sharks as source for CS. Against this background, there are several strategies to replace animal-derived GAGs such as the GAG production via fermentation that is already established for HA [61] as well as the chemical and chemoenzymatical synthesis of GAG analogs based on mono- or oligosaccharide residues [338,339]. A semi-synthetic over-sulfated CS was first synthesized by Maruyama et al. in 1998 [340].

Fondaparinux (Arixtra®) was developed as antithrombotic agent, which mimics the AT-III binding site of HEP (Fig. 2.16). It is a pentasaccharide first synthesized in 55 steps that interacts specifically with AT-III, thereby inhibiting the generation of thrombin. In contrast to HEP, its anti-factor Xa activity cannot be neutralized *in vitro* with protamine sulfate but with the cationic polymer hexadimethrine bromide (Polybrene) [341]. Furthermore, synthetic HEP and HS oligosaccharides are often used to study interactions with proteins [342]. Other strategies include the use of various other biopolymers as GAG mimetics, like sulfated cellulose [343], sulfated dextran [344,345] and crosslinked, positively charged chitosan [346].

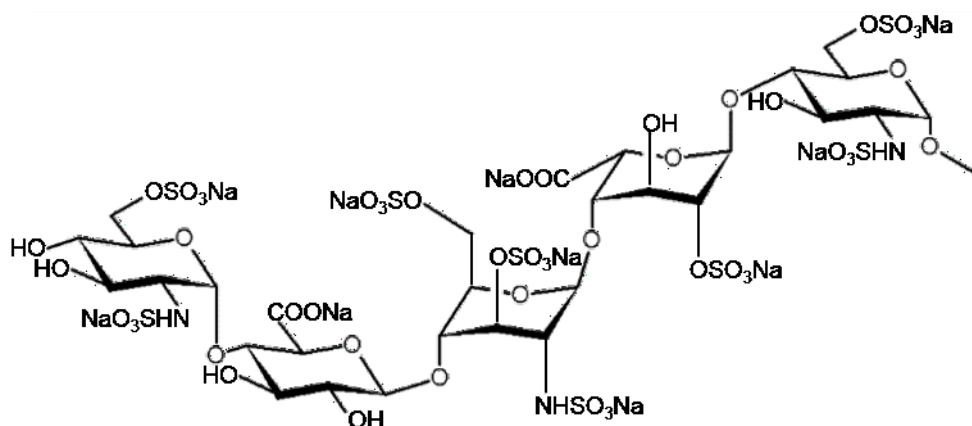


**Fig. 2.16 Structures of the pentasaccharide fondaparinux.**

However, HA as native GAG of the ECM is an ideal starting material for chemical modifications. It is non-immunogenic since it contains no protein epitopes, it is biodegradable by enzymatic digestion via Hyal [83] and it is the simplest GAG molecule that can easily be modified by the introduction of functional groups [9,347] as described in the following sections. Also, HA has no anticoagulative properties since it does not interact with factors of the coagulation cascade [348]. Based on reports from Magnani et al., an anticoagulative activity could be present for sHA derivatives with a degree of sulfation (D.S.s)  $\geq 2.5$  per D.U., which should be considered when selecting GAG derivatives for a future biomedical application. However, they also revealed that this effect can be reversed with protamine and that all examined sHA derivatives had a poor antithrombin activity [349]. An overview on selected biological effects of HA and CS derivatives as solutions or as components of collagen-based aECM coatings on cells relevant for wound healing in skin and bone tissue, which are studied by the research consortium Transregio 67 is given in Tab. 2.7. Until now, though, no data



regarding the impact of multiple sHA derivatives as well as different GAG to collagen mass ratios on the resulting aECM characteristic and the cellular response are available. It remains to be shown whether these variations and especially the combination of different sHA derivatives improve the potential of biomaterials in adjusting the cellular response towards patient specific needs.

**Tab. 2.7 Selected findings of the Transregio 67 obtained with solute or aECM-bound GAG derivatives.** The GAGs or GAG-containing collagen-based aECMs (coll/GAG) mentioned below are those showing the most pronounced biological effects. High-sulfated HA (sHA3), over-sulfated CS (sCS3).

aECM	Biological function	Ref.
coll/sHA1, coll/sHA3	Reduced release of aECM-bound TGF- $\beta$ 1 with increasing sulfation of HA	[350]
coll/sHA3	Reduced bioactivity of sHA3-bound TGF- $\beta$ 1, prevention of the TGF- $\beta$ 1-induced differentiation of fibroblasts to myofibroblasts	[351]
coll/sHA	Increased osteogenic differentiation of hMSCs	[352]
coll/sHA3	Increased metabolic activity of hMSCs, enhanced cell functions of osteogenic differentiated hMSCs like cell-matrix interaction, cell signaling, endocytosis and differentiation	[353]
sCS3, sHA3	Suppression of osteoblast apoptosis, necrosis, reduced osteoblast proliferation, impaired paracrine osteoblast-osteoclast signaling	[354]
coll/sHA3, coll/sCS3	Increased adhesion of human osteoclast precursors, inhibition of osteoclast differentiation and resorption	[355]
sCS3, sHA3	Inhibition of osteocyte apoptosis, no effects on proliferation, reduced expression of sclerostin, increased expression of BMP-2	[356]
coll/sHA3	Reduced release of pro-inflammatory cytokines by macrophages, enhanced differentiation of monocytes into anti-inflammatory M2 macrophages, interference with signaling pathways required for monocyte polarization into inflammatory M1 macrophages	[357,358]
sHA1, sCS3, sHA3	Influence on the Fn and collagen type I matrix assembly	[245,359]

### 2.8.3.1 Methods to adjust the molecular weight of GAGs

Since the  $M_w$  of HA is essential for its function (section 2.1.2.5), several techniques are established to generate HA derivatives with defined  $M_w$  distributions and a reduced polydispersity. HA can be degraded by the incubation of an aqueous HA solution with 0.1 - 2.0 M HCl at 40 - 80°C [360] and HS/HEP and DS are reported to be cleaved by the treatment with nitrous acid [361,362]. Since the depolymerization under acidic conditions is hard to control and leads to several side reaction like the removal of sulfate residues, *N*-deacetylation or elimination at the reducing ends, other methods such as the degradation of

water-solubilized GAGs by ultrasonic [363] or thermal treatment (e.g. autoclave, 130°C, 120 min) [364,365] have been developed. The oxidative depolymerization with reactive oxygen or nitrogen species is also widely used [366]. A further option is the enzymatic degradation of GAGs e.g. with heparinases [367], but this strategy is primarily limited to native GAGs since sulfated HA derivatives for instance are only marginally digested by Hyal [368].

### **2.8.3.2 Synthesis strategies for sulfated GAG derivatives**

The functionalization of GAGs with defined sulfation patterns is challenging [369]. As the biological properties of GAGs are strongly influenced by the D.S.<sub>s</sub> and the sulfate group distribution in the polymer, diverse synthesis pathways or strategies for the sulfation of HA that allow for control of the D.S.<sub>s</sub> and regioselectivity were developed. First approaches to introduce sulfate groups to HA and CS used relatively harsh reaction conditions with chlorosulfonic acid and sulfuric acid as sulfation agents leading to the partial sulfation of free hydroxyl groups but also to a partial depolymerization of GAGs [370].

Nowadays mainly a complex of SO<sub>3</sub> with organic amides or amines is utilized for the chemical sulfation of poly- and oligosaccharides. The reactivity of the SO<sub>3</sub>-complexes increases in the following order: sulfur trioxide-triethylamine complex (SO<sub>3</sub>-Et<sub>3</sub>N) < sulfur trioxide-pyridine complex (SO<sub>3</sub>-pyridine) < sulfur trioxide-*N,N*-dimethylformamide complex (SO<sub>3</sub>-DMF) due to the different stabilities of the Lewis-acid/base-complexes. This makes it possible to obtain defined sulfation degrees in the range of  $0 \leq \text{D.S.}_s \leq 4$  under mild conditions [340,349,371]. For example, the SO<sub>3</sub>-DMF complex is often used to synthesize products with a high D.S.<sub>s</sub>, while SO<sub>3</sub>-pyridine leads to products with low or medium degree of GAG sulfation [59]. Here sHA1 derivatives with a D.S.<sub>s</sub> of 1.0 were shown to be exclusively sulfated at the primary hydroxyl group (C6 position of the *N*-actelyglucosamine residues) (Fig. 3.1) [59,349].

Another strategy is the desulfation of sGAGs. Silylating agents like *N,O*-bis(trimethylsilyl)acetamide can be used to selectively remove sulfate residues at the C6 position [372], while a mixture of water and dimethylsulfoxide (DMSO) randomly remove sulfate residues [373]. Furthermore, *N*-sulfate groups can be introduced to CS and HA after deacetylation (e.g. with 2.5 N NaOH for 72 h at room temperature (RT)) by the sulfation of the resulting free amino groups with SO<sub>3</sub> complexes [374,375].

Regioselectively functionalized sGAGs can also be synthesized by the application of suitable protection strategies [376]. One challenge is that organic sulfates are acid-labile and can be cleaved under such conditions. Options are for instance the use of base- or hydrogenation-labile protection groups and/or photo-labile protection groups. Benzyl groups can be used as permanent protecting groups for aliphatic alcohols during the sulfation step and can be cleaved by hydrogenation with palladium on carbon as a catalyst without cleaving the sulfates. To direct the anomeric specificity, participating groups like benzoyl or acetyl groups can be introduced as permanent protection groups. The base-labile 9-fluorenylmethyl carbonate group and

levulinoyl ester can be removed by hydrazine treatment and are temporary protecting groups often used in oligosaccharides for site-specific reactions via orthogonal protecting strategies [377,378].

### 2.8.3.3 Strategies for cross-linkable GAGs and GAG-based hydrogels

Hydrogels are water-swollen networks of polymers which can be obtained by chemical or physical crosslinking of polymers [379] and provide a promising option for the pharmaceutical and biomedical application of GAGs. Especially HA-based scaffolds have a high potential in regenerative medicine since they provide a 3D cellular microenvironment that is enzymatically degradable and non-immunogenic [380]. The cross-linking of molecules in the presence of cells requires specific mild non-toxic conditions that ensure cell survival. Cell compatible cross-linking schemes include Michael-type addition, triazole formation, click reaction, aldehyde cross-linking, enzymatic cross-linking and photo-induced polymerization [381]. Functional groups for polymerization by a free radical mechanism are for example acrylate, methacrylate, fumarate, cinnamoyl ester and vinyl ester. Vinyl sulfone moieties, *N*-hydroxysuccinimide esters, pyridyl disulfides as well as alkynes, azides and maleimides for highly efficient cycloaddition reactions are other reactive functionalities for cross-linking or derivatization of macromers [382,383].

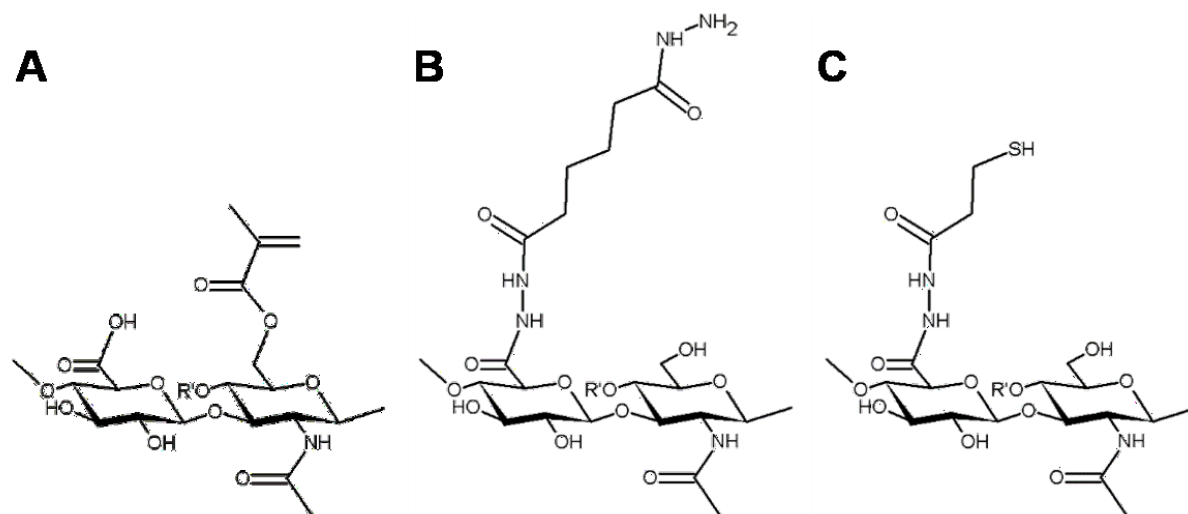


**Fig. 2.17 Structures of cross-linkable HA derivatives.** (A) Methacrylated HA, (B) hydrazido-modified HA and (C) thiolated HA.

Methacrylated GAGs (Fig. 2.17 A) as starting material for cross-linked gels can be formed by functionalizing the hydroxyl groups of GAGs with glycidyl methacrylate or methacrylic anhydride [384,385], while acrylated GAG derivatives are available through a phase-transfer-based synthesis with acryloyl chloride [365]. Hydrazido-modified HA derivatives (Fig. 2.17 B) can be synthesized after activation of the carboxylic groups via carbodiimide chemistry and reaction with dihydrazides like adipic dihydrazide, while thiolated derivatives can be synthesized by using disulfide-linked dehydrazides such as 3,3'-dithiobis(propanic hydrazide) [386,387]. Afterwards the disulfide bonds have to be reduced with dithiothreitol to obtain the

corresponding thiol-functionalized HA derivative (Fig. 2.17 C). To form disulfide cross-linked hydrogels the thiol groups of this HA derivative can be oxidized on air [386].

A further option is the synthesis of HA vinyl esters with tunable degrees of substitution by a lipase-catalyzed transesterification reaction between the hydroxyl groups of HA and divinyl adipate. HA vinyl ester-based hydrogels can be produced by photo-polymerization. These hydrogels can be degraded by i) the enzymatic cleavage of the HA sugar backbone into HA fragments by Hyal and ii) hydrolysis with poly(vinyl alcohol) and adipic acid as degradation products [388].

Star-shaped poly(ethylene glycol) (starPEG)-GAG hydrogels are widely used as biomaterial platforms. They can be produced via Michael addition between a starPEG peptide conjugate with terminal thiol groups and a maleimide-functionalized GAG-peptide conjugates [381] but require further modifications since PEG is known to limit cell adhesion [389].

To further adjust hydrogel properties and tune their degradation behavior, additional hydrolytically cleavable groups or enzymatically cleavable peptide sequences (MMP-cleavable sequences) can be introduced [390,391]. The addition of adhesion sequences like RGD or Gly-Phe-Hyp-Gly-Glu-Arg (GFOGER) enables the interaction of defined amino acid segments with integrin receptors on the cell surface, which can strongly improve the cell adhesion [389,392,393]. Introducing structural proteins such as collagen allows for the tailoring of the mechanical properties, and peptide motif presentation mediates cell adhesion [20,394]. Moreover, sGAG derivatives can be used to sequester, stabilize and control the release of cytokines and growth factors [59,351,395]. This may also make it possible to for instance embed growth factors during hydrogel formation without their losing activity, or to use the hydrogels as scavenger for pro-inflammatory factors. To tune the mechanical stability and the biodegradation behavior of GAG-based hydrogels the degree of substitution is important since an increasing density of cross-linkable groups will enhance the stability of hydrogels [365]. Pores can be introduced into the polymer networks to enhance the seeding efficiency as well as the supply and transport of oxygen and nutrients by different techniques like porogen leaching, templating, electrospinning and freeze-drying [396–399].

Novel approaches are necessary to translate the promising functions of 2.5D collagen-based aECMs (Tab. 2.6) into 3D systems that are able to support healing of vascularized tissues such as skin and bone. Even though HA-based hydrogels are widely studied regarding potential biomedical applications [327], HA-hydrogels with sHA derivatives are rarely described, and mainly for cartilage tissue engineering [400,401]. Hence little is known about the impact of defined substitution patterns of HA and the non-covalent incorporation of collagen fibrils on the resulting hydrogel properties as well as the interaction with mediator proteins and cells.

### 3 MATERIALS AND METHODS

#### 3.1 Chemicals, materials and devices

##### 3.1.1 Chemicals

**Tab. 3.1 Overview of used chemicals.**

<b>Chemical</b>	<b>Specification, catalogue number</b>	<b>Manufacturer</b>
1,9-Dimethylmethylene blue (DMMB)	20335	Serva, Heidelberg, Germany
1-Ethyl-3-(3-dimethylaminopropyl)carbodiimide hydrochlorid (EDC)	E7750	Sigma-Aldrich, Steinheim, Germany
2-Propanol	≥ 99.8%, 6752.2	Sigma-Aldrich, Steinheim, Germany
3,3',5,5'-Tetramethyl-benzidine	Substrate for enzyme linked immunosorbent assay (ELISA), T4444	Sigma-Aldrich, Steinheim, Germany
4-(Dimethylamino)benzaldehyde (DMAB)	99%, 156477	Sigma-Aldrich, Steinheim, Germany
4',6-Diamidino-2-phenylindol (DAPI)	> 90%, 10236276001	Roche, Mannheim, Germany
4-Aminophenylmercuric acetate (APMA)	≥ 90%, A9563	Sigma-Aldrich, Steinheim, Germany
4-Nitrophenyl phosphate disodium salt hexahydrate	≥ 97%, N4645	Sigma-Aldrich, Steinheim, Germany
Acetylacetone	≥ 98%, 00909	Sigma-Aldrich, Steinheim, Germany
Acryloyl chloride	≥ 97%, A24109	Sigma-Aldrich, Steinheim, Germany
Adipic acid dihydracide	≥ 98%, A0638	Sigma-Aldrich, Steinheim, Germany
Agarose	A9539	Sigma-Aldrich, Steinheim, Germany
ATTO 488-NH <sub>2</sub>	AD 488-91	ATTO-TEC, Siegen, Germany
ATTO 565-NH <sub>2</sub>	AD 565-91	ATTO-TEC, Siegen, Germany
Barium acetate	99.999%, 255912	Sigma-Aldrich, Steinheim, Germany
Bovine serum albumin (BSA)	≥ 98%, A7030	Sigma-Aldrich, Steinheim, Germany
Brij® L23 (Polyoxyethylene (23) lauryl ether, Brij 35)	P1254	Sigma-Aldrich, Steinheim, Germany
Bromophenole blue	15375	Serva, Heidelberg, Germany

<b>Chemical</b>	<b>Specification, catalogue number</b>	<b>Manufacturer</b>
Calcium chloride · 2 H <sub>2</sub> O	CN93.1	Carl Roth, Karlsruhe, Germany
Carbon for SEM coating	Ø 6.15 mm x 304 mm, 61-35	Plano, Wetzlar, Germany
Citric acid	≥ 99.5%, 251275	Sigma-Aldrich, Steinheim, Germany
Collagen type I from rat tail tendon	3 - 4 mg/ml in 0.02 N acetic acid, 354236	Corning, New York, USA
Coomassie blue R-250	> 75%, 17525.01	Serva, Heidelberg, Germany
Copper(II) sulfate	≥ 99.99%, 451657	Sigma-Aldrich, Steinheim, Germany
Deuterium oxide (D <sub>2</sub> O)	99.9 atom% D, 151882	Sigma-Aldrich, Steinheim, Germany
Dimethylsulfoxide (DMSO)	> 99.9%, 472301	Sigma-Aldrich, Steinheim, Germany
Disodium hydrogen phosphate	≥ 99%, P030.1	Carl Roth, Karlsruhe, Germany
Ethanol (absolute)	99.98%, 20821.321	VWR, Darmstadt, Germany
Ethanol, denatured	>99.98%, 1% petroleum ether, 1522P	Berkel AHK Alkoholhandel GmbH & Co. KG, Berlin, Germany
Ethanolamine hydrochlorid	≥ 99%, E6133	Sigma-Aldrich, Steinheim, Germany
Ethylenediaminetetraacetic acid trisodium salt hydrate (EDTA)	ED3SS	Sigma-Aldrich, Steinheim, Germany
Folin-Ciocalteu's phenol reagent	2 M, 47641	Sigma-Aldrich, Steinheim, Germany
Formamide	≥ 99.1%, 24311.291	VWR, Darmstadt, Germany
Gelatin from porcine skin	Type A, G8150	Sigma-Aldrich, Steinheim, Germany
Glacial acetic acid	> 99.9%, A6283	Sigma-Aldrich, Steinheim, Germany
Glycerol	≥ 99.5%, ρ = 1.26 g/cm <sup>3</sup> , 3783.2	Carl Roth, Karlsruhe, Germany
Glycine	≥ 99.5%, 3783.1	Sigma-Aldrich, Steinheim, Germany
HEPES buffered saline containing EDTA and P20 (HBS-EP)	10x, 0.1 M HEPES, 1.5 M NaCl, 30 mM EDTA, 0.05% v/v surfactant P20, BR100669	GE Healthcare Europe GmbH, Freiburg, Germany
Hydrochloric acid	37%, 30721	Sigma-Aldrich, Steinheim, Germany

<b>Chemical</b>	<b>Specification, catalogue number</b>	<b>Manufacturer</b>
Lithium phenyl-2,4,6-trimethylbenzoylphosphinate (LAP)	> 98%, L0290	TCI Deutschland GmbH, Eschborn, Germany
Magnesium chloride hexahydrate	M2393	Sigma-Aldrich, Steinheim, Germany
Methanol	≥ 99.8%, 20847.422	VWR, Darmstadt, Germany
Methyl-/vinylether-maleic acid copolymer	184391000, LMW	ACROS, Geel, Belgium
<i>N,N</i> -dimethylformamide (DMF)	99.8%, 227056	Sigma-Aldrich, Steinheim, Germany
<i>N</i> -[Tris(hydroxymethyl)methyl]-2-aminoethanesulfonic acid (TES)	≥ 99%, T1375	Sigma-Aldrich, Steinheim, Germany
<i>N</i> -2-Hydroxyethylpiperazine- <i>N'</i> -2-ethanesulfonic acid (HEPES)	≥ 99.5%, 54457	Sigma-Aldrich, Steinheim, Germany
<i>N</i> -Hydroxy succinimide (NHS)	98%, 130672	Sigma-Aldrich, Steinheim, Germany
<i>N</i> -Isobutyl- <i>N</i> -(4-methoxyphenylsulfonyl)glycyl hydroxamic acid (NNGH)	99%, 316.4 Da, PI-115	Enzo Life Science, Lörrach, Germany
OmniMMP™ Fluorogenic Control	95%, 444.5 Da, P-127	Enzo Life Science, Lörrach, Germany
OmniMMP™ Fluorogenic Substrate	> 98%, 1093.2 Da, P-126	Enzo Life Science, Lörrach, Germany
Pentylamine-biotin	21345	Thermo Fisher Scientific, Langenselbold, Germany
Picric acid	1.2%, 84512.260	VWR, Darmstadt, Germany
Potassium chloride	> 99.6%, 26764.298	Sigma-Aldrich, Steinheim, Germany
Potassium dihydrogen phosphate	> 99.5%, 1.04877.1000	Sigma-Aldrich, Steinheim, Germany
Sirius red (Direct Red 80)	43665	Fluka, Taufkirchen, Germany
Sodium acetate buffer	10 mM, pH 4.5, BR100350	GE Healthcare Europe GmbH, Freiburg, Germany
Sodium azide (NaN <sub>3</sub> )	≥ 99.5%, S2002	Sigma-Aldrich, Steinheim, Germany
Sodium carbonate	≥ 99.5%, 222321	Sigma-Aldrich, Steinheim, Germany
Sodium chloride	≥ 99.5%, S7653	Sigma-Aldrich, Steinheim, Germany
Sodium citrate tribasic dihydrate	99%, C8532	Sigma-Aldrich, Steinheim, Germany
Sodium cyanoborohydride	≥ 95%, 23955696	Molekula, Munich, Germany

<b>Chemical</b>	<b>Specification, catalogue number</b>	<b>Manufacturer</b>
Sodium dodecyl sulfate (SDS), Roti®-Stock	20%, 1057.1	Carl Roth, Karlsruhe, Germany
Sodium formate	≥ 99%, 247596	Sigma-Aldrich, Steinheim, Germany
Sodium hydroxide	≥ 99%, 9356.1	Carl Roth, Karlsruhe, Germany
Sodium hypochloride	available chloride 10 - 15%, 425044	Sigma-Aldrich, Steinheim, Germany
Stains-all	95%, E9379	Sigma-Aldrich, Steinheim, Germany
Sulfur trioxide/dimethylformamide complex (SO <sub>3</sub> -DMF)	≥ 97%, active SO <sub>3</sub> ≥ 45%, 84735	Sigma-Aldrich, Steinheim, Germany
Sulfur trioxide/pyridine complex (SO <sub>3</sub> -pyridine)	≥ 45% SO <sub>3</sub> , 84737	Sigma-Aldrich, Steinheim, Germany
Sulfuric acid	95 - 98%, 258105	Sigma-Aldrich, Steinheim, Germany
Tetra-n-butyl ammonium fluoride hydrate (TBAF)	98%, 241512	Sigma-Aldrich, Steinheim, Germany
Thiazolyl blue tetrazolium bromide (MTT)	≥ 97.5%, M5655	Sigma-Aldrich, Steinheim, Germany
Toluidine blue	80%, T3260	Sigma-Aldrich, Steinheim, Germany
Trichloroacetic acid	≥ 99.0%, T9159	Sigma-Aldrich, Steinheim, Germany
Trifluoroacetic acid (TFA)	99%, T6508	Sigma-Aldrich, Steinheim, Germany
Tris (Tris(hydroxymethyl)aminomethane)- Base	≥ 99.9%, T6066	Sigma-Aldrich, Steinheim, Germany
Tris-HCl	≥ 99%, T5941	Sigma-Aldrich, Steinheim, Germany
Triton-X 100	Laboratory grade, X100	Sigma-Aldrich, Steinheim, Germany
Tween 20	P2287	Sigma-Aldrich, Steinheim, Germany
Ultra pure water	L0020	Biochrom, Berlin, Germany



## 3.1.2 Mediator proteins, enzymes and antibodies

Tab. 3.2 Overview of used mediator proteins, enzymes and antibodies.

Protein	Specification, catalogue number	Manufacturer
AlexaFluor-488 Phalloidin	A12379	Invitrogen, Carlsbad, USA
AlexaFluor-568 secondary antibody	goat anti-mouse, IgG, A11004	Invitrogen, Carlsbad, USA
Anti-phospho-tyrosine-horseradish peroxidase (HRP)	841403	R&D Systems, Wiesbaden, Germany
Collagenase from Clostridium histolyticum (ChC)	EC 3.4.24.3, C1639, 0.4 U/mg (FALGPA)	Sigma-Aldrich, Steinheim, Germany
HA detection reagent	biotinylated recombinant human aggrecan, 842163	R&D Systems, Wiesbaden, Germany
Human Phospho-VEGFR-2/KDR control	841421	R&D Systems, Wiesbaden, Germany
Human Phospho-VEGFR-2/KDR DuoSet IC - ELISA kit	DYC1766-2	R&D Systems, Wiesbaden, Germany
Human TIMP-3 capture antibody	monoclonal, mouse IgG1, 842327	R&D Systems, Wiesbaden, Germany
Human TIMP-3 detection antibody	biotinylated, mouse anti-human, 842328	R&D Systems, Wiesbaden, Germany
Human Total VEGFR-2/KDR DuoSet IC - ELISA kit	DYC1780-2	R&D Systems, Wiesbaden, Germany
Human VEGF capture antibody	monoclonal, mouse IgG2B, MAB293	R&D Systems, Wiesbaden, Germany
Human VEGF detection antibody	biotinylated, goat IgG, BAF293	R&D Systems, Wiesbaden, Germany
Human VEGFR-2/KDR capture antibody	841419	R&D Systems, Wiesbaden, Germany
Human VEGFR-2/KDR detection antibody	841435	R&D Systems, Wiesbaden, Germany
Hyaluronidase (Hyal)	Type I-S, bovine testis, 607 U/mg, EC 3.2.1.35, H3506	Sigma-Aldrich, Steinheim, Germany
Neutravidin™ biotin binding protein	31000	Thermo Fisher Scientific, Langenselbold, Germany
Papain from papaya latex	≥ 10 units/mg protein, P4762	Sigma-Aldrich, Steinheim, Germany
Recombinant human LRP-1 cluster II Fc Chimera	> 90%, 136.2 kDa homodimer, 2368-L2-050	R&D Systems, Wiesbaden, Germany

<b>Protein</b>	<b>Specification, catalogue number</b>	<b>Manufacturer</b>
Recombinant human LRP-1 cluster IV Fc Chimera	> 90%, 153.4 kDa homodimer, 5395-L4-050	R&D Systems, Wiesbaden, Germany
Recombinant human MMP-1	> 95%, 52 kDa zymogen, 901-MP-010, EC 3.4.24.7	R&D Systems, Wiesbaden, Germany
Recombinant human MMP-1 catalytic domain	> 95%, 19.9 kDa, BML-SE180	Enzo Life Science, Lörrach, Germany
Recombinant human MMP-2	> 90%, 71 kDa zymogen, 902-MP-010, EC 3.4.24.24	R&D Systems, Wiesbaden, Germany
Recombinant human MMP-2 catalytic domain	> 90%, 40 kDa, 41.6 U/ $\mu$ l, BML-SE237	Enzo Life Science, Lörrach, Germany
Recombinant human TIMP-3	> 95%, 22 kDa, 973-TM-010	R&D Systems, Wiesbaden, Germany
Recombinant human VEGF <sub>165</sub> (VEGF)	> 97%, 38.4 kDa homodimer, 293-VE-050	R&D Systems, Wiesbaden, Germany
Recombinant human VEGFR-2 (KDR) Fc Chimera	220 kDa homodimer, 357-KD-050/CF	R&D Systems, Wiesbaden, Germany
Rhodamine B labelled Lysozyme	14.3 kDa, LS1-RB-1, EC 3.2.1.17	NANOCS Inc., New York, USA
Streptavidin-horseradish peroxidase (Streptavidin-HRP)	DY998	R&D Systems, Wiesbaden, Germany
Total VEGFR-2 standard	841436	R&D Systems, Wiesbaden, Germany

### 3.1.3 Glycosaminoglycans

**Tab. 3.3 Overview of used commercially available glycosaminoglycans.**

<b>Glycosaminoglycan</b>	<b>Specification, catalogue number</b>	<b>Manufacturer</b>
Chondroitin sulfate (CS)	from porcine trachea, Mixture of 30% chondroitin-6-sulfate and 70% chondroitin-4-sulfate	Kraeber & Co. GmbH, Ellerbek, Germany
CS-, HA- and HEP oligosaccharides	degree of polymerization: 6 (dp 6), CS006, HA06, HO06	Iduron, Manchester, UK
Heparin (HEP)	from porcine intestinal mucosa, H3149	Sigma-Aldrich, Steinheim, Germany
HMW-Hyaluronan (HMW-HA)	from Streptococcus 1.1 · 10 <sup>6</sup> g/mol, PD = 4.8	Aqua Biochem, Dessau, Germany

## 3.1.4 Consumables

Tab. 3.4 Overview of used consumables.

Consumable	Specification, catalogue number	Manufacturer
24 well plate	transparent, F-bottom, sterile, Nunc, 10604903	Thermo Fisher Scientific, Langensfeld, Germany
24 well tissue culture plate	TPP, sterile, 92024	Sigma-Aldrich, Steinheim, Germany
48 well plate	transparent, F-bottom, sterile, Nunc, 10644901	Thermo Fisher Scientific, Langensfeld, Germany
96 well plate	black, Nunclon™ delta surface, sterile, 137101	Thermo Fisher Scientific, Langensfeld, Germany
96 well plate	transparent, F-bottom, Nunc, 10194761	Thermo Fisher Scientific, Langensfeld, Germany
96 well plate	ELISA plate, high binding, F-bottom, transparent, 82.1581.200	Sarstedt, Nümbrecht, Germany
96 well plate	White, half-area, F-bottom, 3992	Corning, New York, USA
Adhesive sticker for AFM	Ø 10 mm, G304	Plano, Wetzlar, Germany
AFM specimen discs	Ø 15 mm, 16218	Ted Pella Inc., Redding, USA
Biopsy punch	sterile, Ø 3 mm, 48301	Pfm medical, Kai Europe GmbH, Solingen, Germany
Cantilever	Tap300-G-10, silicon, resonance frequency: 300 kHz, force constant: 40 N/m	Ted Pella Inc., Redding, USA
Carbon tab for SEM	Ø 12 mm, G3347	Plano, Wetzlar, Germany
Cell counting slides	EVS-050	NanoEnTek, Seoul, South Korea
Cell culture dish	Cellstar®, 60 mm x 15 mm, 628960	Greiner Bio-One, Frickenhausen, Germany
Cell culture flask	175 cm <sup>2</sup> , 83.3912.002	Sarstedt, Nümbrecht, Germany
Cell scarper	16 cm, 83.1832	Sarstedt, Nümbrecht, Germany
Centrifuge tubes	15 ml, 188 271; 50 ml, 227 261	Greiner Bio-One, Frickenhausen, Germany
Cover for 96 well plates	82.1584	Sarstedt, Nümbrecht, Germany
Mica substrate for AFM	11 mm x 11 mm, 0.15 mm thick, G259-3	Plano, Wetzlar, Germany
Microcentrifuge tubes	low binding: 0.65 ml, 1.7 ml, 2.0 ml,	Sorenson Bioscience, Salt Lake City, USA
Microscope cover glasses	Ø 12 mm, No.1, ECN 631-1577	VWR, Darmstadt, Germany
Object slides	Glass, 631-1553	VWR, Darmstadt, Germany
Parafilm	M, PM996	Bemis, Neenah, USA
Pasteur pipette	230 mm, glass, 4522	Carl Roth, Karlsruhe, Germany
Pipet tips	50 - 1000 µl, F167658H; 100 - 5000 µl, F166822H	Eppendorf AG, Hamburg, Germany

Consumable	Specification, catalogue number	Manufacturer
Pipet tips	0.5 - 10 $\mu$ l, 765290; 20 - 200 $\mu$ l, 739296; low binding, sterile: 10 $\mu$ l, 771265; 300 $\mu$ l, 738265	Greiner Bio-One, Frickenhausen, Germany
Pipet tips	low binding, desoxyribonucleic acid (DNA)-, Dnase-, Rnase-free, sterile: 2 - 100 $\mu$ l, 70.760.212; 1250 $\mu$ l, 70.1186.210	Sarstedt, Nümbrecht, Germany
Pipet tips for multichannel pipette	1 - 330 $\mu$ l, 790047	Biozym Scientific GmbH, Hessisch Oldendorf, Germany
Pipet tips for repetitive pipette	5 ml, 0030 069.455; 10 ml, 0030 089.677	Eppendorf AG, Hamburg, Germany
Pipet tips with microcapillary for loading gels	1 - 200 $\mu$ l, 732-0508	VWR, Darmstadt, Germany
Rubber caps for SPR vials	Type 2, ventilated, BR100411	GE Healthcare Europe GmbH, Freiburg, Germany
Rubber caps for SPR vials	Type 3, ventilated, BR100502	GE Healthcare Europe GmbH, Freiburg, Germany
Rubber caps for SPR vials	Type 5, ventilated, BR100655	GE Healthcare Europe GmbH, Freiburg, Germany
Sample holder for SEM	G301, $\varnothing$ 12.5 mm	Plano, Wetzlar, Germany
Scalpel	Nr. 22, 0508	Swann Morton, Sheffield, UK
Sealing films	Rotilabo®, microtest plates, PE, sterile, thickness 50 $\mu$ m, EN77.1	VWR, Darmstadt, Germany
Series S Sensor Chip C1	BR100535	GE Healthcare Europe GmbH, Freiburg, Germany
Series S Sensor Chip CM5	BR100530	GE Healthcare Europe GmbH, Freiburg, Germany
Serological pipettes	2 ml, 86.1252.001	Sarstedt, Nümbrecht, Germany
Serological pipettes	5 ml, 4487; 10 ml, 4488; 25 ml 4489	Corning, New York, USA
Silver dag for SEM	G3692, ACHESON	Plano, Wetzlar, Germany
Syringe	sterile: 5 ml, 4606710V; 20 ml, 4606205V	B. Braun Melsungen AG, Melsungen, Germany
Syringe	sterile: 10 ml, 15E26C8	Henke-Sass Wolf GmbH, Tuttlingen, Germany
Syringe filters	0.2 $\mu$ m pores, 83.1826.001	Sarstedt, Nümbrecht, Germany
Tubes	low binding: 5 ml, D156383K	Eppendorf AG, Hamburg, Germany
Tubes	low binding: 0.65 ml, 7137.1; 1.7 ml, 7154.1; 2.0 ml, 7181.1	Carl Roth, Karlsruhe, Germany
Vials for SPR	7 mm, 0.8 ml, PP, BR100212	GE Healthcare Europe GmbH, Freiburg, Germany

Consumable	Specification, catalogue number	Manufacturer
Vials for SPR	11 mm, 1.5 ml, PP, BR100287	GE Healthcare Europe GmbH, Freiburg, Germany
Vials for SPR	15 mm, 4 ml, PP, BR100654	GE Healthcare Europe GmbH, Freiburg, Germany

### 3.1.5 Devices and software

**Tab. 3.5 Overview of used devices and software.**

Device/software	Specification	Manufacturer
Analytical balance	AX105DR	Mettler Toledo, Greifensee, Switzerland
Atomic force microscope	Nanoscope IIIa Bioscope with Nanoscope software	Digital Instruments/Veeco, New York, USA
Carbon sputter coater	SCD 050	Oerlikon Balzers Coating GmbH, Bingen, Germany
Cell counter	EVE Automatic Cell counter	NanoEnTek, Seoul, South Korea
Centrifuge	5415 D, 5702R, 5804R	Eppendorf AG, Hamburg, Germany
Desiccator	2.4 l, 24 782 57; 5.8 l, 24 782 61	DURAN Group, Mainz, Germany
Digital camera	Digimax V700	Samsung, Schwalbach, Germany
Digital measuring slide	0 - 150 mm	TCM, Hamburg, Germany
Drying cabinet	ED 53, type: 15053300002020	WTB Binder, Tuttlingen, Germany
Electromechanical testing system	Instron 5566 with software Merlin IV	Instron Deutschland GmbH, Darmstadt, Germany
Fluorescence microscope	AxioPhot	Carl Zeiss, Oberkochen, Germany
Fluorescence microscope camera	AxioCam MRm	Carl Zeiss, Oberkochen, Germany
Freeze dryer	Epsilon 2-4 LSC	Martin Christ, Oserode, Germany
Freezer, -20°C	Liebherr Comfort	Liebherr, Biberach an der Riß, Germany
Freezer, -80°C	HERA freeze	Heraeus, Hanau, Germany
Fridge, 5 - 8°C	Liebherr Premium	Liebherr, Biberach an der Riß, Germany
Gel electrophoresis	EasyPhor Page Maxi Wave	Biozym Scientific GmbH, Hessisch Oldendorf, Germany
GraphPad Prism	Version 6	GraphPad Software Inc., La Jolla, USA
Heating plate	MR Hei-End	Heidolph, Schwabach, Germany
Ice dispenser	RF0388A	Manitowoc Ice Inc., Manitowoc, USA
Incubator	MCO-5AC; MCO-18AC	SANYO, Moriguchi, Japan
Liquid nitrogen tank	Locator 4 Plus	Barnstead/Thermolyne, Dubuque, USA
Low voltage power supply	Standard Power Pack P25	Biometra, Göttingen, Germany
Magnetic stirrer	BIG SQUID	IKA-Werke, Staufen, Germany
Microplate reader	Infinite M200 PRO	TECAN, Männedorf, Switzerland

Device/software	Specification	Manufacturer
Microscope	Axiovert 25; Axiovert 40 CFL	Carl Zeiss, Jena, Germany
Microscope camera	AxioCam MRm	Carl Zeiss, Oberkochen, Germany
Microscopy software	AxioVision 4.6, ZEN 2 lite	Carl Zeiss, Jena, Germany
Orbital shaker	Unimax 2010	Heidolph, Schwabach, Germany
pH-meter	pH 526	WTW, Weilheim, Germany
Photo scanner	Epson perfection 4180	Epson Deutschland GmbH, Meerbusch, Germany
Pipette controllers	Accu-jet pro	Braun, Wertheim, Germany
Repetitive pipette (electric)	HandyStep	Brand, Wertheim, Germany
Scanning electron microscope	ESEM XL 30 with microscope control software	FEI Europe, Eindhoven, The Netherlands
Security workbench	KR-170 BW, MSC CL-II EN 12469	Kojair Tech Oy, Vilppula, Finland
Spectrophotometer	NanoDrop 1000 with Program ND-1000	Thermo Fisher Scientific, Langensfeld, Germany
Surface plasmon resonance device	Biacore T100	GE Healthcare Europe GmbH, Freiburg, Germany
Ultrapure water system	Arium 611 VF	Sartorius Stedim, Göttingen, Germany
Ultrasonic bath	USC1200TH	VWR, Darmstadt, Germany
Ultrasonic horn	UP 100 H	Hielscher Ultrasonics GmbH, Teltow, Germany
UV-device	365 nm	Sina (via Canbolat Vertriebsgesellschaft, Würzburg, Germany)
Vacuum pump	PM 12617-86	Biometra, Göttingen, Germany
Vortex	Vortex-Genie 2	Scientific Industries, Bohemia, USA
Water bath	ED-13A	Julabo, Seelbach, Germany

### 3.1.6 Cell culture reagents

**Tab. 3.6** Overview of used cell culture reagents.

Cell culture reagent	Specification, catalogue number	Manufacturer
Aprotinin from bovine lung	1.9 mg protein/ml, A6279	Sigma-Aldrich, Steinheim, Germany
Calcein acetoxymethyl ester (Calcein AM)	≥ 96%, 17783	Sigma-Aldrich, Steinheim, Germany
Dulbecco's modified eagle's medium (DMEM)	F 0415	Biochrom, Berlin, Germany
Dulbecco's phosphate buffered saline (DPBS)	10x, + CaCl <sub>2</sub> , + MgCl <sub>2</sub> , gibco, 14080-048	Thermo Fisher Scientific, Langensfeld, Germany
Fetal bovine serum (FBS)	S 0115	Biochrom, Berlin, Germany
Formaldehyde	36%, 47608	Sigma-Aldrich, Steinheim, Germany

Cell culture reagent	Specification, catalogue number	Manufacturer
Lactate dehydrogenase (LDH) cytotoxicity detection kit	MK401	TaKaRa Bio Europe, Saint-Germain-en-Laye, France
Leupeptin hemisulfate	1167	Tocris Bioscience, Bristol, UK
L-Glutamine	200 mM, K 0283	Biochrom, Berlin, Germany
Mitomycin C	M4287	Sigma-Aldrich, Steinheim, Germany
Mowiol 4-88	81381	Sigma-Aldrich, Steinheim, Germany
NP-40 Alternative	492016	EMD/Calbiochem, San Diego, USA
Oris™ Cell Migration Assay	CMA1.101, 96 well	Platypus Technologies via AMS Biotechnology (Europe) Limited, Frankfurt, Germany
Penicillin/Streptomycin (P/S)	100x, 10000 U/ml, 10000 µg/ml, A 2213	Biochrom, Berlin, Germany
PrestoBlue	Cell viability reagent, A-13261	Invitrogen, Carlsbad, USA
Quant-IT PicoGreen dsDNA reagent	P7581	Invitrogen, Carlsbad, USA
Sodium azide (NaN <sub>3</sub> )	S2002	Sigma-Aldrich, Steinheim, Germany
Sodium orthovanadate (Na <sub>3</sub> VO <sub>4</sub> )	S6508	Sigma-Aldrich, Steinheim, Germany
Trypan blue	0.4%, EBT-001	NanoEnTek, Seoul, South Korea
Trypsin/EDTA	10x, 0.5%/0.2%, L 2153	Biochrom, Berlin, Germany

### 3.2 Preparation and characterization of GAG derivatives

Chemically modified GAG polysaccharides were provided by Dr. Stephanie Möller, Dr. Jana Becher and Dr. Matthias Schnabelrauch from INNOVENT Jena e.V. (TRR67 subproject A2, Z3). HA oligosaccharides were available from Joanna Blaszkiewicz, Sebastian Köhling and Prof. Dr. Jörg Rademann (TRR67 subproject A8). All GAGs (Fig. 3.1) were used as sodium salts. The characterization of GAGs was performed by the groups of Dr. Schnabelrauch and Prof. Dr. Rademann as described in [59,402]. For this nuclear magnetic resonance (NMR) spectra were recorded in D<sub>2</sub>O using a Bruker Advance 400 MHz spectrometer at 373 K. The ratio of the proton signals of the acrylic protons (5.9 - 6.4 ppm) and the -CH<sub>3</sub> of HA or CS (1.9 ppm) in <sup>1</sup>H NMR spectra was used to calculate the degree of acrylation (D.S.<sub>AC</sub>) per D.U. of the respective GAG derivative. Additional Fourier transform-infrared (FT-IR) spectra were obtained with a FT-IR-Spectrometer FTS 175 (Bio-rad, Krefeld, Germany) using the KBr technique. Gel permeation chromatography was used to determine the M<sub>w</sub>. The polydispersity (PD) of the GAGs was calculated by RI detection with standard pullan (PSS, Mainz, Germany)

for calibration, while laser light scattering detection was applied to determine the weight-average  $M_w$  of the polymers. The content of sulfur was quantified with an automatic elemental analyzer (CHNS-932, Leco, Mönchengladbach, Germany). The determined amount was used to calculate the degree of sulfate substitution (D.S.s) of GAG. In addition, the same methods were used to characterize the used commercially available native GAGs (Tab. 3.7, Tab. 3.8, Tab. 3.9).

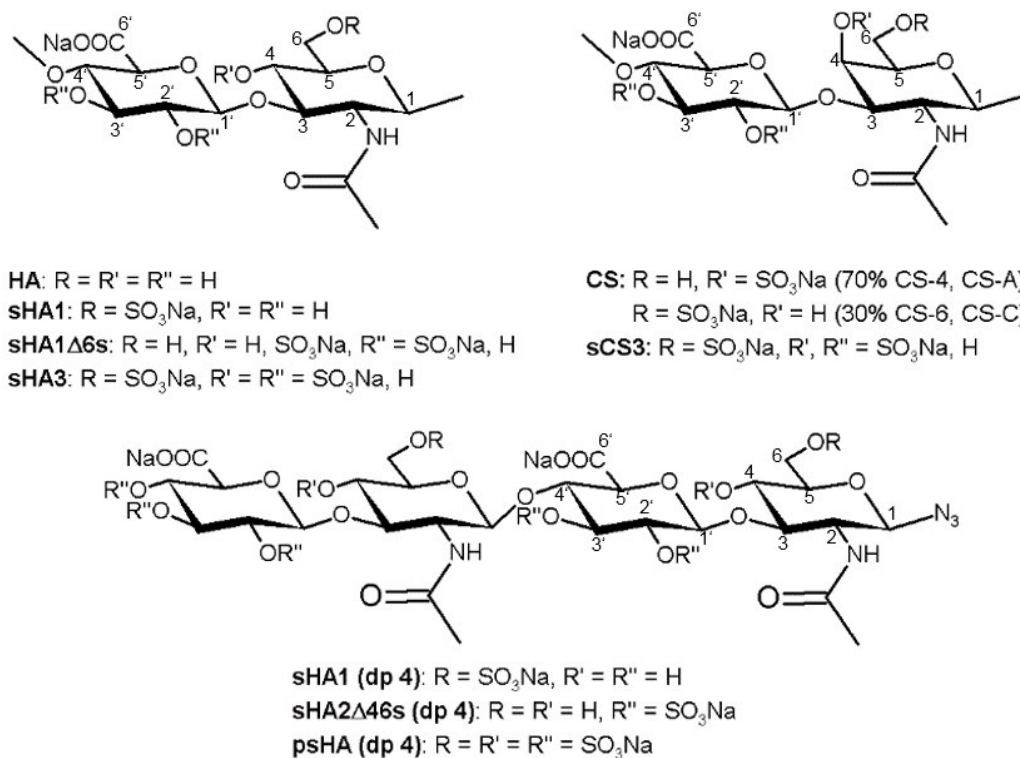


**Fig. 3.1** Structures of sulfated HA and CS derivatives.

### 3.2.1 Preparation of low molecular weight HA

Ozonolysis was used to degrade HMW-HA according to [R316]. To this end a 10 mg/ml solution of native HA dissolved in water was treated for 120 min with 30 g/m<sup>3</sup> O<sub>3</sub> at a flow rate of 20 - 30 l/h, which was generated via an ozone generator (COM-AD-02, ANSEROS Klaus Nonnenmacher, Tübingen, Germany). Free ozone was removed by the treatment with N<sub>2</sub> for 30 min prior to dialysis against water and lyophilization of the remaining solution. Yield: 75 - 85%.

### 3.2.2 Synthesis of low-sulfated HA derivatives

Sulfated HA derivatives exclusively substituted at the C6 position of the *N*-acetylglucosamine sugar unit of HA (sHA1) were synthesized as described in [59,403]. In brief, the sodium salt of HA was transferred into the tetra-butylammonium salt form (TeBA-HA) using a Dowex WX 8 ion exchanger. TeBA-HA served as starting material for the sulfation under argon at RT in the organic solvent DMF. To obtain sHA1, a SO<sub>3</sub>-pyridine complex dissolved in DMF was added



to a suspension of TeBA-HA in DMF (molar polymer/SO<sub>3</sub> ratio: 1:7). Sulfated products were precipitated into acetone and neutralized with ethanolic NaOH solution. The formed sodium salt of sHA1 was washed with acetone and purified by dialysis against distilled water. Yield: 65%.

### 3.2.3 Synthesis of regio-selectively sulfated HA derivatives

Selective sulfation of the secondary hydroxyl groups of HA without sulfation of the primary hydroxyl group at the C6 position of the *N*-acetylglucosamine sugar unit (sHA1Δ6s) can be realized by using benzoyl ester as protecting group as reported in [404,405]. An ion exchanger was used to obtain the TeBA-HA. The primary hydroxyl group at C6 position of the *N*-acetylglucosamine sugar unit was protected by benzylation using benzoyl chloride dissolved in a mixture of DMF and pyridine. The intermediate product was isolated by precipitation in water, then washed and dried in vacuum. The C6-benzoylated HA was afterwards sulfated using SO<sub>3</sub>-DMF (molar polymer/SO<sub>3</sub> ratio 1:15) as sulfation reagent. The reaction mixture was poured into acetone adjusted to pH 10 by the addition of ethanolic NaOH solution and the product was isolated after neutralization with HCl. The protection groups were removed under basic conditions with an aqueous K<sub>2</sub>CO<sub>3</sub> solution overnight. sHA1Δ6s was purified by dialysis against distilled water. Yield: 65%.

### 3.2.4 Synthesis of high-sulfated GAG derivatives

High-sulfated HA (sHA3, sHA4) and over-sulfated CS (sCS3) were synthesized as described in [59,406]. 3.22 mmol TeBA-HA (section 3.2.2) suspended in 400 ml DMF were mixed with 64.4 mmol SO<sub>3</sub>-DMF complex in 40 ml DMF for 60 min at RT under argon atmosphere (polymer/SO<sub>3</sub> ratio: 1:20). In case of sCS3, 6.92 mmol TeBA-CS, which was produced as described for HA, was suspended in 200 ml DMF before adding 138.35 mmol SO<sub>3</sub>-DMF complex in 60 ml DMF and treating it like the respective HA derivatives. Afterwards, the reaction products were isolated by precipitation in acetone and neutralized with ethanolic NaOH. The obtained sodium salts were washed with acetone and dialyzed against water prior to lyophilization and drying under vacuum. Yield: 76% for sCS3; 70% for sHA3, sHA4.

### 3.2.5 Synthesis of acrylated GAG derivatives

HA, CS, sHA1, sHA1Δ6s acrylates (HA-AC, CS-AC, sHA1-AC, sHA1Δ6s-AC) with acryl groups bound directly to the polymer backbone were obtained in a phase-transfer-based synthesis [365]. 10 mg tetra-*n*-butyl ammonium fluoride (TBAF) was added to 100 ml of a 10 mg/ml aqueous solution of GAG. After cooling to 0°C, a 10-fold (in case of HA) or 50-fold (in case of sGAGs) molar excess of acryloyl chloride relative to the D.U. of GAG and 20 ml CH<sub>2</sub>Cl<sub>2</sub> were added. After 240 min of stirring at 4°C, acetone was added to the aqueous phase for precipitation. The precipitate dissolved in water was dialyzed against water prior to lyophilization. Yield: 98%.

### 3.2.6 Fluorescence-labelling of sulfated HA derivatives

Rhodamine derivatives (ATTO 565-NH<sub>2</sub> for sHA1, ATTO 488-NH<sub>2</sub> for sHA4) were bound to the reducing ends of sHA derivatives as described in [R316] (Fig. 3.2). 500 µg fluorescent dye (ATTO 488-NH<sub>2</sub> dissolved in water; ATTO 565-NH<sub>2</sub> dissolved in DMSO) was added to 0.4 mmol GAG in 30 ml water after adjusting the pH to 8 - 8.5 with 0.1 M NaOH and incubated for 360 min under constant stirring at RT. Then, 0.4 mmol NaCNBH<sub>3</sub> was added to the respective sHA1 solution with ATTO 565 at pH 7.5. After 72 h of stirring, the solution was dialyzed against water at pH 8 - 8.5 and afterwards against water at pH 5.5. The obtained products were lyophilized while the solution containing sHA1 with ATTO 488-NH<sub>2</sub> was directly dialyzed without incubation with NaCNBH<sub>3</sub>. The content of fluorescent dye was calculated by fluorescence measurements using the unbound dye for calibration and the unlabeled GAG as blank. Yield: 85%.

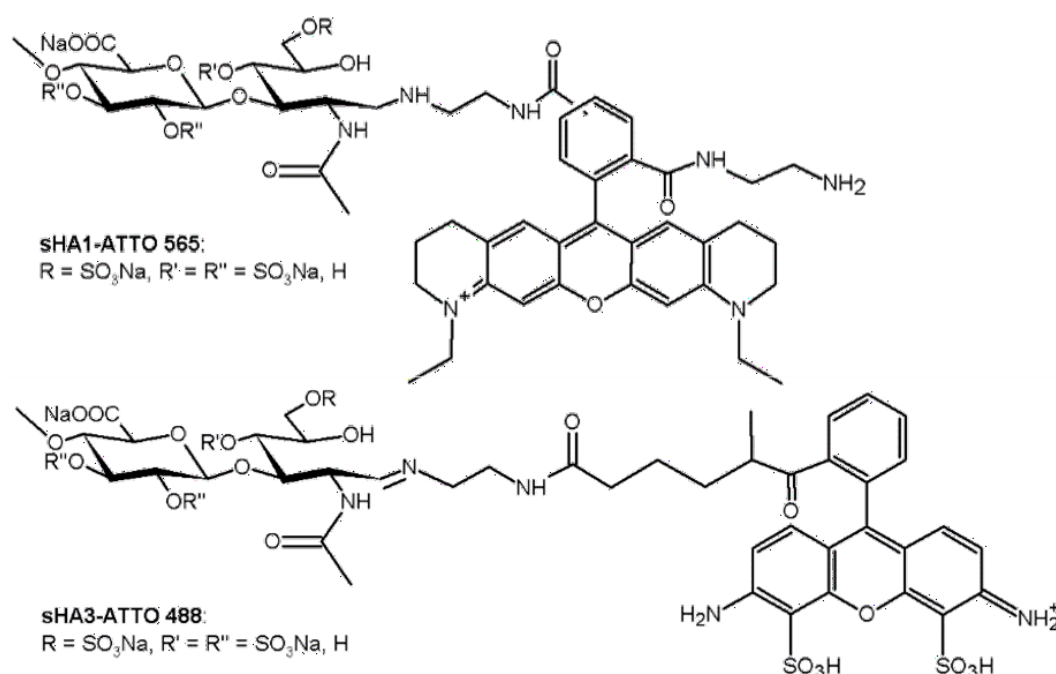
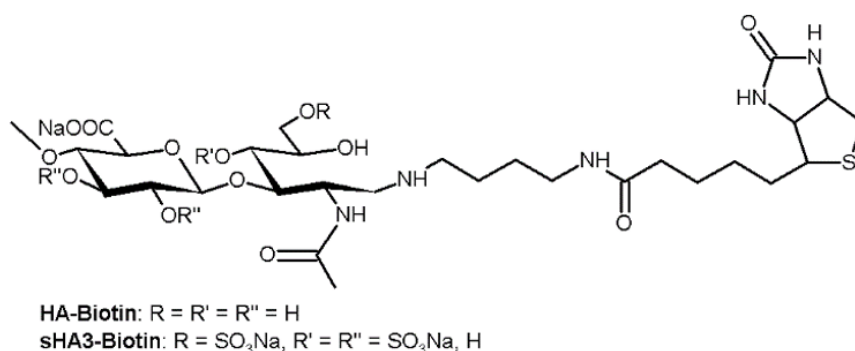


Fig. 3.2 Structure of fluorescence-labeled HA derivatives.

### 3.2.7 Biotin-labelling of HA derivatives

Biotin was introduced to HA and sHA3 at their reducing ends [315] (Fig. 3.3). To this end 0.37 mmol GAG polymer was dissolved in water and 0.1 M NaOH was added to bring the pH to 8.0. Afterwards 3 ml of an aqueous solution containing 0.037 mmol pentylamine-biotin was added to the GAG solution. After 6 h of stirring at RT, the pH was adjusted to 7.5. Then 0.037 mmol NaCNBH<sub>3</sub> was added and the mixture was stirred for 72 h at RT. Free biotin was removed by dialysis against water at pH 8 - 8.5 and afterwards against water at pH 7. The biotinylated GAGs were obtained after filtration and lyophilization. Yield: 75 - 80%.



**Fig. 3.3 Structure of biotin-labeled HA derivatives.**

### 3.2.8 Synthesis of sulfated HA oligosaccharides

Tetra- and hexasaccharides of HA (dp 4, 6) were produced by enzymatic degradation of native HA by bovine testis Hyal (17.5 U per mg of HA) for 10 days at 37°C using 0.1 M acidic sodium acetate with 0.15 M NaCl (pH 4.5) as buffer. Afterwards, the reaction was stopped by boiling the solution for 5 min. The filtered solution was freeze-dried and the products were purified by size exclusion chromatography (Bio-Gel P2-column, extra fine, 3.5 cm x 90 cm; 5 psi pressure; 25% acetic acid as mobile phase) before solvent evaporation and freeze-drying. Yield: 55%.

To fix the anomeric position at the reducing end of the oligosaccharides and to enable anomeric ligation reactions, 0.20 mmol HA oligosaccharide was dissolved in water containing 12.12 mmol sodium azide and 6.06 mmol *N*-methylmorpholine prior to adding 2.11 mmol 2-chloro-1,3-dimethylimidazolium chloride at 0°C to obtain the anomeric azides. After stirring for 15 min at 0°C, the reaction was continued at RT for 30 h. Then the solvent was evaporated and the product was desalted (Sephadex G-10 column, 3 cm x 20 cm; water) and purified via high pressure liquid chromatography (HPLC) (C-18; 95% water with 0.1% TFA and 5% MeCN with 0.1 % TFA; 30 ml/min; UV detection at 214 nm). Yield: 72%.

1.845 mmol SO<sub>3</sub>-pyridine complex (5 equivalents per OH group) was added to 0.041 mol HA azide dissolved in DMF to synthesize per-sulfated HA (psHA) oligosaccharides where all GAG hydroxyl groups were substituted by sulfate esters. After overnight incubation, the mixture was supplemented with further 2 equivalents SO<sub>3</sub>-pyridine complex (0.73 mmol) per OH group of HA azide and incubated for 180 min before ending the reaction by adding 5.16 mmol sodium acetate in ethanol at 0°C. The precipitated product was filtered and washed with water prior to desalting and lyophilization [402]. Yield: 72%.

Low-sulfated HA tetrasaccharides exclusively sulfated at the primary hydroxyl groups (sHA1, dp 4) was also produced by the use of SO<sub>3</sub>-pyridine complexes as sulfating agent. The product was extracted by anion exchange chromatography to obtain the GAG derivative as sodium salt. Yield: 35%.

A medium-sulfated HA tetrasaccharide (sHA2Δ6s, dp 4) sulfated at the C2 and C3 position of the glucuronic acid unit but not at the C4 and C6 position of the *N*-acetylglucosamine was

synthesized after introducing protection groups to the 4,6-diol moieties with phenyl boronic acid. This intermediate product was used for subsequent persulfation. Afterwards the final product was extracted by anion exchange chromatography by applying a gradient of NaCl from 0 - 12 M followed by two desalting steps with Sephadex G-10. Yield: 45%.

**Tab. 3.7 Characteristics of GAG oligo- and polysaccharides used for interaction analyses.**

GAG	D.S.	Mw (kDa)	PD	Biotin content	dp
HA (dp 4)	-	0.777	-	-	4
HA (dp 6)	-	1.204	-	-	6
CS (dp 6)	1.0	1.488	-	-	6
sHA1 (dp 4)	1.0	1.005	-	-	4
sHA2Δ6s (dp 4)	2.0	1.355	-	-	4
HEP (dp 6)	2.0	1.800	-	-	6
psHA (dp 4)	4.0	1.763	-	-	4
psHA (dp 6)	4.0	2.573	-	-	6
LMW-HA	-	48.3	2.3	-	240
sHA1	1.0	31.1	2.2	-	123
HEP	2.2	18.0	not determined	-	58
sHA3	2.8	28.7	1.7	-	84
sHA3	2.9	21.0	1.7	-	60
sCS3	3.1	19.9	1.5	-	56
HA-Biotin	-	33.0	2.2	1.96 µg/mg	164
sHA3-Biotin	3.6	29.0	1.7	5.72 µg/mg	75

**Tab. 3.8 Characteristics of polymeric GAG derivatives used for aECM preparation.**

GAG	D.S.	Mw (kDa)	PD	Fluorescent dye
LMW-HA	-	23.0	2.2	-
sHA1	1.4	20.3	2.8	0.45 µg/mg ATTO 565
sHA4	3.6	28.6	1.7	0.06 µg/mg ATTO 488

**Tab. 3.9 Characteristics of polymeric GAG derivatives used for hydrogel preparation.**

GAG	D.S. <sub>s</sub>	Mw (kDa)*	D.S. <sub>AC</sub>
HA	-	48.3	-
HA-AC	-	145.7	0.6
CS	0.8	19.8	-
CS-AC	0.8	19.9	0.6
sHA1	1.2	26.4	-
sHA1-AC	1.5	27.0	0.7

GAG	D.S. <sub>s</sub>	Mw (kDa)*	D.S. <sub>AC</sub>
sHA1Δ6s	1.4	56.3	-
sHA1Δ6s-AC	1.5	55.1	0.5

\*The given Mw corresponds to the GAGs prior to acrylation. No information regarding the PD were available for these GAG derivatives.

### 3.3 Preparation of biomaterials

#### 3.3.1 aECM coatings composed of collagen type I and GAGs (coll/GAG)

The entropy-driven self-assembly of collagen type I monomers to collagen fibrils at neutral pH in the absence or presence of GAGs was used to prepare 2.5D aECM coatings as described by Williams et al. with modifications [407,408].

##### *Preparation of solutions*

*10 mM acetic acid:* 286 μl glacial acetic acid was added to 400 ml water and the volume was adjusted to 500 ml in a volumetric flask. The solution was autoclaved and stored at 4°C.

*Fibrillogenesis buffer (50 mM Na<sub>2</sub>HPO<sub>4</sub>, 10 mM KH<sub>2</sub>PO<sub>4</sub>, pH 7.4, I 0.08):* 6.719 g Na<sub>2</sub>HPO<sub>4</sub> · 7 H<sub>2</sub>O and 0.760 g KH<sub>2</sub>PO<sub>4</sub> were dissolved in 500 ml water. The solution was sterilized by autoclaving and stored at 4°C.

*Collagen type I solution (1 mg/ml):* The collagen stock solution was diluted with 10 mM acetic acid to obtain 1 mg/ml and stored on ice until use.

*GAG solution (2.5 mM D.U.):* The respective amount of GAG related to the Mw of the D.U. was dissolved in fibrillogenesis buffer for at least 120 min at 4°C prior to usage to always provide the same number of potential protein binding sites.

##### *Preparation of aECM coatings via in vitro fibrillogenesis of collagen type I*

Equal volumes of 1 mg/ml collagen type I dissolved in acetic acid were mixed with fibrillogenesis buffer with or without 2.5 mM D.U. GAGs in multi well plates (105 μg coll/cm<sup>2</sup>) on ice and incubated overnight at 37°C to obtain 1/1 aECMs. 1/0.5 matrices were prepared by mixing 1 mg/ml collagen with 1.25 mM D.U. GAG in fibrillogenesis buffer. Afterwards, the aECMs were dried at RT and washed with water prior to drying. For cell culture experiments, aECMs were prepared under sterile conditions using sterile filtered (0.22 μm) solutions and a laminar airflow cabinet.

#### 3.3.2 Hyaluronan/collagen hydrogels (HA-AC/coll)

##### *Preparation of solutions*

10 mM acetic acid and the fibrillogenesis buffer were prepared as described in section 3.3.1.

*1% acrylated GAG in water:* 10 mg acrylated GAG were dissolved in 1 ml water under exclusion of light. The solution was made freshly directly prior to use.

*2% acrylated GAG in water:* 20 mg acrylated GAG were dissolved in 1 ml water in the dark. The solution was made fresh directly prior to use.

*1% LAP in water:* 1 mg LAP was freshly dissolved in 100  $\mu$ l water and protected from light.

*Collagen type I solution (2 mg/ml):* The collagen stock solution was diluted with 10 mM acetic acid to obtain 2 mg/ml and stored on ice until use.

### ***Preparation of HA-AC/collagen hydrogels***

HA-containing hydrogels were obtained after photocrosslinking of HA-AC as reported by Becher et al. [365]. Tab. 3.10 describes the preparation of HA/coll hydrogels in detail, while the compositions of the respective polymer formulations are given in Tab. 3.11.

**Tab. 3.10 Preparation of HA-AC/collagen hydrogels.**

<b>Step</b>	<b>Procedure</b>
<i>In vitro</i> fibrillogenesis	Equal volumes of 2 mg/ml collagen type I dissolved in 10 mM acetic acid and fibrillogenesis buffer were mixed in low-binding tubes on ice, followed by an incubation for 16 hours at 37°C.
Preparation of polymer formulations	20 $\mu$ l 1% LAP was added to 200 $\mu$ l 1% HA-AC for the preparation of gels w/o collagen and sGAG-AC. Collagen-containing gels were prepared from mixtures of 100 $\mu$ l 2% HA-AC or 75 $\mu$ l 2% HA-AC and 25 $\mu$ l 2% sGAG-AC with 100 $\mu$ l of a suspension of 1 mg/ml fibrillar collagen and 20 $\mu$ l 1% LAP. For cell culture experiments, 200 $\mu$ l polymer mixture containing LAP were added per well of a 48 well plate under sterile conditions. For characterization studies, the gels were prepared non-sterile with 200 $\mu$ l polymer mixture in 96 well plates, with 250 $\mu$ l polymer mixture in cylindrical silicon casting molds or with 50 $\mu$ l polymer mixture between two glass cover slides ( $\varnothing$ 12 mm).
Photocrosslinking	The polymer mixtures were irradiated for 10 min with UV light ( $\lambda = 365$ nm, 0.17 W/cm <sup>2</sup> ).
First freeze-drying	The gels were frozen for 60 min at -80°C prior to freeze-drying. The following program was used: 1) 20 min freezing at -10°C; 2) 105 min drying at -10°C and 1.030 mbar; 3) 150 min drying at 20°C and 1.030 mbar, 4) 690 min drying at 20°C and 1.030 mbar; 5) 10 min drying at 20°C and 0.001 mbar; 6) 50 min drying at 30°C and 0.001 mbar and 7) 120 min drying at 30°C and 0.001 mbar.
Washing	The freeze-dried gels were washed twice with water to remove salts and LAP.
Second freeze-drying	After the second freeze-drying step under the same conditions as the first one, porous HA/coll-gels were obtained with the following sizes: i) from 48 well plates: h = 1.1 mm, $\varnothing$ = 8.5 mm; ii) from 96 well plates: h = 5 mm, $\varnothing$ = 4 mm; iii) from silicon casting molds: h = 3.3 mm, $\varnothing$ = 5 mm; iv) from glass cover slides after punching with a biopsy punch: h = 0.2 mm, $\varnothing$ = 3 mm.

**Tab. 3.11 Composition of 1 ml aqueous acrylated polymer mixture.**

Hydrogel	HA-AC	sGAG-AC	Collagen
HA-AC	10 mg	-	-
HA-AC/coll	10 mg	-	0.5 mg
HA-AC/CS/coll	7.5 mg	2.5 mg	0.5 mg
HA-AC/sHA1/coll	7.5 mg	2.5 mg	0.5 mg
HA-AC/sHA1Δ6s/coll	7.5 mg	2.5 mg	0.5 mg

### 3.4 Analytical and further methods

GAGs are polydisperse macromolecules differing in their sugar chain length as well as their molecular weight according to their net amount of substitute residues (e.g. sulfate groups). To compare similar numbers of potential GAG binding sites, equal molar concentrations related to the molecular weight of the respective GAG D.U. were used in all following experimental analyses if not stated otherwise.

#### 3.4.1 Immobilization of GAGs on polystyrene surfaces

##### *Preparation of solutions*

*1% adipic acid dihydrazide solution:* 200 mg adipic acid dihydrazide were dissolved in 20 ml water. This solution should always be prepared freshly.

*0.5% methyl vinyl ether/maleic acid copolymer solution:* 75 mg methyl vinyl ether/maleic acid copolymer were dissolved in 15 ml DMSO. This solution should be made freshly before usage.

*25 mM citric acid phosphate buffer (pH 5.0):* 480.3 mg citric acid and 445 mg Na<sub>2</sub>HPO<sub>4</sub> · H<sub>2</sub>O were dissolved in 80 ml water. The pH was adjusted to 5.0 by adding 3 N NaOH prior to adjusting the volume to 100 ml in a volumetric flask.

*1% sodium cyanoborohydride solution:* 20 mg NaBH<sub>3</sub>CN were freshly dissolved in 2 ml methanol.

*Tris buffered saline (TBS) buffer (10 mM Tris-HCl, 50 mM NaCl, pH 7.4):* 121 mg Tris-base and 292 mg NaCl were dissolved in 80 ml water, the pH was adjusted to 7.4 via the addition of 6 M and 1 M HCl and water was added to reach a final volume of 100 ml in a volumetric flask.

*2% BSA in TBS buffer:* 100 mg BSA were freshly dissolved in 5 ml TBS buffer before use.

*1% BSA in phosphate buffered saline (PBS) buffer:* 150 mg BSA were dissolved in 15 ml PBS. This solution should be made freshly each day.

To assess the binding of solute mediator proteins to GAG-coated surfaces or the degradation of immobilized HA, GAGs were immobilized according to the following protocols.

### ***Covalent immobilization of GAGs via their reducing ends***

The immobilization of GAGs was performed as previously described [59,409]. To introduce acid anhydride groups onto polystyrene surfaces (96 well plates Maxi-Sorp™ or 24 well plates) 0.5% methyl vinyl ether/maleic acid copolymer dissolved in DMSO was added for 30 min, followed by a treatment with 1% adipic acid dihydrazide for 150 min to functionalize the plate with hydrazine groups.

Afterwards, the plates were washed three times with water before incubating them overnight at 4°C with 2.5 mM D.U. GAGs dissolved in phosphate buffer containing 25 mM citric acid (pH 5.0). The formyl groups of the reducing end of the GAGs then react with hydrazine groups on the surfaces. The next day the formed Schiff's bases were reduced by adding 1% sodium cyanoborohydride dissolved in methanol for 30 min via reductive amination. Before use, the GAG-coated surfaces were washed with Tris-buffered saline (TBS, 10 mM Tris-HCl, 50 mM NaCl, pH 7.4). Non-specific interactions were blocked via the incubation with 2% BSA in TBS for 120 min.

### ***Immobilization of biotinylated GAGs to neutravidin-coated surfaces***

Biotinylated GAGs were immobilized to neutravidin coated 96 well ELISA plates, which were pre-treated with 100 µl of 10 µg/ml neutravidin dissolved in PBS overnight at 4°C and washed with 0.05% Tween 20 in PBS for three times as described in [315]. 50 µl of a 2.5 mM D.U. GAG solution in PBS was added per well and incubated at RT for 120 min. Afterwards the wells were washed thrice with 0.05% Tween 20 in PBS and blocked with 2% BSA in PBS for 120 min.

## **3.4.2 Binding of mediator proteins to GAG-coated surfaces**

### ***Preparation of solutions***

*TIMP-3 solutions:* A 100 µg/ml TIMP-3 stock solution was diluted with 1% BSA in PBS to obtain 1.8 nM TIMP-3 as final concentration.

*VEGF-A solutions:* A 100 µg/ml VEGF-A<sub>165</sub> stock solution was diluted with 1% BSA in PBS to obtain 1.8 nM VEGF-A.

*Lysozyme solution:* The 1000 µg/ml Rhodamine B labeled lysozyme stock solution was 1:500 diluted with 2% BSA in PBS to achieve a concentration of 140 nM lysozyme.

### ***Interaction of proteins with GAG-surfaces***

The binding capacity of GAG-coated surfaces (section 3.4.1) was determined after incubation of the GAG-containing wells with the respective protein (TIMP-3, VEGF-A, and fluorescence-labeled lysozyme) overnight at 4°C. Competitive GAG-binding studies between TIMP-3 and VEGF-A were performed with biotinylated HA and sHA3 immobilized to neutravidin-coated wells of a 96 well plate, while the binding of TIMP-3 or VEGF-A was studied with GAGs covalently immobilized via their reducing ends in wells of a 96 well plate. Since the detection



of fluorescence-labeled lysozyme requires significantly higher protein amounts compared to the quantification via ELISA, wells of a 24 well plate with covalently immobilized GAGs were used to examine their interaction with lysozyme. The added volume of the respective protein solution was 100  $\mu\text{l}$  per well of a 96 well plate, while 300  $\mu\text{l}$  were used for wells of a 24 well plate.

The supernatants were analyzed via sandwich-ELISA (section 3.4.4) to quantify the amounts of TIMP-3 and VEGF-A that were not bound to GAGs, while the intensity of the fluorescence signal ( $\lambda_{\text{ex}} = 544 \text{ nm}$ ,  $\lambda_{\text{em}} = 576 \text{ nm}$ ) was used to measure the amount of lysozyme in the supernatants.

### 3.4.3 Binding of lysozyme or VEGF-A to hydrogels

#### *Preparation of solutions*

*2% BSA in PBS:* 20 mg BSA were dissolved in 1 ml PBS prior to use.

*Lysozyme in 2% BSA/PBS (8  $\mu\text{g}/\text{ml}$ ):* The 1000  $\mu\text{g}/\text{ml}$  Rhodamine B labeled lysozyme stock solution was diluted with 2% BSA in PBS to obtain a concentration of 8  $\mu\text{g}/\text{ml}$  lysozyme.

*1% BSA in PBS:* 10 mg BSA were freshly dissolved in 1 ml PBS.

*VEGF-A solution (500 ng/ml):* A 100  $\mu\text{g}/\text{ml}$  VEGF-A stock solution was diluted 1:200 with 1% BSA in PBS to achieve a final concentration of 500 ng/ml.

*Hyal solution (1600 U/ml):* A Hyal solution of 1600 U/ml in PBS was freshly prepared prior to use.

#### *Binding and release of lysozyme*

Freeze-dried gels with a diameter of 4 mm and a height of 5 mm prepared from 200  $\mu\text{l}$  polymer mixture in 96 well plates were used. The gels were incubated with 500  $\mu\text{l}$  8  $\mu\text{g}/\text{ml}$  Rhodamine B labeled lysozyme in 2% BSA/PBS overnight at 4°C. Afterwards, 250  $\mu\text{l}$  of the supernatants were collected and replaced by 250  $\mu\text{l}$  freshly prepared 2% BSA/PBS. Then the hydrogels were incubated at 37°C under constant shaking (125 rpm) and the supernatants were collected at different time points (1 h, 4 h, 24 h, 192 h) and stored at 4°C in the dark until analysis. The amount of non-bound lysozyme in the supernatants was determined by measuring the fluorescence intensity ( $\lambda_{\text{ex}} = 544 \text{ nm}$ ,  $\lambda_{\text{em}} = 576 \text{ nm}$ ) relative to a lysozyme calibration curve. To calculate the amounts of hydrogel-bound lysozyme, the determined lysozyme values in the supernatants were subtracted from the initially used lysozyme concentration.

#### *Binding and release of VEGF-A*

Gels with a diameter of 3 mm and a height of 0.2 mm were obtained from freeze-dried gels prepared with 50  $\mu\text{l}$  polymer solution between two glass discs ( $\text{\O} 12 \text{ mm}$ ) using a biopsy punch. The gels were incubated with 400  $\mu\text{l}$  500 ng/ml VEGF-A in 1% BSA/PBS overnight at 37°C prior to replacing the supernatant by 400  $\mu\text{l}$  freshly prepared 1% BSA/PBS solution. The

supernatants were collected at each time point (initial, 1 h, 1 d, 8 d, 21 d, 30 d), stored at  $-80^{\circ}\text{C}$  until VEGF-A quantification by ELISA (section 3.4.4) and replaced by  $400\ \mu\text{l}$  1% BSA/PBS after the respective incubation times. After 30 days of incubation, the gels were degraded in  $200\ \mu\text{l}$  1600 U/ml hyaluronidase solution and the obtained solution was analyzed via VEGF-A ELISA as well. The initial amount of VEGF-A bound to the gels was calculated by adding up the remaining VEGF-A amount in the gels after 30 days of incubation and the released amounts of VEGF-A over time.

#### **3.4.4 Quantification of TIMP-3 and VEGF-A via ELISA**

The amount of solute TIMP-3 or solute VEGF-A was quantified via Sandwich-ELISA using specific antibodies according to the manufacturer's protocols (R&D Systems). TIMP-3 and VEGF-A concentrations ranging from 62.5 pg/ml to 4000 pg/ml in 1% BSA/PBS were used as standards for quantification.

##### ***Preparation of solutions***

*Mouse anti-human TIMP-3 capture antibody stock solution:* 360  $\mu\text{g}$  lyophilized TIMP-3 capture antibody were dissolved in 1 ml PBS to a final concentration of 360  $\mu\text{g}/\text{ml}$  according to the manufacturer's instructions and 55.5  $\mu\text{l}$  aliquots were stored at  $-80^{\circ}\text{C}$ .

*Biotinylated mouse anti-human TIMP-3 detection antibody stock solution:* 360  $\mu\text{g}$  lyophilized TIMP-3 detection antibody were dissolved in 1 ml 1% BSA in PBS to a final concentration of 360  $\mu\text{g}/\text{ml}$  according to the manufacturer's protocol and 55.5  $\mu\text{l}$  aliquots were stored at  $-80^{\circ}\text{C}$ .

*Mouse anti-human TIMP-3 capture antibody solution:* The stock solution was 1:180 diluted to achieve a concentration of 2  $\mu\text{g}/\text{ml}$  in PBS.

*Biotinylated mouse anti-human TIMP-3 detection antibody solution:* The stock solution was 1:180 diluted to obtain a concentration of 2  $\mu\text{g}/\text{ml}$  with 1% BSA in PBS.

*Mouse anti-human VEGF capture antibody stock solution:* 500  $\mu\text{g}$  lyophilized VEGF capture antibody were dissolved in 1 ml PBS to receive a final concentration of 500  $\mu\text{g}/\text{ml}$  according to the manufacturer's instructions and 20  $\mu\text{l}$  aliquots were stored at  $-80^{\circ}\text{C}$ .

*Biotinylated goat anti-human VEGF detection antibody stock solution:* 50  $\mu\text{g}$  lyophilized VEGF detection antibody were dissolved in 250  $\mu\text{l}$  PBS to obtain a final concentration of 200  $\mu\text{g}/\text{ml}$  according to the manufacturer's protocol and 5  $\mu\text{l}$  aliquots were stored at  $-80^{\circ}\text{C}$ .

*Mouse anti-human VEGF capture antibody solution:* The stock solution was 1:500 diluted to achieve a concentration of 1  $\mu\text{g}/\text{ml}$  in PBS.

*Biotinylated goat anti-human VEGF detection antibody solution:* The stock solution was 1:2000 diluted to obtain a concentration of 0.1  $\mu\text{g}/\text{ml}$  with 1% BSA in PBS.

*Wash buffer (0.05% Tween 20 in PBS, pH 7.4):* 250 µl Tween 20 was added to 400 ml PBS and the volume was adjusted to 500 ml with PBS in a volumetric flask.

*Reagent diluent (1% BSA in PBS, pH 7.4):* 500 mg BSA were freshly dissolved in 50 ml PBS.

*Streptavidin-HRP working dilution:* The streptavidin-HRP stock solution was diluted 1:200 with reagent diluent prior to use.

*Stop solution (1 M H<sub>2</sub>SO<sub>4</sub>):* 56 ml concentrated H<sub>2</sub>SO<sub>4</sub> was diluted with water to a final volume of 1000 ml in a volumetric flask.

### ***Plate preparation***

100 µl of the respective capture antibody solution was added per well of a 96 well ELISA plate. The sealed plate was incubated overnight at RT. The next day the supernatants were removed and each well was washed three times with 300 µl wash buffer. The nonspecific binding sites were blocked for 60 min by incubation with 300 µl reagent diluent per well. Afterwards, the wells were washed thrice.

### ***ELISA procedure***

100 µl sample or standard solution was added per well and incubated for 120 min at RT. Then the wells were washed three times with wash buffer (300 µl) prior to the incubation with 100 µl detection antibody solution for 120 min. After three washing steps with wash buffer, 100 µl diluted streptavidin-HRP solution was added to each well and incubated in the dark for 20 min. The wells were washed again three times with wash buffer, and then 100 µl substrate solution (3,3',5,5'-tetramethyl-benzidine) was added per well. The plates were incubated in the dark for 5 min - 20 min at RT before stopping the reaction by the addition of 50 µl stop solution. The absorbance was measured at 490 nm.

### **3.4.5 HA degradation via Hyal in the presence of GAGs**

A direct ELISA was used to detect the remaining amounts of immobilized HA in transparent 96 well plates after incubation with hyaluronidase in the absence or presence of GAGs. The degradation of HA was calculated relative to the absorbance of the non-degraded HA control wells during ELISA.

### ***Preparation of solutions***

*Hyal solution:* Hyal solutions of 0.02 U/ml in PBS were freshly prepared each day prior to usage.

*2M NaCl solution:* 11.688 g NaCl were dissolved in 80 ml water and the volume was adjusted to 100 ml in a volumetric flask.

*Biotinylated HA detection reagent stock solution:* 24 µg lyophilized biotinylated recombinant human aggrecan were dissolved in 250 µl PBS to a final concentration of 96 µg/ml according to the manufacturer's instructions and 25 µl aliquots were stored at -80°C.

*Biotinylated HA detection reagent working solution:* The HA detection reagent stock solution was diluted with 1% BSA/PBS to achieve a final concentration of 400 ng/ml directly prior to use.

#### ***Plate preparation***

Native HA was covalently immobilized via its reducing ends in 96 well ELISA plates by adding 100  $\mu$ l 2.5 mM D.U. GAG solution per well as described in section 3.4.1.

#### ***HA degradation via Hyal***

For HA degradation 50  $\mu$ l 0.02 U/ml Hyal solution with or without 2.5 mM D.U. solute GAG was added to each well and the plate was incubated at 37°C for 30 or 120 min. After the respective time points, the supernatants were discarded and the wells were washed three times with PBS and thrice with 2 M NaCl. Wells incubated with PBS without Hyal, served as control.

#### ***Quantification of remaining HA via ELISA***

100  $\mu$ l HA detection reagent solution was added to each well for 120 min. After aspirating this solution the wells were washed with wash buffer (3x), prior to adding 100  $\mu$ l diluted streptavidin-HRP solution per well and incubation of the plate in the dark for 20 min. The wells were washed again (3x) with wash buffer, then 100  $\mu$ l substrate solution (3,3',5,5'-tetramethylbenzidine) was added to each well. After 5 - 10 min of incubation protected from light the reaction was stopped with 50  $\mu$ l 1 M H<sub>2</sub>SO<sub>4</sub> per well and the absorbance at 490 nm was measured.

### **3.4.6 Enzyme kinetic analysis**

#### ***Preparation of solutions***

*Assay buffer for MMP catalytic domains (50 mM HEPES, 10 mM CaCl<sub>2</sub>, 0.05% Brij-L23, pH 7.5):* 50 mg Brij-L23, 1.192 g HEPES and 147 mg CaCl<sub>2</sub> · H<sub>2</sub>O were dissolved in 80 ml water. The pH was adjusted to 7.5 via the addition of 1 M NaOH. Afterwards, the solution was transferred to a 100 ml volumetric flask and the volume was adjusted to 100 ml with water. The solution was filtered (0.02  $\mu$ m) and stored at RT until usage.

*TIMP buffer - assay buffer for full-length MMPs (50 mM Tris, 10 mM CaCl<sub>2</sub>, 150 mM NaCl, 0.05% Brij-L23, pH 7.5):* 50 mg Brij-L23, 605.7 mg Tris, 147 mg CaCl<sub>2</sub> · 2H<sub>2</sub>O and 876.6 mg NaCl were dissolved in 80 ml water. After adjusting the pH to 7.5 by the addition of 0.5 M HCl, the solution was transferred to a 100 ml volumetric flask and the volume was adjusted to 100 ml with water. The solution was filtered (0.02  $\mu$ m) and stored at RT until usage.

*100 mM APMA stock solution:* 0.3908 g APMA (4-Aminophenylmercuric acetate) dissolved in DMSO were adjusted to 10 ml in a 10 ml volumetric flask with DMSO. Aliquots of 200  $\mu$ l were prepared in 0.65 ml low binding tubes and stored at -20°C until use.

*1.3 mM NNGH stock solution:* 5 mg NNGH were dissolved in 12.165 ml DMSO to a final concentration of 411  $\mu$ g/ml and stored in aliquots at -80°C.

400  $\mu\text{M}$  OmniMMP<sup>TM</sup> fluorogenic substrate stock solution: 1 mg OmniMMP<sup>TM</sup> fluorogenic substrate was dissolved in 2.288 ml DMSO (437  $\mu\text{g}/\text{ml}$ ) and 200  $\mu\text{l}$  aliquots of this solution were stored at  $-80^\circ\text{C}$  in the dark until usage.

#### **Performance of the MMP kinetic analysis**

The remaining enzyme activity of full-length MMP-1 and MMP-2 after allosteric activation with APMA according to R&D Systems (Tab. 3.12) and the corresponding catalytic domains was determined by measuring the increase of the fluorescence signal ( $\lambda_{\text{ex}}$ : 328 nm,  $\lambda_{\text{em}}$ : 420 nm) over time, represented by the cleavage of a fluorescent substrate peptide (Mca-Pro-Leu-Dpa-Ala-Arg-NH<sub>2</sub> [Mca: (7-methoxycoumarin-4-yl)-acetyl, Dpa: *N*-3-(2,4-dinitrophenyl)-L- $\alpha$ - $\beta$ -diamino-propionyl]). Enzyme kinetics were performed for 10 min with 30 sec time intervals in white half-area 96 well plates after 60 min of MMP incubation with the respective GAG solution or with preformed TIMP-3/GAG complexes at  $37^\circ\text{C}$  according to the manufacturer's protocol (Enzo Life Science) and Tab. 3.13.

**Tab. 3.12 Activation of proMMP-1 and proMMP-2 via APMA.**

Step	Activation of proMMP-1	Activation of proMMP-2
1	Dilution of proMMP-1 to 50 $\mu\text{g}/\text{ml}$ in assay buffer	Dilution of proMMP-2 to 100 $\mu\text{g}/\text{ml}$ in assay buffer
2	Addition of 100 mM APMA to obtain a final concentration of 1 mM APMA in solution	
3	Incubation for 120 min at $37^\circ\text{C}$	Incubation for 60 min at $37^\circ\text{C}$
4	Dilution of the activated full-length MMP with assay buffer to 38.48 nM (2 ng/ $\mu\text{l}$ MMP-1, 2.73 ng/ $\mu\text{l}$ MMP-2)	
5	Immediate performance of enzyme kinetic analysis with 3.8 nM activated MMP	

The remaining enzyme activity was calculated from the slope of a linear regression curve in which the increase of the fluorescence signal over time was linear relative to the negative control buffer without GAGs or TIMP-3 representing 100% enzyme activity. 10  $\mu\text{l}$  6.5  $\mu\text{M}$  NNGH served as positive control for inhibition and the final volume within the assay was adjusted to 90  $\mu\text{l}$  via the addition of assay buffer prior to the addition of the substrate peptide.

**Tab. 3.13 Scheme for the performance of MMP kinetic analysis.** The respective solutions were added in the described order.

Step	Kinetics with catalytic domains of MMPs	Kinetics with activated full-length MMPs	Kinetics with activated MMPs and TIMP-3
1	20 $\mu\text{l}$ 12.5 - 125 mM D.U. GAG		20 $\mu\text{l}$ 12.5 mM D.U.
2		---	10 $\mu\text{l}$ 50 nM or 25 nM TIMP-3 for MMP-1 or -2
3	50 $\mu\text{l}$ assay buffer for MMP catalytic domains	60 $\mu\text{l}$ assay buffer for full-length MMPs	50 $\mu\text{l}$ assay buffer for full-length MMPs

Step	Kinetics with catalytic domains of MMPs	Kinetics with activated full-length MMPs	Kinetics with activated MMPs and TIMP-3
4		w/o incubation	Incubation for 30 min at 37°C
5	20 $\mu$ l 0.450 U*/ $\mu$ l catalytic domain of MMP-1/-2	10 $\mu$ l 38.48 nM activated full-length MMP-1/-2**	
6		Incubation for 60 min at 37°C	
7	Addition of 10 $\mu$ l 40 $\mu$ M fluorescent substrate peptide and start of fluorescence measurement		

\*1 U = 100 pmol/min at 37°C using the Ac-Pro-Leu-Gly-S-Leu-Leu-Gly-OEt as substrate according to certificate of analysis (Enzo Life Science); \*\*Equal nM concentrations instead of activities were used in case of activated full-length MMPs since the activity U of the activated full-length MMPs could not be determined like for the catalytic domains due to the interference of APMA with the substrate Ac-Pro-Leu-Gly-S-Leu-Leu-Gly-OEt [410].

### 3.4.7 Surface plasmon resonance (SPR)

Molecular interaction analysis in real time was performed with a Biacore T100 instrument.

#### *Preparation of solutions*

All solutions used within SPR measurements were prepared with ultra pure water and filtered (0.22  $\mu$ m) if not stated otherwise.

*HBS-EP buffer (0.01 M HEPES, 0.15 M NaCl, 3 mM EDTA, 0.005% surfactant P20, pH 7.4):* The commercially available HBS-EP stock solution (GE Healthcare) was diluted 1:10 with water for the preparation of the running buffer.

*391.2 mM EDC solution:* 750 mg EDC were dissolved in 10 ml water and aliquots (110  $\mu$ l) were kept at -20°C until usage.

*100 mM NHS solution:* 115 mg NHS were dissolved in 10 ml water and aliquots of 110  $\mu$ l were stored at -20°C until use.

*1 M ethanolamine-HCl-NaOH (pH 8.5):* 4.88 g ethanolamine-HCl were dissolved in 40 ml water and the pH was adjusted to 8.5 by adding 1 M NaOH prior to transferring this solution to a 50 ml volumetric flask and adjusting the volume with water. The solution was aliquoted (1 ml) and stored at -20°C.

*1 M HCl regeneration stock solution:* 4.1404 ml HCl (37%) were added to about 40 ml water before adjusting the volume to 50 ml in a volumetric flask with water.

*5 M NaCl regeneration solution:* 14.61 g NaCl were dissolved in about 40 ml water prior to bringing the volume to 50 ml in a volumetric flask.

*Conditioning solution for C1 sensor chips (100 mM glycine-NaOH with 0.3% Triton X-100, pH 12):* 375 mg glycine were dissolved in about 40 ml water, the pH was adjusted to 12 with

NaOH (4 M, 1 M) prior to adding 160.5 mg Triton X-100 and bringing the volume to 50 ml in a volumetric flask.

*BIAdesorb solution 1 (0.5% SDS):* 2.50 ml SDS were dissolved in about 80 ml water before adjusting the volume to 100 ml in a volumetric flask.

*BIAdesorb solution 2 (50 mM glycine-NaOH, pH 9.5):* 375 mg glycine were dissolved in about 80 ml water, the pH was adjusted to 9.5 with NaOH (1 M, 0.5 M) prior to volume adjustment to 100 ml in a volumetric flask. This solution was stored at 4°C until use.

*BIAdisinfecant solution (sodium hypochloride with 0.7 - 1% active chloride):* 3 ml sodium hypochloride (10 - 15% active chloride) were mixed with 40 ml water.

*LRP-1 cluster II stock solution:* 50 µg lyophilized LRP-1 cluster II were dissolved in 100 µl PBS to a final concentration of 500 µg/ml according to the manufacturer's instructions and aliquots (1 - 5 µl) were stored at -80°C.

*LRP-1 cluster IV stock solution:* 50 µg lyophilized LRP-1 cluster IV were dissolved in 500 µl PBS to a final concentration of 100 µg/ml according to the manufacturer's instructions and aliquots (2 - 10 µl) were stored at -80°C.

*TIMP-3 stock solution:* Lyophilized TIMP-3 was dissolved in water to a final concentration of 100 µg/ml according to the manufacturer and aliquots (1 - 3 µl) were stored at -80°C.

*VEGFR-2 stock solution:* 50 µg lyophilized VEGFR-2 were dissolved in PBS to a final concentration of 100 µg/ml according to the manufacturer's instructions and aliquots (2 - 10 µl) were stored at -80°C.

#### ***Immobilization of ligands on the sensor chip surface***

The amine coupling reaction according to the manufacturer's instructions (GE Healthcare Europe GmbH, Freiburg, Germany) at 25°C was used to covalently immobilize the respective protein on the sensor chip surfaces. The surfaces of C1 sensor chips were washed twice with 100 mM glycine-NaOH (pH 12) containing 0.3% Triton X-100 for 60 sec each before ligand immobilization.

The carboxyl groups on the SPR sensor chip surfaces (100 nm carboxymethylated dextran matrix on CM5 sensor chips, matrix-free carboxymethylated surface on C1 sensor chips) were transferred to active esters via the injection of a mixture containing 195.6 mM EDC and 50 mM NHS for 420 sec at a flow rate of 10 µl/min of the running buffer. Immediately after this the proteins were randomly immobilized via their primary amine groups by injecting them according to the conditions given in Tab. 3.14. Afterwards 1 M ethanolamine-HCl-NaOH (pH 8.5) was injected for 420 sec with a flow rate of 10 µl/min to react with excessive reactive groups on the chip surface. A flow cell treated with EDC/NHS and ethanolamine without immobilized protein served as reference.

**Tab. 3.14 Immobilization conditions used for the different SPR measurements.**

Studied interaction	Ligand*	Sensor chip	Immobilization conditions	Immobilization level (RU)
Polymeric GAG/TIMP-3	TIMP-3	CM5	120 sec, 5 $\mu$ l/min, 10 $\mu$ g/ml in acetate buffer (pH 4.5)	830
Oligomeric GAG/TIMP-3	TIMP-3	CM5	120 sec, 5 $\mu$ l/min, 50 $\mu$ g/ml in acetate buffer (pH 4.5)	4700
GAG/VEGF-A	VEGF-A	CM5	120 sec, 5 $\mu$ l/min, 10 $\mu$ g/ml in acetate buffer (pH 5.5)	5000 - 6500
TIMP-3/GAG with LRP-1 cluster II	LRP-1 cluster II	CM5	120 sec, 5 $\mu$ l/min, 12.5 $\mu$ g/ml in acetate buffer (pH 4.5)	500
TIMP-3/GAG with LRP-1 cluster IV	LRP-1 cluster IV	CM5	120 sec, 5 $\mu$ l/min, 12.5 $\mu$ g/ml in acetate buffer (pH 4.5)	380
TIMP-3/VEGFR-2	TIMP-3	C1	120 sec, 5 $\mu$ l/min, 10 $\mu$ g/ml in acetate buffer (pH 4.5)	140
VEGF-A/VEGFR-2	VEGF-A	C1	40 sec, 5 $\mu$ l/min, 0.7 $\mu$ g/ml in acetate buffer (pH 5.5)	30
TIMP-3/VEGF-A/GAG with VEGFR-2	VEGFR-2	C1	120 sec, 5 $\mu$ l/min, 80 $\mu$ g/ml in acetate buffer (pH 4.0)	50

\*Immobilized interaction partner on the sensor chip surface

### ***Performance of SPR measurements***

Sensorgrams as plots of the resonance signal in RU (resonance units) over time were used to trace the association, dissociation as well as kinetics of interactions. All SPR analyses were performed at 37°C using a flow rate of 30  $\mu$ l/min of the respective running buffer. Tab. 3.15 summarizes the specific analysis and regeneration conditions for each examined interaction. In case of competitive SPR experiments, the mediator proteins were pre-incubated with GAGs for 1 h prior to analysis. GAG solutions and protein solutions were injected after a defined number of interaction analyses as controls to ensure a continuous binding capacity of the immobilized ligand. Prior to injection the sample solutions were stored at 12°C in the Biacore sample compartment to maintain the protein activity.

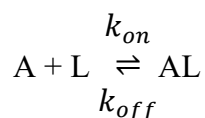


**Tab. 3.15 Analysis and regeneration conditions of the different SPR measurements.**

Studied interaction	Analysis conditions	Regeneration
GAG/TIMP-3	Binding analysis, running buffer: TIMP buffer, 100 - 600 $\mu$ M D.U. polymeric GAGs, 10 - 500 $\mu$ M D.U. oligomeric GAGs, 300 sec analyte injection, 600 sec dissociation phase	1. 5 M NaCl (60 sec, 30 $\mu$ l/min), 2. 1000 sec stabilization
GAG/VEGF-A	Binding analysis, running buffer: HBS-EP, 10 nM D.U. GAG, 300 sec analyte injection, 600 sec dissociation phase	1. 60 mM HCl (200 sec, 5 $\mu$ l/min), 2. 5 M NaCl (60 sec, 30 $\mu$ l/min), 3. 1000 sec stabilization
TIMP-3/LRP-1 cluster II or IV	Single cycle kinetics, running buffer: TIMP buffer, 12.5 - 200 nM TIMP-3, 220 sec analyte injection, 1000 sec dissociation phase	1. 5 M NaCl (60 sec, 30 $\mu$ l/min), 2. 1000 sec stabilization
TIMP-3/VEGFR-2	Single cycle kinetics, running buffer: HBS-EP, 1.58 - 25.25 nM VEGFR-2, 240 sec analyte injection, 600 sec dissociation phase	1. 60 mM HCl (200 sec, 5 $\mu$ l/min), 2. 5 M NaCl (60 sec, 30 $\mu$ l/min), 3. 1000 sec stabilization
VEGF-A/VEGFR-2	Single cycle kinetics, running buffer: HBS-EP, 0.44 - 7.10 nM VEGFR-2, 240 sec analyte injection, 600 sec dissociation phase	1. 60 mM HCl (200 sec, 5 $\mu$ l/min), 2. 5 M NaCl (60 sec, 30 $\mu$ l/min), 3. 1000 sec stabilization
TIMP-3/VEGF- A/GAG with VEGFR-2	Binding analysis, running buffer: HBS-EP, 20 - 100 nM TIMP-3, 20 nM VEGF-A, 20 - 100 $\mu$ M D.U. polymeric GAGs, 40 - 80 $\mu$ M D.U. oligomeric GAGs, 120 sec analyte injection, 600 sec dissociation	1. 60 mM HCl (200 sec, 5 $\mu$ l/min), 2. 5 M NaCl (60 sec, 30 $\mu$ l/min), 3. 1000 sec stabilization
Sequential binding of 1. TIMP-3, 2. sHA3, 3. VEGF-A or 1. VEGF-A, 2. sHA3, 3. TIMP-3 to VEGFR-2	Sequential binding analysis, running buffer: HBS-EP, 40 nM VEGF-A or TIMP-3, 40 $\mu$ M D.U. sHA3, 120 sec analyte injection, 30 sec dissociation without regeneration after the first two injections, 600 sec dissociation after the third injection	1. 60 mM HCl (200 sec, 5 $\mu$ l/min), 2. 5 M NaCl (60 sec, 30 $\mu$ l/min), 3. 1000 sec stabilization

The Biacore T100 evaluation software 2.03 was used to study the potential binding of analytes to immobilized ligands and to determine specific interaction parameters. The binding levels were measured 10 sec before the end of analyte injection. The sensorgram adjustment relative to the baseline as well as to the running buffer after subtraction of the reference surface without immobilized ligand was conducted according to the literature to improve the sensorgram quality [411]. In some cases, the binding was normalized relative to the binding response of the highest concentration of sHA3 to enable a ranking between measurements with different immobilization levels or between measurements where no complete regeneration of the ligand binding capacity could be achieved after the regeneration step.

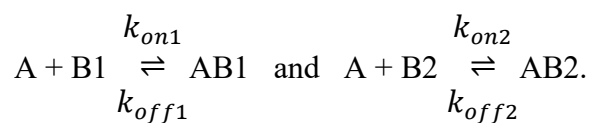
After performing single cycle kinetic analyses the kinetic parameters were determined by fitting the measured data to the heterogeneous ligand model in case of LRP-1 or to a 1:1 Langmuir binding fitting model in case of VEGFR-2 via the Biacore evaluation software 2.03. The 1:1 Langmuir binding model describes the simplest interaction where one analyte A in solution interacts with one immobilized ligand L, thereby forming the complex AL:



with  $k_{on}$  representing the association rate constant, which describes the number of formed complexes per time, and  $k_{off}$  being the dissociation rate constant that reflects the stability of the complex. At equilibrium, the concentration-independent equilibrium dissociation constant  $K_D$  can be determined according to this formula:

$$K_D = \frac{k_{off}}{k_{on}}.$$

The heterogeneous ligand model can be used for more complex binding interactions where the same solute analyte A interacts with two independent binding sites B1 and B2 of one ligand:



To validate the obtained parameters,  $\chi^2$  was calculated as statistical parameter for assessing the quality of the fitted model according to this formula:

$$\chi^2 = \frac{\sum_1^n (r_f - r_x)^2}{n-p}$$

with  $r_f$  representing the fitted value at a particular point,  $r_x$  being the experimental value at this point, n reflecting the number of data points and p giving the number of fitted parameters. This parameter can be used to assess how well the fitted curve coincides with the measured data. Low values indicate a good agreement. Furthermore, the significance of the determined  $K_D$  values for the 1:1 Langmuir binding fitting model was determined via the corresponding standard error calculated by the Biacore evaluation software.

### ***Cleaning routine and maintenance of the system***

The “Desorb” program was performed weekly, while the “Desorb and Sanitize” cleaning program was conducted every four weeks according to the manufacturer’s instructions to ensure optimal system performance.

### **3.4.8 Enzymatic degradation of aECMs via collagenase**

The degradability of collagen-based aECM coatings can be studied *in vitro* by incubating the matrices with bacterial collagenase (ChC). The amount of degraded matrix could be quantified by determining the protein concentration in the supernatant using the method of Lowry (section 3.4.11).

#### ***Preparation of solutions***

*ChC solution:* ChC was freshly dissolved in PBS (1x) to a final concentration of 500 µg/ml. Prior to use, the ChC solution was incubated for 15 min at 37°C.

#### ***Performance of the enzymatic degradation of aECMs***

Collagen-based coatings were prepared in 24 well plates as described in section 3.3.1. Prior to use the aECMs were washed two times with water and incubated with PBS for 60 min at 37°C to remove non-associated GAGs. 400 µl PBS was added per well prior to incubation of the matrices for 30 min at 37°C. Afterwards 100 µl ChC solution was added (0.02 U per well) and the matrices were incubated for up to 180 min at 37°C under constant shaking (50 rpm). Matrices incubated with 500 µl PBS without ChC served as controls. At the respective time points the supernatants were collected on ice and stored at 4°C until usage for the Lowry assay.

### **3.4.9 Qualitative analysis of collagen - Sirius red staining**

The interaction of the anionic dye Sirius red with basic groups of the collagen molecule [412] was used to visualize the collagen content of 2.5D and 3D aECMs as reported previously [350].

#### ***Preparation of solutions***

*Sirius red staining solution (0.1% in saturated picric acid):* 10 mg Sirius red were dissolved in 10 ml saturated picric acid. The solution could be stored in the dark for several months.

*Wash solution (0.01 M HCl):* 1 ml 1 M HCl was diluted with water to a final volume of 100 ml in a volumetric flask.

#### ***Staining of collagen***

500 µl Sirius red staining solution were added to each aECM-coated well or hydrogel in a 24 well plate and incubated for 30 min at RT. Unbound dye was removed by washing the wells 3 - 4 times with wash solution until the supernatant remains colorless. Afterwards the stained collagen was documented via a camera.

### 3.4.10 Qualitative analysis of sulfated glycosaminoglycans - Toluidine blue staining

The cationic dye Toluidine blue interacts with anionic residues of proteoglycans and GAGs leading to the formation of a blue-colored complex [413]. However, non-sulfated HA cannot be visualized by Toluidine blue staining [414].

#### *Preparation of solutions*

*Toluidine blue staining solution (0.04% in 0.1 M HCl containing 2 mg/ml NaCl):* 20 mg Toluidine blue and 100 mg NaCl were dissolved in 40 ml of water prior to the addition of 5 ml 1 M HCl and adjusting the volume with water to 50 ml in a volumetric flask.

#### *Staining of sulfated GAGs*

500  $\mu$ l Toluidine blue staining solution was added per aECM-coated well or hydrogel in a 24 well plate and incubated for 240 min at RT. Unbound Toluidine blue was removed by washing the wells 3 - 4 times with water. Afterwards pictures of the stained sulfated GAGs were taken with a camera.

### 3.4.11 Quantification of collagen - Lowry assay

The amount of proteins such as collagen can be determined via the method of Lowry [415].

#### *Preparation of solutions*

*2% Na<sub>2</sub>CO<sub>3</sub> in 0.1 M NaOH:* 400 mg NaOH and 2 g Na<sub>2</sub>CO<sub>3</sub> were dissolved in 80 ml water before bringing the volume to 100 ml with water in volumetric flask. The solution can be stored at 4°C for several months.

*0.5% CuSO<sub>4</sub> in 1% sodium citrate:* 50 mg CuSO<sub>4</sub> and 100 mg sodium citrate were dissolved in 8 ml water before bringing the volume to 10 ml with water in volumetric flask. The solution can be stored at 4°C for several months.

*Lowry working solution:* Directly before usage, 1 ml 2% Na<sub>2</sub>CO<sub>3</sub> in 0.1 M NaOH was mixed with 0.5% CuSO<sub>4</sub> in 1% sodium citrate.

#### *Performance of the Lowry assay*

200  $\mu$ l sample solution or collagen standard (8 - 500  $\mu$ g/ml collagen type I dissolved in 10 mM acetic acid) was mixed with 1000  $\mu$ l of the Lowry working solution and incubated for 15 min in the dark. Afterwards 100  $\mu$ l Folin-Ciocalteu's phenol reagent was added and the mixture was incubated for 80 min protected from light. 200  $\mu$ l of these solutions were then transferred to the wells of transparent 96 well plates. The absorbance of the respective solutions was measured at 700 nm.

### 3.4.12 Quantification of sulfated glycosaminoglycans - Dimethylmethylene blue assay

The amount of sulfated GAGs in aECMs was determined by using the specific interaction of the positively charged dye DMMB with negatively charged GAGs [416], which results in the

formation of DMMB/GAG complexes with an absorbance maximum at 525 nm and a decreased intensity of the DMMB peak at 595 nm.

#### ***Preparation of solutions***

*Papain solution (0.1 mg/ml):* 5 mg papain were dissolved in 50 ml PBS at RT for 30 min. The solution should be made freshly each time.

*DMMB solution:* 2.1 mg DMMB were dissolved in 500  $\mu$ l absolute ethanol before mixing with 100 ml 0.2 mg/ml sodium formate solution (pH 1.5). This solution can be stored in the dark at RT for several month.

#### ***Protein degradation via papain***

Interfering matrix proteins like collagen were degraded via papain to release the aECM-bound GAGs prior to their quantification. To this end 500  $\mu$ l papain solution was added per aECM-coated well of a 24 well plate and incubated overnight at 60°C.

#### ***Quantification of sulfated GAGs***

The papain-treated sample solutions were cooled down to RT and mixed. 40  $\mu$ l of sample solution was added per well of a transparent 96 well plate prior to the addition of 200  $\mu$ l DMMB solution. The absorbance was measured immediately at 595 nm. GAG solutions with defined concentrations of the respective GAG (1 - 75  $\mu$ g/ml) in PBS served as calibration standards for quantification.

### **3.4.13 Quantification of glycosaminoglycans - Hexosamine assay**

The Elson-Morgan reaction was used to quantify the amount of GAGs, especially non-sulfated HA in aECMs. Here the *N*-acetylglucosamine as a hexosamine at the reducing end of the GAGs reacts with acetylacetone resulting in the formation of a pyrrole derivative which is able to interact with DMAB. *N*-acetyl-glycosamines can convert to glucoxazole and glucoxoline that can react with DMAB. Via the formation of different chromogens a colored product with an absorption maximum at 586 nm is obtained [417–419].

#### ***Preparation of solutions***

*Acetylacetone solution (4% in 1.25 M Na<sub>2</sub>CO<sub>3</sub>):* 1.324 g Na<sub>2</sub>CO<sub>3</sub> were dissolved in 5 ml water prior to adding 400  $\mu$ l acetylacetone. The volume of this solution was adjusted to 10 ml in a volumetric flask. The solution should be prepared freshly each day.

*DMAB solution (2.66% in 3 M HCl containing 47.5% ethanol):* 266 mg DMAB were dissolved in a mixture of 5 ml 6 M HCl and 5 ml ethanol (95%). The solution should be made freshly.

#### ***Performance of the hexosamine assay***

The GAG content of aECMs was quantified as described in Tab. 3.16. Defined concentrations of the respective GAG dissolved in PBS (1 - 100  $\mu$ g/ml) treated like the samples were used as standards for calibration.

**Tab. 3.16 Sample preparation and performance of the hexosamine assay.**

<b>Step</b>	<b>Procedure of the hexosamine assay</b>
Protein degradation with papain	The collagen matrix was degraded with 0.1 mg/ml papain in PBS as reported for the DMMB assay (section 3.4.12).
Hydrolyses with HCl	200 µl of the sample solution after papain treatment was mixed with 200 µl 12 M HCl and incubated for 6 h at 100 °C.
Drying and neutralization	The samples were cooled on ice after hydrolysis and dried under vacuum over NaOH in a desiccator at 40°C for 120 - 168 h.
Reaction with DMAB	The dried samples were dissolved in 50 µl water prior to adding 250 µl acetylacetone solution and incubating for 60 min at 95°C. 300 µl cooled sample solution was added to 1.25 ml ethanol, mixed with 250 µl DMAB solution and incubated for 60 min at RT.
Photometric measurement	The absorbance of 200 µl solution per well was measured at 540 nm in a transparent 96 well plate.

### 3.4.14 Agarose gel electrophoresis of GAGs

#### *Preparation of solutions*

*Papain solution (0.1 mg/ml):* 5 mg papain were dissolved in 50 ml PBS at RT for 30 min. The solution should be made freshly each time.

*Trichloroacetic acid (100%):* 5 g trichloroacetic acid were dissolved in 2.270 ml water.

*50 mM barium acetate electrophoresis buffer (pH 5.5):* For the preparation of 1 l buffer 12.771 g barium acetate were dissolved in 900 ml water prior to adjusting the pH with glacial acetic acid to 5.5 and adjusting the volume to 1000 ml in a volumetric flask.

*Sample loading solution (0.25% bromophenol blue in 40% glycerol):* 2 ml glycerol were mixed with 3 ml of water before the addition of 12.5 mg bromophenol blue. The solution was stored at 4°C until usage.

*Stains-all staining solution:* 2.5 mg Stains-all were dissolved in 50 ml 50% ethanol and kept in the dark. This solution should be prepared freshly each time.

*Toluidine blue staining solution (0.2%):* 400 mg Toluidine blue were dissolved in 200 ml of a mixture containing ethanol, water and glacial acetic acid (50/49/1, v/v/v). This solution should be made freshly each time.

*Toluidine blue destaining solution:* 250 ml ethanol was mixed with 245 ml water and 5 ml glacial acetic acid.

**Sample preparation**

The aECM-associated GAGs were extracted by ethanol precipitation after matrix degradation with papain (section 3.4.12) and protein removal according to [420]. To this end 400  $\mu$ l 0.1 mg/ml papain in PBS was added to each aECM-coated well of a 24 well plate and incubated for 24 h at 60°C. Then 100% trichloroacetic acid was added to a final concentration of 6% trichloroacetic acid. The proteins were allowed to precipitate for 120 min on ice before centrifugation for 30 min at 4°C with 15000·g. The remaining GAGs in the supernatants were precipitated overnight with 4 times the volume of ethanol at -20°C and obtained after centrifugation (30 min, 4°C, 15000·g). The dried pellets were dissolved in a defined volume of water.

**Performance of the agarose gel electrophoresis**

The separation of GAGs according to their charge was performed as described previously [421] (Tab. 3.17). Images of the stained gels were taken with a camera or a photo scanner. The electrophoretic mobility  $\mu$  of the GAGs was calculated according to:

$$\mu = l \cdot d / t \cdot U$$

with  $l$  defining the migration distance of the GAG in cm,  $d$  representing the distance between the electrodes in cm,  $t$  being the time of electrophoretic separation in hours and  $U$  as voltage in V.

**Tab. 3.17 Sample preparation and performance of the agarose gel electrophoresis.**

Step	GAG separation by their charge
Casting of the gel	A 1% agarose gel (0.5 cm thick) was cast in 50 mM barium acetate buffer (pH 5.5).
Loading of the gel	10 $\mu$ l sample (0.5 mg/ml GAG dissolved in water) were mixed with 3 $\mu$ l sample loading solution. 10 $\mu$ l of this mixture or 5 $\mu$ l HA size marker was loaded per lane.
Running of the gel	60 V for 60 min in 50 mM barium acetate buffer (pH 5.5).
Staining of the gel	For 30 min with Toluidine blue and destained with destaining solution, followed by Stains-all staining

**3.4.15 Determination of the elastic modulus of hydrogels**

Mechanical compression of cylindrical hydrogels ( $h \approx 5$  mm,  $\varnothing \approx 6$  mm) prepared in silicon casting molds was measured at RT directly after photocrosslinking. The uniaxial compression test (0.05 N, compression speed: 10 mm/min) was done with an electromechanical testing system (Instron 5566) using a 2 kg load cell and the Merlin IV software. The linear slope of the stress-strain curves was used to calculate the elastic modulus  $E$ . The following formulas were used to calculate the compressive stress  $\delta$ , the strain  $\varepsilon$  and the elastic modulus  $E$  of the gels:

$$\delta = F_B / A_0$$

$$\varepsilon = \Delta L / L_0$$

$$E = \delta / \varepsilon$$

with  $F_B$  being the maximal force at gel burst,  $A_0$  representing the initial contact area of the hydrogels,  $\Delta L$  defined as way until gel burst and  $L_0$  as initial height of the hydrogel.

#### 3.4.16 Analysis of hydrogel swelling properties and characteristics

To determine the volume loss of the gels during freeze-drying, the diameter and height of the gels were measured before and after freeze-drying using a digital measuring slide. The respective water content of the gels was calculated from their weight after crosslinking in comparison to their mass after lyophilization. The swelling ratio of the freeze-dried gels was determined as described in [422] by measuring their weight after 5, 10, 30 and 60 min of incubation with water at RT. The following formula was used to calculate the swelling ratio:

$$\text{swelling ratio} = (m_T - m_D)/m_D$$

with  $m_T$  defining the mass of the swollen gel and  $m_D$  representing the initial mass of the gel after freeze-drying.

#### 3.4.17 Degradation of hydrogels via Hyal

##### *Preparation of solutions*

*Hyal solution (1000 U/ml)*: 16.5 mg Hyal were dissolved in 10 ml of PBS directly prior to use.

##### *Degradation of hydrogels*

The freeze-dried gels were incubated with 400  $\mu$ l of Hyal solution (1000 U/ml) at 37°C for up to 48 h. After 3, 6 and 24 h, 200  $\mu$ l of the respective supernatants were removed and replaced by 200  $\mu$ l new Hyal solution. The supernatants and the sample solutions were analyzed regarding their GAG content via the hexosamine assay (section 3.4.13) after 48 h of incubation. The amount of degraded gels was calculated indirectly by subtracting the released GAG amounts in the supernatant from the initial GAG amounts of the gels.

#### 3.4.18 Scanning electron microscopy (SEM)

Freeze-dried gels were cut into halves, mounted on carbon tabs onto sample holders and coated with a thin carbon layer via a carbon sputter coater. The carbon sputtering was performed by Dipl.-Ing. Silvia Mühle (Institute of Materials Science, TU Dresden). Secondary electron images of the gel structures were obtained by SEM using a Philips ESEM XL30 under high vacuum with a back-scattering electron detector and 3 kV acceleration voltage.

#### 3.4.19 Atomic force microscopy (AFM)

The fibril morphology of aECMs was studied via AFM as reported by Miron et al. [359R].

##### *Sample preparation*

*In vitro* fibrillogenesis of collagen type I in tubes at 37°C with or without the addition of GAGs to the fibrillogenesis buffer was performed as described in section 3.3.1. The formed aECMs were washed with 30 mM phosphate buffer (pH 7.4, obtained by a 1:1 dilution of fibrillogenesis



buffer with water) after centrifugation (15 min, 25°C, 5000·g). The aECM pellet obtained after a second centrifugation was resuspended in 30 mM phosphate buffer via short pulses with an ultrasonic horn. The aECM suspension was then added to a mica substrate ( $\approx 0.4 \mu\text{g}$  collagen/ $\text{mm}^2$ ) and the collagen fibrils were allowed to adsorb to the surface for 15 min. After three washing steps with water, the aECM-coated mica was dried at RT.

### ***AFM analysis***

The fibril morphology was analyzed with a Nanoscope IIA Bioscope in tapping mode in air using a silicon cantilever without coating. The height and amplitude images were recorded in parallel using the Nanoscope software (scanning rate: 1.0 - 1.2 Hz, 512 lines per image).

## **3.5 Cell culture**

The stable transfection of PAE (porcine aortic endothelial) cells with VEGFR-2 was performed by Prof. Dr. Johannes Waltenberger (Department of Cardiovascular Medicine, University Münster, Germany) as described in [423].

### **3.5.1 Cultivation of endothelial cells (PAE/KDR cells)**

The cultivation of PAE/KDR cells was carried out under sterile conditions using a laminar flow cabinet and an incubator (37°C, 5% CO<sub>2</sub>, humidified atmosphere). Prior to use in cell culture, all solutions were heated to 37°C if not stated otherwise. The cell number was determined with an automatic cell counter after staining with trypan blue using the following parameters: sensitivity level 9, minimal cell size 8  $\mu\text{m}$ , maximal cell size 40  $\mu\text{m}$  and circularity 85%. The cells were used between passages 3 - 7 for the cell culture studies. During cell expansion, the cells were cultured in cell culture flasks (175 cm<sup>2</sup>) containing 25 ml cell culture medium with serum. The medium was changed every 2 - 3 d. The cells were detached from the flask surface after washing with PBS via the addition of 10 ml trypsin/EDTA (1x) for 4 min at 37°C and split when they reached 85 - 90% confluence or prior to use in cell culture experiments. The cell morphology and confluence were continuously monitored with a microscope.

### ***Preparation of solutions***

*PBS (phosphate buffered saline) stock solution (10x):* 80.0 g NaCl, 2.0 g KCl, 14.4 g Na<sub>2</sub>HPO<sub>4</sub> and 2.4 g KH<sub>2</sub>PO<sub>4</sub> were dissolved in 800 ml water. The volume was adjusted to 1000 ml in a volumetric flask.

*PBS solution (136.9 mM NaCl, 2.68 mM KCl, 10.14 mM Na<sub>2</sub>HPO<sub>4</sub>, 1.76 mM KH<sub>2</sub>PO<sub>4</sub>, pH 7.4):* The PBS stock solution was diluted 1:10 with water. The pH was checked to be 7.4 prior to autoclaving the solution.

*Cell culture medium for PAE/KDR cells with serum (DMEM, 2 mM L-Gln, 100 U/ml penicillin, 100  $\mu\text{g}/\text{ml}$  streptomycin, 10% FBS):* 440 ml DMEM were supplemented with 50 ml FBS, 5 ml

penicillin/streptomycin (P/S) stock solution (100x) and 5 ml 200 mM L-glutamine. The media was stored at 4°C and used within 3 weeks after preparation.

*Cell culture medium for PAE/KDR cells without serum (DMEM, 2 mM L-Gln, 100 U/ml penicillin, 100 µg/ml streptomycin, 0.1% BSA):* 500 mg BSA were dissolved in a mixture of 490 ml DMEM, 5 ml P/S stock solution (100x) and 5 ml 200 mM L-glutamine. The filtered media (0.22 µm) was stored at 4°C and used within one week after preparation.

*Trypsin-EDTA solution (1x):* The 10x stock solution was diluted 1:10 with PBS. Sterile 10 ml aliquots were stored at -20°C until use.

### 3.5.2 Stimulation of VEGFR-2 phosphorylation on PAE/KDR cells

The phosphorylation of VEGFR-2 on PAE/KDR cells was stimulated according to [424].

#### *Preparation of solutions*

Mediator protein solutions were prepared in medium w/o FBS with 0.1% BSA prior to use. The GAG/protein solutions were pre-incubated for 30 min on ice.

*200 mM activated Na<sub>3</sub>VO<sub>4</sub>:* For the activation of sodium orthovanadate 1.84 g were dissolved in 40 ml water. The pH was adjusted to 10 via the addition of 1 N NaOH or 1 N HCl resulting in a color change of the solution to yellow. This solution was heated to 90 - 100°C for 10 min until it appeared colorless and completely dissolved and then cooled down to RT. The pH is again adjusted to 10 and the first steps were repeated until pH 10 was constantly reached and the solution remained colorless. Afterwards, the final volume of the solution was adjusted to 50 ml with water. After mixing, aliquots of 1 ml of activated sodium orthovanadate were frozen at -20°C until usage.

*100 µM Na<sub>3</sub>VO<sub>4</sub> in PBS:* 20 µl 200 mM Na<sub>3</sub>VO<sub>4</sub> were added to 39.980 ml PBS. This solution was prepared directly prior to usage.

*Aprotinin stock solution (1 mg/ml):* 526 µl 1.9 mg/ml aprotinin solution were mixed with 474 µl diluent 1 (section 3.5.3). This solution was stored at 4°C.

*Leupeptin stock solution (1 mg/ml):* 1.2 mg leupeptin were dissolved in 1200 µl diluent 1. The solution was kept at 4°C.

*Lysis buffer (1 % NP-40 Alternative, 20 mM Tris (pH 8.0), 137 mM NaCl, 10% glycerol, 2 mM EDTA, 1 mM activated Na<sub>3</sub>VO<sub>4</sub>, 10 µg/ml aprotinin, 10 µg/ml leupeptin):* 45 µl 1 mg/ml aprotinin and 45 µl 1 mg/ml leupeptin were added to 4.41 ml of diluent 1 (section 3.5.3).

#### *Stimulation of VEGFR-2 phosphorylation*

VEGFR-2 phosphorylation was induced on PAE/KDR cells as described in Tab. 3.18.

**Tab. 3.18 Procedure to stimulate VEGFR-2 phosphorylation on PAE/KDR cells.**

Step	VEGFR-2 stimulation
Cell seeding (day 1)	2 · 10 <sup>6</sup> PAE/KDR cells in 3 ml medium containing 10% FBS were seeded in petri dishes (Ø 6 cm) and were allowed to adhere.
Cell starving (day 2)	After overnight incubation of the cells in the incubator with serum-containing medium, the supernatant was discarded and the cells were starved for 120 min with 0.1% BSA/medium without serum.
VEGFR-2 stimulation (day 2)	Then the medium was removed and the cells were washed with PBS. Afterwards the cells were pre-incubated with 50 nM TIMP-3 for 30 min in the incubator before stimulation with 1 nM VEGF in the absence or presence of 200 µM D.U. sHA3 in a total volume of 750 µl for 10 min.
Cell lysis (day 2)	Immediately after cell stimulation, the cells were washed with 2 ml 100 µM Na <sub>3</sub> VO <sub>4</sub> in PBS and lysed with 250 µl lysis buffer on ice for 15 min. The cell lysates were harvested via a cell scraper and collected in tubes. After centrifugation (15 min, 4°C, 10000·g), the supernatants were stored at -80°C until use for ELISA (section 3.5.3).

### 3.5.3 Quantification of VEGFR-2 and phosphorylated VEGFR-2 via ELISA

The total amount of VEGFR-2 or phosphorylated VEGFR-2 was quantified with sandwich-ELISAs according to the manufacturer (R&D Systems). VEGFR-2 and phosphorylated VEGFR-2 concentrations ranging from 125 - 4000 pg/ml or 250 - 8000 pg/ml in diluent 1 were used as standards for quantification.

#### **Preparation of solutions**

*Diluent 1 (1% NP-40 Alternative, 20 mM Tris (pH 8.0), 137 mM NaCl, 10% glycerol, 2 mM EDTA, 1 mM activated Na<sub>3</sub>VO<sub>4</sub>):* 242.4 mg Tris were dissolved in 70 ml water and the pH was adjusted to 8.0. Afterwards, 1 g NP-40 Alternative, 0.80 g NaCl, 10 g glycerol, 71.6 mg EDTA and 500 µl 200 mM Na<sub>3</sub>VO<sub>4</sub> were added and the solution was filled up to 100 ml in a volumetric flask. The solution was stored at 4°C.

*Diluent 2 (20 mM Tris, 137 mM NaCl, 0.05% Tween 20, 0.1% BSA):* 242.4 mg Tris, 801 mg NaCl and 50 µl Tween 20 were dissolved in 80 ml water before adjusting the volume to 100 ml in a volumetric flask. This solution could be stored at RT. Prior to use, 0.1% BSA was added (e.g. 2 mg BSA dissolved in 2 ml 20 mM Tris, 137 mM NaCl, 0.05% Tween 20).

*Block buffer (1% BSA, 0.05% NaN<sub>3</sub> in PBS):* 300 mg BSA and 15 mg NaN<sub>3</sub> were dissolved in 30 ml PBS directly prior to use.

*Wash buffer (0.05% Tween 20 in PBS, pH 7.4):* 250 µl Tween 20 were added to 400 ml PBS and the volume was adjusted to 500 ml with PBS in a volumetric flask.

*Stop solution (1 M H<sub>2</sub>SO<sub>4</sub>):* 56 ml concentrated H<sub>2</sub>SO<sub>4</sub> were diluted with water to a final volume of 1000 ml in a volumetric flask.

*Total VEGFR-2 capture antibody stock solution:* 144 µg lyophilized mouse anti-human VEGFR-2 capture antibody were dissolved in 200 µl PBS to obtain a final concentration of 720 µg/ml. 10 µl aliquots were stored at -80°C.

*Total VEGFR-2 detection antibody stock solution:* 7.2 µg lyophilized biotinylated goat anti-human VEGFR-2 detection antibody were dissolved in 1000 µl diluent 2 to obtain a final concentration of 7.2 µg/ml. 50 µl aliquots were stored at -80°C.

*Phospho-VEGFR-2 capture antibody stock solution:* 288 µg lyophilized mouse anti-human VEGFR-2 capture antibody were dissolved in 200 µl PBS to obtain a final concentration of 1440 µg/ml. 10 µl aliquots were stored at -80°C.

*Total VEGFR-2 capture antibody working solution:* The 720 µg/ml VEGFR-2 capture antibody stock solution were diluted 1:180 in PBS to achieve a concentration of 4 µg/ml.

*Total VEGFR-2 detection antibody working solution:* The 7.2 µg/ml VEGFR-2 detection antibody stock solution were diluted 1:36 in diluent 2 to have a concentration of 200 ng/ml.

*Phospho-VEGFR-2 capture antibody working solution:* The 1440 µg/ml VEGFR-2 capture antibody stock solution was diluted 1:180 in PBS to obtain a concentration of 8 µg/ml.

*Anti-phospho-tyrosine-HRP working solution:* The stock solution was diluted 1:1500 with diluent 2 (e.g. 5 µl stock solution mixed with 7.495 ml diluent 2).

*Phospho-VEGFR-2 control:* 195 ng lyophilized recombinant human phosphorylated VEGFR-2 were dissolved in 500 µl diluent 1 to achieve a final concentration of 390 ng/ml. 10 µl aliquots were stored at -80°C.

*Total VEGFR-2 control:* 25 ng lyophilized recombinant human VEGFR-2 were dissolved in 500 µl diluent 1 to achieve a final concentration of 50 ng/ml. 55 µl aliquots were stored at -80°C.

### ***Plate preparation and ELISA procedure***

Each well of a 96 well ELISA plate was coated with 100 µl of the respective capture antibody solution overnight at RT as described in section 3.4.4. The ELISA procedure to quantify the total amount of VEGFR-2 was similar to section 3.4.4. In case of the phosphorylated VEGFR-2 ELISA, 100 µl anti-tyrosine-HRP was added to each well and incubated for 120 min at RT instead of adding a detection antibody and streptavidin-HRP separately.

### **3.5.4 Migration of PAE/KDR cells**

Cell migration was determined after culturing a monolayer of PAE/KDR cells around a physical barrier (silicon stopper) by detecting the number of cells which migrated into the exclusion zone after removal of the silicon stopper. Cell proliferation was blocked via the pre-incubation of the cells with mitomycin C which inhibits the DNA synthesis by forming inter- and intrastrand crosslinks [425]. The number of migrated cells at a certain time point was indirectly determined by measuring the intensity of the fluorescence signal after cell metabolism of the non-fluorescent calcein AM to fluorescent calcein by esterases of living cells [426].

**Preparation of solutions**

*Calcein AM stock solution:* Calcein AM was dissolved in DMSO to a final concentration of 1 mg/ml and aliquots (2.5 - 100  $\mu$ l) were stored at -20°C.

*Mitomycin C stock solution (0.5 mg/ml):* 2 mg mitomycin C were dissolved in 4.0 ml PBS. The filtered solution (0.22  $\mu$ m) was aliquoted (100  $\mu$ l) and stored at -20°C.

*10  $\mu$ g/ml Mitomycin C in 0.1% BSA/DMEM:* 120  $\mu$ l 0.5 mg/ml mitomycin C were added to 5.880 ml 0.1% BSA/DMEM directly prior to use.

*Calcein AM working solution:* 2.5  $\mu$ l 1 mg/ml Calcein AM solution were freshly diluted with 5 ml DPBS containing calcium and magnesium ions and stored in the dark until use.

**Performance of the migration assay**

Oris<sup>TM</sup> cell migration assay was performed according to the manufacturer's instructions (Platypus Technologies) as described in Tab. 3.19.

**Tab. 3.19 Migration assay procedure.**

Step	Procedure
Cell seeding and starving (day 1)	3 · 10 <sup>5</sup> cells in 100 $\mu$ l medium containing 10% FBS were seeded per well around the silicon stopper and allowed to adhere for 4 h. Afterwards, the medium was aspirated and the cells were washed with PBS. The cells were starved overnight in 100 $\mu$ l medium with 0.1% BSA.
Blocking of cell proliferation (day 2)	2 h prior to the start of the migration assay, the medium was replaced by medium supplemented with 10 $\mu$ g/ml mitomycin C.
Stimulation of cell migration (day 2)	The silicon stoppers were removed, the medium was aspirated and the cells were washed with PBS. 100 $\mu$ l of medium without FBS containing 10 nM VEGF-A, 100 nM TIMP-3 and/or 200 $\mu$ M D.U. GAG was added per well and the cells were allowed to migrate into the exclusion zone for 26 h.
Fluorescent staining of cells	After aspirating the medium, the cells were washed with PBS. 100 $\mu$ l calcein AM working solution was added per well and incubated for 60 min at 37°C. Then, the detection mask was applied to the plate and the fluorescence intensity was measured at $\lambda_{\text{ex}} = 485$ nm and $\lambda_{\text{em}} = 528$ nm.

**3.5.5 Influence of solute GAGs and VEGF-A on the proliferation and tube formation of PAE/KDR cells cultivated on collagen coatings**

PAE/KDR cells were cultivated on collagen-coated wells (section 3.3.1) with or without stimulation of VEGF-A in the absence or presence of solute GAG derivatives. The effects of the respective treatments were assessed via DNA assay (section 3.5.8) and MTT staining.

### ***Preparation of solutions***

**69.4 ng/ml VEGF-A solution:** A 100 µg/ml VEGF-A stock solution was diluted with 0.1% BSA/DMEM to a final concentration of 69.4 ng/ml.

**GAG solutions:** Solutions containing 416.67 µM D.U. of the respective GAGs in 0.1% BSA/DMEM were used after sterile filtration (0.22 µm). Prior to this, the GAGs were allowed to dissolve for at least 30 min at RT.

**GAG/VEGF-A solutions:** 1 µl 100 µg/ml VEGF-A was added to 1440 µl 416.67 µM D.U. GAG in 0.1% BSA/DMEM. The mixture was freshly prepared and allowed to incubate for 60 min on ice prior to usage.

**MTT solution:** MTT was dissolved in PBS to a final concentration of 5 mg/ml prior to usage and filtered (0.22 µm).

### ***Cell seeding on collagen coatings and stimulation with VEGF-A in the presence of GAGs***

30 µl cell suspension containing  $5 \cdot 10^4$  PAE/KDR cells were added per well of a 24 plate, while  $2.5 \cdot 10^4$  cells were used for MTT staining to facilitate the cell visualization even at later time points. 720 µl 69.4 ng/ml VEGF-A solution, the same volume of a 416.67 µM D.U. GAG solution or a 416.67 µM D.U. GAG solution containing 50 ng VEGF-A were added to the cells directly after seeding. The cells were cultivated for up to 3 days.

### ***Performance of the MTT assay***

50 µl of the MTT solution was added per well to the medium and the cells. Afterwards, the cells were allowed to metabolize the MTT dye for 120 min by further cultivation at 37°C. Then, the supernatants were removed, the cells were washed with PBS und used for microscopic examination of the tube formation.

### **3.5.6 Quantification of the protein content in cell lysates - Nanodrop**

2 µl cell lysate after centrifugation (15 min, 4°C, 10000·g) were used to determine the respective protein concentration. The program ND-1000 measuring the absorbance at 290 nm was used for quantification.

### **3.5.7 Cultivation of PAE/KDR cells on hydrogels**

The direct effects of the hydrogel composition on the cell viability and proliferation were studied in the presence of serum, while hydrogels pre-incubated with VEGF-A were used to analyze the potential stimulatory effect of hydrogel-bound VEGF-A on endothelial cells. Cells cultivated on tissue culture poly styrene (PS) served as reference.

#### ***3.5.7.1 Cell proliferation on hydrogels in the presence of serum***

$2 \cdot 10^5$  PAE/KDR cells in 50 µl medium with 10% FBS were seeded per freeze-dried hydrogel (h = 1.1 mm, Ø = 8.5 mm) using 24 well plates. The cells were incubated with the gels for 60 min in the incubator before adding 700 µl medium and cultivating for up to 72 h. After

defined time points (2 h, 24 h and 72 h) the medium was discarded, the gels were washed with PBS, placed in new wells and stored at  $-80^{\circ}\text{C}$  until further analysis.

#### ***3.5.7.2 Effects of VEGF-A-loaded gels on PAE/KDR cells***

To increase the sensitivity of endothelial cells for VEGF-A stimulation, these experiments were conducted in the presence of BSA instead of serum. Cell culture experiments with hydrogels pre-incubated with medium without VEGF-A as well as cells seeded onto PS served as references.

#### ***Preparation of solutions***

*100 ng/ml VEGF-A solution:* A 100  $\mu\text{g/ml}$  VEGF-A stock solution was diluted 1:1000 with medium containing 0.1% BSA to achieve a final concentration of 100 ng/ml directly prior to use.

#### ***Loading of hydrogels with VEGF-A***

Freeze-dried hydrogels ( $h = 1.1 \text{ mm}$ ,  $\text{Ø} = 8.5 \text{ mm}$ ) were incubated overnight with 500  $\mu\text{l}$  medium with or without 100 ng/ml VEGF-A at  $37^{\circ}\text{C}$ . The next day the supernatant was collected and analyzed via ELISA (section 3.4.4). The amount of bound VEGF-A was calculated by subtracting the amount of non-bound VEGF-A in the supernatant from the initially applied VEGF-A amount (50 ng). The VEGF-A-loaded hydrogels were transferred into new wells of a 24 well plate and were used immediately for the cell culture experiment.

#### ***Cell seeding of hydrogels***

24 hours before use, the cells were starved with 0.1% BSA medium.  $5 \cdot 10^4$  PAE/KDR cells in 30  $\mu\text{l}$  medium containing 0.1% BSA were seeded onto each hydrogel and incubated for 60 min at  $37^{\circ}\text{C}$  in the incubator prior to the addition of 720  $\mu\text{l}$  medium and cell cultivation for up to 72 h. Cells which were seeded onto PS and cultivated with 750  $\mu\text{l}$  medium containing 50 ng VEGF-A were used as positive controls.

#### **3.5.8 Determination of the LDH activity and DNA amount**

The LDH activity can be determined using the reduction of  $\text{NAD}^+$  to  $\text{NADH/H}^+$  during the conversion of lactate to pyruvate, which is catalyzed by LDH. Afterwards  $\text{H/H}^+$  transfer to iodonitrotetrazolium chloride is catalyzed by diaphorase, reducing the yellow tetrazolium salt to a red formazan dye. The formation of a fluorescent complex between double-strained DNA and the nucleic acid staining dye PicoGreen is used to quantify the amount of DNA. The LDH activity and DNA amount were determined according to the manufacturer's protocols as previously reported [427,428].

#### ***Preparation of solutions***

For both assays, DNase free ultra pure water was used for all solutions. The absorbance or fluorescence signal of the lysis buffer served as reagent blank value. Cell lysates containing

defined cell numbers ( $0 - 4 \cdot 10^5$ ) were used to correlate the respective LDH activity or DNA amount with the number of cells.

*Lysis buffer (1% Triton X-100 in PBS)*: 1 g Triton X-100 was dissolved in 80 ml PBS before adjusting the volume with PBS to 100 ml. The solution was made freshly each time and stored on ice until use.

*Tris-EDTA buffer stock solution (200 mM Tris-base, 20 mM EDTA, 20x)*: 1.2114 g Tris-base and 292.2 mg EDTA were dissolved in 40 ml of water, the pH was adjusted to 7.5 by adding 4 M HCl and the solution was adjusted to 50 ml with water in a volumetric flask. The autoclaved solution was aliquoted to 1 ml and stored at  $-20^{\circ}\text{C}$ .

*Tris-EDTA buffer (10 mM Tris-base, 1 mM EDTA, 1x)*: 1 ml Tris-EDTA stock solution (20x) was mixed with 19 ml of water.

*Catalyst (diaphorase/ $\text{NAD}^+$ ) stock solution*: The lyophilisate was dissolved in 1000  $\mu\text{l}$  water and 50  $\mu\text{l}$  aliquots were stored at  $-20^{\circ}\text{C}$ .

*LDH substrate solution*: 250  $\mu\text{l}$  catalyst stock solution were mixed with 11.250 ml iodonitrotetrazolium chloride (INT) dye solution directly prior to use.

*PicoGreen working solution*: The commercially available PicoGreen ds DNA reagent stock solution was diluted 1:800 directly prior to use and protected from light (e.g. 10  $\mu\text{l}$  PicoGreen stock mixed with 7.990 ml Tris-EDTA buffer (1x)).

### ***Cell lysis***

The cells, which were stored at  $-80^{\circ}\text{C}$ , were thawed for 10 min on ice. Then, the cells were incubated with 500  $\mu\text{l}$  lysis buffer per well for 60 min on ice. Hydrogels were afterwards treated for 10 min on ice in an ultrasonic bath. The cell lysates were carefully mixed prior to use.

### ***Determination of the LDH activity***

50  $\mu\text{l}$  cell lysate were mixed with 50  $\mu\text{l}$  LDH substrate solution from the LDH cytotoxicity detection kit (TaKaRa) in a transparent 96 well plate and allowed to incubate for 5 - 10 min in the dark. Then, 50  $\mu\text{l}$  0.5 M HCl were added per well to stop the reaction. The absorbance of the solutions was measured at 492 nm.

### ***Quantification of the DNA amount***

10  $\mu\text{l}$  cell lysate were supplemented with 190  $\mu\text{l}$  PicoGreen working solution in a black 96 well plate. The fluorescence intensity ( $\lambda_{\text{ex}}$ : 485 nm,  $\lambda_{\text{em}}$ : 535 nm) was measured after 5 - 10 min of incubation in the dark at RT.

## **3.5.9 Immunofluorescence staining**

### ***Preparation of solutions***

*Fixation solution (3.6% formaldehyde in PBS)*: 1 ml formaldehyde solution (36%) was mixed with 9 ml cooled PBS directly prior to use.



*0.1% Triton X-100 in PBS:* 500  $\mu$ l Triton X-100 were dissolved in 500 ml PBS.

*AlexaFluor-488 phalloidin working solution:* The 1000 U/ml AlexaFluor-488 phalloidin stock solution was diluted 1:200 with blocking buffer to achieve 5 U/ml.

*DAPI working solution:* The DAPI stock solution (1000  $\mu$ g/ml) was diluted with blocking buffer to 0.2  $\mu$ g/ml (1:5000 dilution).

*Blocking buffer (0.05% Tween 20, 1% BSA in PBS):* 500 mg BSA and 25  $\mu$ l Tween 20 were dissolved in 40 ml PBS before adjusting the volume to 50 ml in a volumetric flask. The solution should be made freshly each time.

*Embedding medium (Mowiol 4-88):* 6.0 g glycerol and 2.4 g Mowiol 4-88 were mixed with 6.0 ml water and incubated for 60 min at RT. Then, 12.0 ml 0.2 M Tris-HCl (pH 8.5) was added and the solution was heated to 50°C for 10 min. After centrifugation for 1 min at 13000-g the supernatant was aliquoted to 15 ml and stored at -20°C or 4°C until use.

### ***Performance of the immunofluorescence staining***

The cells were stained with DAPI for their nuclei and with AlexaFluor-488 phalloidin for their cytoskeletal F-actin filaments according to Tab. 3.20. In case of cells cultivated on hydrogels, the gels were cut into halves prior to embedding with the inner part of the gels visible for microscopic examination.

**Tab. 3.20 Immunofluorescence staining procedure.**

<b>Step</b>	<b>Procedure of immunofluorescence staining</b>
Cell fixation	After removing the cell culture medium, the cells were washed with warm PBS prior to the addition of 1.0 ml cooled fixation solution per well. After 30 min of incubation at 4°C, 900 $\mu$ l of the fixation solution were replaced by 900 $\mu$ l cooled PBS. These samples could be stored at 4°C until staining.
Immuno-fluorescence staining	The supernatant was aspirated before permeabilizing the cell membranes with 0.1% Triton X-100 in PBS for 20 min. Then, the samples were washed with PBS and incubated with blocking buffer for 10 min. Afterwards they were incubated with AlexaFluor-488 working solution for 60 min in the dark. DAPI working solution was added for 10 min after washing with PBS. Finally the samples were washed three times with PBS.
Embedding of samples	The samples were embedded in Mowiol 4-88 between two glass cover slides. Afterwards the samples were dried in the dark at RT for 48 - 72 h.
Fluorescence microscopy	Fluorescence filter for DAPI: $\lambda_{ex}$ : 350 - 403 nm, $\lambda_{em}$ : 420 nm; Fluorescence filter for AlexaFluor-488: $\lambda_{ex}$ : 473 - 498 nm, $\lambda_{em}$ : 515 - 565 nm

### 3.6 Statistics

All assays were performed at least in triplicates. One-way or two-way ANOVA were applied to statistically evaluate the determined data. Tukey and Bonferroni post-tests were used to reveal differences between groups. If not stated otherwise, all results are displayed as mean  $\pm$  standard deviation. The standard error is given for  $K_D$  values, which were determined by SPR measurements and fitted to the 1:1 Langmuir binding fitting model.

## 4 RESULTS AND DISCUSSION

Since the number of pathological conditions like non-healing chronic wounds rises notably in the aging population, new strategies for the development of functional materials, which are able to restore functions and properties of damaged vascularized tissues such as bone and skin are in high demand [261,429]. PG-bound sGAGs and non-sulfated HA are major functional components of the native ECM able to interact with several biological mediator proteins involved in cellular processes such as wound healing. Many evidences stress that GAG sulfation strongly influences these interactions and furthermore has direct effects on cells [9R]. Hence, chemically modified GAGs are promising compounds for the described biomaterials.

One promising option to treat for example chronic wounds is to reduce the extensive matrix degradation caused mainly by the continuous production and activity of ECM degrading enzymes such as MMPs in combination with low tissue levels of TIMPs, their natural counterparts [430]. In this context TIMP-3 is of special interest since it i) binds to HSPGs within the native ECM, ii) is suggested to be a major regulator of tissue remodeling and iii) contributes to the regulation of angiogenesis by competing with VEGF-A for the VEGFR-2 binding that initiates the activation of endothelial cells. It is consequently of great interest to identify GAG derivatives that interact with MMP-1 and -2 as well as with TIMP-3 and VEGF-A, and to evaluate how these derivatives could modulate matrix degradation and mediator protein activity if used as functional component of biomaterials.

To mimic the *in vivo* situation more closely, it is necessary to develop new multi-component 2.5D and 3D aECMs based on polymeric GAG derivatives and collagen type I. The goal is to engineer defined aECMs with specific and complex interaction profiles for biological mediators and cells. To this end, it is essential to characterize these aECMs regarding their composition, topography, enzymatic degradation behavior, their binding and release profiles for mediator proteins as well as their influence on endothelial cells.

### 4.1 Selection of GAGs and GAG derivatives

To analyze the effect of the carbohydrate backbone as well as sulfation degree and pattern on the interaction of GAGs with mediator proteins and enzymes, native and chemically modified GAG polysaccharides were used. GAG oligosaccharides were chosen to further determine the minimal structural requirements in case of the MMP-1 activity in the presence of TIMP-3, the interplay of TIMP-3 with GAGs as well as the influence of GAGs on the TIMP-3 binding to LRP-1 or VEGFR-2 and on the VEGF-A/VEGFR-2 complex formation. Since lysozyme, which served as positively charged model protein, and VEGF-A were to be used to load HA/collagen-based hydrogels, additional binding studies of non- and low-sulfated polymeric acrylated GAG derivatives in comparison to their corresponding GAG derivatives were conducted. For the development of aECM coatings differently sulfated HA polysaccharides were used.

Acrylated HA and CS served as crosslinkable polymers to engineer 3D HA/collagen-based hydrogels. To achieve an acrylation degree ( $D.S._{AC}$ ) sufficient for the production of dimensionally stable hydrogels, only low-sulfated HA derivatives (sHA1, sHA1 $\Delta$ 6s) could be used as both chemical modifications (sulfation and acrylation) target the primary and secondary hydroxyl groups.

## 4.2 Interaction of GAGs with mediator proteins and enzymes

### 4.2.1 Influence of GAGs on MMP-1/-2 activity

Since the matrix degradation via MMPs is crucial for tissue remodeling during wound healing, the direct effects of GAG derivatives on the activity of the catalytic domains as well as the full-length MMP-1 and -2 were analyzed (Fig. 4.1).

GAG concentrations in the mM D.U. range were necessary to alter MMP activity. This indicates that GAGs are less potent than TIMPs in influencing MMP activity, as the latter have  $IC_{50}$  values in the nM range [432]. MMP-2 was more sensitive to high GAG concentrations (25 mM D.U.) compared to MMP-1. The presence of HA, CS, HEP and sCS3 enhanced the activity of both catalytic MMP domains in a concentration-dependent manner, while sHA3 led to no detectable effects (Fig. 4.1 A, C). However, HEP and sCS3 were able to promote the activity of the catalytic domains at a concentration of 2.5 mM D.U. GAG. Only sHA1 slightly decreased substrate cleavage by the catalytic domains of MMP-1 and -2.

The increased activity of the catalytic domains of MMP-1 and -2 in the presence of native GAGs like HEP is in accordance with reports from Yu and Woessner demonstrating an enhanced detection of pro- and activated full-length MMP-1, -7 and -13 via zymography in the presence of HEP within the gel [176]. The authors proposed that HEP may induce conformational changes or facilitate refolding of the enzymes leading to higher enzymatic activity, or that HEP reduces autolysis. GAGs can also interact with the prodomain of MMPs, which could result in the allosteric activation of proMMPs by causing a conformational perturbation of the cysteine switch that may disrupt the zinc-thiol binding. This could be a further explanation for the proMMP activation by GAGs.

To closer mimic the conditions *in vivo*, the full-length enzymes of MMP-1 and -2 were used after activation (Fig. 4.1 B, D). Interestingly, nearly all GAGs decreased the enzyme activities at 25 mM D.U., which is opposed to the effects detected for their corresponding catalytic domains. In line with this Kliemt et al. described a decreased MMP-2 activity for cells cultivated on aECMs with sHA3 [353]. The inhibitory effect of GAGs on MMP-1 was found to be sulfation-dependent for HA derivatives, with the strongest effects detected for sHA3 and the lowest for HA. A similar trend was observed for sCS3 compared to CS (Fig. 4.1 B). Even though the remaining activity of MMP-2 in the presence of 25 mM D.U. sHA3 was comparable to that of MMP-1 (about 50%), no clear trend regarding the GAG sulfation could be observed

for former (Fig. 4.1 D), showing that the effect of GAGs on the MMP activity cannot be simply correlated with the overall charge density of the polysaccharides. However, at a lower GAG concentration of 2.5 mM D.U. there were no or less pronounced effects of GAGs on the activity of full-length MMP-1 and -2. These results agree with previous reports demonstration a weak interaction between HEP and MMP-1 or proMMP-2 [8,177].

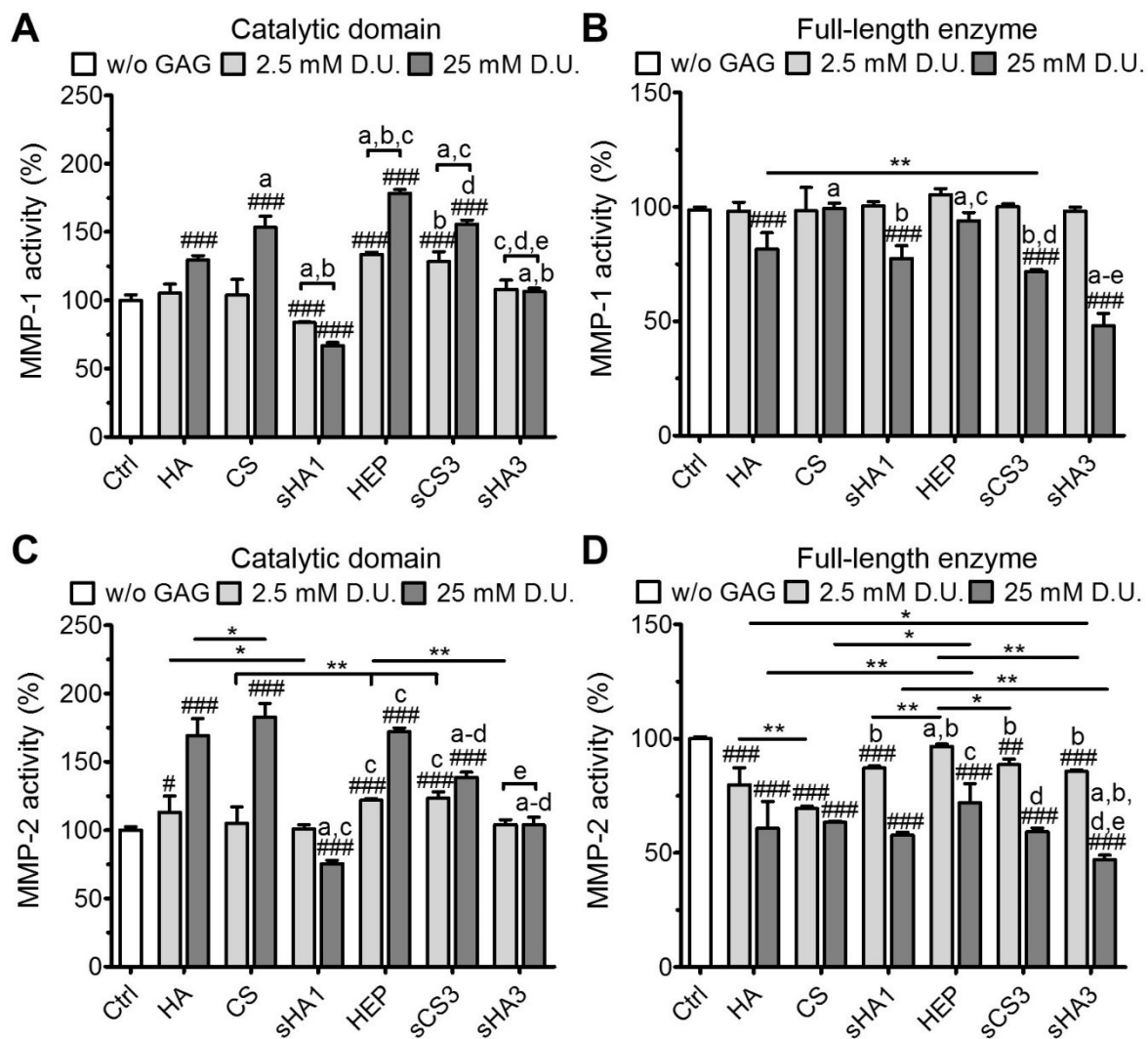


**Fig. 4.1 Activity of MMP-1 and -2 in the presence of GAG polysaccharides.** Enzyme kinetic analysis of the activity of the catalytic domains of MMP-1 (A) or -2 (C) and full-length MMP-1 (B) and -2 (D) in the presence of solute GAGs. Two-way ANOVA: # ( $p < 0.05$ ), ## ( $p < 0.01$ ), ### ( $p < 0.001$ ) vs. Ctrl; \* ( $p < 0.05$ ), \*\* ( $p < 0.01$ ) vs. respective treatment, a ( $p < 0.001$ ) vs. HA, b ( $p < 0.001$ ) vs. CS, c ( $p < 0.001$ ) vs. sHA1, d ( $p < 0.001$ ) vs. HEP and e ( $p < 0.001$ ) vs. sCS3. Adapted from [R431] with modifications.

The conflicting data on the positive or negative effects of GAGs on the activity of active full-length MMPs between this study and the reports of Yu and Woessner likely result from the different presentation of the MMPs (in solution during enzyme kinetics vs. embedded in a gel matrix during zymography). As stressed by the authors, a direct contact of the MMP with the GAG in the gel is mandatory for an improved zymographic detection [176]. The potential

partial denaturation of the MMP due to the denaturing conditions during electrophoresis and its limited flexibility when bound within the gel may allow a direct interplay between HEP and the catalytic domain that initiates the increased substrate cleavage. However, as soon as solute MMPs are used as during enzyme kinetics, the enzymes have more options to interact with solute GAGs due to their enhanced flexibility in solution. Furthermore, the access of GAGs to the catalytic MMP domain may be sterically hindered by other non-catalytic regions of the enzyme. The different effects of GAGs on the MMP activity of full-length enzyme and the catalytic domain suggest a potential role of non-catalytic domains such as the HPX-like domain or the hinge-region, and these may contribute to the GAG-induced alterations of the enzyme activity. An interplay of the HPX-like domain of MMP-2 with HEP was already described [180]. Moreover, GAGs may sequester divalent cations like  $\text{Ca}^{2+}$  via their sulfate residues, albeit a clear proof of a direct binding of  $\text{Ca}^{2+}$  to HEP is still missing [48]. Since 2 - 3  $\text{Ca}^{2+}$  and one structural  $\text{Zn}^{2+}$  are present in the catalytic domain of MMPs [433], any changes of the concentrations of these cation may affect MMP activity.

#### 4.2.2 Interaction of TIMP-3 with GAGs

TIMP-3 is of particular interest as modulator of matrix remodeling since it occurs GAG-bound in the ECM *in vivo* [7]. With an isoelectric point of 9.1 [434] is positively charged under physiological conditions, suggesting an interaction of GAG derivatives with TIMP-3.

SPR binding analyses showed immobilized TIMP-3 to have a concentration- and sulfation-dependent interaction with GAG polysaccharides with (Fig. 4.2). sCS3 and sHA3 exhibited the highest binding levels (Fig. 4.2, A-C). There were no significant differences between the binding strength of CS compared to sHA1 or sCS3 and sHA3, while non-sulfated HA showed almost no binding. To exclude any effects of protein immobilization, additional ELISA experiments were conducted with GAG derivatives immobilized to PS and incubated with solute TIMP-3 in 1% BSA/PBS. BSA was added to reduce the non-specific protein adsorption and can be used in GAG/mediator protein interaction analysis since it is known that sHA has a low affinity for albumin [435]. The detected amounts of GAG-bound TIMP-3 confirmed that the TIMP-3 binding depends on GAG sulfation (Fig. 4.2 D). High-sulfated GAGs bound most of the applied TIMP-3 ( $\approx 72\%$ ), while HA retained significantly less ( $\approx 34\%$ ). The binding strength of TIMP-3 to CS, sHA1 or HEP was comparable and lay between these two values. BSA-coated reference surfaces bound significantly less TIMP-3 than GAG-coated wells, demonstrating the specific interplay of GAGs with TIMP-3. In summary, these data show that solute as well as immobilized sGAGs are potent interaction partners of TIMP-3.

Previous studies regarding the interplay of BMP-2 and TGF- $\beta$ 1 with GAG derivatives also revealed an increase in binding strength for HA with an increasing sulfation degree [253,436]. In contrast to these data, no significant differences between binding strength of CS and sHA1 or sHA3 and sCS3 polysaccharides with a comparable D.S.<sub>s</sub> were found. This indicates that the

binding of TIMP-3 to GAGs is driven mostly by electrostatic interactions between the positively charged amino acids of TIMP-3 and the negatively charged sulfate and carboxylic groups of GAGs [48]. The carbohydrate backbone is of secondary importance. A similar sulfation-dependent interaction of TIMP-3 with CS and HEP was detected via SPR by Robinson et al. [437] but with no clear trend for the amounts of TIMP-3 bound to HEP and HS. The authors suggested that TIMP-3 has different binding sites for GAGs, which may lead to these results [437].

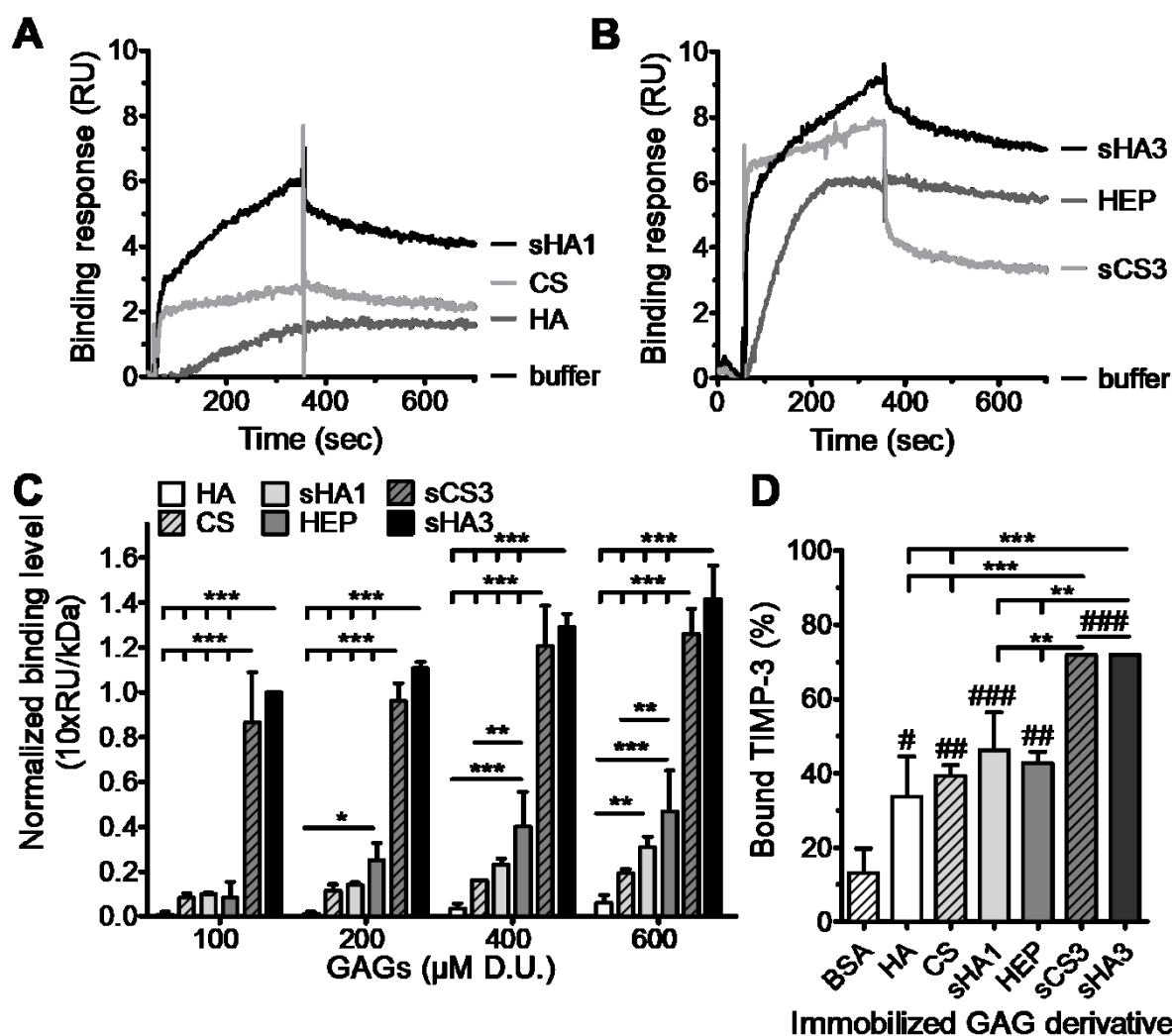


**Fig. 4.2 Interaction of GAG polysaccharides with TIMP-3.** Representative SPR sensorgrams showing the binding response of 600 μM D.U. GAG to immobilized TIMP-3 (830 RU) (A, B) and normalized binding levels of 100 - 600 μM D.U. GAG polysaccharides relative to 100 μM D.U. sHA3 corrected for their molecular weight differences (C). Two-way ANOVA: \* ( $p < 0.05$ ), \*\* ( $p < 0.01$ ), \*\*\* ( $p < 0.001$ ). Amounts of TIMP-3 bound to GAG-coated surfaces after o/n incubation with 1.8 nM TIMP-3 in 1% BSA/PBS as determined via ELISA (D). One-way ANOVA: # ( $p < 0.05$ ) vs. BSA, ## ( $p < 0.01$ ) vs. BSA, ### ( $p < 0.001$ ) vs. BSA, \*\* ( $p < 0.01$ ), \*\*\* ( $p < 0.001$ ). Adapted from [R431] with modifications.

Zhang et al. characterized the TIMP-3 interaction with native GAGs like HEP via competition SPR experiments with solute TIMP-3/GAG complexes and HEP-surfaces. They showed that

the *N*-sulfation as well as the sulfation at the C6 position of the glucosamine residue and the chain-length have a strong influence on the HEP/TIMP-3 interplay. CS-A, CS-C or HS only weakly interfered with the TIMP-3 binding to immobilized HEP [203].

Defined sHA oligosaccharides (Fig. 3.1) were used in comparison to commercially available HA, CS and HEP hexasaccharides (indicated as dp 6) to investigate the impact of sulfation pattern and GAG structure in detail and to analyze whether such short GAG sequences are already sufficient for an interaction with TIMP-3 (Fig. 4.3). The HA tetrasaccharides revealed a sulfation-dependent binding to immobilized TIMP-3 (Fig. 4.3 A). While both non-sulfated HA oligosaccharides displayed low binding responses to TIMP-3 surfaces, all sHA tetra- and hexasaccharides exhibited significantly higher binding levels in case of 100 or 500  $\mu$ M D.U. GAG (Fig. 4.3 B). In general the binding response increases in a concentration-dependent manner. In contrast, very low binding responses with a fast dissociation of TIMP-3-bound GAG were measured for HEP and CS (both dp 6). This indicates that a higher number of D.U. is necessary to stabilize TIMP-3/GAG complex formation in these cases. This is in contrast to findings of Zhang et al., reporting the binding of a HEP disaccharide to TIMP-3 via SPR [203]. Structural variations between the used HEP samples may be responsible for these differences. Overall, the following ranking of the normalized binding levels was detected at 500  $\mu$ M D.U.: HEP (dp 6)  $\approx$  CS (dp 6) < HA (dp 4)  $\approx$  HA (dp 6) < psHA (dp 6) < sHA1 (dp 4) < psHA (dp 4). Interestingly, psHA (dp 4), where all hydroxyl groups are transferred to sulfate esters, displayed a significantly higher binding response to TIMP-3 than psHA (dp 6), indicating different binding profiles for TIMP-3.

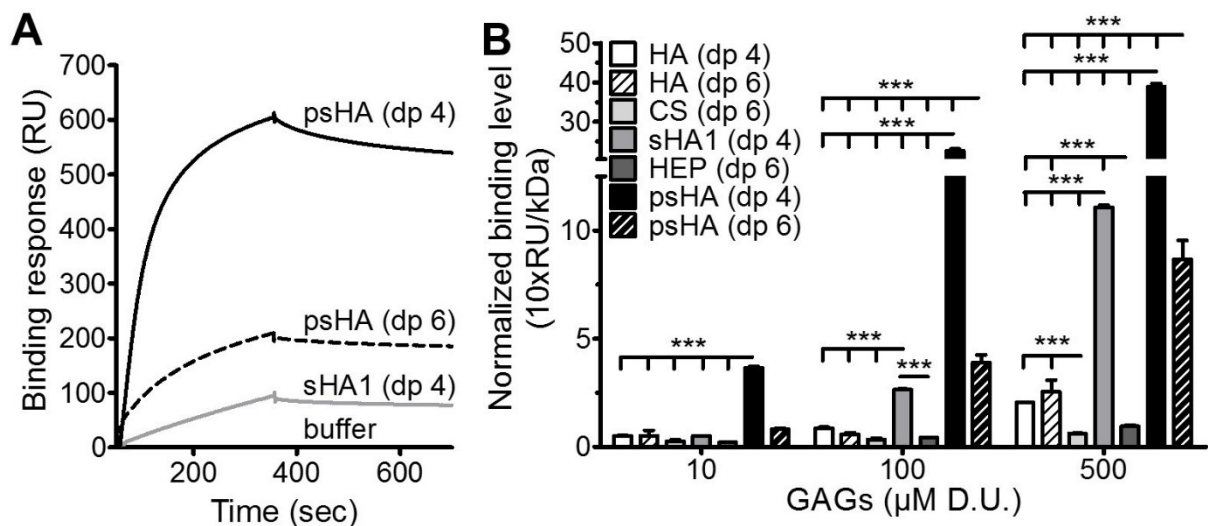


**Fig. 4.3 Binding of GAG oligosaccharides to TIMP-3.** Representative SPR sensorgrams displaying the binding response of 500  $\mu$ M D.U. GAG oligosaccharides to immobilized TIMP-3 (4700 RU) (A) and normalized binding levels of 10 - 500  $\mu$ M D.U. GAG oligosaccharides relative to 100  $\mu$ M D.U. psHA (dp 4) (B). Two-way ANOVA: \*\*\* ( $p < 0.001$ ). Adapted from [R431] with modifications.

Thus, distinct structural properties of GAGs determine their interaction with TIMP-3. Only one sulfate residue per D.U. at the C6 position as in case of sHA1 (dp 4) was already sufficient to



strongly increase the binding to TIMP-3 compared to HA (dp 4). Since sHA1 (dp 4) showed a higher binding level to TIMP-3 than HEP or CS even though the D.S.<sub>s</sub> was lower or comparable, these results demonstrate that the sulfation pattern as well as the sugar backbone further alter the TIMP-3 interaction with GAG oligosaccharides and cannot be simply correlated to the overall negative charge density of the respective GAG oligosaccharides. In contrast, a sulfation-dependent increase of the GAG/TIMP-3 complex formation was observed for the corresponding GAG polysaccharides. Due to missing data regarding the exact distribution of sulfate residues in case of CS (dp 6) and the HEP polysaccharide, a coherent interpretation of this factor is challenging. However, differences between their sulfation patterns are possible reasons here as well.

Moreover, the results for psHA (dp 4 vs. dp 6) indicate that an elongated GAG chain does not automatically enhance or stabilize the binding to TIMP-3. This suggests that the short and highly negatively charged psHA tetrasaccharide is accessing and binding further small GAG binding regions on the TIMP-3 surface. Accordingly, amide hydrogen/deuterium exchange mass spectrometry with psHA (dp 4) and TIMP-3 and molecular modeling experiments demonstrated that the *N*- and *C*-terminal domains of TIMP-3 contain a number of amino acids that form three GAG binding sites [R431]. In particular the contribution of Lys-76, Arg-163 and Lys-165 is in line with previous mutagenesis studies conducted by Lee et al. [202].

#### 4.2.3 Interaction of acrylated GAGs with lysozyme

GAG acrylation is necessary to prepare hydrogels via photocrosslinking (section 4.4.1). To examine the potential influence of acrylation on the protein binding capacity, Rhodamine B labeled lysozyme was incubated with GAG-coated wells (Fig. 4.4). Since native sGAGs are reported to bind lysozyme [438,439], it served as model protein to estimate the impact of GAG modification on protein binding. Lysozyme is comparable to several proteins involved during the wound healing process due to its pI of 11.35, positive net charge and molecular weight of 14.3 kDa. The good availability and comparatively low cost are further advantages [440,441]. However, the possible additional influences of GAGs on the enzymatic activity of lysozyme, as reported for HEP [438], were not considered in these studies.

BSA-coated control wells retained only low lysozyme amounts (about 6%), while surfaces with sGAGs captured significantly more protein than the control or HA-coated surfaces (about 22 - 39% vs. about 17%). Based on these values it is likely that the binding capacity of GAG-coated surfaces for lysozyme is exhausted under the chosen experimental conditions. The lysozyme binding capacity of GAG-coated surfaces showed a ranking as follows: BSA < HA  $\approx$  HA-AC < sHA1-AC  $\approx$  sHA1 < sHA1 $\Delta$ 6s-AC  $\approx$  CS-AC  $\approx$  CS < sHA1 $\Delta$ 6s.

Interestingly, lysozyme preferred the binding to CS and sHA1 $\Delta$ 6s over HA or sHA1. Hintze et al. also detected a higher binding level of sHA1 $\Delta$ 6s compared to sHA1 for BMP-2 surfaces in SPR measurements [436]. In case of HA, CS and sHA1, no significant differences could be

detected compared to their acrylated forms. In contrast, acrylation of sHA1 $\Delta$ 6s markedly decreased the amount of GAG-bound lysozyme. This indicates that the introduction of acryl residues at the C6 position of the glucosamine moiety of sHA1 $\Delta$ 6s hinders the interplay with this protein, while the acrylation of secondary hydroxyl groups has no apparent effects on the GAG/lysozyme interaction.

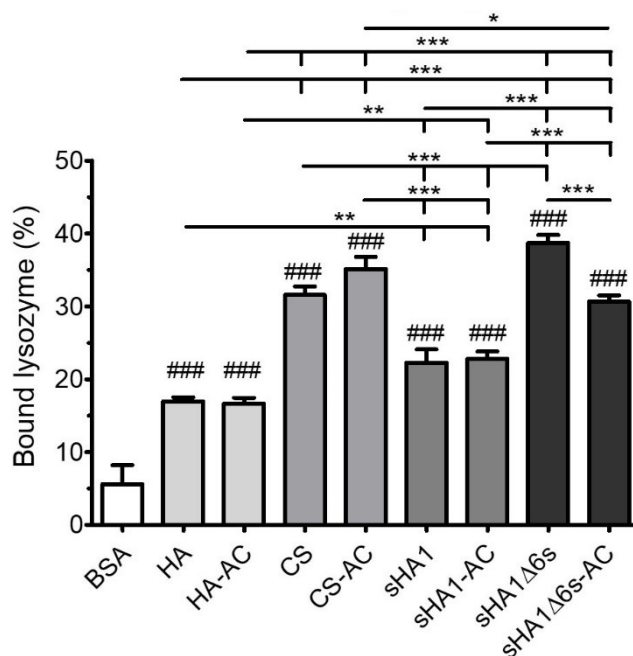


**Fig. 4.4 Binding of lysozyme to immobilized GAGs.** Each GAG-coated well was incubated with 600 ng fluorescence-labeled lysozyme in 2% BSA/PBS overnight at 4°C. The amount of non-bound lysozyme was determined in the supernatants via fluorescence measurements and the amounts of bound lysozyme were calculated by subtracting these values from the initially used concentrations. One-way ANOVA: ### ( $p < 0.001$ ) vs. BSA and \* ( $p < 0.05$ ), \*\* ( $p < 0.01$ ), \*\*\* ( $p < 0.001$ ) vs. respective group.

#### 4.2.4 Interaction of acrylated GAGs with VEGF-A

The potential influence of acrylation on the interaction profile of GAG derivatives with VEGF-A (pI of  $\approx 8.5$ ) [442] was analyzed via ELISA with immobilized GAGs and SPR measurements with immobilized VEGF-A (Fig. 4.5, Fig. 4.6). The amount of GAG-bound VEGF-A increased with the presence of sulfate residues to HA (Fig. 4.5 A). Likewise, Anderson et al. described that VEGF-A binds to HEP surfaces mainly via electrostatic interaction [443]. Interestingly, sHA1 $\Delta$ 6s bound almost all VEGF-A, suggesting that the sulfation of the secondary hydroxyl groups favors the binding of VEGF-A compared to sHA1, where the C6 position is completely sulfated. There was no significant difference between the VEGF-A binding of HA and CS. Acrylation of sHA1 $\Delta$ 6s significantly reduced the amount of VEGF-A bound, while this was only seen by trend for HA and sHA1. sHA derivatives released less VEGF-A compared to HA (Fig. 4.5 B). HA and sHA1 acrylation led to a significantly enhanced retention of VEGF-A, possibly due to a partial crosslinking of GAGs during the unavoidable

short exposure of the GAG-coated plate to light. In the case of CS and sHA1 $\Delta$ 6s, no significant differences in the release of VEGF-A were apparent compared to their acrylated counterparts.

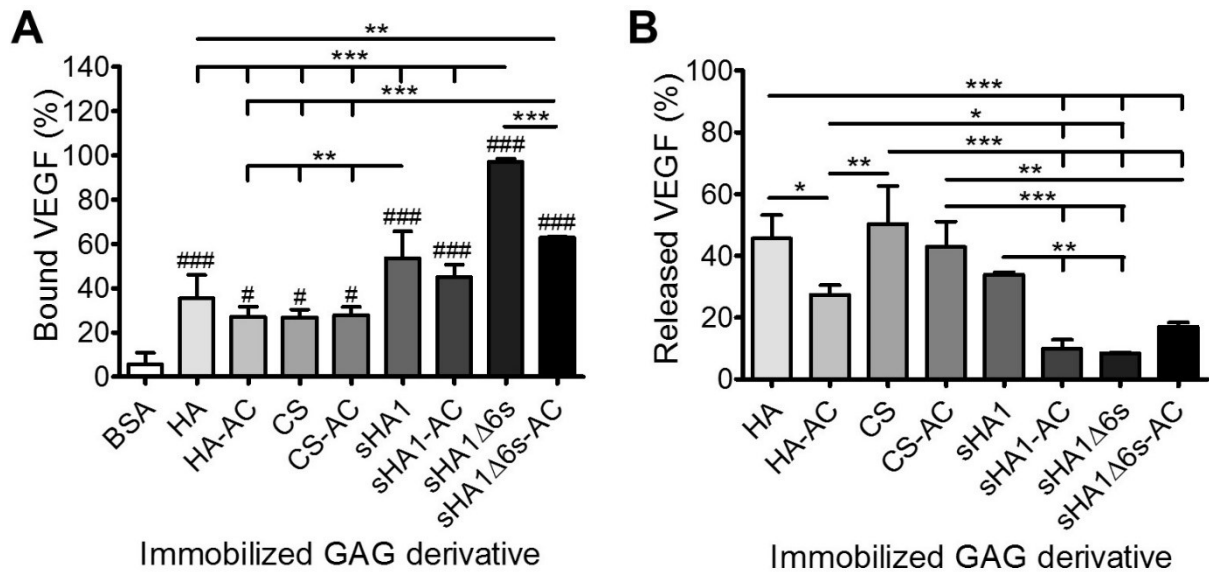


**Fig. 4.5 Interaction of VEGF-A with immobilized GAG derivatives.** The amounts of VEGF-A were quantified via sandwich ELISA. The amounts of GAG-bound VEGF-A after o/n incubation with 1.8 nM VEGF-A in 1% BSA/PBS at 4°C are displayed in (A) and the amounts of released VEGF-A after incubation with 1% BSA/PBS at 37°C for 120 hours in (B). One-way ANOVA: # ( $p < 0.05$ ), ### ( $p < 0.001$ ) vs. BSA and \* ( $p < 0.05$ ), \*\* ( $p < 0.01$ ), \*\*\* ( $p < 0.001$ ) vs. respective group.

Additional SPR measurements with an immobilization set-up reversed compared to ELISA studies were performed to analyze the potential impact of GAG acrylation on their binding to immobilized VEGF-A (Fig. 4.6). Representative sensorgrams display a reduced binding response of sHA1 $\Delta$ 6s-AC compared to the respective GAG without acrylation (Fig. 4.6 A). However, after analyte injection all sHA derivatives revealed only a slight dissociation over time, indicating a high stability of the formed sHA/VEGF-A complexes. In summary, the binding responses increased in the following order: HA  $\approx$  HA-AC < CS  $\approx$  CS-AC < sHA1-AC  $\approx$  sHA1 $\Delta$ 6s-AC < sHA1 < sHA1 $\Delta$ 6s (Fig. 4.6 B). Hintze et al. also detected higher binding levels for sHA derivatives than for HA or CS during SPR binding studies with TGF- $\beta$ 1, BMP-2 and -4 [59,253,436]. In contrast to these findings, Ono et al. reported that desulfation of HEP at the C6 position strongly decreased the interaction with VEGF-A compared to non-modified HEP [444]. Compared to lysozyme, which preferentially binds to CS and not to sHA1, VEGF-A exhibited an opposed preference, clearly demonstrating that the carbohydrate backbone is an important factor that can direct the mediator protein/GAG interaction profiles.

The decrease of the VEGF-A binding capacity due to the acrylation of sHA derivatives is in line with the ELISA findings, implicating that the introduction of acrylate residues into the carbohydrate backbone, especially at the C6 position as in case of sHA1 $\Delta$ 6s-AC, strongly affect the binding affinity for VEGF-A. This was also observed for lysozyme. In contrast, SPR showed a significant increase of the binding level for CS and CS-AC compared to HA or

HA-AC. This was not apparent in the ELISA studies for the examined VEGF-A concentration, possibly due to the higher sensitivity of the SPR technique.

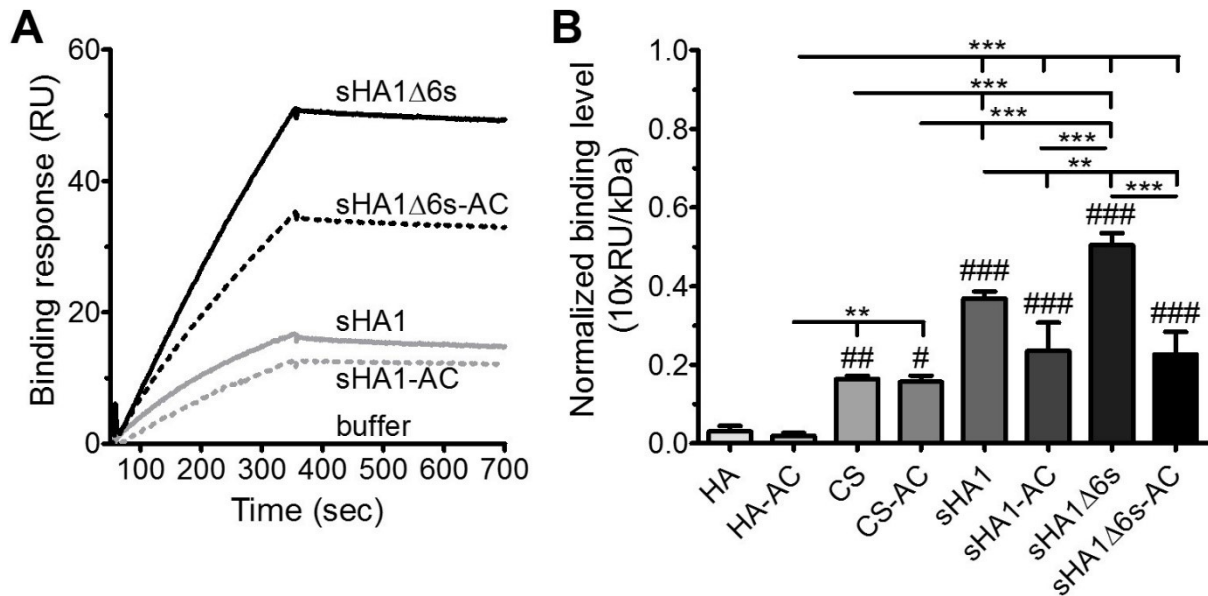


**Fig. 4.6 Interaction of solute GAG derivatives with immobilized VEGF-A.** Representative sensorgrams showing the binding response of 10 nM D.U. GAG to a VEGF-A surface (5159 RU) (A) and normalized binding levels of 10 nM D.U. GAG relative to 10 nM D.U. sHA1 (B). One-way ANOVA: # ( $p < 0.05$ ), ## ( $p < 0.01$ ), ### ( $p < 0.001$ ) vs. HA and \* ( $p < 0.05$ ), \*\* ( $p < 0.01$ ), \*\*\* ( $p < 0.001$ ) vs. respective treatment.

### 4.3 Consequences of GAG/protein interactions on protein functions, receptor binding and intracellular signaling

#### 4.3.1 Influence of GAGs on the TIMP-3 induced MMP inhibition

As shown in section 4.2.2, native as well as chemically modified GAGs are able to interact with TIMP-3. However, the biological consequences on MMP inhibition by TIMP-3 remain unclear. For this reason, the effect of GAGs on the inhibitory activity of TIMP-3 was investigated by analyzing the activity of MMP-1 and -2 as native targets in the presence of TIMP-3 and GAGs.

The enzyme activity in the presence of pre-formed GAG/TIMP-3 complexes compared to TIMP-3 without GAGs is displayed in Fig. 4.7. To decrease the MMP-1 or -2 activity to about 40%, 5 or 2.5 nM TIMP-3 were required, respectively. Neither the presence of 2.5 mM D.U. GAG polysaccharides nor 2.5 mM D.U. HA or psHA tetrasaccharides had a significant effect on the TIMP-3 mediated MMP-1 and -2 inhibition. This is in accordance with molecular modeling results showing no overlapping of the suggested GAG binding regions on the TIMP-3 surface with the known binding site for proteases like ADAM-17 or MMPs [R431]. In conclusion, these findings suggest that GAG binding to TIMP-3 does not alter protease/TIMP-3 interactions. However, Butler et al. detected a slightly decreased MMP-2 activity in the presence of TIMP-3 and HEP, and Troeberg et al. reported an enhanced affinity of TIMP-3 for

ADAMTS-5 in the presence of native GAGs like HS and HEP due to a reduced dissociation rate of the formed TIMP-3/ADAMTS-5 complex. The different results concerning the impact of HEP on the MMP-2 inhibition via TIMP-3 could be attributed to the different protein sources as well as batch-to-batch variations of the used HEP. In accordance with these data, however, Butler et al. found no or only marginal alterations of the MMP-2 inhibition by TIMP-3 in the presence of HA, HS, dermatan sulfate and de-*N*-sulfated HEP [193].

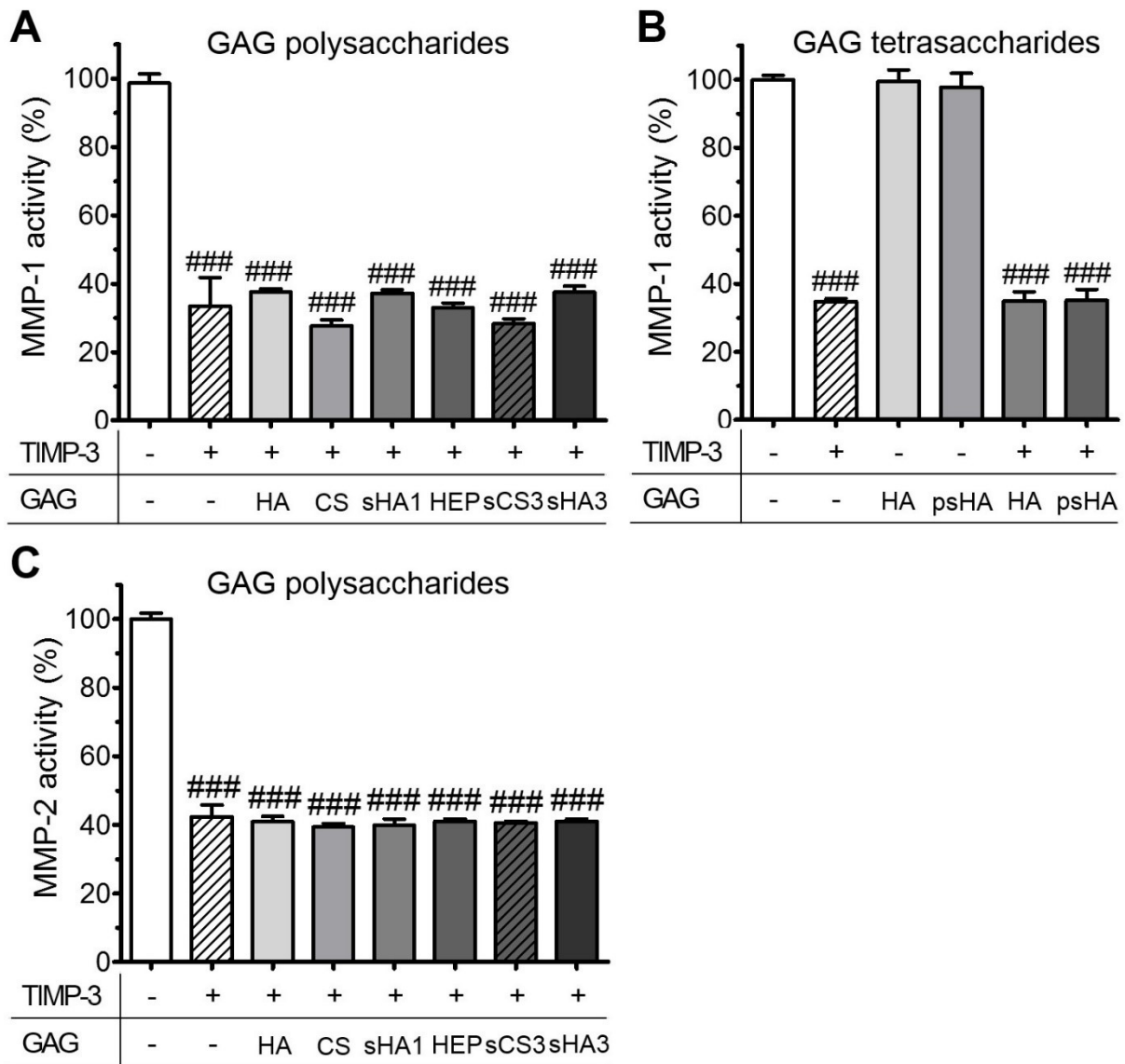


**Fig. 4.7 MMP activity in the presence of TIMP-3 and GAGs.** Inhibition of MMP-1 (A, B) and MMP-2 (C) by 5 nM TIMP-3 or 2.5 nM TIMP-3 in case of MMP-2 in the presence or absence of 2.5 mM D.U. GAGs. One-way ANOVA: ### ( $p < 0.001$ ) vs. Ctrl w/o TIMP-3 and GAG or vs. HA tetrasaccharides in the absence of TIMP-3. Adapted from [R431] with modifications.

#### 4.3.2 Interaction of TIMP-3 with LRP-1 cluster II and IV

Since tissue homeostasis and remodeling as complex processes have to be strictly regulated by the presence, activity and interplay of several factors [5,445], TIMP-3 concentrations must be tightly controlled depending on the biological requirements. Even though it is known that the

up-take and degradation of TIMP-3 via the endocytic receptor LRP-1 is an important mechanism to adjust extracellular TIMP-3 levels, available results on the TIMP-3/LRP-1 interaction are restricted to binding experiments using the whole LRP-1 ectodomain ( $\approx 80\%$  purity) [10]. Hence, it had to be clarified whether LRP-1 clusters II and/or IV are responsible for the binding of TIMP-3 as these are the clusters known to be required for the interaction between LRP-1 and most of its ligands [226,446]. Kinetic parameters for the TIMP-3 binding to LRP-1 clusters II and IV were determined via SPR single cycle kinetics (Fig. 4.8, Tab. 4.1).

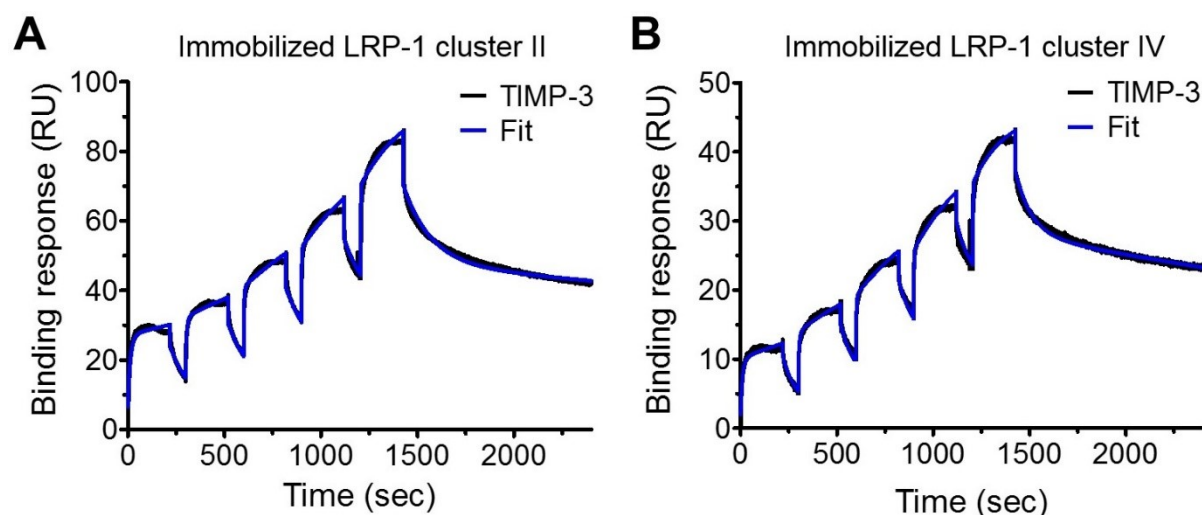


**Fig. 4.8 Kinetic analyses of the TIMP-3/LRP-1 cluster II and IV interaction.** 12.5 - 200 nM TIMP-3 were sequentially injected over LRP-1 cluster II (A) (738 RU) and cluster IV (B) (354 RU) surfaces without regeneration between the injections. The fitted curves according to the heterogeneous ligand model are displayed in blue. Adapted from [R447] with modifications.

**Tab. 4.1 Kinetic parameters characterizing the TIMP-3 interaction with LRP-1.**

Interaction	$k_{on1}$ ( $M^{-1}s^{-1}$ )	$k_{off1}$ ( $s^{-1}$ )	$K_{D1}$ (nM)	$k_{on2}$ ( $M^{-1}s^{-1}$ )	$k_{off2}$ ( $s^{-1}$ )	$K_{D2}$ (nM)	$\chi^2$
TIMP-3/LRP-1 cluster II	$1.98 \cdot 10^4$	$1.11 \cdot 10^{-4}$	5.6	$5.30 \cdot 10^6$	$6.99 \cdot 10^{-3}$	1.3	2.25
TIMP-3/LRP-1 cluster IV	$2.76 \cdot 10^4$	$1.94 \cdot 10^{-4}$	7.0	$6.48 \cdot 10^6$	$12.2 \cdot 10^{-3}$	1.9	1.51

In line with previous reports [10], nM TIMP-3 concentrations were sufficient for a detectable binding to LRP-1 cluster II and IV surfaces. The binding response of TIMP-3 to both clusters increased in a concentration-dependent manner. The heterogeneous ligand model was used assuming the potential binding of TIMP-3 to multiple binding regions. Compared to the  $K_D$  for the whole LRP-1 ectodomain ( $\approx 28$  nM) [10], the  $K_D$  values for LRP-1 cluster II and IV were slightly lower indicating a higher affinity of TIMP-3 for the distinct clusters. The calculated parameters like complex stability ( $k_{off1}$ ) were comparable for both examined LRP-1 clusters. Likewise, Neels et al. did not detect major differences between the interaction of apolipoprotein E, RAP or  $\alpha 2$ -macroglobulin with these two receptor fragments [226].

### 4.3.3 Influence of GAGs on the TIMP-3/LRP-1 interplay

After revealing the interaction of TIMP-3 with GAG derivatives (section 4.2.2) and the direct binding of TIMP-3 to LRP-1 cluster II and IV, the potential impact of GAGs on the TIMP-3/LRP-1 complex formation was analyzed via SPR (Fig. 4.9) to study their influence on the endocytic regulation of extracellular TIMP-3 levels. Control experiments measuring the binding response of 100  $\mu$ M D.U. GAG polysaccharides to LRP-1 cluster II and IV surfaces showed no detectable binding for the GAGs alone (Appendix Fig. 7.1). Hence, any alterations of the TIMP-3/LRP-1 interaction after pre-incubation of TIMP-3 with GAGs should be a consequence of the GAG binding to TIMP-3.

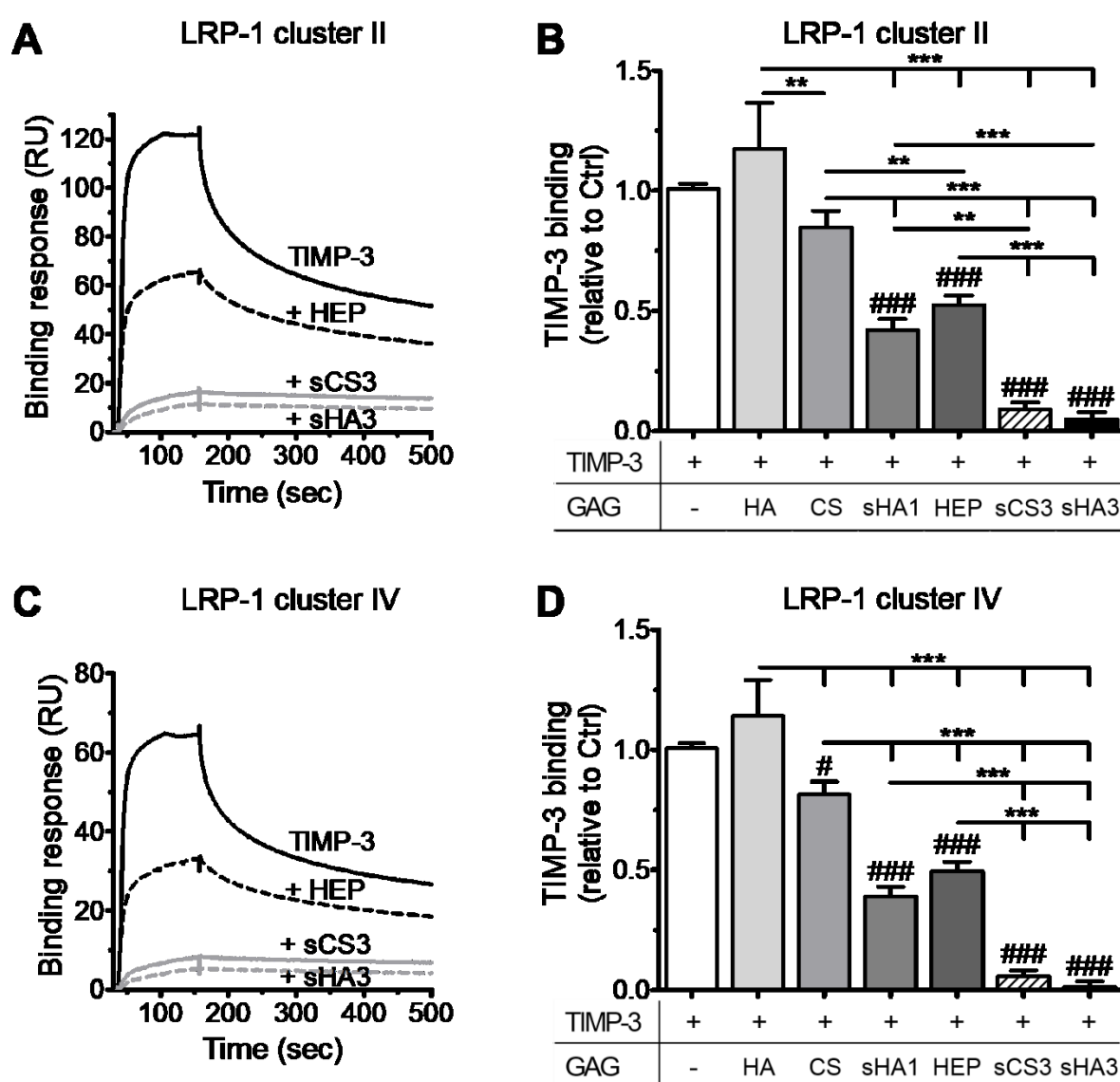


**Fig. 4.9** Influence of GAG polysaccharides on the interaction of TIMP-3 with LRP-1 cluster II and IV. Representative sensorgrams showing the interference of high-sulfated GAG derivatives with the TIMP-3/LRP-1 cluster II (A) or cluster IV (C) complex formation. Binding levels relative to 100 nM TIMP-3 alone for the interaction with immobilized LRP-1 cluster II (B) or cluster IV (D) after pre-incubation with 100  $\mu$ M D.U. GAGs. One-way ANOVA: \*\* ( $p < 0.01$ ), \*\*\* ( $p < 0.001$ ) vs. respective treatment; # ( $p < 0.05$ ), ### ( $p < 0.001$ ) vs. TIMP-3 alone. Adapted from [R447] with modifications.

The binding of TIMP-3/GAG to LRP-1 cluster II (Fig. 4.9 A, B) and cluster IV (Fig. 4.9 C, D) decreased with an increasing degree of GAG sulfation in the following order: HA < CS < HEP  $\approx$  sHA1 < sCS3  $\approx$  sHA3. Only HA showed a slight trend of enhancing the TIMP-3 binding response, while all other sGAGs revealed an inhibitory effect on the TIMP-3/LRP-1 cluster interaction. In particular the high-sulfated GAGs sCS3 and sHA3 markedly reduced the protein association to the endocytic receptor clusters, interfering stronger with the TIMP-3/LRP-1 cluster II and IV binding than native GAGs. It is of note that 100  $\mu$ M D.U. CS significantly lowered the binding response of TIMP-3 to LRP-1 cluster IV, while this was only a trend for cluster II (Fig. 4.9 B, D). Interestingly, the interference of sHA1 and HEP were comparable for both clusters even though sHA1 had a lower D.S.s. These binding analyses demonstrated a comparable ranking for both clusters, indicating no cluster-specific differences between the GAG effects on the TIMP-3/LRP-1 interplay.

HA tetrasaccharides were used to study whether such short GAG sequences are already sufficient to alter the binding of TIMP-3 to the LRP-1 clusters (Fig. 4.10). As for the GAG polysaccharides, HA (dp 4) and sHA1 (dp 4) alone displayed no or only marginal binding responses to both clusters. psHA (dp 4) showed a concentration-dependent interaction with LRP-1 cluster II, implying an interaction of psHA (dp 4) with regions other than the complement-like domains (Appendix Fig. 7.2). However, this was not very pronounced for cluster IV, where 100 and 400  $\mu$ M D.U. psHA (dp 4) displayed only binding responses of about 12.3 - 13.6% relative to TIMP-3. Pre-incubation of 100 nM TIMP-3 with 100  $\mu$ M D.U. sHA1 (dp 4) and psHA (dp 4) significantly decreased the TIMP-3 binding to LRP-1 cluster II in a comparable manner, while only sHA1 (dp 4) interfered with the TIMP-3/LRP-1 cluster IV interaction at this concentration. However, the contribution of the psHA (dp 4)/cluster II interplay to the binding response of TIMP-3/psHA (dp 4) cannot be readily assessed since the used method cannot distinguish between the two binding events. For psHA (dp 4), higher GAG concentrations were necessary to interfere with the TIMP-3/LRP-1 cluster IV interplay (Appendix Fig. 7.3), which could correspond to the additional psHA (dp 4) binding to this cluster. This is supported by the altered sensorgram curvature of the mixture of TIMP-3 with psHA (dp 4) injected over a LRP-1 cluster IV surface (Fig. 4.10 C). Compared to TIMP-3 alone, this curve is characterized by a higher slope during the association phase, suggesting that the binding of psHA (dp 4) and of TIMP-3 to this cluster are two independent events.

Since comparable concentrations of HA tetra- and polysaccharides were used, the enhanced interference of the latter indicates that longer GAG chains are more efficient in blocking the TIMP-3 binding to LRP-1 (Fig. 4.9, Fig. 4.10). The sHA1 polysaccharide (dp 123) for example resulted in an about 3 - 3.8-fold higher decrease of the TIMP-3 binding response than the corresponding tetrasaccharide. Similar effects of the GAG size on the TIMP-3 endocytosis were described for HEP, where HEP (dp 9, 14, 36) but not HEP (dp 5) inhibited the interaction with this endocytic receptor [10]. Taken together, this indicates a stabilizing effect of longer GAG



chains on the GAG binding to TIMP-3, which corresponds with the inhibitory potential of GAGs on the TIMP-3/LRP-1 complex building. Possibly, such negatively charged GAG polysaccharides are more efficient in preventing the binding of TIMP-3 to negatively charged CR LRP-1 domains.

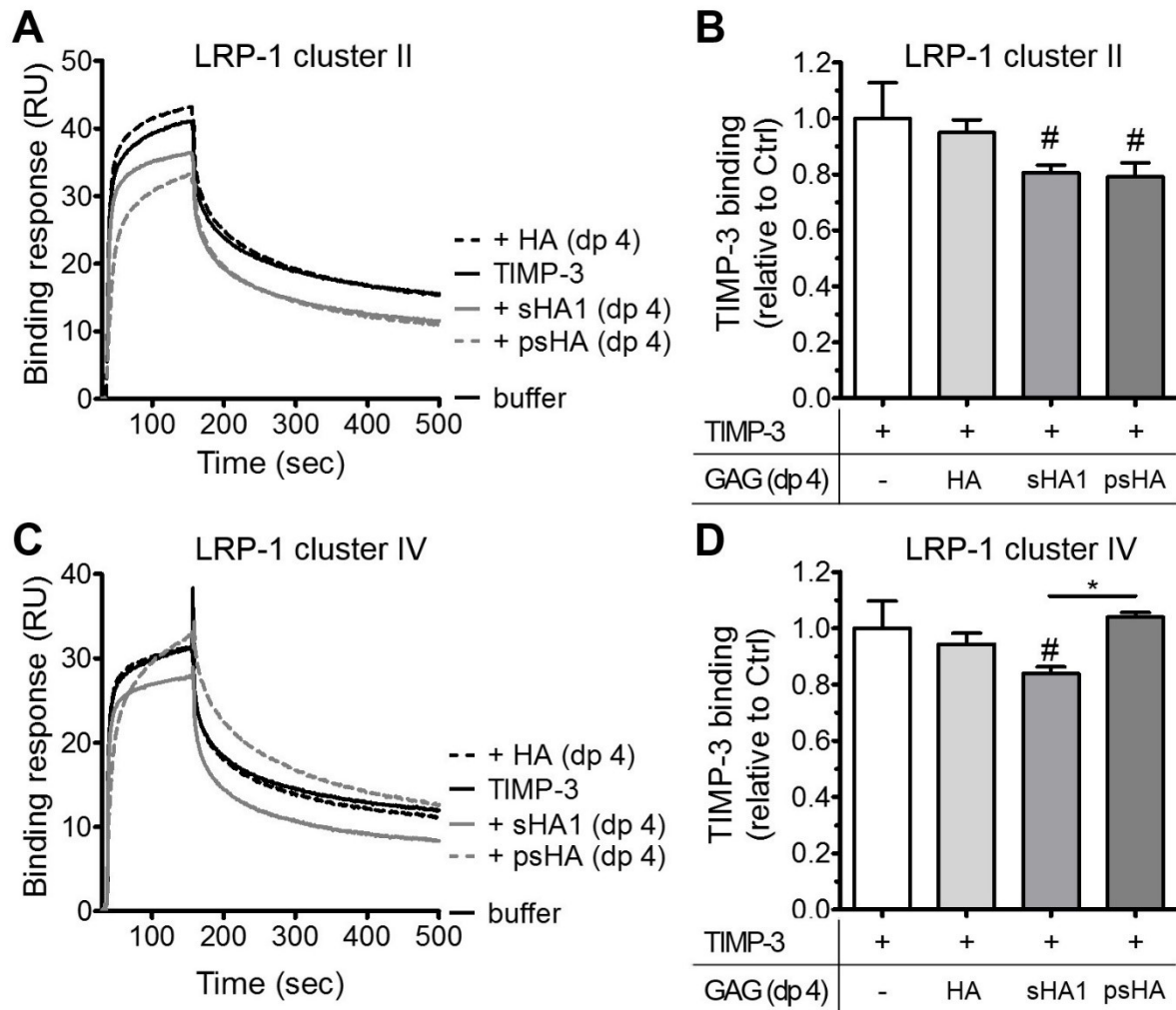


**Fig. 4.10 Influence of HA tetrasaccharides on the TIMP-3/LRP-1 cluster II and IV interaction.** Sensorgrams showing the influence of HA tetrasaccharides on the binding of TIMP-3 to LRP-1 cluster II (A) and cluster IV (C). The relative binding levels of TIMP-3 pre-incubated with 100  $\mu$ M D.U. HA tetrasaccharides compared to 100 nM TIMP-3 w/o GAG are displayed in (B) for LRP-1 cluster II and in (D) for cluster IV. One-way ANOVA: # ( $p < 0.05$ ) vs. TIMP-3 w/o GAG; \* ( $p < 0.05$ ) vs. respective treatment. Adapted from [R447] with modifications.

Besides the binding of TIMP-3 to native GAGs such as HS, CS and HEP, only limited data are available regarding the influence of GAG binding on biological processes like the LRP-1-mediated endocytosis of TIMP-3. In accordance with these SPR findings, Troeberg et al. demonstrated that HS, HEP and CS-E can decrease the TIMP-3 endocytosis via LRP-1 *in vitro* for HTB94 chondrosarcoma cells [10]. Likewise, HEP can decrease the up-take of thrombospondin-1 via LRP-1 as shown for endothelial cells [448,449].

Regarding the structural requirements of GAGs to interfere with the TIMP-3/LRP-1 cluster II and IV interaction, especially the sulfation at the C6 of the glucosamine residue seems to be important. This is highlighted when comparing the inhibitory effects of sHA1 and CS polysaccharides. Even though their D.S.s is comparable, sHA1, which is exclusively sulfated at the mentioned position, had a much stronger impact on the receptor binding than CS, which is mainly sulfated at the C4 position. A similar effect was apparent for TGF- $\beta$ 1 and BMP-2, where CS showed lower binding responses compared to sHA1 [253,436]. Interestingly, this difference was only seen as a trend during SPR binding analysis of the TIMP-3/GAG interaction (Fig. 4.2).

Despite the importance of sulfation location, an additional role of the sugar backbone as well as the GAG size cannot be excluded. Even sHA1 (dp 4) was sufficient to significantly decrease the TIMP-3/LRPR-1 binding, underlining the role of sulfate residues at the C6 position. In line with this Troeberg et al. described that the desulfation of HEP at the C6 position reduced the binding capacity for TIMP-3 as well as the blocking effect on the TIMP-3 up-take. It is of note that they observed no binding of TIMP-3 to CS-A or CS-C [10], while the SPR and ELISA studies performed here clearly demonstrate an interaction of TIMP-3 with CS (Fig. 4.2) as well as a partially blocked receptor interaction with TIMP-3.

It can be hypothesized that the formation of TIMP-3/GAG complexes blocking the binding of TIMP-3 to LRP-1 cluster II and IV is a general GAG-mediated mechanism that could result in a decreased cellular up-take and degradation of TIMP-3 via LRP-1. This hypothesis is supported by results detecting increased TIMP-3 concentrations in the media of hMSCs after cultivation with sHA1 but not with CS or HA. Furthermore, slightly lower protein levels of LRP-1 are observed after the hMSC treatment with sHA1 compared to CS by proteomic analysis [450], which could be a further regulatory effect of the altered LRP-1 functions in the presence of sHA derivatives.

#### 4.3.4 Interaction of TIMP-3 and VEGF-A with VEGFR-2

VEGFR-2-mediated signaling that activates endothelial cells and thereby stimulates angiogenesis must be tightly controlled e.g. via the interplay of pro- and anti-angiogenic factors such as VEGF-A and TIMP-3 [119,292]. Since VEGF-A and TIMP-3 are both able to interact with native as well as chemically modified GAG derivatives (section 4.2.2, 4.2.4) and compete for the binding to VEGFR-2, the potential influence of GAG derivatives on the TIMP-3 and VEGF-A interplay with VEGFR-2 is analyzed to obtain a deeper understanding of this complex signaling process.

Single cycle kinetic measurements with SPR were performed to determine the kinetic parameters characterizing the interplay of TIMP-3 or VEGF-A with VEGFR-2 in the absence of GAGs (Fig. 4.11). The calculated parameters are summarized in Tab. 4.2. Here for the first time we determined the  $K_D$  value with about 215 pM for the TIMP-3/VEGFR-2 interaction.

The  $K_D$  value of 737 pM for the VEGF-A/VEGFR-2 complex formation is in accordance with previously determined values [287,288,300,451,452]. Interestingly, these data show that the  $K_D$  values for the binding of TIMP-3 as well as VEGF-A to VEGFR-2 are both in the same pM range.

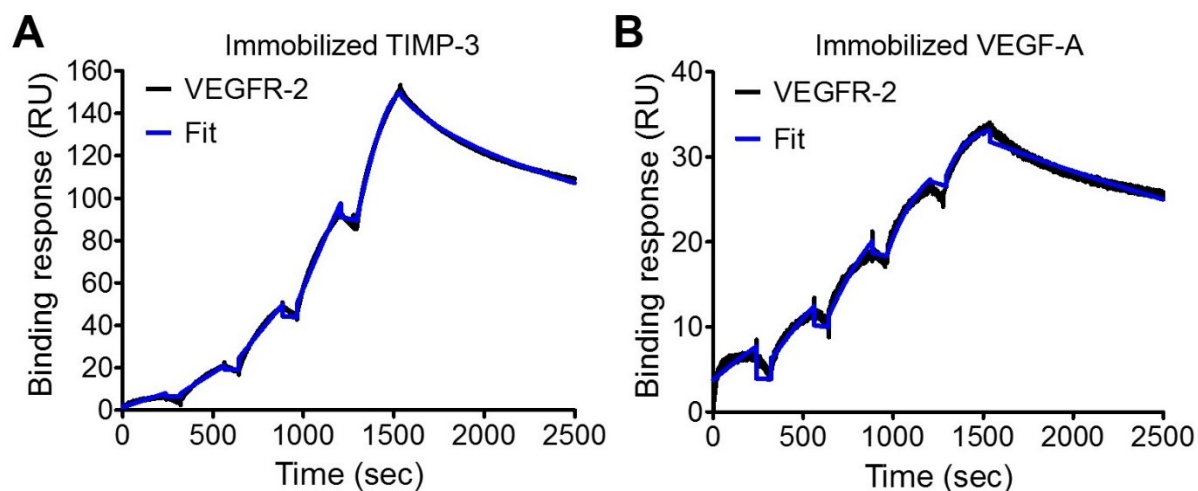


**Fig. 4.11 Kinetic analyses of TIMP-3/VEGFR-2 and VEGF-A/VEGFR-2 interactions.** 0.44 - 7.10 nM VEGFR-2 were sequentially injected over TIMP-3 surfaces (A) (142 RU), while 1.58 - 25.25 nM VEGFR-2 were injected over VEGF-A surfaces (B) (33 RU). The fitted curves according to the 1:1 Langmuir binding fitting model are displayed in blue. Adapted from [R453] with modifications.

**Tab. 4.2 Kinetic parameters of the TIMP-3/VEGFR-2 and VEGF-A/VEGFR-2 interplay.**

Interaction	$k_{on}$ ( $M^{-1}s^{-1}$ )	$k_{off}$ ( $s^{-1}$ )	$K_D$ (pM)	$\chi^2$
TIMP-3/VEGFR-2	$(4.89 \pm 0.06) \cdot 10^6$	$(1.05 \pm 0.01) \cdot 10^{-3}$	215	2.26
VEGF-A/VEGFR-2	$(3.40 \pm 0.02) \cdot 10^5$	$(2.50 \pm 0.01) \cdot 10^{-3}$	737	0.63

#### 4.3.5 Influence of GAGs on the TIMP-3/VEGFR-2 interaction

To study the consequences of the TIMP-3/GAG complex formation on the TIMP-3/VEGFR-2 binding, SPR measurements were conducted. Additional effects of a potential direct interaction of GAGs with VEGFR-2 could be excluded since control experiments showed no detectable binding response for the used GAGs (Appendix Fig. 7.4). Binding analysis revealed a sulfation-dependent blocking of the TIMP-3 binding to VEGFR-2, which was most pronounced for the high-sulfated derivatives sHA3 and sCS3 (Fig. 4.12). In accordance with this Robinson et al. also measured a higher binding of TIMP-3 to CS surfaces compared to HA surfaces [437]. Overall, the TIMP-3 binding signal decreased in the presence of GAG polysaccharides as follows: HA < CS < HEP  $\leq$  sHA1 < sHA3  $\approx$  sCS3, which corresponds well with the detected ranking of the TIMP-3/GAG interaction (section 4.2.2) as well as the interference of GAGs on the TIMP-3/LRP-1 docking (section 4.3.3). However, in contrast to the latter interaction where HA did not significantly altered the receptor binding, even non-sulfated HA reduced the TIMP-3/VEGFR-2 interplay. Additional experiments using a broader range of sHA3

concentrations showed that even 2 nM D.U. were sufficient to lower the TIMP-3 binding response to VEGFR-2 (Appendix Fig. 7.5 A).

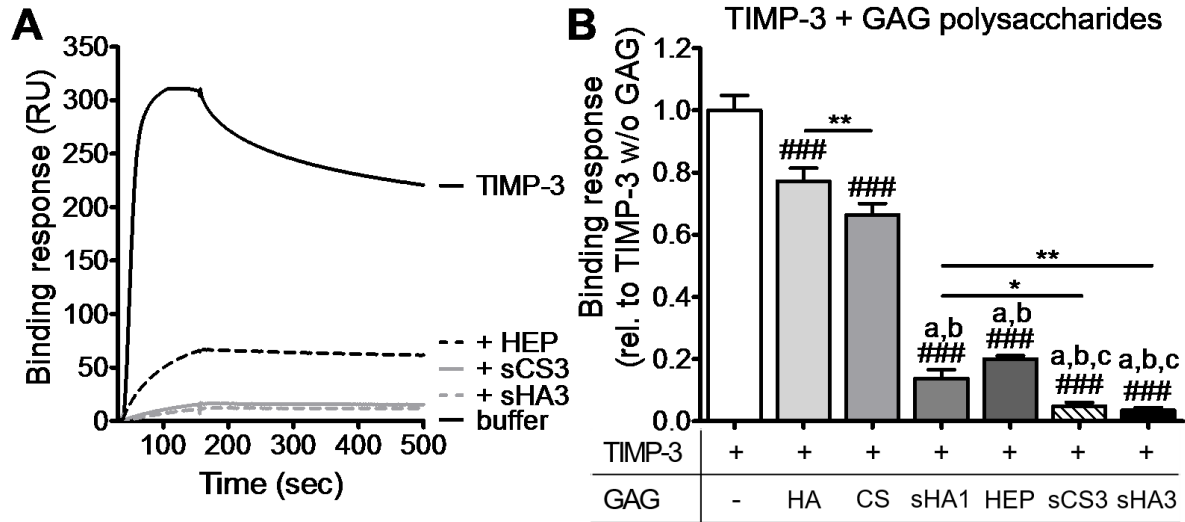


**Fig. 4.12 Influence of GAG polysaccharides on the binding of TIMP-3 to VEGFR-2.** Representative sensorgrams (A) and relative binding levels (B) displaying the binding response of 100 nM TIMP-3 with or without pre-incubation with 100  $\mu$ M D.U. GAG polysaccharides to immobilized VEGFR-2 (A: 124 RU; B: 124 RU, 69 RU). One-way ANOVA: ### ( $p < 0.001$ ) vs. TIMP-3 w/o GAG; \* ( $p < 0.05$ ), \*\* ( $p < 0.01$ ) vs. respective treatment; a ( $p < 0.001$ ) vs. TIMP-3 + HA; b ( $p < 0.001$ ) vs. TIMP-3 + CS; c ( $p < 0.001$ ) vs. TIMP-3 + HEP. Adapted from [R453] with modifications.

GAG oligosaccharides were also analyzed using the same experimental set-up. Here a four times higher GAG to TIMP-3 ratio (4  $\mu$ M D.U. to 1 nM TIMP-3) (Fig. 4.13, Appendix Fig. 7.6) compared to the studies with GAG polysaccharides was examined since even for a 2:1 GAG to TIMP-3 ratio (2  $\mu$ M D.U. to 1 nM TIMP-3) significant effects were only apparent for sHA1 (dp 4), HEP (dp 6) as well as psHA (dp 4, dp 6) (Appendix Fig. 7.6). HA (dp 4, dp 6) and CS (dp 6) revealed no or only a slightly interference with the TIMP-3/VEGFR-2 binding. In contrast, HEP (dp 6) and all examined sHA oligosaccharides significantly reduced the receptor binding of TIMP-3. The exception was sHA2 $\Delta$ 6s (dp 4), which contains two sulfate residues at the glucuronic acid unit but non at the glucosamine unit. It is of note that psHA (dp 4) blocked the TIMP-3/VEGFR-2 complex building more efficiently compared to psHA (dp 6), which is in line with the observed lower binding response of the latter compared to its corresponding tetrasaccharide during TIMP-3/GAG binding analyses (Fig. 4.3). Zhang et al. also detected a more pronounced competition by HEP disaccharides with unknown sulfation pattern for the TIMP-3/HEP binding than by HEP tetrasaccharides. However, they found no significant differences between the effects of HEP tetra- and hexasaccharides [203].

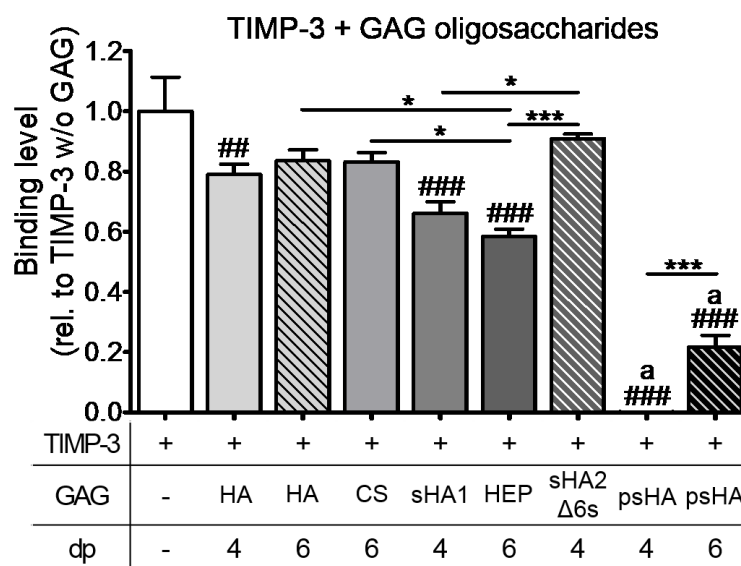


**Fig. 4.13 Effects of GAG oligosaccharides on the TIMP-3/VEGFR-2 interaction.** Relative binding levels are shown for the binding of 20 nM TIMP-3 after pre-incubation with 80 μM D.U. GAG oligosaccharides to VEGFR-2 surfaces (124, 69 RU). One-way ANOVA: ## ( $p < 0.01$ ), ### ( $p < 0.001$ ) vs. TIMP-3 w/o GAG; \* ( $p < 0.05$ ), \*\*\* ( $p < 0.001$ ) vs. respective treatment; a ( $p < 0.001$ ) vs. HA (dp 4, dp 6), CS (dp 6), sHA1 (dp 4), HEP (dp 6), sHA2Δ6s (dp 4). Adapted from [R453] with modifications.

#### 4.3.6 Influence of GAGs on the VEGF-A/VEGFR-2 interaction

Since VEGF-A<sub>165</sub>, as a natural ligand of VEGFR-2 that contains a HEP-binding domain [454], was proven to interact with native GAGs and chemically modified HA derivatives (section 4.2.2), the influence of the GAG/VEGF-A interaction on the growth factor/receptor docking was examined via SPR as well. Sulfated GAG derivatives and HEP blocked the interaction of VEGF-A with VEGFR-2 in a sulfation-dependent manner, while HA and CS had no significant influence on the receptor binding of VEGF-A (Fig. 4.14). The high-sulfated GAG polysaccharides sHA3 and sCS3 completely diminished the VEGF-A binding response. Further binding analyses revealed that sHA3 concentration-dependently affect the VEGF-A/VEGFR-2 interplay in the range of 0.2 to 200 μM D.U., while 2 nM D.U. sHA3 had no significant effect (Appendix Fig. 7.5 B). Compared to the TIMP-3/VEGFR-2 interplay (Appendix Fig. 7.5 A), the VEGF-A/VEGFR-2 was less sensitive against 2 nM D.U. sHA3.

Additional SPR studies with pre-formed VEGF-A/GAG oligosaccharide complexes likewise showed that HEP (dp 6), sHA1 (dp 4) and psHA (dp 4, dp 6) partially block the VEGF-A/VEGFR-2 complex building (Fig. 4.15, Appendix Fig. 7.7). All other used oligosaccharides did not alter this interaction. It is of note that HEP (dp 6) but not sHA2Δ6s (dp 4) interfered strongly with the VEGF-A/receptor binding, although they have a comparable D.S.s. This is in line with the fact that HS oligosaccharides exclusively sulfated at the C2 position were reported to be weak competitors for the HS/VEGF-A interplay [455]. In contrast, the SPR binding studies with GAG polysaccharides and immobilized VEGF-A revealed the

highest binding response for sHA1 $\Delta$ 6s (section 4.2.4). However, these differences could be a result of the GAG chain length as well as the additional presence of sulfate residues at the C4 position of the glucosamine unit in the latter case.

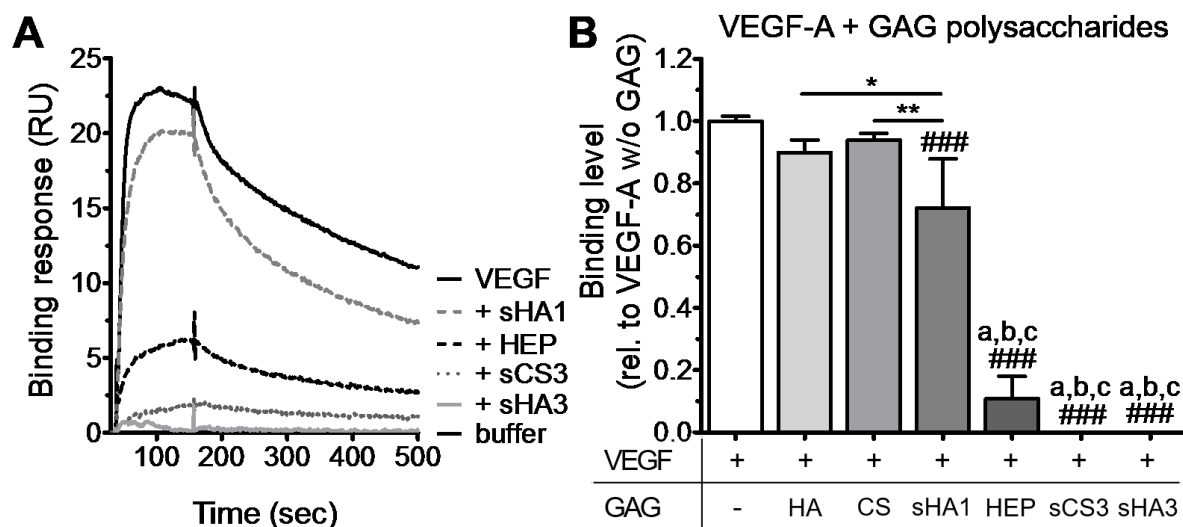


**Fig. 4.14 Interference of GAG polysaccharides with the VEGF-A/VEGFR-2 binding.** Sensorgrams obtained for the binding of 20 nM VEGF-A after pre-incubation with 20  $\mu$ M D.U. GAG polysaccharides to VEGFR-2 surfaces (53 RU) are displayed in (A). The relative binding levels for this interaction is shown in (B). One-way ANOVA: ### ( $p < 0.001$ ) vs. VEGF-A w/o GAG; \* ( $p < 0.05$ ), \*\* ( $p < 0.01$ ) vs. respective treatment; a ( $p < 0.001$ ) vs. VEGF-A + HA; b ( $p < 0.001$ ) vs. VEGF-A + CS; c ( $p < 0.001$ ) vs. VEGF-A + sHA1.

Interestingly, a lower binding response was observed in the presence of psHA (dp 6) compared to psHA (dp 4), suggesting an enhanced affinity of psHA for VEGF-A with increasing GAG chain length. A similar effect of the GAG chain length was reported for HEP, where HEP (dp 40) exhibited a higher affinity for VEGF-A ( $K_D \approx 22 - 42$  nM) than HEP (dp 10) ( $K_D \approx 660 - 840$  nM) [300]. Teran and Nugent likewise observed an altered interplay between VEGF-A and its receptors in the presence of HEP. In contrast to the obtained findings, these authors reported that the addition of HEP to a VEGF-A solution without an explicitly mentioned pre-incubation time increased the interaction of VEGF-A with immobilized VEGFR-2. They assumed that HEP induced the formation of a new high affinity ternary complex between HEP, VEGF-A and VEGFR-2. It has to be noted that apart from the molecular weight of the GAGs, no additional information regarding the chemical characteristics of the used GAGs are provided within this study [11]. Clear conclusions are challenging since HEP is known for its high structural variability depending on the source, and this may cause these opposed effects on the VEGF-A/VEGFR-2 complex formation.

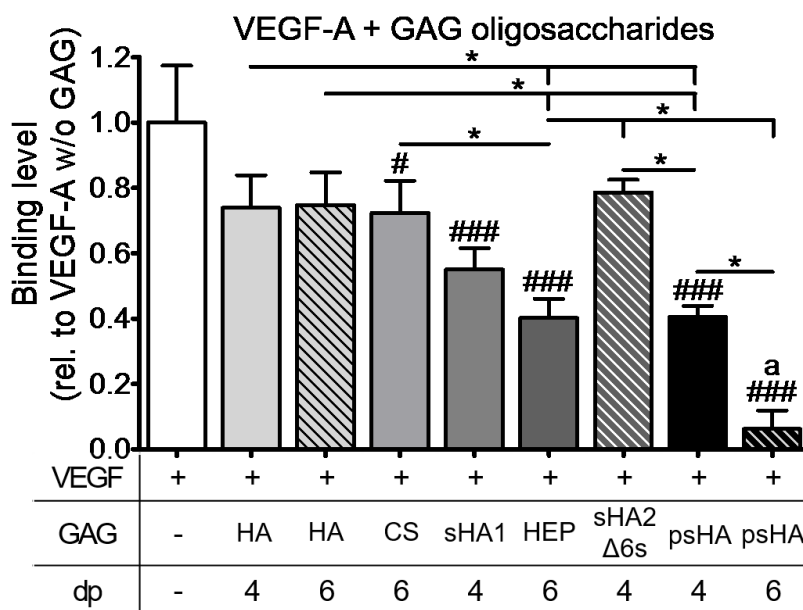


**Fig. 4.15 Effects of GAG oligosaccharides on the VEGF-A/VEGFR-2 interplay.** The binding levels after pre-incubation of 20 nM VEGF-A with 80  $\mu$ M D.U. GAG oligosaccharides relative to the binding response of VEGF-A w/o GAGs to VEGFR-2 (53, 69 RU) are displayed. One-way ANOVA: # ( $p < 0.05$ ), ### ( $p < 0.001$ ) vs. VEGF-A w/o GAG; \* ( $p < 0.05$ ) vs. respective treatment; a ( $p < 0.001$ ) vs. VEGF-A + HA (dp 4, dp 6), VEGF-A + CS (dp 6), VEGF-A + sHA1 (dp 4) and VEGF-A + sHA2 $\Delta$ 6s.

#### 4.3.7 Influence of GAGs on the TIMP-3/VEGF-A/VEGFR-2 interaction

To better reflect the native situation, binding analyses were conducted to evaluate the impact of GAG poly- and oligosaccharides on the TIMP-3/VEGF-A competition for the VEGFR-2 binding. To this end solutions containing VEGF-A and TIMP-3 were pre-incubated with GAGs before SPR analysis. This ensured that any detected changes of the protein/receptor interaction were a consequence of direct binding of sGAGs to VEGF-A and TIMP-3, as we could exclude any GAG binding to VEGFR-2 (Appendix Fig. 7.4) under the chosen experimental conditions as well as an interplay between VEGF-A and TIMP-3.

Similar data were described previously [11,119], although Di Benedetto et al. found an interaction between VEGFR-2 and HEP-albumin [456]. TIMP-3 alone revealed a higher binding response than VEGF-A alone in accordance with the measured kinetic parameters (section 4.3.4, Tab. 4.2), while the TIMP-3/VEGF-A mixture exhibited a comparable binding level to TIMP-3 alone (Fig. 4.16 A, B). The latter can be explained with the competition between VEGF-A and TIMP-3 for the binding to VEGFR-2 [119], which precludes a cumulative binding response compared to the binding levels of both proteins alone.

Like the GAG effects on the VEGF-A or TIMP-3 binding to VEGFR-2 (sections 4.3.5, 4.3.6), sHA polysaccharides concurrently induced a sulfation-dependent reduction of the binding response of VEGF-A together with TIMP-3. Non-sulfated HA and the lowest examined

concentration of 5 nM D.U. sHA3 had no significant impact on the VEGF-A/TIMP-3 interplay with VEGFR-2. This is in line with findings of Hintze et al., demonstrating that sHA derivatives block the binding of BMP-2 to its receptor IA in a sulfation-dependent manner [457].

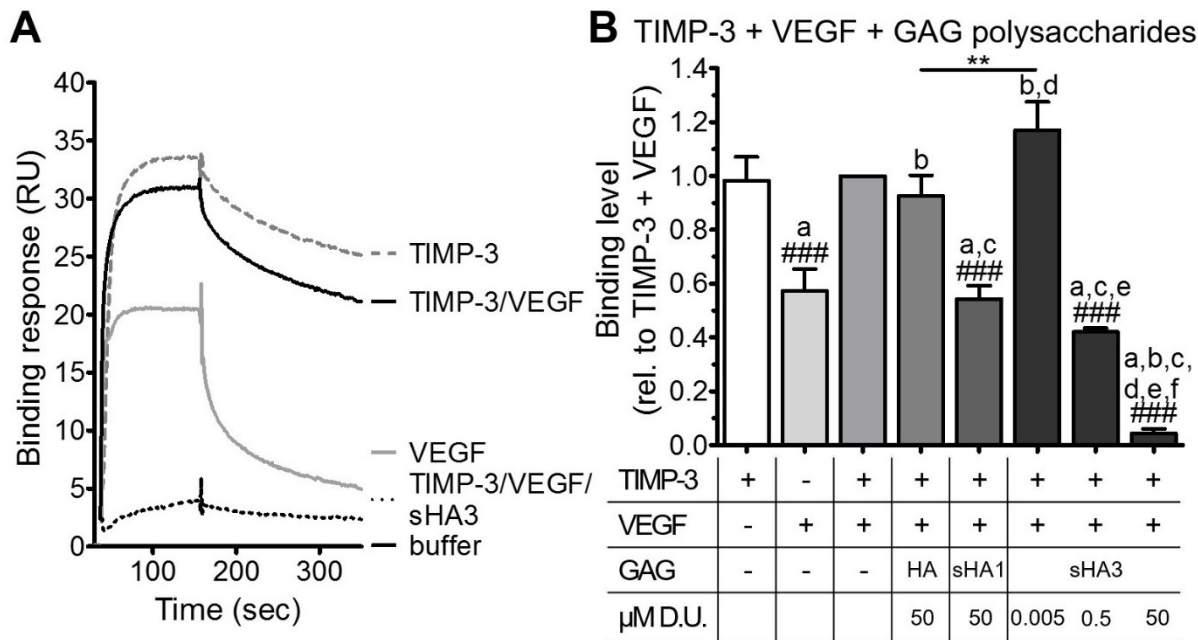


**Fig. 4.16 Interference of GAG polysaccharides with the TIMP-3/VEGF-A competition for VEGFR-2.** Representative sensorgrams showing the binding response of a mixture of 50 nM TIMP-3 and 50 nM VEGF-A in comparison to TIMP-3 or VEGF-A alone or in the presence of 50 μM D.U. sHA3 during injection over a VEGFR-2 surface (53 RU) (A). The binding levels normalized to the binding level of the TIMP-3/VEGF-A mixture in the presence of HA and sHA derivatives is displayed in (B). One-way ANOVA: ### ( $p < 0.001$ ) vs. TIMP-3 + VEGF-A; \*\* ( $p < 0.01$ ) vs. respective treatment; a ( $p < 0.001$ ) vs. TIMP-3; b ( $p < 0.001$ ) vs. VEGF-A; c ( $p < 0.001$ ) vs. TIMP-3 + VEGF-A + HA; d ( $p < 0.001$ ) vs. TIMP-3 + VEGF-A + sHA1; e ( $p < 0.001$ ) vs. TIMP-3 + VEGF-A + 5 nM D.U. sHA3; f ( $p < 0.001$ ) vs. TIMP-3 + VEGF-A + 500 nM D.U. sHA3. Adapted from [R453] with modifications.

Similar to the previous results (sections 4.3.5, 4.3.6) enhanced GAG to protein ratios were necessary for GAG oligosaccharides compared to GAG polysaccharides to induce significant alterations of the binding levels (Fig. 4.17). This indicates a stabilizing effect of a longer GAG chain on the protein/GAG binding and possibly an increased sterical hindrance that enhance the efficiency of receptor blocking. Here only sHA1 (dp 4) and psHA (dp 4, dp 6) but not native GAG oligosaccharides significantly blocked the binding of both proteins to VEGFR-2. It should be noted that this effect was just seen as trend for HEP (dp 6). Overall these data correspond well with the obtained findings that show the influence of GAG polysaccharides on the TIMP-3/VEGFR-2 complex building (section 4.3.5). They potentially result from the enhanced negative net charge of high-sulfated GAGs that may enhance the electrostatic part of the GAG/protein interplay. Accordingly, sCS3 and sHA3 revealed higher binding levels to TIMP-3 surfaces than native GAGs such as HEP (section 4.2.2). A comparable trend was also observed



for the GAG effect on the VEGF-A/VEGFR-2 binding, even if there were no significant differences between sCS3, sHA3 and HEP (section 4.3.6). However, additional alterations due to the different carbohydrate backbones of these GAGs cannot be excluded.

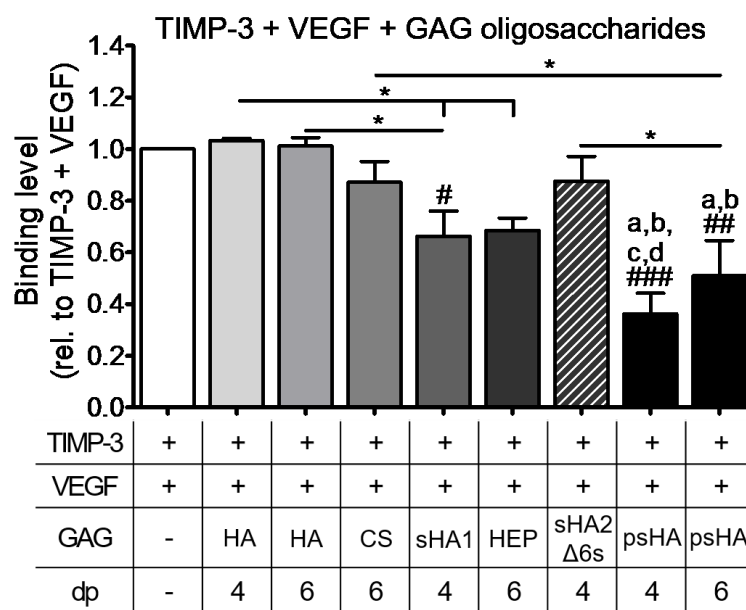


**Fig. 4.17 Interference of GAG oligosaccharides with the TIMP-3/VEGF-A competition for VEGFR-2.** Normalized binding levels relative to the binding level of 20 nM TIMP-3 and 20 nM VEGF-A in the presence of 80  $\mu$ M D.U. GAG oligosaccharides to VEGFR-2 surfaces (53 RU) are shown. One-way ANOVA: # ( $p < 0.05$ ), ### ( $p < 0.001$ ) vs. TIMP-3 + VEGF-A; \* ( $p < 0.05$ ) vs. respective treatment; a ( $p < 0.001$ ) vs. TIMP-3 + VEGF-A + HA (dp 4); b ( $p < 0.001$ ) vs. TIMP-3 + VEGF-A + HA (dp 6); c ( $p < 0.001$ ) vs. TIMP-3 + VEGF-A + CS (dp 6); d ( $p < 0.001$ ) vs. TIMP-3 + VEGF-A + sHA2 $\Delta$ 6s. Adapted from [R453] with modifications.

In summary, a mainly sulfation-dependent interference of GAGs was demonstrated for all examined protein interaction with VEGFR-2. Even sHA tetrasaccharides were potent enough to significantly block the receptor binding, if at a high molar excess. Furthermore, the results of these SPR measurements showed that sulfate residues at the C6 position of the glucosamine residues of HA play a particular role in the inhibitory potential of GAGs on the VEGF-A/VEGFR-2 and TIMP-3/VEGFR-2 complex building. This was especially evident for HA tetrasaccharides, where sHA1 (dp 4) significantly decreased the binding of TIMP-3, VEGF-A or of a TIMP-3/VEGF-A-mixture (Fig. 4.13, 4.15, 4.17), whereas sHA2 $\Delta$ 6s (dp 4) and CS (dp 6) with a higher or comparable D.S.<sub>s</sub> had no or at least lower effects compared to sHA1 (dp 4). This is in line with previous observations where HEP without sulfation at the C6 position exhibited no interaction with VEGF-A and possessed a decreased affinity for TIMP-3 compared to unmodified HEP [203,444]. However, an additional effect of the sugar backbone on the protein/VEGFR-2 binding could be a considerable factor that might contribute to the differences between sHA1 (dp 4) and CS (dp 6) as well.

Molecular modeling techniques support these SPR results. They suggest that VEGF-A and TIMP-3 use similar binding regions on the VEGFR-2 surface and show that negatively charged regions of VEGFR-2 compete with the negatively charged GAGs for the docking to positively charged TIMP-3 regions. This may be the underlying mechanism for the observed inhibitory effects of GAGs on the receptor binding [R453], and agrees with literature data where three distinct GAG binding regions present at the *N*- and *C*-terminal domains of TIMP-3 were identified earlier, and especially the *C*-terminal of TIMP-3 is reported to compete with VEGF-A for the VEGFR-2 binding [295,R431].

To provide further insights into the molecular interplay, additional SPR binding studies were performed to examine whether the order of binding events affects the receptor binding. When injecting solutions with only one analyte present (VEGF-A or TIMP-3 or sHA3) after each other without regeneration after the first or second analyte injection over VEGFR-2 surfaces, comparable binding levels were recorded for the respective analyte independent of the order of analyte injection (Fig. 4.18 A compared to B). Thus, the order of protein injection has no significant influence on the detected binding levels. Furthermore, these sequential binding analyses revealed that sHA3 does not bind or only marginally binds to pre-formed TIMP-3/VEGFR-2 (Fig. 4.18 A) or VEGF-A/VEGFR-2 (Fig. 4.18 B) complexes. This clearly indicates that the GAG binding regions of VEGF-A as well as of TIMP-3 are already occupied after the binding to VEGFR-2, explaining why sHA3 shows a strongly decreased protein binding capacity and is no longer able to significantly interact with TIMP-3 or VEGF-A during sequential injection.

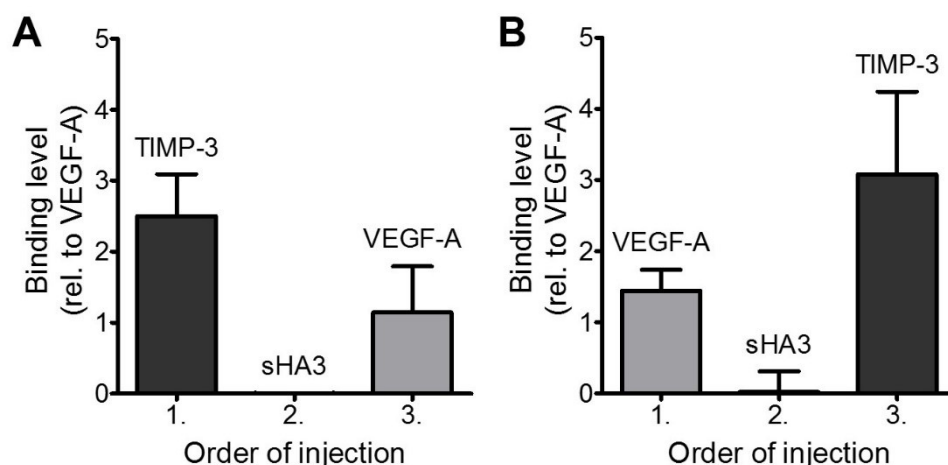


**Fig. 4.18 Sequential interaction analysis of TIMP-3, sHA3 and VEGF-A binding to VEGFR-2.** The SPR binding levels relative to the binding level of 40 nM VEGF-A are shown for the sequential injection of first 40 nM TIMP-3, second 40  $\mu$ M D.U. sHA3 and third 40 nM VEGF-A (A) or of first 40 nM VEGF-A, second 40  $\mu$ M D.U. sHA1 and third 40 nM TIMP-3 (B) over VEGFR-2 surfaces (53 RU, 69 RU, 51 RU). Adapted from [R453] with modifications.

Displacement ELISA experiments with immobilized GAGs were conducted to study whether the presence of VEGF-A and TIMP-3 together as potential GAG interaction partners influences their GAG binding (Fig. 4.19). The retardation of VEGF-A (Fig. 4.19 A) and TIMP-3 alone (Fig. 4.19 B) by GAGs increased with the degree of GAG sulfation (white bars). The presence of additional TIMP-3 did not significantly affect the VEGF-A recovery in the supernatants (Fig. 4.19 A, grey bars) for the examined surfaces compared to VEGF-A alone. It is of note that the presence of VEGF-A enhanced the recovered TIMP-3 amounts in the supernatants (grey bars, striped) after incubation with sHA3-coated wells from about 23% to about 62% (Fig. 4.19 B), while the TIMP-3 recovery remained unaffected in case of the BSA-coated control wells and non-sulfated HA. Thus, these data demonstrate that VEGF-A represents the preferred sHA3 binding partner, which is able to reduce but not to eliminate the interaction of TIMP-3 with sHA3. This is in accordance with findings showing an 1.4 - 2.7 times enhanced affinity of HEP for VEGF-A compared to TIMP-3 with a  $K_D$  of about 59 nM [203,300]. This corresponds also with the increased interference of HEP poly- and oligosaccharides with the VEGF-A/VEGFR-2 interplay compared to the TIMP-3 binding to VEGFR-2 during SPR measurements, where 80  $\mu$ M D.U. HEP (dp 6) reduced the VEGF-A binding level to 40%, while equal GAG concentrations decreased the TIMP-3 binding level only to about 58%.

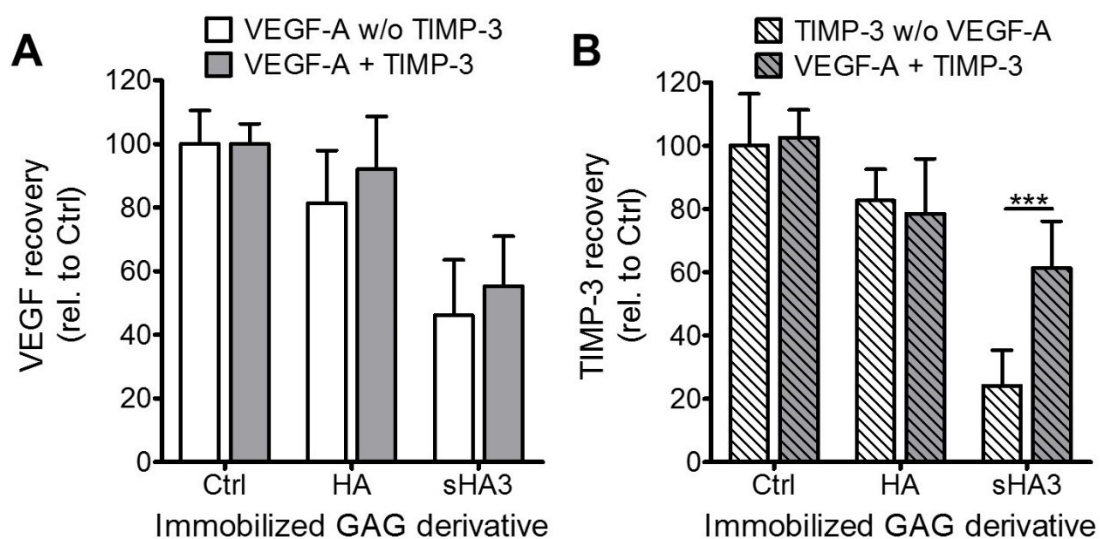


**Fig. 4.19 Binding of VEGF-A or TIMP-3 to GAG surfaces.** Wells with immobilized HA or sHA3 were incubated o/n at 4°C with 1.8 nM VEGF-A, 1.8 nM TIMP-3 or a solution containing both proteins dissolved in 1% BSA/PBS. Afterwards, the amounts of non-bound VEGF-A or TIMP-3 were quantified via ELISA. BSA-coated wells served as control (Ctrl). Two-way ANOVA: \*\*\* ( $p < 0.001$ ) vs. respective treatment. Adapted from [R453] with modifications.

#### 4.3.8 Biological consequences on the VEGFR-2 signaling

Though sGAGs were shown to have a blocking effect on VEGF-A and TIMP-3 binding to VEGFR-2, the biological consequences of this on VEGFR-2 signaling remained unknown. To investigate how sHA3 affects the VEGF-A-induced VEGFR-2 phosphorylation as first

intracellular step of VEGF-A signaling in the presence or absence of competing TIMP-3 *in vitro* cell culture experiments using confluent endothelial cells that represent the physiological state in adults [262] were conducted (Fig. 4.20 A). Cell migration was used to study angiogenic and anti-angiogenic effects in parallel to assess whether HA or sHA3 alter the biological activity of VEGF-A and TIMP-3 in a way that modulates endothelial cell behavior (Fig. 4.20 B). Since human endothelial cells like HUVECs since they typically require a cultivation with HEP-containing cell culture media [458] and this means that potential GAG-induced side effects cannot be excluded, porcine aortic endothelial cells which heterotopically express VEGFR-2 (PAE/KDR cells) were used instead. The expression of VEGFR-2 by PAE/KDR cells was verified and quantified via a specific VEGFR-2 ELISA, showing that on average  $1347 \pm 167$  VEGFR-2 are detectable on each cell surface.

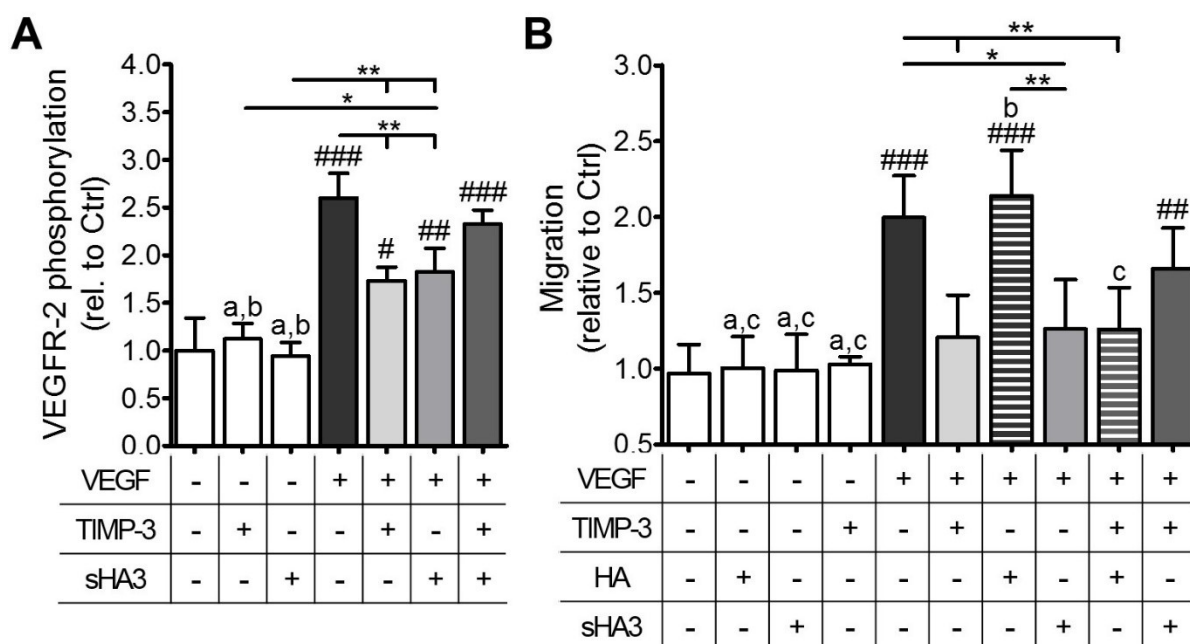


**Fig. 4.20 Effects of sHA3 on the VEGF-A/TIMP-3 controlled phosphorylation of VEGFR-2 and on endothelial cell migration.** (A) After PAE/KDR cell stimulation with 1 nM VEGF-A in the absence or presence of 50 nM TIMP-3 and/or 200  $\mu$ M D.U. sHA3, the VEGFR-2 phosphorylation was quantified via ELISA and normalized to the total amount of VEGFR-2, which is also determined via ELISA relative to total protein concentrations of the respective cell lysates. (B) PAE/KDR cells were initially seeded around a physical barrier, after its removal the cells were stimulated with 10 nM VEGF-A to migrate into the exclusion zone for 26 hours in the presence of 100 nM TIMP-3 and/or 200  $\mu$ M D.U. HA or sHA3. The migration was measured by determining the fluorescence intensity after cell incubation with calcein AM. One-way ANOVA: # ( $p < 0.05$ ), ## ( $p < 0.01$ ), ### ( $p < 0.001$ ) vs. Ctrl (media w/o VEGF-A, TIMP-3 and GAG); \* ( $p < 0.05$ ), \*\* ( $p < 0.01$ ) vs. respective treatment; in (A): a ( $p < 0.001$ ) vs. VEGF-A and b ( $p < 0.001$ ) vs. a mixture containing VEGF-A, TIMP-3 and sHA3; in (B): a (0.001) vs. VEGF-A, b ( $p < 0.001$ ) vs. VEGF-A + TIMP-3 and c ( $p < 0.001$ ) vs. VEGF-A + HA. Adapted from [R453] with modifications.

Compared to the SPR measurements, higher TIMP-3 concentrations were necessary to significantly inhibit the biological activity of VEGF-A during the cell culture experiments. Similar observations were reported previously. There it was suggested that just high doses of solute TIMP-3 compete with VEGF-A for the binding to VEGFR-2 [119,295]. However, the applied protein concentrations should resemble potential *in vivo* concentrations because sHA derivatives were shown to increase the amount of pericellular TIMP-3 [R447] by blocking the TIMP-3 endocytosis via LRP-1 (section 4.3.3). No sHA3-induced VEGFR-2 phosphorylation could be detected, which corresponds well the SPR data showing no direct interplay of GAGs with this receptor (Appendix Fig. 7.4). Based on this it can be suggested that any potential direct effects of GAGs on endothelial cells are not VEGFR-2 mediated. Neither HA nor sHA3 alone affected the endothelial cell migration. In contrast, the presence of sHA3 strongly decreased the VEGF-A-stimulated VEGFR-2 phosphorylation and cell migration, while HA did not alter the VEGF-A effects on cell migration, which corresponds well with the SPR results.

In contrast to these findings, Ashikari-Hada et al. reported that the addition of HEP to VEGF-A can enhance the VEGFR-2 phosphorylation of human endothelial cells, though no information regarding the HEP source is provided by the authors [308]. In accordance with the obtained findings, Freudenberg et al. observed a decreased VEGF-A-induced migration of HUVECs in the presence of HEP-containing gels compared to gels with desulfated HEP [459] and Cole et al. detected that HS oligosaccharides inhibit the VEGF-induced HUVEC migration [455].

It should be noted that the inhibitory effect of sHA3 on the VEGF-A-stimulated VEGFR-2 phosphorylation was less pronounced than for SPR binding analysis with VEGFR-2 surfaces (Appendix Fig. 7.8). This could be explained by the fact that sHA3 can interact with other proteins present at the cell surface or released by the cells during the cell culture studies, while VEGF-A and TIMP-3 represent the only possible binding partners for sHA3 during the conducted SPR approach. The assumed additional sHA3/protein interactions potentially decrease the number of free binding sites within the sHA3 polysaccharide chain, which may result in the detected lower inhibitory potential of sHA3 in the cell culture assay compared to the SPR studies.

TIMP-3 significantly reduced the VEGF-A-induced VEGFR-2 phosphorylation and endothelial cell migration. Interestingly, both increased receptor phosphorylation ( $\approx 35\%$ ) and cell migration ( $\approx 38\%$ ) were observed in the presence of sHA3, VEGF-A and TIMP-3 compared to the mixture of VEGF-A and TIMP-3. However, 200  $\mu\text{M}$  D.U. GAG did not completely restore the bioactivity of VEGF-A. To support the *in vitro* findings additional SPR experiments were conducted using similar VEGF-A, TIMP-3 and sHA3 concentrations as in the VEGFR-2 phosphorylation stimulation assay (Appendix Fig. 7.8). SPR measurements likewise showed significantly decreased binding levels of 50 nM TIMP-3 or 1 nM VEGF-A after pre-incubation with 200  $\mu\text{M}$  D.U. sHA3, and at least by trend a slightly higher binding signal for the

combination of VEGF-A, TIMP-3 and sHA3 in comparison to VEGF-A/sHA3 or TIMP-3/sHA3 complexes was detected.

Importantly, these data highlight that albeit VEGF-A/sHA3 complexes exhibit a decreased biological activity compared to VEGF-A alone, the simultaneous formation of VEGF-A/sHA3 and TIMP-3/sHA3 complexes enables a partially rescued VEGF-A/VEGFR-2 signaling as proven by the VEGFR-2 phosphorylation as well as the endothelial cell migration. As a consequence, a co-regulatory role of TIMP-3 and sGAG derivatives on the biological activity of VEGF-A can be hypothesized (Fig. 4.21). This might be translated into the development of sGAG-containing biomaterials able to rebalance abnormal angiogenesis associated with increased levels of VEGF-A and VEGFR-2 as e.g. present in atherosclerosis or rheumatoid arthritis [273,460].

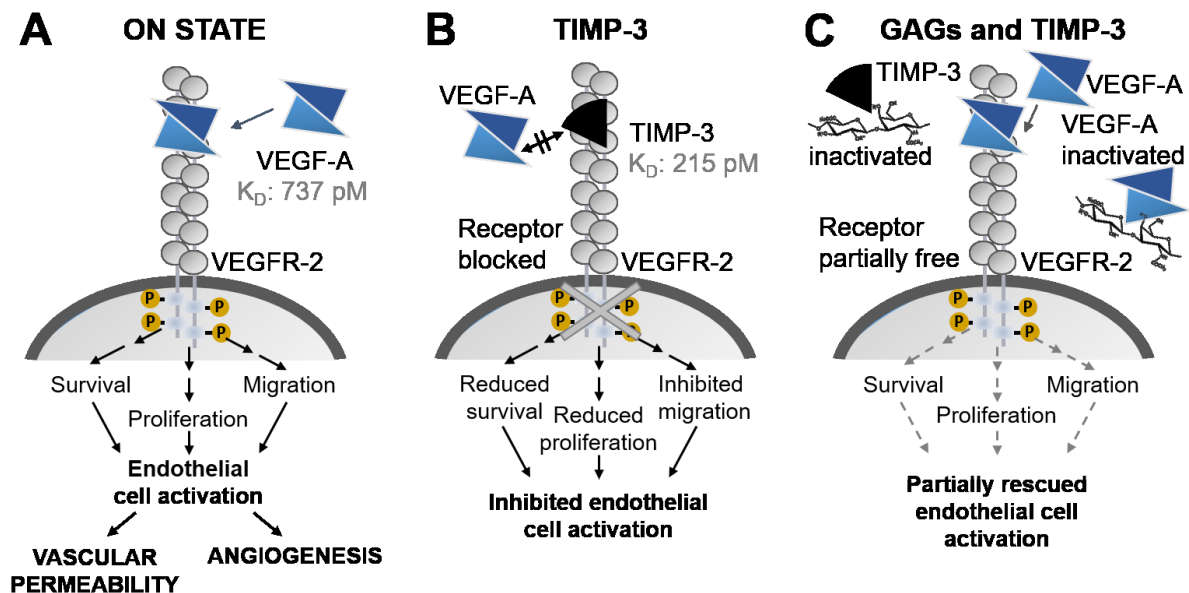


**Fig. 4.21 Simplified scheme of VEGF-A/VEGFR-2 signaling in the presence of TIMP-3 and GAGs.**

(A) Successful docking of a VEGF-A dimer to extracellular domains of VEGFR-2 induces the dimerization of VEGFR-2, which initiates the autophosphorylation of intracellular tyrosine residues. This signaling process activates endothelial cell survival, migration and proliferation. (B) Extracellular TIMP-3 as natural VEGF-A competitor binds to VEGFR-2, thereby blocking the VEGF-A/VEGFR-2 complex formation and consequential the VEGF-A-induced signal transduction cascade and endothelial cell activation. (C) VEGF-A and TIMP-3 interact both with extracellular sGAGs. Solute TIMP-3/sGAG and VEGF-A/sGAG complexes exhibit a reduced binding to VEGFR-2, which decreases the biological activity of TIMP-3 and VEGF-A. However, the simultaneous formation of TIMP-3/sGAG complexes partially rescues the successful binding of VEGF-A to VEGFR-2 and allows a controlled VEGF-A/VEGFR-2 signal transduction and endothelial cell stimulation. Adapted from [R453] with modifications.

#### 4.4 Biomaterial coatings functionalized with HA derivatives (2.5D aECMs)

The native ECM represents a complex system containing a high number of cues that control and modulate the cellular response. Thus, model systems that partially replicate this biocomplexity are required to analyze biochemical signals that alter for example tissue homeostasis. Against this background, aECMs that include GAG derivatives associated with collagen fibrils are reported as promising biomaterials with favorable properties that may improve the regeneration of skin and bone tissue [9R]. However, these data are restricted to aECMs with only one GAG. Only little is known about the potential influence of altered sHA concentrations or the presence of multiple sHA derivatives during the *in vitro* fibrillogenesis of collagen type I, potentially altering the biochemical composition, the resulting fibril morphology as well as the enzymatic aECM degradation. Especially evaluating whether GAG derivatives affect the enzymatic stability of aECMs is of special interest for a future application for example as implant coatings.

##### 4.4.1 Development and characterization of aECMs with one or two GAGs

HA, sHA derivatives with different sulfation degrees (sHA1 and sHA4) as well as a combination of sHA1 and sHA4 were integrated into single-GAG- or multi-GAG-aECMs. To systemically modify GAG concentrations during the collagen self-assembly process, the collagen amount per aECM was kept constant while altering the number, concentration and sulfation degree of the used GAG derivatives. Afterwards, aECMs were dried and analyzed regarding their composition and stability at 37°C in PBS (Fig. 4.22) without any additional crosslinking to allow a certain release of GAG polysaccharides and degradation of collagen.

85 - 90% of the initially applied GAG amounts were released from aECMs during their initial washing with water (Fig. 4.22 A). During the first 60 min of incubation with PBS an additional GAG release occurred, while the GAG contents remaining after this time was comparatively stable for up to eight days. These release profiles imply that the association of GAGs to collagen fibrils is restricted by a limited number of GAG binding sites on collagen, explaining the burst release of non-associated GAGs during early incubation period. Interestingly, the aECM with a higher collagen to sHA4 ratio during *in vitro* fibrillogenesis (1/0.5 stands for 1 mg/ml collagen, which is mixed with 1.25 mM D.U. GAG) revealed a higher percentage of remaining GAG per matrix than the aECM with a lower collagen to sHA4 ratio of 1/1 (1 mg/ml collagen mixed with 2.5 mM D.U. GAG). However, we observed no significant differences between the other sHA containing coatings. It is of note that the percentage of remaining GAG in the single-GAG matrices was comparable to the percentage of integrated GAG determined for the multi-GAG aECM, where both sHA1 and sHA4 were present during aECM formation. Since the GAG concentrations were related to their D.U. during the aECM preparation and almost comparable percentages of remaining GAGs per matrix were calculated, we found that the GAG amounts associated to collagen increased with the D.S.<sub>s</sub> as well as the used GAG concentration,

which is in line with previous results [359R,461–463]. However, as reported by Bierbaum et al. and Miron et al., the integrated GAG amounts do not linearly correlate with the applied GAG amounts [359R,464].

Collagen constitutes the main component of the developed aECM coatings. These coatings contain about 90 - 95% of the initially applied collagen amount of 200  $\mu\text{g}$ , irrespective of the used GAG to collagen ratio or GAG type (Fig. 4.22 B). Importantly, the collagen content decreased only marginally over the incubation time, indicating that all aECMs were quite stable for at least eight days at 37°C. This is in line with previous reports on the stability of collagen-based coatings [350].

In summary, the developed matrices were characterized by the following GAG to collagen mass ratios after 60 min of incubation at 37°C: 1:19 for coll/HA (1/1), 1:27 for coll/sHA1 (1/0.5), 1:13 for coll/sHA1 (1/1), 1:11 for coll/sHA1/sHA4 (1/0.5/0.5), 1:16 for coll/sHA4 (1/0.5) and 1:12 for coll/sHA4 (1/1), respectively. van der Smissen et al. revealed a comparable GAG to collagen mass ratio for aECMs with LMW-HA, but they reported an increased amount of high-sulfated HA in their coatings [351]. This may result from differences between the molecular weights and sulfation degree of the used sHA derivatives. Interestingly, comparable GAG concentrations as in the here prepared aECMs were also found in bone, where the native ECM contains about 4 - 5% sGAGs related to the collagen dry weight [107,359R]. Thus, these aECM coatings could function as biomimetic materials in a range of applications such as implant coatings.

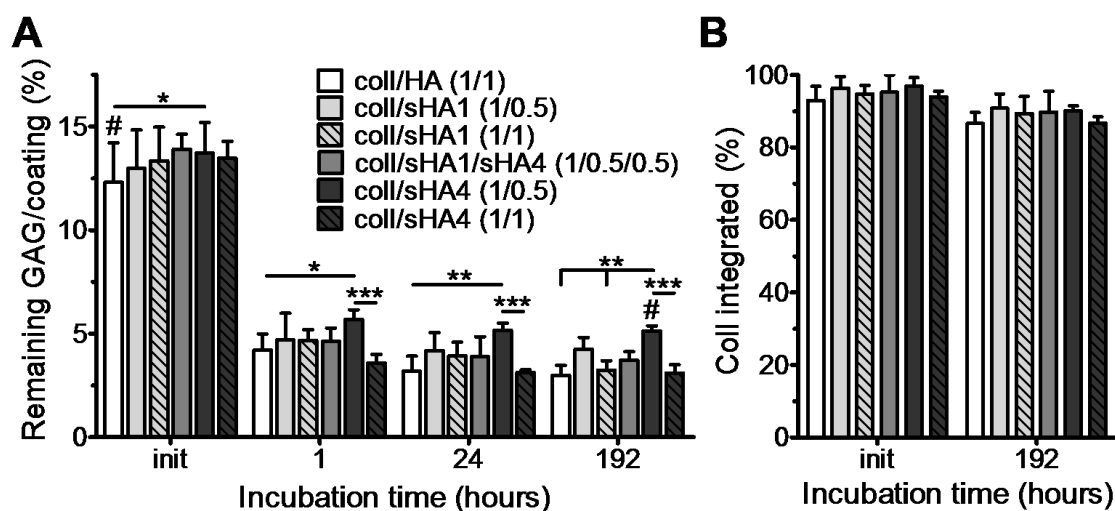


**Fig. 4.22 Composition of aECMs.** Collagen-based coatings were washed with water (init) and afterwards incubated with PBS at 37°C for up to eight days. The remaining GAG (A) and collagen (coll) (B) amounts per aECM were indirectly calculated by subtracting the quantified GAG or collagen amounts in the supernatants from the initially applied amounts. The legend shown in (A) is also applied to (B). Two-way ANOVA: \* ( $p < 0.05$ ), \*\* ( $p < 0.01$ ), \*\*\* ( $p < 0.001$ ) vs. respective aECM; # ( $p < 0.05$ ) vs. coll/sHA1/sHA4 (1/0.5/0.5). Adapted from [R316] with modifications.



In general the analysis of GAG derivatives is challenging [369]. For example, sHA1 and sHA4 only differ in their sulfation degree and cannot be distinguished by their sugar backbone. In addition, the number of available assays that are sensitive enough to detect GAG concentrations in the low  $\mu\text{g}$  range as expected for collagen-based aECMs is limited, no antibodies exist that reliably recognize chemically sulfated HA derivatives and no fragment-based GAG analysis can be performed due to the insufficient degradation of sHA derivatives via hyaluronidase [368]. Thus, fluorescence-labeled sHA derivatives were used to quantify them separately within the multi-GAG coating (Fig. 4.23 A) since none of the standard methods for sGAGs such as the DMMB assay allow any discrimination between such GAGs [416,419]. Also, agarose gel electrophoresis was applied for the first time to sHA derivatives to separate sHA1 from sHA4 (Fig. 4.23 B). Staining of the sGAGs within the gel using the cationic dyes toluidine blue and Stains-all visualized sHA1 as blue and sHA4 as purple bands. Both GAGs could be separated with this method due to the ion pair formation of the sulfate residues of the GAGs with  $\text{Ba}^{2+}$  ions present in the electrophoresis buffer. Since formed ion pairs have a decreased electrophoretic mobility, sHA4 and sHA1 revealed a mobility of 3.7 cm/(A·h) or 5.1 cm/(A·h), respectively, when applying an electric field strength of 451 V/m. Here, both sHA derivatives could be detected within the multi-GAG aECM even after the incubation with PBS at 37°C, indicating that sHA1 as well as sHA4 were integrated into the aECM during *in vitro* fibrillogenesis of collagen type I.

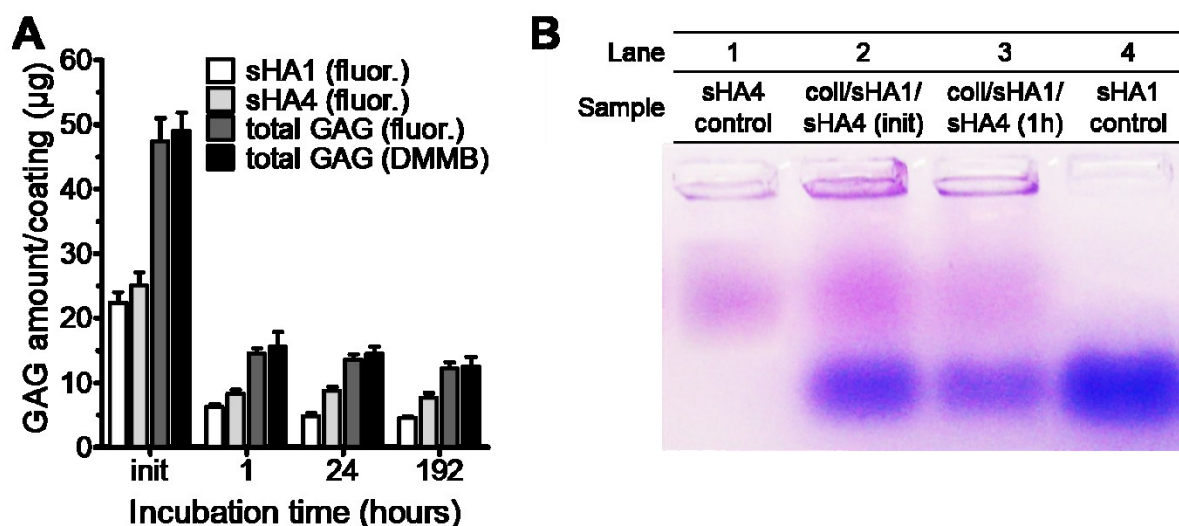


**Fig. 4.23 Quantification and separation of sHA derivatives from the multi-GAG aECM.** Multi-GAG coatings prepared with ATTO-labeled sHA1 and sHA4 were washed twice with water (init) and afterwards incubated with PBS at 37°C for up to eight days. The amount of sGAGs was quantified via DMMB assay and via fluorescence measurements (A). GAGs were stained with toluidine blue and Stains-all after GAG extraction from aECMs and subsequent separation by agarose gel electrophoresis. 10  $\mu\text{g}$  sHA1 and sHA4 were applied as references. Adapted from [R316] with modifications.

Negatively charged sHA derivatives within the aECM coatings alter the surface charge of the matrices in a sulfation-dependent manner, as shown by  $\zeta$ -potential measurements, and aECM

coll/sHA1/sHA4 (1/0.5/0.5) displayed an pI of 4.25, which is between the pI of coll/sHA1 (1/1) and coll/sHA4 (1/1) (pI of 4.65 or 3.95). Interestingly, additional cell culture studies using the GAG-containing matrices developed here revealed an enhanced viability of murine osteoclast-precursor-like RAW264.7 cells on aECMs with sHA4. Furthermore, the presence of sHA derivatives inhibited the osteoclast maturation in a defined manner, depending on the GAG sulfation as well as the GAG combination [R316]. In summary, these data highlight the potential of especially multi-sHA-containing matrices to potentially adjust the activity of bone-resorbing osteoclasts without completely inhibiting their crosstalk with osteoblasts, which is crucial for bone regeneration.

#### 4.4.2 Morphology of aECMs

Native GAGs such as CS, HA and HEP function as modulators that alter the structural ECM organization e.g. by influencing the assembly of collagen type I into fibrils [359R]. Thus, we hypothesized that the presence of GAG derivatives during fibrillogenesis may have an effect on the fibril morphology as well.

AFM analysis revealed that especially sHA derivatives individually altered the structure of the resulting collagen fibrils depending on their concentration as well as their D.S.s, while HA had no obvious effect on the aECM morphology at the investigated concentration (Fig. 4.24). This is in accordance with previous observations revealing a decreased surface roughness of collagen-based aECMs with increasing HA sulfation [353].

Large collagen fibrils showing the characteristic banding pattern were observed for collagen and coll/HA (1/1) (Fig. 4.24 A, E). The collagen fibril diameter after *in vitro* fibrillogenesis in the absence of sGAG was comparable to native collagen, which can be 10 - 500 nm depending on the tissue and developmental stage [465]. In contrast, concentration-dependently decreased fibril diameters were apparent for sHA1-containing matrices (Fig. 4.24 B, C). While coll/sHA1 (1/0.5) is characterized by thin fibrils, network-like structures with some embedded microfibrils were seen for coll/sHA1 (1/1). sHA4 exhibited the strongest interference with the collagen fibril formation leading to the development of homogeneous collagen-networks composed of thin, fine microfibrils without apparent banding pattern for both coll/sHA1 (1/0.5) and coll/sHA1 (1/1) (Fig. 4.24 F, G). Previous studies with single GAGs present during *in vitro* fibrillogenesis also reported that enhanced GAG concentrations and sulfation can decrease the fibril diameter of collagen type I and II [359R,407].

A heterogeneous mix of microfibrils and thin fibrils was detected for the multi-GAG aECM that contained both sHA1 and sHA4 (Fig. 4.24 D). This suggests that both GAGs individually contributed to the fibril organization, as sHA4 alone lead to microfibrils and sHA1 alone to thin fibrils.

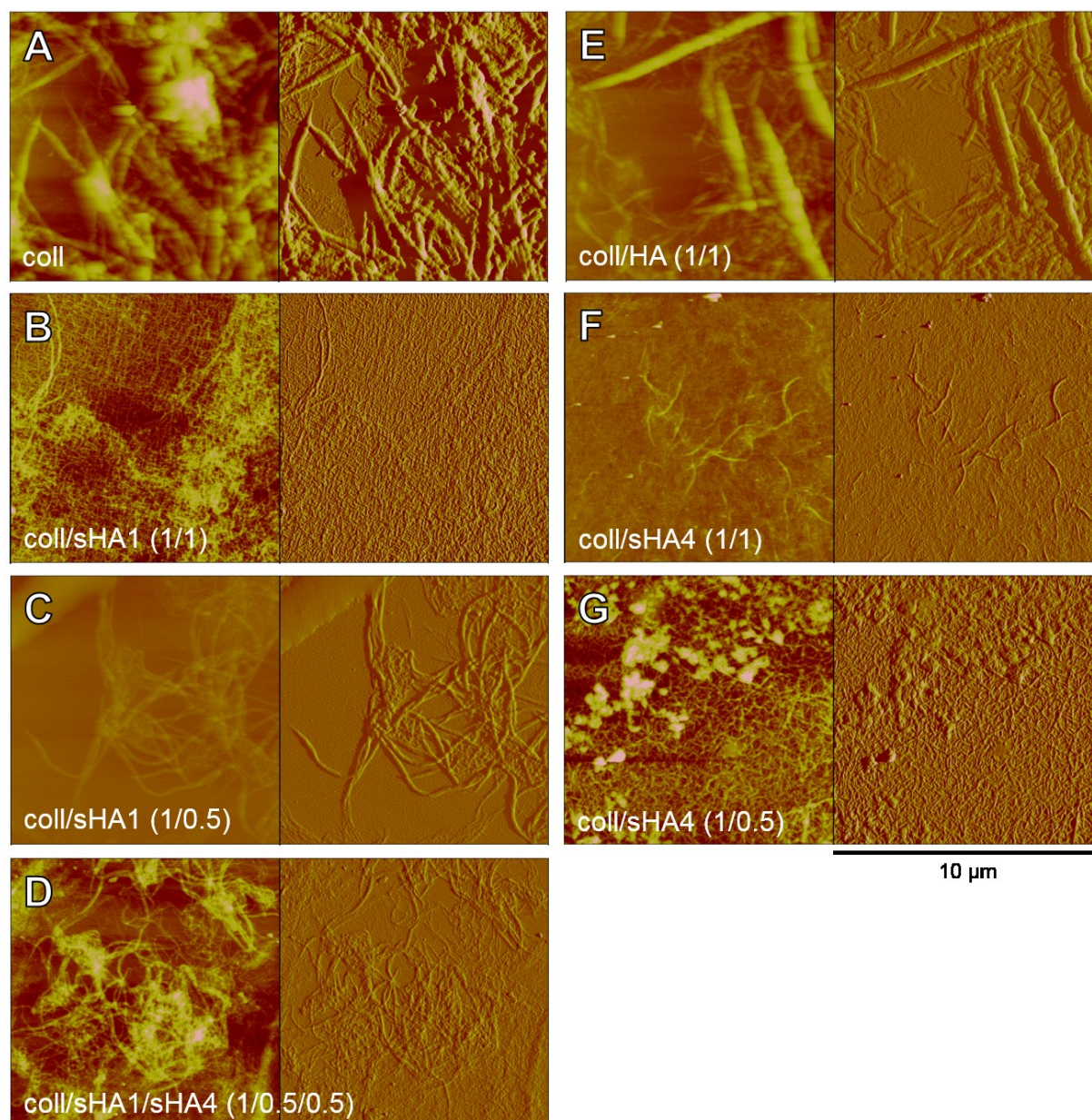


**Fig. 4.24 Fibril morphology of aECMs.** (A) coll fibrils in the absence of GAGs (z range height 250 nm, amplitude 0.8 V); (B) coll/sHA1 (1/1) (z range height 50 nm, amplitude 0.6 V); (C) coll/sHA1 (1/0.5) (z range height 300 nm, amplitude 0.8 V); (D) coll/sHA1/sHA4 (1/0.5/0.5) (z range height 50 nm, amplitude 0.8 V); (E) coll/HA (1/1) (z range height 200 nm, amplitude 1.1 V); (F) coll/sHA4 (1/1) (z range height 50 nm, amplitude 0.5 V) and (G) coll/sHA4 (1/0.5) (z range height 100 nm, amplitude 1.0 V). Images represent 10  $\mu\text{m}$  x 10  $\mu\text{m}$  details showing height images (left) and amplitude images (right). Adapted from [R316].

In summary, these findings demonstrate that the matrix morphology can be altered by varying the GAG sulfation, concentration and composition. Overall, the effects of GAG derivatives on the self-assembly of collagen type I were much more prominent for sHA4 compared to HA or sHA1, suggesting that the HA sulfation has a stronger influence on the fibril morphology than sHA concentration. This indicates that especially the negative net charge of sHA directs the fibril formation, which is consistent with previous findings showing that the interplay between

GAGs and collagen is mainly driven by their electrostatic interaction [24,466–468]. Accordingly, kinetic analyses of fibril formation revealed that sHA3 to collagen mass ratios above 1:1000 lead to an altered shape of the fibrillogenesis curve that indicates an aggregation rather than an ordered fibril assembly and results in an dose-dependent reduction of the resulting fibril diameter [359R].

#### 4.4.3 Enzymatic aECM degradation via collagenases

The enzymatic degradation of aECMs with or without associated GAGs by ChC was analyzed to estimate their degradability (Fig. 4.25). After 3 hours of ChC treatment, about 80 - 95% of the aECMs were degraded with most of the degradation occurring during the first 60 min. Likewise, Shi et al. observed an almost complete degradation of reconstituted human collagen type I after overnight incubation with ChC at 37°C [469].

There were no significant differences regarding the degradability of the analyzed matrices, which correlated well with the findings that show no or only a marginal decrease of the MMP-1/-2 activity in the presence of 2.5 mM D.U. GAG (Fig. 4.1). Since aECMs contain just 2 - 7% of the initially applied GAG solution (2.5 mM D.U) [9R], the remaining GAG amounts appear to be too low to influence the enzymatic aECM degradation.

ChC is widely used for *in vitro* enzymatic degradation studies [170] due to good availability and a degradation mechanism similar to MMPs [470], but is known to be more active than mammalian collagenases [170] and since it represents a mixture of six collagenases [471] we assume a much slower degradation of the aECMs *in vivo*.

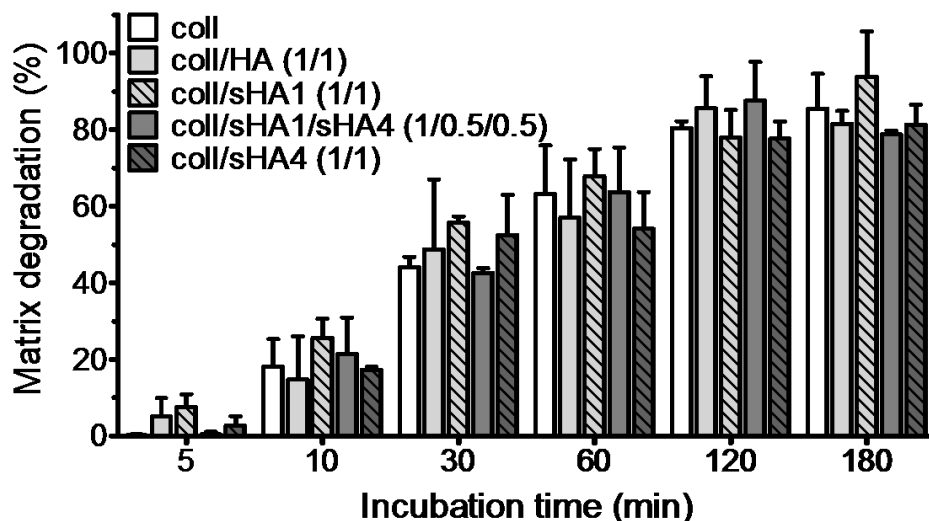


**Fig. 4.25 Enzymatic degradation of aECMs.** Matrices were incubated with PBS for 1 hour at 37°C prior to the treatment with 0.02 U ChC for up to 180 min at 37°C. The amount of degraded collagen was quantified via Lowry assay in the supernatants.

#### 4.5 Hydrogels as 3D aECMs for mediator protein binding and cell cultivation

Novel multi-functional 3D biomaterials are needed to meet the growing demands of a rising number of multi-morbid patients in the aging population [429], and using natural ECM components such as GAGs and structural proteins is advantageous to engineer biomaterials that mimic specific ECM properties and functions [5]. To translate the promising effects of GAG-containing 2.5D aECM coatings [9,R316], HA-based hydrogels crosslinked via HA- and sGAG-acrylates with embedded collagen type I fibrils were developed. To this end collagen fibrils obtained via *in vitro* fibrillogenesis were used without additional crosslinking within the GAG-based hydrogel network to maintain the characteristic properties and structure of collagen.

An similar combination of preparation techniques was previously described by Guo et al., who developed collagen/CS/HA hydrogels based on methacrylated HA and CS derivatives for cartilage tissue engineering [472]. These gels had 10 times higher collagen concentrations and lower GAG to collagen mass ratios (1:2 vs. 20:1 in the here developed gels). The advantages of the compositions used here are i) decreasing the necessary amounts of the animal-derived component collagen and at the same time ii) obtaining hydrogels that contain collagen fibrils which provide cell adhesion ligands. Moreover, the here prepared gels are iii) characterized by much higher sHA to HA mass ratios than those described previously [400,401], providing an enhanced number of sulfated GAG residues as potential interaction sites for the interplay with mediator proteins and cells.

The aim is to use these hydrogels as mediator protein binding or scavenging systems as well as growth promoting substrates for cells relevant during the healing of vascularized tissues such as skin. Against this background, these gels were analyzed to examine their characteristic hydrogel parameters, composition, stability, structure, enzymatic degradation and their binding and release profiles for lysozyme and VEGF-A. Afterwards endothelial cells were cultivated in the gels in the absence or presence of VEGF-A to reveal the effects of the hydrogel composition on the adhesion, proliferation and functional morphology of these cells.

##### 4.5.1 Hydrogel characteristics, composition and structure

To characterize the developed hydrogels the water content, the volume loss after lyophilization, the swelling ratio as well as the elastic modulus were determined as typical hydrogel parameters (Fig. 4.26). All gels contained about 97 - 99% water after crosslinking and their volume decreased during freeze-drying by about 10 - 40% (Fig. 4.26 A, B). In line with this, Cai et al. detected high water contents above 97% for their HEP/HA-PEG hydrogels and concluded that this is especially favorable for the exchange of hydrophilic molecules and nutrients for cells within the gel [473]. The highest water content, volume loss due to lyophilization and elastic modulus were found for pure HA-AC gels without sGAG or collagen (Fig. 4.26 A-C). In contrast, significantly decreased values were observed for these three parameters in case of

collagen-containing gels. Segura et al. reported a comparable effect of collagen on the water content for HA/collagen hydrogels that were crosslinked with poly(ethylene glycol) diglycidyl ether [474].

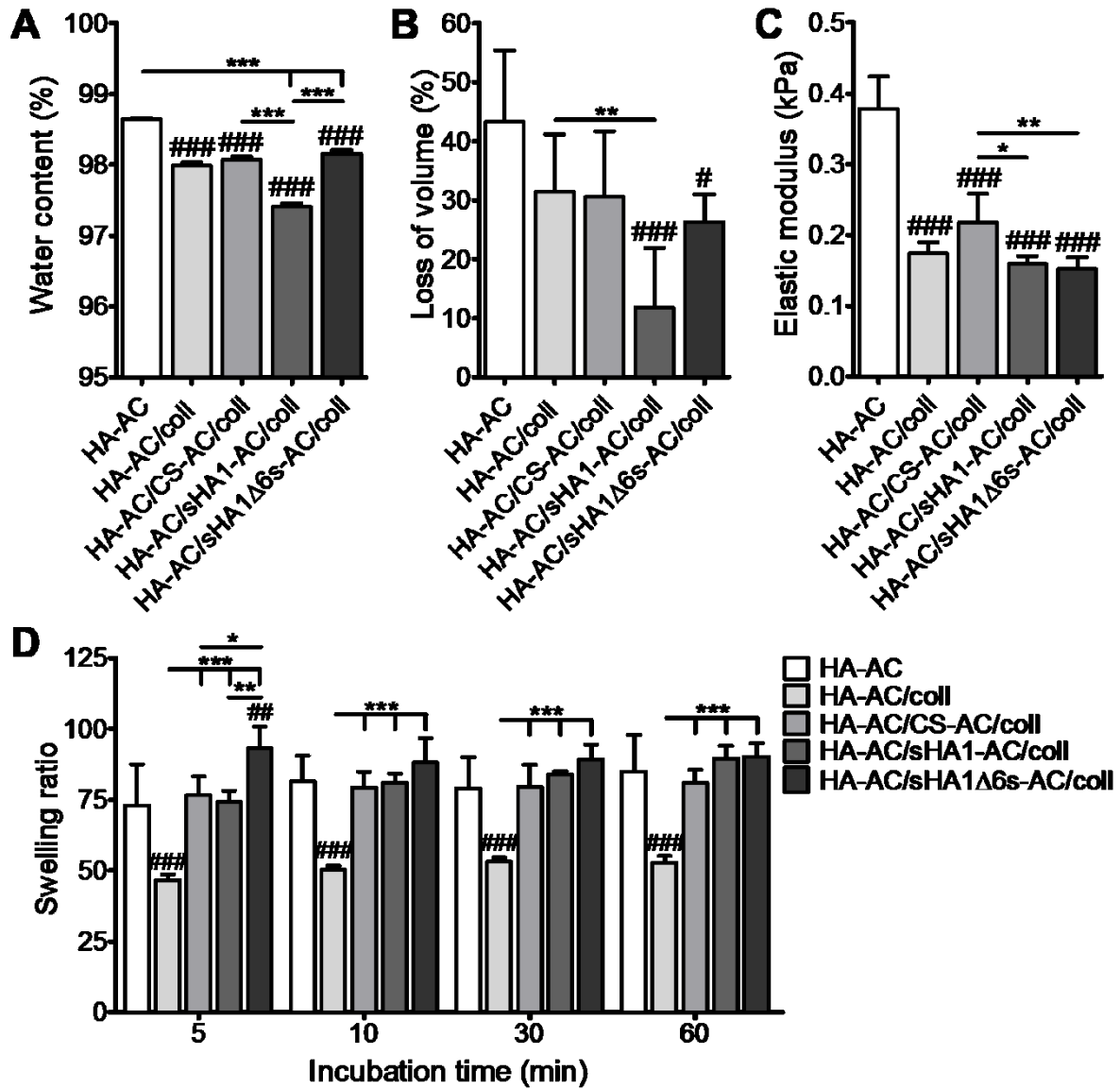


**Fig. 4.26 Characterization of HA/collagen hydrogels.** The water content of the respective gels (A), the loss of volume due to lyophilization (B), the elastic modulus (C) and the swelling ratio after incubation of the freeze-dried gels with water (D) are displayed. One-way ANOVA for (A-C) and two-way ANOVA for (D): # ( $p < 0.05$ ), ## ( $p < 0.01$ ), ### ( $p < 0.001$ ) vs. HA-AC; \* ( $p < 0.05$ ), \*\* ( $p < 0.01$ ), \*\*\* ( $p < 0.001$ ) vs. respective hydrogel. Adapted from [R475] with modifications.

It is of note that HA-AC/sHA1-AC/coll was the gel with the lowest water content as well as the lowest loss of volume after freeze-drying compared to HA-AC/coll. However, there were no significant differences between the water content and volume loss for gels with CS-AC or sHA1Δ6s-AC and HA-AC/coll. The elastic modulus of HA-AC was 43 - 60% higher than for HA-AC/coll and those hydrogels with additional sGAG-AC, which all showed elastic moduli in the range of 0.15 - 0.22 kPa. This suggests that collagen fibrils may be sterical obstacles that

partially hinder effective GAG-crosslinking, thereby possibly resulting in the formation of less crosslinks per respective gel volume compared to pure HA-AC gels, which in turn leads to decreased elastic moduli. The here determined elastic modulus of HA-AC is supported by previous studies of Becher et al. [365]. A slightly enhanced elastic modulus was, however, detected for HA-AC/CS-AC/coll compared to sHA-AC-containing hydrogels, which could correlate to the altered polysaccharides backbone or with the enhanced D.S.s of both sHA-AC derivatives.

The swelling ratio of hydrogels is defined as an increase of the gel weight from the binding of water relative to the initial gel mass after lyophilization. In general, all hydrogels absorbed a higher mass of water than their dry weight within the first five minutes of incubation. The addition of collagen in case of HA-AC/coll significantly decreased the swelling ratio of HA-AC gels (Fig. 4.26 D) while it was enhanced for all sGAG-AC-containing hydrogels compared to HA-AC/coll, reaching swelling ratios almost comparable to pure HA-AC gels. Additional collagen fibrils present within the crosslinked HA network could hinder the binding of further water molecules to HA, which may explain the decreased swelling ratio of HA-AC/coll. This effect was not apparent for hydrogels with additional sGAG-AC derivatives, probably due to a compensating effect as a result of their enhanced water binding capacity in comparison to HA [476]. Purcell et al. likewise reported an increased swelling ratio for gels containing 10% sHA derivatives compared to pure HA hydrogels [400]. After five minutes of gel incubation in distilled water, HA-AC/sHA1 $\Delta$ 6s-AC/coll revealed the highest water binding capacity, while this was insignificantly increased compared to the other sGAG-AC gels and HA-AC at later time points.

After crosslinking and freeze-drying, the composition and stability of the obtained hydrogel scaffolds were analyzed (Fig. 4.27). Almost the whole amount of GAG-AC was integrated into the gels during crosslinking (Fig. 4.27 A).

During the gel incubation in PBS at 37°C for up to 192 hours, only low amounts of sGAG-AC (< 10%) were released, mainly within the first 60 min of incubation, while the HA-AC content remained nearly unaffected over time. In line with this, Hu et al. observed no release of crosslinked HA from hydrogels containing HA, gelatin and CS after 15 days of incubation in PBS at 37°C [477]. Here significantly higher percentages of remaining GAGs were found compared to non-crosslinked collagen-based aECM coatings with associated GAGs, which typically contain only 10 - 50% of the initially used GAG amounts after 60 min of incubation with PBS at 37°C.

The 2.5D aECM had about 90 - 95% of their initial collagen stably incorporated [350] (section 4.4.1). In contrast, significant amounts of collagen were detected in the supernatants during incubation of the hydrogels in PBS (Fig. 4.27 B). This was more pronounced for hydrogels with additional sGAG-AC than for HA-AC/coll ( $\approx$  40 - 50% collagen release vs.  $\approx$  30%). Together

with the higher release of sGAG-AC compared to HA-AC, this suggests that the GAG sulfation may alter the crosslinking network of the gels.

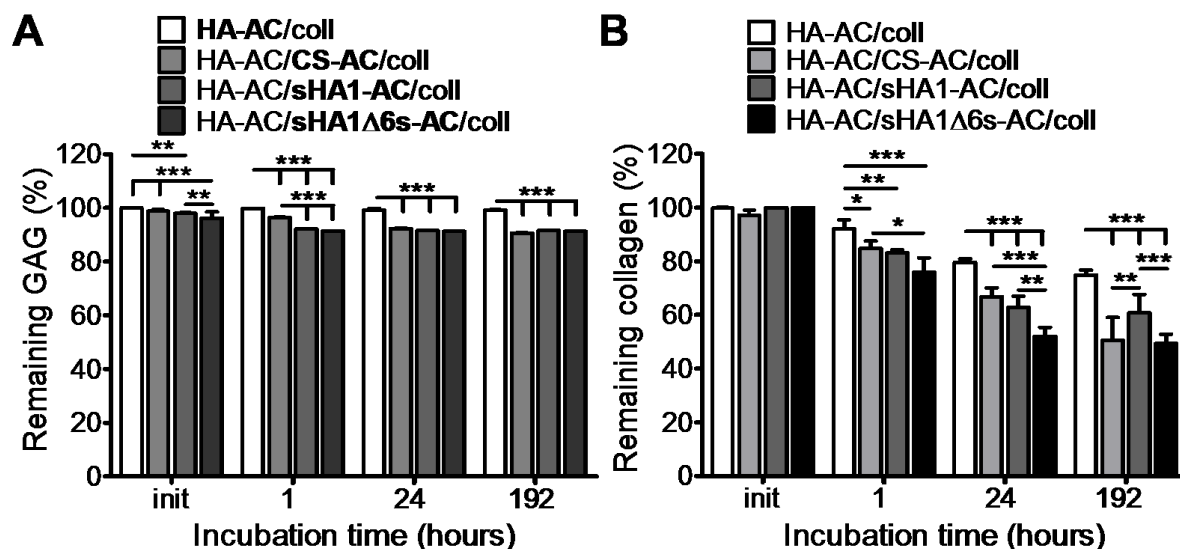


**Fig. 4.27 Composition of HA/collagen hydrogels.** Hydrogels were incubated in PBS at 37°C for up to 192 hours. The remaining GAG content in the gels (shown in bold) was indirectly calculated by measuring the amount of released GAG in the supernatants via hexosamine or DMMB assay (A). The collagen content was assessed via the method of Lowry (B). Two-way ANOVA: \* ( $p < 0.05$ ), \*\* ( $p < 0.01$ ), \*\*\* ( $p < 0.001$ ) vs. respective hydrogel. Adapted from [R475] with modifications.

Additional staining methods were used to qualitatively examine the GAG and collagen content of these gels (Appendix Fig. 7.9). Some light blue background staining was observed in case of HA-AC and HA-AC/coll, while hydrogels with sGAG-AC displayed a higher color intensity after incubation with Toluidine blue indicating a homogeneous incorporation of sGAGs within the gels (Appendix Fig 7.9, top). For all collagen-containing gels an uniform distribution of collagen was shown after staining with Sirius red (Appendix Fig. 7.9, bottom).

The resulting GAG-AC to coll mass ratios calculated for the freeze-dried hydrogel scaffolds and for gels after incubation in PBS at 37°C are summarized in Tab. 4.3. Overall, the GAG to collagen mass ratios of the HA/collagen hydrogels were almost inverted compared to non-crosslinked collagen-based aECM coatings (section 4.4.1).

**Tab. 4.3 GAG to collagen mass ratios of HA-AC/collagen hydrogels.**

Hydrogel	After freeze-drying	After 192 hours in PBS
HA-AC/coll	20:1	26:1
HA-AC/CS-AC/coll	21:1	38:1
HA-AC/sHA1-AC/coll	20:1	32:1
HA-AC/sHA1Δ6s-AC/coll	20:1	39:1



SEM was used to analyze the structure of the hydrogel scaffolds after freeze-drying (Fig. 4.28). All samples showed a porous structure characterized by pore diameters predominantly above 100  $\mu\text{m}$ . Gels containing collagen displayed randomly distributed collagen fibrils with diameters of about 100 - 300 nm and an apparent banding pattern (red arrows in Fig. 4.28 G-J), while smooth surfaces were observed for HA-AC. Similar collagen fibril morphologies were reported for collagen type I-based matrices after the *in vitro* fibrillogenesis of collagen monomers as well for collagen fibrils present in native tissue [359R,478]. As expected, there were no obvious differences between HA-AC/coll and those gels with additional amounts of sGAG-AC (Fig. 4.28 B-E, G-J).

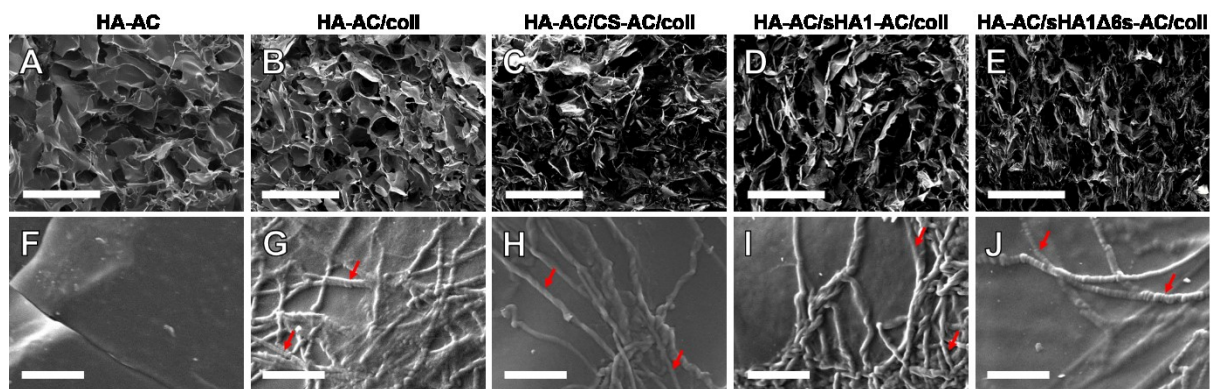


**Fig. 4.28 Morphology of hydrogels.** SEM images of lyophilized hydrogel cross-sections. Scaffolds without collagen (A/F), with collagen (B/G) and additional CS-AC (C/H), sHA1-AC (D/I) and sHA1 $\Delta$ 6s-AC (E/J) are shown. Arrows highlight the typical banding pattern of collagen fibrils. Scale bars in the upper panel indicate 400  $\mu\text{m}$  and in the lower panel 2  $\mu\text{m}$ . Adapted from [R475].

#### 4.5.2 HA and hydrogel degradation via Hyal

The enzymatic activity of Hyal can be inhibited by native sGAGs like HEP [478]. We therefore investigated how solute and hydrogel-bound sGAG derivatives affect the Hyal-mediated degradation of native HA immobilized on PS surfaces as well as of HA-based hydrogels (Fig. 4.29). This is of particular interest since the biodegradability of a material is important for its potential biomedical application.

Hyal was shown to time-dependently degrade immobilized HA. The presence of all examined sGAGs resulted in decreased amounts degraded HA after 30 min of incubation compared to the control without GAGs (about 35 - 51% HA degradation vs. about 66%) (Fig. 4.29 A). It is of note that both sHA derivatives revealed a stronger impact on the HA cleavage than native CS. HEP retarded HA degradation in a manner comparable to sHA1 and CS, while the presence of sHA1 $\Delta$ 6s showed the most pronounced effects on HA degradation. This indicates that all examined sGAGs had an inhibitory potential against Hyal activity.

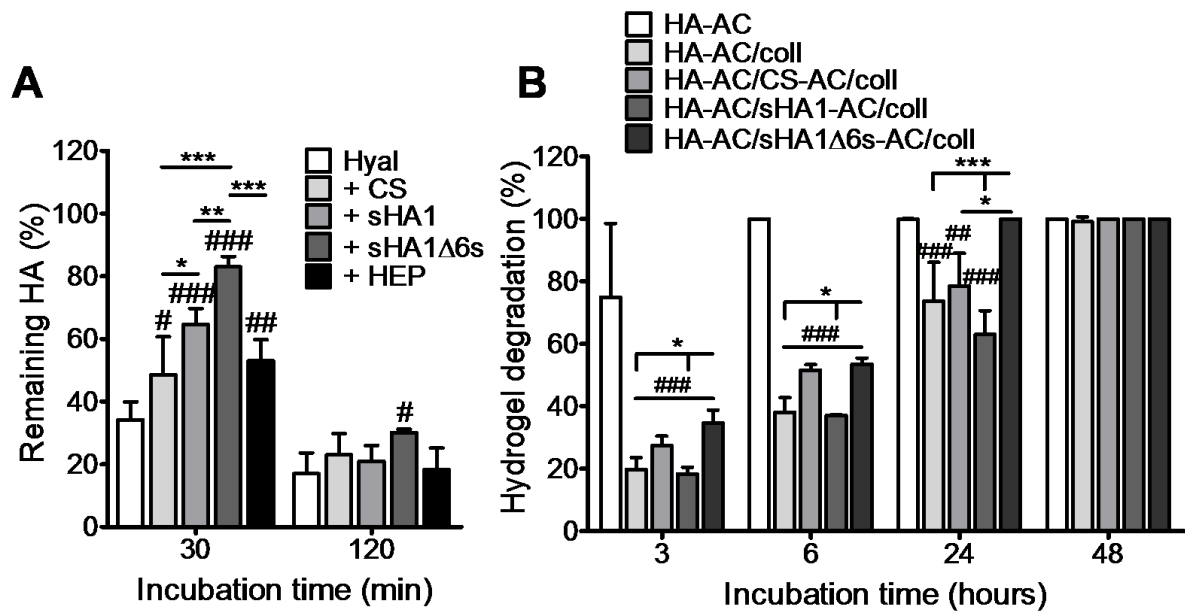


**Fig. 4.29 Enzymatic degradation of HA coatings and HA/collagen hydrogels via Hyal.** (A) Native HA was immobilized via its reducing ends onto PS surfaces prior to the incubation with 0.001 U Hyal per well in the absence or presence of solute sGAGs at 37°C. The remaining HA was afterwards quantified via ELISA. (B) Degradation of HA/collagen hydrogels via 400 U Hyal per gel at 37°C. The amount of degraded gels was examined by determining GAG amounts in the supernatants via hexosamine assay. Two-way ANOVA: # ( $p < 0.05$ ), ## ( $p < 0.01$ ), ### ( $p < 0.001$ ) vs. Hyal w/o GAG or HA-AC; \* ( $p < 0.05$ ), \*\* ( $p < 0.01$ ), \*\*\* ( $p < 0.001$ ) vs. respective group. Adapted from [R475] with modifications.

HA sulfation is likewise reported to block the HA degradation by Hyal and native GAGs such as CS are suggested to function as modulators of the Hyal activity [368,478]. In line with the obtained findings, Suzuki et al. found a decreased Hyal activity in the presence of per-sulfated HA [479]. The significantly stronger effect of sHA1Δ6s compared to sHA1 points to an influence of the sulfation position, while the comparably lower interference of CS implies that the sugar backbone plays a role as well. This is supported by the fact that even though HEP has a higher D.S.<sub>s</sub> it revealed a lower or similar inhibitory effect on the HA cleavage compared to sHA derivatives with less sulfate residues per D.U. We observed a trend to a slightly lower HA degradation in the presence of HEP than in the presence of CS, which may correlate with the previously demonstrated higher binding levels for the HEP interaction with Hyal compared to CS-A during SPR analysis [480].

After a further 90 min of incubation with the respective mixtures of Hyal and sGAGs the detected amounts of non-degraded HA were mainly comparable to the control (about 17 - 30% remaining HA). The fact that we could not measure a complete HA degradation after 120 min of treatment with Hyal may result from the concurrent further degradation of HA present in the supernatants after its cleavage from the wells, and from a potential sterical hindrance of lysozyme that hampers the cleavage of remaining HA close to the well surface. However, we cannot exclude a slight overassessment of the inhibition of the Hyal activity due to a potential

additional sHA degradation via Hyal, even though this is suggested to be of secondary importance.

Pure HA-AC hydrogels were quickly degraded within 3 - 6 hours of incubation (Fig. 4.29 B), while collagen-containing gels with or without sGAG-AC were only decomposed after 24 - 48 hours. Feng et al. reported a similar degradation of hydrogels composed of methacrylated HA with or without methacrylated sHA during early time points of Hyal incubation [401]. In contrast to the obtained findings with collagen-containing HA-hydrogels, though, they found a decreased hydrogel degradation for gels with methacrylated sHA compared to pure HA-based gels at later stage of their degradation study; however, this does not correspond with the sulfation degree of the used GAGs (D.S.s of 0.4 for methacrylated sHA vs. D.S.s of 1.5 for sHA1-AC).

Interestingly, gels with additional sHA1 $\Delta$ 6s-AC were less resistant against Hyal activity than HA-AC/sHA1-AC/coll or HA-AC/coll gels. This indicates that the position of acrylation strongly affects the hydrogel stability against enzymatic degradation, as we observed a diametrically opposed impact for solute, non-acrylated sHA1 $\Delta$ 6s on the degradation of HA (Fig. 4.29 A, B). However, there were no significant differences between the degradation rate of HA-AC/coll gels with or without additional sHA1-AC or CS-AC.

In summary, low-sulfated sHA derivatives do not hinder the enzymatic cleavage of immobilized HA or of crosslinked HA/collagen hydrogels in general, since native HA was degraded within 120 min in the presence of sGAGs and all hydrogel compositions were fully decomposed within 48 hours via Hyal activity. Moreover, the presence of collagen fibrils significantly enhanced the resistance of the hydrogels against enzymatic degradation. This should be favorable regarding the fast HA degradation *in vivo* that usually limits the biomedical application of HA-based hydrogels. Though *in vitro* data can only give an indication regarding degradation time *in vivo*, it can be assumed to be longer since the Hyal concentrations used here were above physiological levels [481].

#### 4.5.3 Interaction of lysozyme with hydrogels

To analyze the protein binding and release profiles of the developed HA/collagen hydrogels depending on their composition, the gels were loaded with fluorescence-labeled lysozyme prior to incubation in buffer (Fig. 4.30). Lysozyme was used as model protein to analyze the potential interaction with GAGs since its size is in the range of several GAG-binding mediator proteins such as pro-inflammatory cytokines or growth factors like bFGF, and it is positively charged at physiological pH 7.4 [440,441,482].

Hydrogels with additional sHA1-AC and CS-AC captured significantly higher amounts of lysozyme than the respective gels without sGAG-AC (Fig. 4.30 A). This is in accordance with previously reported results showing an enhanced interaction of lysozyme with CS-A or CS-E

compared to HA [439]. Overall, HA-AC/CS-AC/coll gels bound the highest protein amounts even in comparison to sHA-AC containing hydrogels, although their sulfation degree is lower. This is in line with the GAG/lysozyme binding studies (Fig. 4.4) and suggests that the sugar backbone of GAGs plays an important role for lysozyme binding to GAGs.

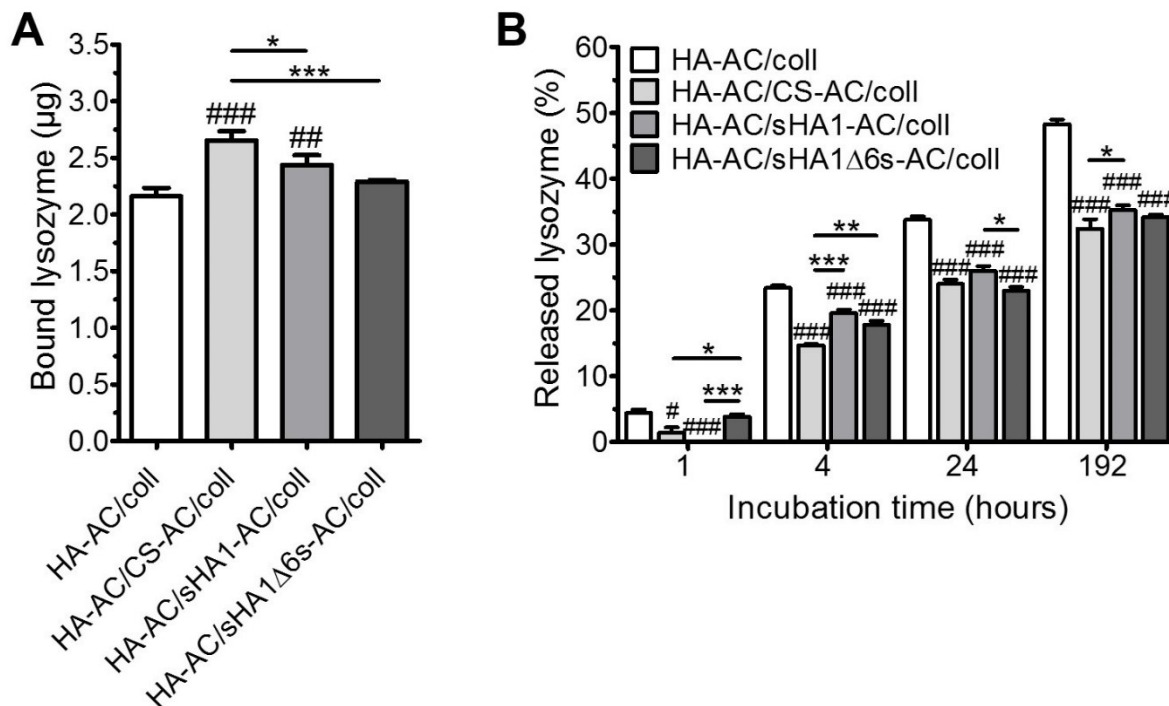


**Fig. 4.30 Binding and release of lysozyme after incubation with hydrogels.** Each hydrogel was incubated with 4 µg Rhodamine B-labeled lysozyme dissolved in 2% BSA/PBS o/n at 4°C. Afterwards, the gels were incubated in 2% BSA/PBS at 37°C to study their lysozyme release over time. The lysozyme binding (A) and release (B) was quantified via fluorescence measurement. One-way ANOVA for (A) and two-way ANOVA for (B): # ( $p < 0.05$ ), ## ( $p < 0.01$ ), ### ( $p < 0.001$ ) vs. HA-AC/coll; \* ( $p < 0.05$ ), \*\* ( $p < 0.01$ ), \*\*\* ( $p < 0.001$ ) vs. respective hydrogel composition. Adapted from [R475] with modifications.

Surprisingly, the addition of sHA1Δ6s-AC had no significant impact on the amount of gel-bound lysozyme compared to HA-AC/coll, only a tendency for a higher protein binding capacity was observed. These results highlight that the type of substitution, their pattern and the crosslinking of GAGs strongly alters the protein binding since sHA1Δ6s-coated surfaces revealed the highest lysozyme binding capacity. This markedly decreased after acrylation (section 4.2.3, Fig. 4.4) and, as seen for HA-AC/sHA1Δ6s-AC/coll gels, seem to further decrease after crosslinking. This implies that the introduction and crosslinking of acryl groups at the C6 position of HA after sulfation of secondary hydroxyl groups may affect the GAG structure and thereby the formed GAG network as well as the gel interaction with lysozyme. Since the characteristic hydrogel parameters of the HA-AC/sHA1Δ6s-AC/coll gels were mainly comparable to the other sGAG-containing gels, it is not possible to deduce from these parameters on the changed lysozyme binding behavior.

A time-dependent lysozyme release was observed during the gel incubation with PBS (Fig. 4.30 B). The highest percentage of previously gel-bound lysozyme was measured in the supernatants after 4 hours of incubation (about 15 - 23%). The amount of lysozyme released during the following 188 hours was almost comparable to the initially released amount with 16 - 25%, indicating a slower lysozyme release. All gels with sGAG-AC showed a retarded protein release compared to HA-AC/coll gels, showing that the lysozyme/hydrogel interaction is mainly controlled via binding to sGAG derivatives. Cai et al. likewise demonstrated that the addition of HEP to HA-PEG or CS-PEG hydrogels significantly decreased the release of bFGF from the hydrogels [473]. In addition, the presence of gelatin in HA-PEG-hydrogels containing HEP was shown to increase the release of several growth factors like bFGF or VEGF-A. The possible reason may be a reduced sterically hindrance that affects the diffusion of the growth factors through gelatin-containing gels due to the lower molecular weight of gelatin compared to HA [482]. Thus, it can be assumed that the presence of collagen within the gels also contributes to the release characteristics.

#### 4.5.4 Interaction of VEGF-A with hydrogels

Based on the results with the model protein lysozyme (section 4.5.3) the binding capacity of the hydrogels for VEGF-A as well as their growth factor release profiles were examined via ELISA (Fig. 4.31). Thin small hydrogels were used for these experiments to enable the incubation with VEGF-A amounts above their respective binding maxima.

All hydrogels bound about 30 - 43 ng VEGF-A (Fig. 4.31 A). Even though there were no significant differences between the gels, sGAG-AC-containing gels showed a trend to capture higher amounts of VEGF-A compared to HA-AC/coll. Release analysis revealed a sulfation-dependent VEGF-A retardation (Fig. 4.31 B). While HA-AC/coll and HA-AC/CS-AC/coll released about 80 - 90% of the initially gel-bound VEGF-A within eight days of incubation, gels with sHA1-AC and sHA1 $\Delta$ -AC showed a significantly slower VEGF-A release which might be favorable for applications that require a long-term delivery of the growth factor. In general, the VEGF-A release increased in the following order: HA-AC/sHA1-AC/coll < HA-AC/sHA1 $\Delta$ 6s-AC/coll < HA-AC/CS-AC/coll  $\approx$  HA-AC/coll. Feng et al. also demonstrated a retarded release of TGF- $\beta$ 1 from hydrogels containing methacrylated sHA compared to pure HA-based hydrogels, making an increased electrostatic interaction of the negatively charged sulfate residues with positively charged regions of the growth factor responsible [401]. In accordance with findings with HA-AC/sHA1 $\Delta$ 6s-AC/coll compared to HA-AC/sHA1-AC/coll, binding and release studies with VEGF-A and starPEG-HEP hydrogels containing differently desulfated HEP derivatives revealed that gels containing a 6-*O*-desulfated HEP release higher amounts of VEGF-A compared to gels with non-modified HEP, even though their VEGF-A binding capacity was similar [459].

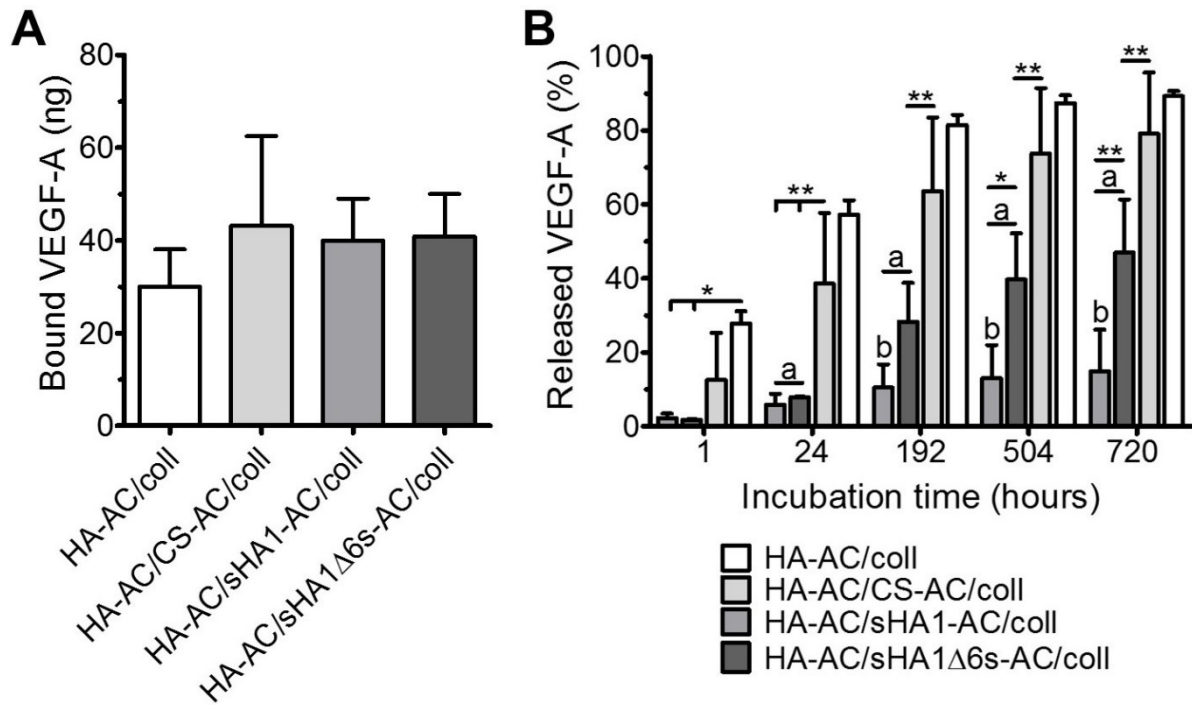


**Fig. 4.31 Binding and release of VEGF-A after incubation with hydrogels.** Each hydrogel was incubated with 200 ng VEGF-A dissolved in 1% BSA/PBS o/n at 37°C. Afterwards, the gels were incubated in 1% BSA/PBS at 37°C to study their VEGF-A release over time. The VEGF-A binding (A) and release (B) was measured via ELISA. Two-way ANOVA: \* ( $p < 0.05$ ), \*\* ( $p < 0.01$ ) vs. respective hydrogel composition; a ( $p < 0.001$ ) vs. HA-AC/coll, b ( $p < 0.001$ ) vs. HA-AC/CS-AC/coll.

There were no differences between the binding of VEGF-A to CS-AC, sHA1-AC or sHA1Δ6s-AC containing gels, which agreed with SPR data using acrylated sGAG derivatives (section 4.2.4). In contrast, SPR binding analysis demonstrated a higher binding response of CS-AC and sHA-AC derivatives compared to HA-AC, suggesting a higher binding capacity of hydrogels with sGAG-AC compared to gels with HA-AC. However, all hydrogels with sGAG-AC mainly contain HA-AC (75%) regarding their GAG content and only 25% are sGAG-AC. This may lead to no significant differences in their VEGF-A binding behavior. This could be advantageous for future *in vitro* and *in vivo* studies since it allows the direct comparison of effects resulting from the different release characteristics of sGAG-AC containing gels without considering further effects due to different initial VEGF-A amounts within the gels. The comparably high amounts of gel-bound VEGF-A within HA-AC/coll gels together with the fast growth factor release indicate that VEGF-A is mainly entrapped in the hydrogel meshwork rather than specifically bound in this hydrogel type.

The retarded VEGF-A release from HA-AC/sHA1-AC/coll and HA-AC/sHA1Δ6s-AC/coll compared to the other gels is in accordance with ELISA experiments with the respective immobilized GAGs (section 4.2.4). The impact of acrylation at the C6 position of sHA1Δ6s lead to a strongly decreased interaction with VEGF-A during SPR and ELISA analyses. This was even more pronounced after crosslinking and resulted in a higher release of VEGF-A from gels with sHA1Δ6s-AC compared to sHA1-AC-containing ones, something that was not

observed for the non-crosslinked GAGs in ELISA studies (section 4.2.4). A similar effect was seen for the binding of lysozyme to sHA1 $\Delta$ 6s-AC surfaces compared to sHA1 $\Delta$ 6s surfaces (section 4.2.3). Thus, the release profiles of the developed HA/collagen-based hydrogels for VEGF-A can be specifically adjusted via the usage of acrylated sHA derivatives with different substitution patterns.

#### 4.5.5 Endothelial cell growth within hydrogels in the presence of serum

Since endothelial cells are indispensable for angiogenesis during regeneration of vascularized tissues such as skin or bone [483], the endothelial cell line PAE/KDR was used to examine the biocompatibility of the hydrogels. To this end the cells were cultivated on hydrogels in the presence of serum. Their metabolic activity, cell number and cell morphology were analyzed over time to reveal the direct effects of the hydrogel composition on the cellular response *in vitro* (Fig. 4.32). Pure HA-AC gels could not be included in cell culture studies since they quickly lost their physical stability and were almost decomposed within one day after cell seeding.

About 50% of the seeded endothelial cells were found within the HA-AC/coll gels after 2 hours of cultivation. HA-AC/sHA1 $\Delta$ 6s-AC/coll gels had the highest seeding efficiency with about 99% of the seeded cells determined via DNA assay (Fig. 4.32 A). A similar trend with about 1.7 - 1.9 and 1.5 - 1.7-fold higher values was detected for the metabolic activity determined via LDH assay for PAE/KDR cells cultivated within sHA1 $\Delta$ 6s-AC- or sHA1-AC-containing hydrogels (Fig. 4.32 B). This indicates that the presence of sHA-AC derivatives strongly enhance the PAE/KDR cell proliferation and metabolic activity. In line with this van der Smissen et al. detected an increased adhesion and proliferation of human dermal fibroblast after cultivation on collagen-based aECM coatings with sHA derivatives [406]. However, the cell counting technique used here do not allow to differentiate between proliferation, survival (necrosis or apoptosis) or both. The underlying mechanism how especially sHA derivatives exert their effects on cells is not fully understood hitherto.

The cell numbers time-dependently increased for all gel compositions proving HA/collagen gels to be nontoxic. The strongest rise of the cell numbers after 72 hours was observed for both gels with sHA-AC derivatives showing an about 1.7 - 2.1-fold increase in cell number for HA-AC/sHA1 $\Delta$ 6s-AC/coll and an about 2.0 - 2.6-fold increase for HA-AC/sHA1-AC/coll gels.

Important aspects could be that GAG derivatives affect cell adhesion, which is mediated via integrins as well as the actin cytoskeleton signaling processes [353]. The presence of CS-AC within the gels led to almost no significant effects on the cell proliferation and none for the metabolic activity compared to HA-AC/coll. The only exception was a slightly increased DNA content after 72 hours within HA-AC/CS-AC/coll gels compared to HA-AC/coll, which may result from the slightly higher initial seeding efficiency. A growth promoting effect of CS coatings on endothelial cells compared to HA coatings was also reported by Heng et al. [55]. It

is of note that the examined release of collagen from gels over time (section 4.5.1) led to no apparent negative effects during the cell culture studies.

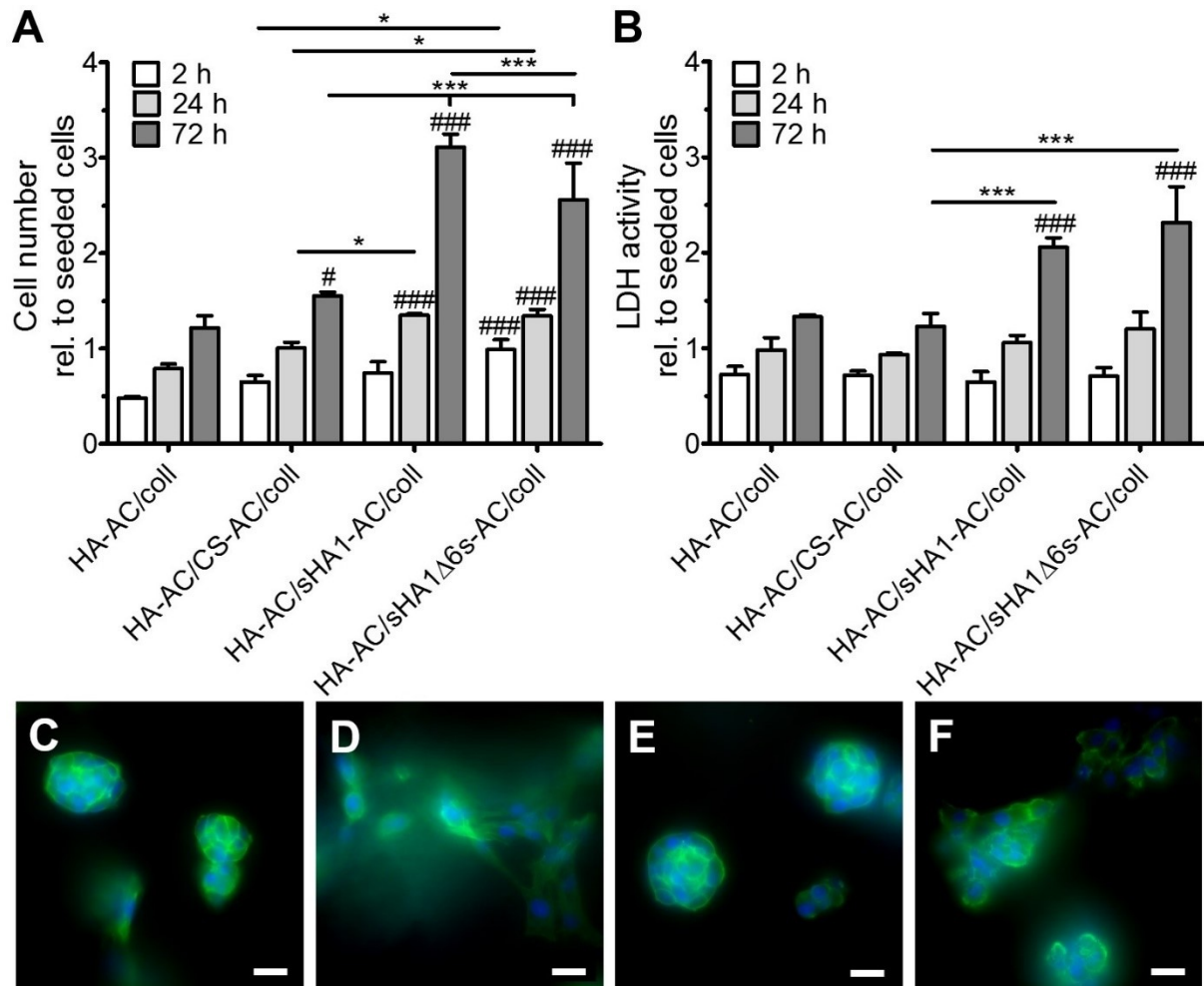


**Fig. 4.32 Effects of hydrogel composition on endothelial cells.** 200000 PAE/KDR cells were seeded per freeze-dried hydrogel ( $h = 1.1$  mm,  $\varnothing = 8.5$  mm) and cultivated for up to 72 hours in the presence of serum. The respective cell number was indirectly calculated by quantifying the DNA content (A) and the metabolic activity was determined by measuring the LDH activity (B). The endothelial cell morphology on HA-AC/coll (C), HA-AC/CS-AC/coll (D), HA-AC/sHA1-AC/coll (E) and HA-AC/sHA1Δ6s-AC/coll was visualized after 72 hours by immunofluorescence staining of F-actin (green) and the nuclei with DAPI (blue). Two-way ANOVA: # ( $p < 0.05$ ), ### ( $p < 0.001$ ) vs. HA-AC/coll; \* ( $p < 0.05$ ), \*\*\* ( $p < 0.001$ ) vs. respective hydrogel composition. Adapted from [R475] with modifications.

The PAE/KDR cell morphology after 72 hours of cultivation was examined after immunofluorescence staining of the cell nuclei and cytoskeletal F-actin filaments (Fig. 4.32 C-F). Since the gels were cut into halves and the inner parts of the gels were used for microscopic observations, the obtained fluorescence images proved the presence of endothelial cells in the inner part of the hydrogels. This indicates that the provided gel structures allow PAE/KDR cell migration. The 3D growth of the cells in the gels is also apparent in the images where cells are out of the plane of focus.



Endothelial cells within hydrogels with CS-AC or sHA1 $\Delta$ 6s-AC (Fig. 4.32 D, F) revealed a more spread morphology compared to those within the other gels (Fig. 4.32 C, E) which mainly showed bigger cell clusters. This implies an enhanced cell-matrix interaction for gels with CS-AC or sHA1 $\Delta$ 6s-AC and a more preferred cell-cell contact in the latter cases. However, PAE/KDR cells in gels containing sHA1 $\Delta$ 6s-AC had a more rounded shape than those in gels with CS-AC (Fig. 4.32 D, F), which may result from the increased elastic modulus of the latter gels compared to the other sGAG-AC-containing hydrogels (Fig. 4.32 C). Only in the latter case did endothelial cells show spread F-actin filaments, while the cells within the other gels exhibited a denser F-actin network. Heng et al. also observed that endothelial cells cultivated on HA coatings had a more rounded and less elongated shape than those on CS surfaces [55].

#### 4.5.6 Influence of solute GAGs on VEGF-A stimulated endothelial cells

To determine GAG-mediated effects on the VEGF-A-stimulated proliferation and tube formation of PAE/KDR cells, the cells were cultivated on collagen type I coatings to facilitate adhesion in the absence or presence of VEGF-A and/or solute GAG derivatives under serum free conditions (Fig. 4.33).

No toxic effects were observed for the examined GAG derivatives. PAE/KDR cells cultivated in the presence of VEGF-A without GAGs demonstrated an about two-fold increase in cell number after 72 hours compared to non-stimulated control cells, but no significant difference after 4 hours of seeding (Fig. 4.33 A, B). For native GAGs a slightly enhanced cell number was only observed for CS-AC + VEGF-A compared to the cultivation with CS alone (Fig. 4.33 A). However, sHA1 $\Delta$ 6s alone and sHA1 $\Delta$ 6s-AC + VEGF-A significantly enhanced the cell adhesion after 4 hours compared to the Coll reference (Fig. 4.33 C). The addition of none of the other GAGs had a detectable influence on the cell numbers after 4 hours of cultivation (Fig. 4.33 A, C). It is of note that the calculated cell numbers in the presence of sHA1 $\Delta$ 6s-AC + VEGF-A were also higher than those in the presence of sHA1 and sHA1-AC either with or without VEGF-A (Fig. 4.33 C).

After 72 hours of cell cultivation, treatment with HA and sGAGs led to significantly increased cell numbers compared to non-stimulated control cells (Fig. 4.33 B, D). This is in line with previous studies reporting that the binding of HA (dp 10 - 15) to the HA receptor CD44 stimulates endothelial cell proliferation [484]. The presence of sHA derivatives alone (white bars) led to about 2.2 - 3.0-fold higher cell numbers compared to PAE/KDR cells treated with VEGF-A alone (Fig. 4.33 D), while the other GAGs caused only a 1.4 - 1.8-fold increase of the cell numbers (Fig. 4.33 B, white bars). An additional GAG-induced stimulatory effect on the endothelial cell proliferation was no longer apparent in the presence of VEGF-A for HA, HA-AC, CS and CS-AC (Fig. 4.33 B, grey bars). In contrast, about 60% higher cell numbers were determined in the presence of sHA1 and sHA1-AC, while sHA1 $\Delta$ 6s and sHA1 $\Delta$ 6s-AC caused a rise in cell number of about 80 - 90% compared to the VEGF-A-treated control cells

w/o GAGs (Fig. 4.33 D, grey bars). In line with this, Cole et al. found an enhance proliferation of HUVECs in the presence of VEGF-A and HS oligosaccharides compared to VEGF-A alone. However, no data regarding the effects of these oligosaccharides on endothelial cell proliferation in the absence of VEGF-A were provided in the study [455].

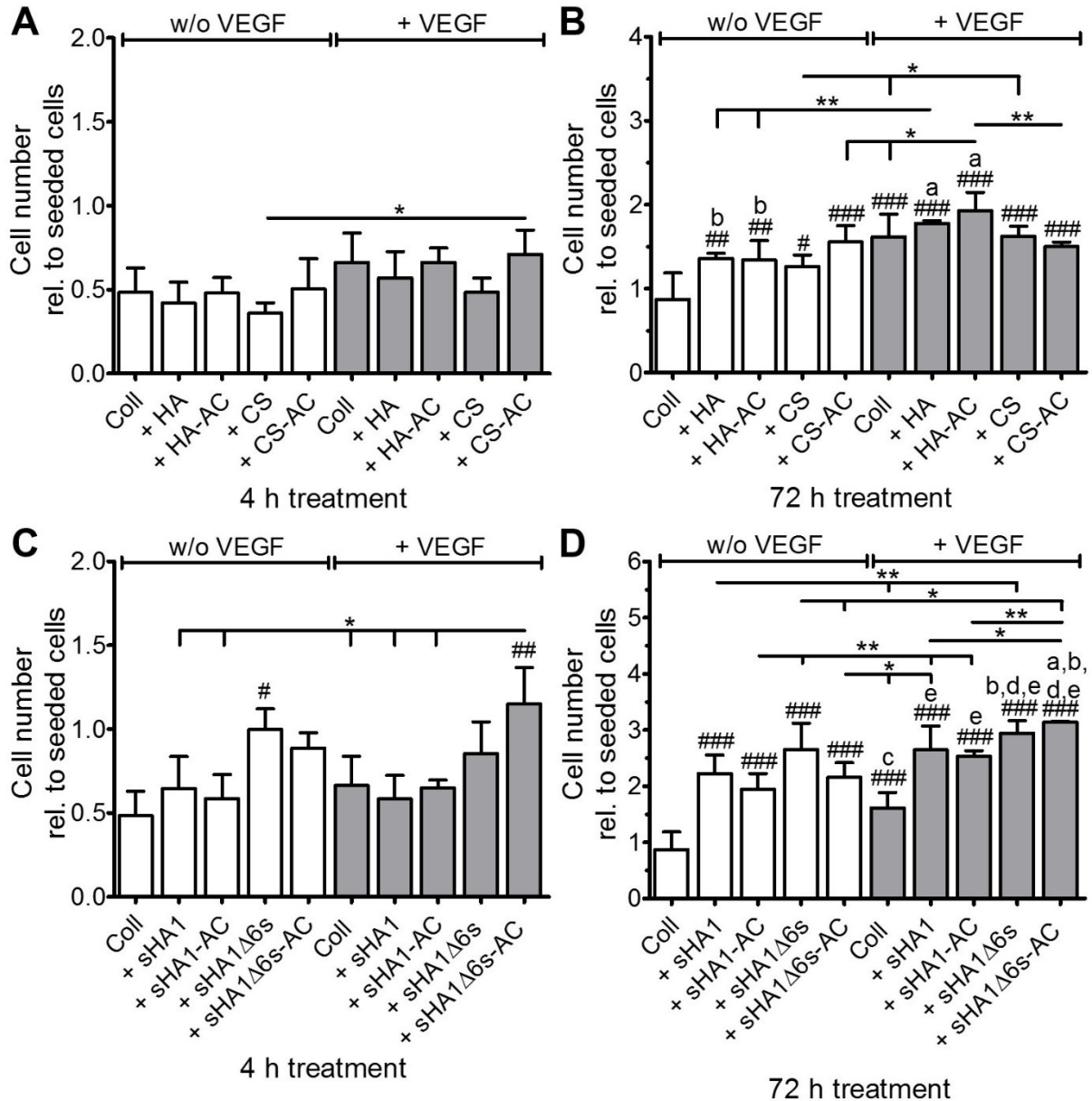


**Fig. 4.33 Influence of VEGF-A and solute GAGs on PAE/KDR cells.** 50000 PAE/KDR cells were seeded on collagen-coated wells and cultivated in the presence or absence of 400  $\mu$ M D.U. solute native GAGs (A, B), sHA derivatives (C, D) in comparison to their acrylated derivatives with (gray bars) or without the addition of 50 ng VEGF-A (white bars) per well. The cell number was calculated indirectly by determining the DNA content after 4 or 72 hours of cultivation. Two-way ANOVA: # ( $p < 0.05$ ), ## ( $p < 0.01$ ), ### ( $p < 0.001$ ) vs. Coll. \* ( $p < 0.05$ ), \*\* ( $p < 0.01$ ) vs. respective treatment. (B): a ( $p < 0.001$ ) vs. + CS, b ( $p < 0.001$ ) vs. + HA-AC + VEGF-A. (D): a ( $p < 0.001$ ) vs. + sHA1, b ( $p < 0.001$ ) vs. + sHA1-AC, c ( $p < 0.001$ ) vs. sHA1 $\Delta$ 6s, d ( $p < 0.001$ ) vs. + sHA1 $\Delta$ 6s-AC, e ( $p < 0.001$ ) vs. Coll + VEGF-A.

Since GAGs were shown to interfere with the VEGF-A binding to VEGFR-2 (section 4.3.6) and potentially causing decreased VEGFR-2 signaling and endothelial cell activation (section 4.3.8), and since SPR binding analysis and VEGFR-2 phosphorylation studies revealed no direct interplay of GAGs with VEGFR-2, it is likely that the VEGF-A activity is altered in the presence of GAGs.

When comparing the VEGF-A-induced increase in cell number of the control with the cell numbers determined in the presence of GAGs both without and with VEGF-A (values from Fig. 4.33, white bars compared to the respective gray bars), a reduced endothelial cell stimulatory activity of VEGF-A was observed for almost all GAGs (Fig. 4.34). It is noteworthy that the VEGF-A activity was only partially affected and not completely inhibited by the examined GAGs. The addition of sHA1 $\Delta$ 6s-AC had no significant impact on the VEGF-A activity whereas sHA1 $\Delta$ 6s reduced the VEGF-A activity, which is in line with the SPR data showing that the acrylation of sHA1 $\Delta$ 6s strongly decrease the binding to VEGF-A (section 4.2.4).

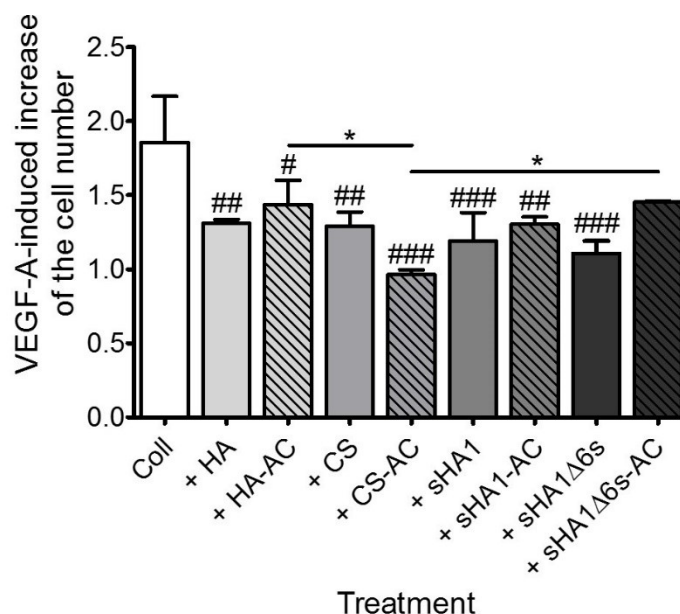


**Fig. 4.34 Endothelial cell stimulatory activity of VEGF-A in the presence of GAGs.** The VEGF-A-induced effects on the cell number of PAE/KDR cells after 72 hours of cultivation in the absence (coll) or presence of solute GAGs were shown relative to the determined cell numbers in the absence of VEGF-A for the respective treatments. One-way ANOVA: # ( $p < 0.05$ ), ## ( $p < 0.01$ ), ### ( $p < 0.001$ ) vs. Coll; \* ( $p < 0.05$ ) vs. respective treatment.

However, the inhibitory effects of HA, CS and their acrylated counterparts compared to sHA derivatives calculated here (Fig. 4.34) were higher than expected based on the results on the binding studies done by ELISA and SPR (section 4.2.4). Thus it can be suggested that the possibly higher number of formed sHA/VEGF-A complexes decreases the available number of D.U. of these sHA derivatives in the medium. As these are required for the direct effects on the endothelial cell proliferation, this might lead to an underestimation of the inhibitory effect of

sHA derivatives on the VEGF-A activity when simply comparing the cell numbers in the presence or absence of VEGF-A for the respective GAG treatments.

It should be noted that the direct effects of sGAGs on endothelial cells (Fig. 4.33) do not seem to be mediated via VEGFR-2, based on the SPR binding analysis with solute GAGs that showed no detectable binding response during injection over VEGFR-2 surfaces (Appendix Fig. 7.4). This is in accordance with the results of the VEGFR-2 stimulation assay revealing no sHA3-induced receptor phosphorylation (Fig. 4.20 A, section 4.3.8). Thus, other mechanism, which remain to be elucidated, must be responsible for the detected effects (compare section 4.5.5).

The effect of the potential VEGF-A/GAG interaction on the angiogenic ability of endothelial cells was also qualitatively assessed by examining the *in vitro* tube formation after staining living cells with MTT (Appendix Fig. 7.10). As indicated by the intense blue color of the cells, almost all cells present were metabolically active. In line with the determined cell numbers, a much higher cell density was observed for cells treated with sHA derivatives. After 72 hours of incubation with VEGF-A in the absence or presence of GAGs, all PAE/KDR cells formed tube-like structures proving that VEGF-A is at least partially active to stimulate the tube formation of endothelial cells. Freudenberg et al. observed a similar formation of tubular structures after cultivation of HUVECs in the presence of VEGF-A on a collagen type I/starPEG-HEP gel sandwich containing desulfated HEP or sulfated HEP, although the tube density was lower in the latter case [459].

#### 4.5.7 Effects of VEGF-A-loaded hydrogels on endothelial cells

VEGF-A is crucial for angiogenesis during wound healing, but when administered topically is quickly degraded by proteases in the chronic wound fluid. Kleinheinz et al. found that solute VEGF-A<sub>165</sub> has a biological half-life of only about 90 minutes in aqueous solution [485]. Consequently high amounts of expensive growth factors are needed to stimulate wound healing for example of chronic foot ulcers, always with the risk of overdosage [486,487]. Thus, hydrogel systems that allow a defined binding and thereby protection of the growth factor against degradation as well as an adjustable release of VEGF-A could be beneficial to stimulate wound healing of vascularized tissues.

The biological activity of hydrogel-bound VEGF-A was assessed by cultivating PAE/KDR cells on pre-loaded gels (Fig. 4.35). Since larger hydrogel volumes were used for cell culture experiments than for VEGF-A binding and release studies (200  $\mu$ l instead of less than 50  $\mu$ l) with a consequently much higher VEGF-A binding capacity, we assume that all applied VEGF-A is bound to the gels. This is supported by additionally performed ELISA experiments analyzing the VEGF-A contents in the supernatants after incubation of the gels with the growth factor, where only marginal amounts (< 0.6%) of solute VEGF-A were found (Appendix Fig. 7.11).

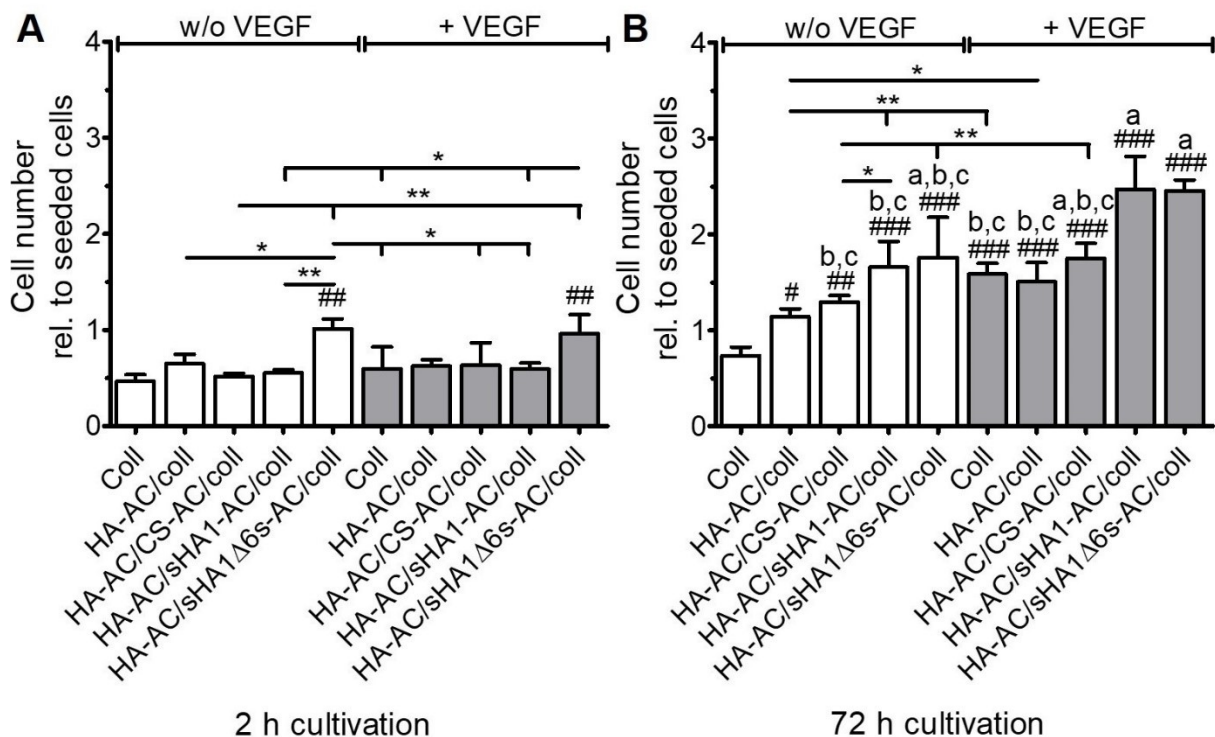


**Fig. 4.35 Influence of VEGF-A on PAE/KDR cells cultivated on HA-AC/collagen hydrogels.** 50000 PAE/KDR cells were seeded on HA/coll hydrogels in the absence of VEGF-A (white bars) or pre-loaded with 50 ng VEGF-A per gel (gray bars). In case of the control, cells were seeded onto collagen coated surfaces and directly stimulated with solute 50 ng VEGF-A after seeding. The cells were cultivated for 2 (A) or 72 hours (B). Afterwards, the cell number per gel was determined by quantifying the DNA content. Two-way ANOVA: # ( $p < 0.05$ ), ## ( $p < 0.01$ ), ### ( $p < 0.001$ ) vs. Coll, \* ( $p < 0.05$ ), \*\* ( $p < 0.01$ ) vs. respective treatment. (B): a ( $p < 0.001$ ) vs. HA-AC/coll, b ( $p < 0.001$ ) vs. HA-AC/sHA1-AC/coll + VEGF-A, c ( $p < 0.001$ ) vs. HA-AC/sHA1Δ6s-AC/coll + VEGF-A.

An enhanced cell number after 2 hours was detected for gels with sHA1Δ6s-AC in the presence or absence of VEGF-A, while there were no significant differences between the other hydrogel compositions and the collagen-coated reference wells (Fig. 4.35 A).

Cell stimulation with solute as well as gel-bound VEGF-A induced a rise of the cell number after 72 hours compared to the non-treated samples (Fig. 4.35 B). In both cases the highest cell numbers were observed for HA-AC/sHA1-AC/coll and HA-AC/sHA1Δ6s-AC/coll gels. This is in line with findings showing a strongly enhanced endothelial cell proliferation in the presence of solute sHA1, sHA1-AC, sHA1Δ6s and sHA1Δ6s-AC under serum free conditions (section 4.5.6) and after cultivation within HA-AC/sHA1-AC/coll and HA-AC/sHA1Δ6s-AC/coll hydrogels in the presence of serum (section 4.5.5). However, there were no significant differences between HA-AC/coll and HA-AC/CS-AC/coll gels for the respective conditions. While solute VEGF-A combined with the collagen control lead to an about 2.2-fold higher cell number, gel-bound VEGF-A exhibited a lower activity with about 1.3 - 1.5 increase compared to the respective gels w/o VEGF-A. This is likely the result of a partial inactivation of VEGF-A by binding to GAGs (sections 4.3.6, 4.3.8).

Sprouting can be seen by the network formation of branching structures as result of the VEGF-A-induced chemotaxis and chemokinesis of endothelial cells [488] and was qualitatively assessed (Fig. 4.36). Immunofluorescence staining of PAE/KDR cells within the gels showed the sprouting of the cells after pre-loading of CS-AC- and sHA1 $\Delta$ 6s-AC-containing hydrogels with VEGF-A (Fig. 4.36 F, H). However, no cell sprouting was detected for VEGF-A-loaded hydrogels with sHA1-AC, which may be due to the comparably low release of gel-bound VEGF-A (section 4.5.4). Freudenberg et al. also described that the formation of tubular structures correlated with the amount of released VEGF-A from HEP-containing hydrogels [459]. Cells within HA-AC/coll gels with or without VEGF-A appeared as cell clusters (Fig. 4.36 A, E) similar to what was observed under serum containing conditions (section 4.5.5).

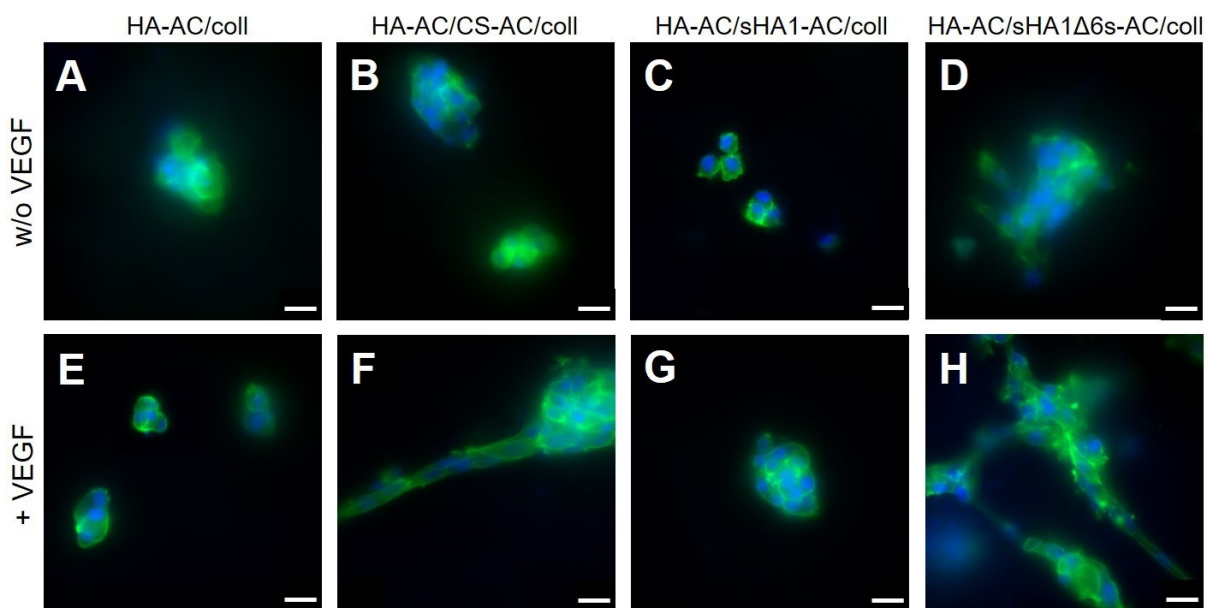


**Fig. 4.36 Influence of VEGF-A on the morphology of PAE/KDR cells cultivated on HA-AC/collagen hydrogels.** Cells after 72 hours of cultivation under serum free conditions of initially 50000 PAE/KDR cells without (A - D) or with 50 ng VEGF-A per gel (E - H) stained for their nuclei in blue with DAPI and for F-actin in green. The scale bar represents 20  $\mu$ m.

The absence of serum significantly affected the endothelial cell morphology after cultivation within hydrogels with CS-AC (Fig. 4.36 B vs. Fig. 4.32 section 4.5.5), while there were no apparent differences in case of HA-AC/sHA1-AC/coll or HA-AC/sHA1 $\Delta$ 6s-AC/coll in the presence or absence of serum (Fig. 4.36 C, D vs. Fig. 4.32 section 4.5.5). Even though HA-AC/coll and HA-AC/CS-AC/coll gels revealed almost comparable VEGF-A binding and release profiles (Fig. 4.30 section 4.5.4), tube-like structures were only seen in the latter case. This suggests that the binding of VEGF-A to sGAGs like CS-AC protects or maintains the VEGF-A functional activity to some extent, for instance by protecting the growth factor against proteolytic degradation as reported for native GAGs [280].

The stiffness (elastic modulus) of hydrogels with about 200 Pa (Fig. 4.26) was in between that of the firm and rigid HA/gelatin hydrogels (85 - 780 Pa) prepared by Hanjaya-Putra et al. These

authors described that the tube length, area and thickness formed by VEGF-stimulated endothelial progenitor cells increased when decreasing the matrix stiffness [489]. Moreover, HUVECs were shown to form stable networks only on soft but not on stiffer gels (140 Pa vs. 2500 Pa) even after stimulation with bFGF or VEGF-A, since in the latter case, cell-substrate adhesion is increased while cell-cell adhesion was enhanced on soft substrates [490]. Even though the stiffness of HA/collagen-hydrogels is lower than the stiffness of human tissues, which usually range from 1 - 100 kPa [491], this property could facilitate the sprouting of endothelial cells and thereby possibly promote the regeneration of injured vascularized tissues. Overall, pre-loading of sHA-AC-containing hydrogels with VEGF-A enhanced the proliferation of endothelial cells compared to hydrogels with sHA-AC or VEGF-A alone. This highlights the potential of the gels to stimulate endothelial cells and may result in an improved repair of damages vascularized tissues.

#### 4.6 Potential limitations

The conducted *in vitro* studies and the utilized methods have potential restrictions. The biophysical interaction analysis via SPR for example requires the immobilization of one interaction partner onto the sensor chip surface. Amine coupling was used for this, leading to a random immobilization of the proteins, for which reason a potential influence on the protein activity and functional availability of binding sites cannot be excluded. However, since additional ELISA experiments with immobilized GAGs revealed rankings almost comparable to the SPR binding strengths, we assume that these effects are of minor importance.

Another point is that all binding studies were performed with a strictly limited number of interaction partners. The obtained data is thus based on a simplified model that cannot replicate the complexity *in vivo* where other potential GAG interaction partners are present. Further, competitive SPR binding studies with two analytes (TIMP-3, VEGF-A) that can bind to the immobilized ligand (VEGFR-2) allow no clear distinction between the two possible binding events (TIMP-3/VEGFR-2 or VEGF-A/VEGFR-2).

During cell culture experiments, additional influences of a potential interplay of GAGs with serum proteins on the cellular behavior with serum containing media have to be considered. In contrast, the cell cultivation under serum-free conditions is more artificial but enables the analysis of distinct factors and conditions on the cellular level.

Overall larger amounts of GAG oligosaccharides would be required to validate the obtained SPR data in cell culture models. Further defined GAG oligosaccharides with a broader range of different sizes and sulfation patterns would be desirable to allow more conclusions regarding the influence of the GAG structure, molecular size and substitution patterns on the interplay and activity of biologically relevant mediator proteins with GAGs.

## 5 SUMMARY

Bone fractures and pathologic conditions like chronic wounds significantly reduce the quality of life for the patients, which is especially dramatic in an elderly population with considerable multi-morbidity and lead to substantial socio-economic costs. To improve the wound healing capacity of these patients, new strategies for the design of novel multi-functional biomaterials are required: they should be able to decrease extensive pathologic tissue degradation and specifically control angiogenesis in damaged vascularized tissues like bone and skin.

Glycosaminoglycans (GAGs) like hyaluronan (HA) and chondroitin sulfate (CS) as important extracellular matrix (ECM) components are involved in several biological processes such as matrix remodeling and growth factor signaling, either by directly influencing the cellular response or by interacting with mediator proteins. This could be useful in functionalizing biomaterials, but native sulfated GAGs (sGAGs) show a high batch-to-batch variability and are limited in their availability. Chemically modified HA and CS derivatives with much more defined characteristics regarding their carbohydrate backbone, sulfate group distribution and sulfation degree are favorable to study the structure-function relationship of GAGs in their interaction with mediator proteins and/or cells and this might be used to precisely modulate activity profiles to stimulate wound healing.

By combining collagen type I as the main structural protein of the bone and skin ECM with these GAG derivatives, 2.5-dimensional (2.5D) and 3D artificial ECM (aECM) coatings and hydrogels were developed. These biomaterials as well as the respective GAG derivatives alone were compared to native GAGs and used to analyze how the sulfation degree, pattern and carbohydrate backbone of GAGs influence:

- i) the activity of tissue inhibitor of metalloproteinase-3 (TIMP-3) and vascular endothelial growth factor-A (VEGF-A) as main regulators of ECM remodeling and angiogenesis,
- ii) the composition and characteristics of the developed 2.5D and 3D aECMs,
- iii) the enzymatic degradation of collagen-based aECMs and HA/collagen-based hydrogels,
- iv) the proliferation and functional morphology of endothelial cells.

Surface plasmon resonance (SPR) and enzyme linked immunosorbent assay (ELISA) binding studies revealed that sulfated HA (sHA) derivatives interact with TIMP-3 and VEGF-A in a sulfation-dependent manner. sHA showed an enhanced interplay with these proteins compared to native GAGs like heparin (HEP) or CS, suggesting a further impact of the carbohydrate backbone and sulfation pattern. sGAGs alone were weak modulators of the matrix metalloproteinase-1 and -2 (MMP-1 and -2) activity and did not interfere with the inhibitory potential of TIMP-3 against these proteinases during enzyme kinetic analyses. However, the formation of TIMP-3/GAG complexes reduced the binding of TIMP-3 to cluster II and IV of its endocytic receptor low-density lipoprotein receptor-related protein-1 (LRP-1, mediates the up-take and degradation of TIMP-3 from the extracellular environment) in a sulfation- and



GAG type-dependent manner. It is of note that the determined complex stabilities of TIMP-3 with cluster II and IV were almost identical indicating for the first time that both clusters contribute to the TIMP-3 binding. Competitive SPR experiments demonstrated that GAG polysaccharides interfere stronger with the TIMP-3/LRP-1 interplay than GAG oligosaccharides. The importance of the position of sulfation is highlighted by the finding that a sHA tetrasaccharide exclusively sulfated at the C6 position of the *N*-acetylglucosamine residues significantly blocked the receptor binding, while CS and HEP hexasaccharides had no detectable effects. Thus, sHA derivatives as part of biomaterials could be used to sequester and accumulate TIMP-3 in aECMs in a defined manner where sHA-bound TIMP-3 could decrease the matrix breakdown by potentially restoring the MMP/TIMP balance. GAG binding might extend the beneficial presence of TIMP-3 into wounds characterized by excessive pathologic tissue degradation (e.g. chronic wounds, osteoarthritis).

Mediator protein interaction studies with sHA coated surfaces showed the simultaneous binding of TIMP-3 and VEGF-A, even though the sHA/VEGF-A interplay was preferred. Moreover, kinetic analysis revealed almost comparable affinities of both proteins for VEGF receptor-2 (VEGFR-2), explaining their competition that mainly regulates the activation of endothelial cells. Additional SPR measurements demonstrated that the binding of sGAGs to TIMP-3 or VEGF-A decreases the binding of the respective mediator protein to VEGFR-2. Likewise, a sulfation-dependent reduction of the binding signal was observed after pre-incubation of a mixture of TIMP-3 and VEGF-A with sGAG poly- and oligosaccharides. The biological consequences of GAGs interfering with VEGF-A/VEGFR-2 and TIMP-3/VEGFR-2 were assessed *in vitro* using porcine aortic endothelial cells stably transfected with VEGFR-2 (PAE/KDR cells). The presence of sHA both decreased VEGF-A activity and the activity of TIMP-3 to inhibit the VEGF-A-induced VEGFR-2 phosphorylation. The same decreased activities could be observed for the migration of endothelial cells. However, if sHA, TIMP-3 and VEGF-A were present simultaneously, sHA partially restored the TIMP-3-mediated blocking of VEGF-A activity. These findings provide novel insights into the regulatory potential of sHA during endothelial cell activation as an important aspect of angiogenesis, which could be translated into the design of biomaterials to treat abnormal angiogenesis. These sHA-containing materials might control the angiogenic response by modulating the activity of TIMP-3 and VEGF-A.

The *in vitro* fibrillogenesis of collagen type I in the presence of sHA derivatives led to 2.5D collagen-based aECM coatings with stable collagen contents and GAG contents that resemble the organic part of the bone ECM. A burst release of GAGs was observed during the first hour of incubation in buffer with the GAG content remaining almost constant afterwards, implying that the number of GAG-binding sites of collagen restricts the amounts of associated GAGs. Moreover, two differently sulfated HA derivatives could for the first time be incorporated into one multi-GAG aECM as verified via agarose gel electrophoresis and fluorescence

measurements. This illustrates the multiple options to modify the aECM composition and thereby potentially their functionality. Atomic force microscopy showed that the presence of sHA derivatives during fibrillogenesis significantly reduced the resulting fibril diameter in a concentration- and sulfation-dependent manner, indicating an interference of the GAGs with the self-assembly of collagen monomers. In line with enzyme kinetic results, none of the GAGs as part of aECMs altered the enzymatic collagen degradation via a bacterial collagenase. Thus aECMs were proven to be biodegradable independent from their composition, which is favorable concerning a potential biomedical usage of the aECMs e.g. as implant coatings.

HA/collagen-based hydrogels containing fibrillar collagen embedded into a network of crosslinked HA and sGAGs were developed as 3D aECMs. Scanning electron microscopy demonstrated a porous structure of the gels after lyophilization, which could favor the cultivation of cells. The presence of collagen markedly enhanced the stability of the gels against the enzymatic degradation via hyaluronidase, something beneficial to clinical use as this is often limited by the generally fast breakdown of HA. Binding and release experiments with lysozyme, as positively charged model protein for e.g. pro-inflammatory cytokines, and VEGF-A revealed that the sulfation of GAGs increased the protein binding capacity for pure GAG coatings and retarded the protein release from hydrogels compared to hydrogels without sGAGs. Moreover, the additional acrylation of sHA was shown to strongly reduce the interaction with both proteins when the primary hydroxyl groups were targets of acrylation. This stresses the influence of the substitution pattern on the protein binding properties of the GAG derivatives. However, hydrogel characteristics like the elastic modulus remained unaffected. The different interaction profiles of lysozyme and VEGF-A with GAGs demonstrated a protein-specific preference of different monosaccharide compositions, suggesting that the mediator protein binding could be simultaneously adjusted for several proteins by combining different GAG derivatives. This might allow the scavenging of pro-inflammatory cytokines and at the same time a binding and release of wound healing stimulating growth factors.

Since there is a growing demand for biomaterials to regenerate injured vascularized tissues like bone and skin, endothelial cells were used to examine the direct effects of solute GAGs and hydrogels containing these GAGs *in vitro*. In both cases, sHA strongly enhanced the proliferation of PAE/KDR cells. A VEGFR-2-mediated effect of GAGs on endothelial cells as underlying mechanism is unlikely since GAGs alone did not bind to VEGFR-2 and had no influence on VEGFR-2 phosphorylation. Other factors like GAG-induced alterations of cell-matrix interactions and cell signaling could be responsible. In accordance with SPR results, a decreased endothelial cell proliferation stimulating activity of VEGF-A was observed in the presence of solute GAGs or after binding to hydrogels compared to the respective treatment without VEGF-A. However, tube formation could be observed in the presence of solute VEGF-A and GAGs and within hydrogels with sGAGs that released sufficient VEGF-A

amounts over time. Overall the presence of GAGs and VEGF-A strongly promoted the endothelial cell proliferation compared to the treatment with GAGs or VEGF-A alone. Thus, HA/collagen-based hydrogels functionalized with sHA derivatives offer a promising option for the design of “intelligent” biomaterials that direct and regulate the cellular behavior instead of simply acting as inert filling material. They could be used for the controlled delivery and/or scavenging of multiple mediator proteins, thus enhancing the local availability or reducing the activity of these GAG-interacting mediator proteins, or by directly influencing the cellular response. This might be applied to a range of pathological conditions by tuning the biomaterial compositions to patient-specific needs.

However, extensive *in vivo* validation is required to show whether these *in vitro* findings could be used to control the biological activity of for instance TIMP-3 and VEGF-A, especially under the pathological conditions of extended matrix degradation and dysregulated angiogenesis.

## ZUSAMMENFASSUNG

Knochenbrüche und pathologische Zustände wie chronische Wunden reduzieren die Lebensqualität der Patienten deutlich. Dies ist besonders bei der alternden Bevölkerung mit häufiger Multimorbidität dramatisch und geht mit erheblichen sozioökonomischen Kosten einher. Zur Verbesserung der Wundheilungskapazität multimorbider Patienten sind neue Strategien für die Entwicklung multifunktionaler Biomaterialien nötig. Besondere Bedeutung kommt hierbei der Verringerung eines übermäßigen pathologischen Gewebeabbaus und der Kontrolle der Angiogenese in geschädigten vaskularisierten Geweben (z.B. Knochen- und Hautgewebe) zu.

Glykosaminoglykane (GAGs) wie Hyaluronsäure (HA) und Chondroitinsulfat (CS) als wichtige Komponenten der extrazellulären Matrix (ECM) sind an zahlreichen biologischen Prozessen wie der Matrixremodellierung und der Signaltransduktion von Wachstumsfaktoren durch die direkte Beeinflussung des zellulären Verhaltens oder durch die Interaktion mit Mediatorproteinen beteiligt, weshalb GAGs für die Funktionalisierung von Biomaterialien vielversprechend sind. Allerdings zeigen native sulfatierte GAGs (sGAGs) eine stark chargenabhängige Variabilität und sind in ihrer Verfügbarkeit begrenzt. Daher sind chemisch modifizierte HA- und CS-Derivate mit deutlich definierten Eigenschaften hinsichtlich ihres Kohlenhydratgrundgerüsts, der Sulfatgruppenverteilung und des Sulfatierungsgrades vorteilhaft, um die Struktur-Eigenschafts-Beziehungen von GAGs in ihrer Interaktion mit Mediatorproteinen und/oder Zellen zu untersuchen. Dies könnte zur präzisen Einstellung von Wirkprofilen dienen, welche die Wundheilung stimulieren. Durch die Kombination von Kollagen Typ I als Hauptstrukturprotein der Knochen- und Haut-ECM mit diesen GAG-Derivaten wurden 2,5-dimensionale (2,5D) und 3D artifizielle ECM (aECM)-Beschichtungen und -Hydrogele entwickelt. Diese Biomaterialien sowie die jeweiligen GAG-Derivate allein im Vergleich zu nativen GAGs wurden verwendet, um zu analysieren, wie der Sulfatierungsgrad, das Sulfatierungsmuster und das Kohlenhydratgrundgerüst der GAGs die folgenden Aspekte beeinflussen:

- i) die Aktivität des Gewebeinhibitors von Metalloproteinase-3 (TIMP-3) und des vaskulären endothelialen Wachstumsfaktor-A (VEGF-A) als Hauptmodulatoren der ECM-Remodellierung und Angiogenese;
- ii) die Zusammensetzung und Eigenschaften der entwickelten 2,5D und 3D aECMs;
- iii) den enzymatischen Abbau von kollagenbasierten aECMs und HA/kollagen-basierten Hydrogelen;
- iv) die Proliferation und funktionelle Morphologie von Endothelzellen.

Oberflächenplasmonresonanz (Surface Plasmon Resonance (SPR)) und Enzyme-linked Immunosorbent Assay (ELISA) Bindungsstudien zeigten, dass sulfatierte HA (sHA)-Derivate mit TIMP-3 und VEGF-A sulfatierungsabhängig wechselwirken. Dabei wiesen sHA-Derivate eine verstärkte Interaktion mit diesen Proteinen im Vergleich zu nativen GAGs wie Heparin

(HEP) oder CS auf. Dies deutet auf einen weiteren Einfluss des Kohlenhydratrückgrats und des Sulfatierungsmusters hin. sGAGs allein wirkten als schwache Modulatoren der Matrix Metalloproteinase-1 und -2 (MMP-1 und -2)-Aktivitäten und beeinflussten das inhibitorische Potential von TIMP-3 gegenüber diesen Proteinase in enzymkinetischen Messungen nicht. Allerdings reduzierte die Bildung von TIMP-3/GAG-Komplexen sulfatierungs- und GAG-typabhängig die Bindung von TIMP-3 an Cluster II und IV seines Endozytose-Rezeptors low-density lipoprotein receptor-related protein-1 (LRP-1), welcher die Aufnahme und den Abbau von TIMP-3 aus der extrazellulären Umgebung steuert. Die ermittelten Komplexstabilitäten von TIMP-3 mit Cluster II und IV waren fast identisch und wiesen erstmals nach, dass beide Cluster zur TIMP-3-Bindung beitragen. Kompetitive SPR-Experimente zeigten, dass GAG-Polysaccharide stärker mit der TIMP-3/LRP-1-Interaktion interferieren als GAG-Oligosaccharide. Die Bedeutung der Sulfatierungsposition wird daran deutlich, dass ein sHA-Tetrasaccharid, das ausschließlich an der C6-Position der *N*-Acetylglucosamineinheiten sulfatiert ist, die Rezeptorbindung signifikant blockierte, während CS- und HEP-Hexasaccharide keine nachweisbaren Wirkungen hatten. Abgeleitet aus diesen Untersuchungen könnten sHA-Derivate als Teil von funktionellen Biomaterialien genutzt werden, um TIMP-3 in aECMs definiert zu sequestrieren und zu akkumulieren. Dabei könnte sHA-gebundenes TIMP-3 den Matrixabbau verringern, indem es das MMP/TIMP-Gleichgewicht wiederherstellt, und die GAG-Bindung könnte die Anwesenheit von TIMP-3 in Wunden, welche durch einen übermäßigen pathologischen Gewebeabbau charakterisiert sind (z.B. chronische Wunden, Osteoarthritis), verlängern.

Mediatorprotein-Interaktionsstudien mit sHA-beschichteten Oberflächen zeigten die gleichzeitige Bindung von TIMP-3 und VEGF-A, wobei die sHA/VEGF-A-Interaktion bevorzugt war. Darüber hinaus ergaben kinetische SPR-Analysen nahezu vergleichbare Affinitäten beider Proteine für VEGF-Rezeptor-2 (VEGFR-2). Dies erklärt deren Konkurrenz, welche im Wesentlichen die Aktivierung von Endothelzellen reguliert. Zusätzlich zeigte sich, dass die Interaktion von sGAGs mit TIMP-3 oder VEGF-A die Bindung des jeweiligen Mediatorproteins an VEGFR-2 verringert. Ebenso wurde nach der Vorinkubation einer Mischung aus TIMP-3 und VEGF-A mit sGAG-Poly- und -Oligosacchariden eine sulfatierungsabhängige Reduktion des Bindungssignals beobachtet. Die biologischen Konsequenzen dieser Beeinflussung der VEGF-A/VEGFR-2- und TIMP-3/VEGFR-2-Interaktionen durch GAGs wurden *in vitro* durch mit VEGFR-2 transfizierte porcine Aortenendothelzellen (PAE/KDR-Zellen) untersucht. Die Anwesenheit von sHA verringerte die biologische Aktivität von VEGF-A, die VEGFR-2-Phosphorylierung und Migration von Endothelzellen zu stimulieren. Des Weiteren hemmte sHA die inhibierenden Effekte von TIMP-3 auf VEGF-A, wodurch in einem kombinierten Ansatz mit sHA, TIMP-3 und VEGF-A sHA die TIMP-3-vermittelte Blockierung der VEGF-A-Aktivität teilweise wiederherstellte. Diese Erkenntnisse liefern neue Einblicke in das regulatorische Potential von sHA zur

Aktivierung von Endothelzellen als wichtigen Aspekt der Angiogenese, die in die Entwicklung von Biomaterialien umgesetzt werden könnte, um Zustände abnormaler Angiogenese zu behandeln. Derartige sHA-haltige Materialien können dazu dienen, die angiogene Antwort von Endothelzellen durch Modulierung der Aktivität von TIMP-3 und VEGF-A zu kontrollieren.

Die *in vitro* Fibrillogenese von Kollagen Typ I in Gegenwart von sHA-Derivaten führte zu 2,5D kollagenbasierten aECM-Beschichtungen mit stabilen Kollagengehalten und GAG-Anteilen, die dem organischen Teil der Knochen-ECM ähneln. Eine starke Freisetzung von GAGs wurde während der ersten Stunde der Inkubation in Puffer beobachtet, während der GAG-Gehalt anschließend nahezu konstant blieb. Demnach beschränkt die Anzahl der GAG-Bindungsstellen des Kollagens die Menge an assoziiertem GAG. Darüber hinaus verifizierten Agarose-Gelelektrophorese- und Fluoreszenzanalysen den erstmaligen Einbau von zwei unterschiedlich sulfatierten HA-Derivaten in eine multi-GAG-aECM. Dies verdeutlicht die vielfältigen Möglichkeiten zur Modifizierung der aECM-Zusammensetzung und dadurch deren Funktionalität. Rasterkraftmikroskopie zeigte, dass die Anwesenheit von sHA-Derivaten während der Fibrillogenese den resultierenden Fibrillendurchmesser konzentrations- und sulfatierungsabhängig verringert. GAGs beeinflussen hierbei wahrscheinlich die Selbstorganisation von Kollagenmonomeren. Im Einklang mit enzymkinetischen Ergebnissen änderte keines der GAGs als Teil von aECMs den enzymatischen Kollagenabbau durch bakterielle Kollagenase. Somit erwiesen sich die aECMs unabhängig von ihrer Zusammensetzung als biologisch abbaubar. Hinsichtlich einer möglichen biomedizinischen Verwendung dieser, z.B. als Implantatbeschichtungen, ist dies günstig.

HA/Kollagen-basierte Hydrogele, die fibrilläres Kollagen, eingebettet in ein Netzwerk aus vernetzter HA und sGAGs, enthalten, wurden als 3D aECMs entwickelt. Raster-elektronenmikroskopische Aufnahmen zeigten eine poröse Struktur der gefriergetrockneten Gele, die vorteilhaft für die Zellkultivierung sein sollte. Die Anwesenheit von Kollagen erhöhte die Stabilität der Gele gegen den enzymatischen Abbau durch Hyaluronidase deutlich. Da die klinische Nutzung von HA-Hydrogelen oft durch den schnellen Abbau von HA beschränkt ist, sollte dies vorteilhaft sein. Bindungs- und Freisetzungsexperimente mit Lysozym, als positiv geladenes Modellprotein für z. B. pro-inflammatorische Zytokine, und VEGF-A zeigten, dass die Sulfatierung von GAGs die Proteinbindungskapazität von reinen GAG-Beschichtungen erhöht und die Proteinfreisetzung aus Hydrogelen im Vergleich zu Hydrogelen ohne sGAGs verzögert. Darüber hinaus wurde ermittelt, dass die Acylierung der primären Hydroxylgruppen von sHA die Wechselwirkung mit beiden Proteinen stark verringert. Dies unterstreicht den Einfluss des Substitutionsmusters auf die Proteinbindungseigenschaften der GAG-Derivate. Dabei blieben Hydrogel-Charakteristika wie der Elastizitätsmodul unverändert. Beim Vergleich der verschiedenen Wechselwirkungsprofile von Lysozym und VEGF-A mit GAGs wurde eine proteinspezifische Präferenz verschiedener Monosaccharid-Zusammensetzungen beobachtet. Dies deutet darauf hin, dass die Bindung von Mediatoren aus Mischungen durch

Kombination verschiedener GAG-Derivate spezifisch angepasst werden kann. Dadurch könnte die Sequestrierung von pro-inflammatorischen Zytokinen und gleichzeitig die Bindung und Freisetzung von die Wundheilung stimulierenden Wachstumsfaktoren ermöglicht werden.

Aufgrund des steigenden Bedarfs an Biomaterialien zur Regeneration von verletzten vaskulären Geweben wie Knochen und Haut, dienten Endothelzellen zur *in vitro* Untersuchung der direkten Effekte von gelösten GAGs und Hydrogelen, die diese GAGs enthalten. In beiden Fällen stimulierten sHA-Derivate die Proliferation von PAE/KDR-Zellen deutlich. Eine VEGFR-2-vermittelte Wirkung von GAGs auf Endothelzellen als zugrunde liegender Mechanismus ist jedoch unwahrscheinlich, da GAGs selbst nicht an VEGFR-2 banden und keinen Einfluss auf die VEGFR-2-Phosphorylierung hatten. Andere Faktoren wie GAG-induzierte Veränderungen von Zell-Matrix-Wechselwirkungen und der Zellkommunikation könnten involviert sein. Übereinstimmend mit SPR-Ergebnissen wurde eine verminderte stimulierende Aktivität von VEGF-A auf die Proliferation von Endothelzellen in Gegenwart gelöster GAGs oder nach Bindung an Hydrogele im Vergleich zur jeweiligen Behandlung ohne VEGF-A detektiert. Dennoch konnte die Tube-Formation von Endothelzellen in Gegenwart von gelöstem VEGF-A und GAGs und innerhalb von Hydrogelen mit sGAGs, die ausreichende VEGF-A-Mengen freisetzen, beobachtet werden.

Insgesamt steigerte die Anwesenheit von GAGs und VEGF-A die Proliferation der Endothelzellen im Vergleich zur Behandlung mit GAGs oder VEGF-A alleine. So bieten mit sHA-Derivaten funktionalisierte HA/Kollagen-basierte Hydrogele eine vielversprechende Möglichkeit für die Gestaltung von „intelligenten“ Biomaterialien, die die zelluläre Reaktion steuern und regulieren, anstatt nur als inertes Füllmaterial zu dienen. Diese Materialien könnten z. B. zum kontrollierten Transport und/oder zur Bindung mehrerer Mediatorproteine dienen, um eine definiert regulierte Zellantwort durch eine Verbesserung der lokalen Verfügbarkeit oder eine Verringerung der Aktivität dieser GAG-interagierenden Mediatorproteine auszulösen. Ein solches Prinzip könnte auf eine Reihe pathologischer Bedingungen angewandt werden, indem die Biomaterial-Zusammensetzung auf patientenspezifische Bedürfnisse abgestimmt wird.

Insgesamt ist jedoch eine umfangreiche *in vivo*-Validierung dieser Daten erforderlich, um zu zeigen, ob diese *in vitro*-Befunde zur Steuerung der biologischen Aktivität von z. B. TIMP-3 und VEGF-A unter pathologischen Bedingungen übermäßigen Matrixabbaus und dysregulierter Angiogenese genutzt werden können.

## 6 OUTLOOK

*In vivo* studies to validate the results of the conducted *in vitro* experiments are highly warranted especially for health-compromised conditions in appropriate pre-clinical models. These data are crucial for a potential future local biomedical application of chemically modified GAG derivatives as functional part of aECM coatings or HA/collagen-based hydrogels to regulate biological processes at the tissue/biomaterial interface.

In addition, *in vitro* studies regarding the interplay of GAGs with further growth factors important for the complex process of angiogenesis - like bFGF in combination with for example VEGF-A - or a focus on the suggested interplay of HA derivatives with the HA receptor CD44 could contribute to an in-depth understanding of the multiple functions of GAGs. It might also serve to elucidate the molecular mechanism responsible for the detected direct effects of GAGs on the proliferation of endothelial cells. Moreover, additional cell types relevant for skin and bone healing as well as co-culture studies with these cells need to be performed to further assess the properties of the developed biomaterials.

Another interesting aspect would be to analyze the potential impact of sGAG derivatives on the activity of cathepsin K, which is a critical collagenase in bone remodeling that is known to interact with native GAGs. Further studies are necessary to address the question whether the binding of LRP-1 ligands to GAGs is a general mechanism to post-translationally control their LRP-1-mediated endocytosis and intracellular degradation by blocking the ligand/LRP-1 interplay. MMP-9 and TGF- $\beta$ 1, both known to contain a HEP-binding region, could be analyzed in competitive SPR approaches.

The development of even more complex aECM systems containing multiple GAG derivatives with defined spatial distributions of GAGs and mediator proteins as planned for the third funding period of the “Transregio 67” could additionally foster the engineering of cellular microenvironments that mimics several functions of the native ECM. This may lead to a patient-specific tailoring of biomaterial properties and interaction profiles in future.



## 7 APPENDIX

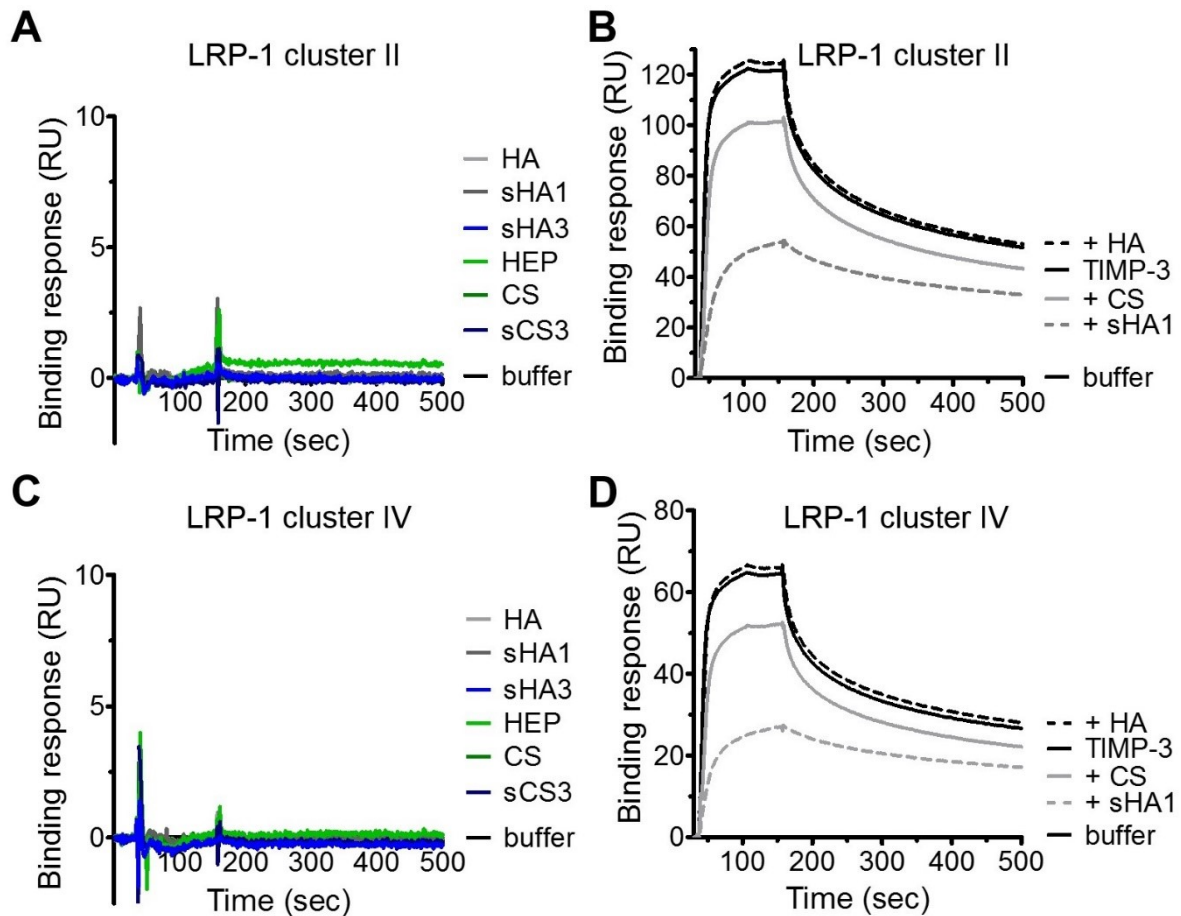


**Fig. 7.1 Influence of solute GAGs on the TIMP-3/LRP-1 complex formation.** The binding response of 100  $\mu\text{M}$  D.U. GAG solution to LRP-1 cluster II (500 RU) (A) or cluster IV (380 RU) (C) surfaces is displayed. Representative sensorgrams showing the binding response of 100 nM TIMP-3 to LRP-1 cluster II (B) or cluster IV (D) in the presence of 100  $\mu\text{M}$  D.U. non- or low-sulfated GAGs. Adapted from [R447] with modifications.

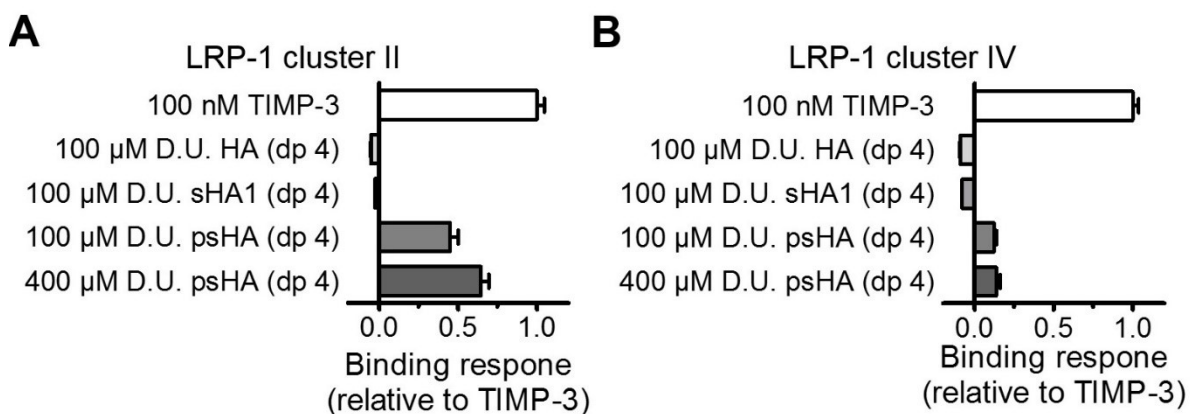


**Fig. 7.2 Interaction of HA tetrasaccharides with LRP-1.** Binding response of HA tetrasaccharides to LRP-1 cluster II (690 RU) (A) and IV (380 RU) (B) surfaces relative to the response of 100 nM TIMP-3. Adapted from [R447] with modifications.

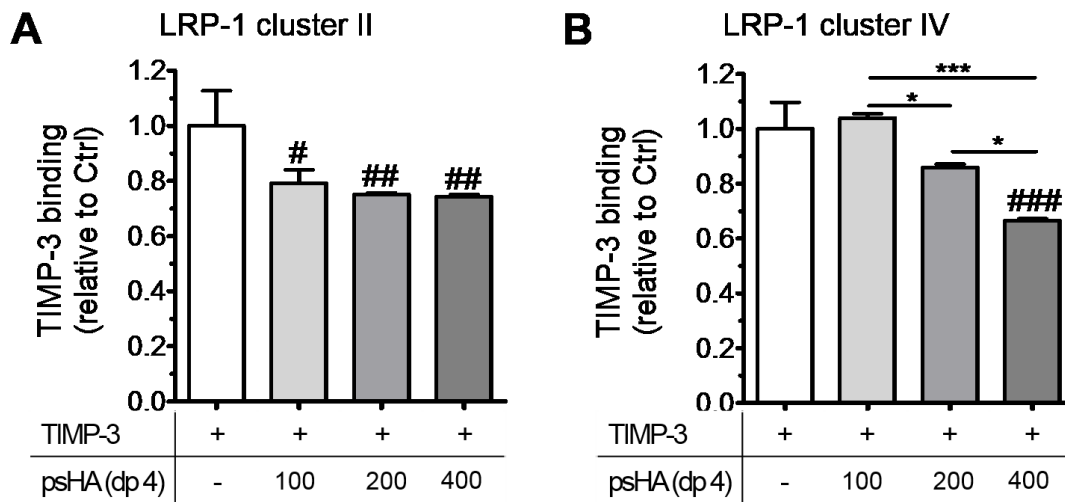


**Fig. 7.3 Effects of a psHA tetrasaccharide on the TIMP-3/LRP-1 cluster II and IV binding.** The binding response of TIMP-3 after pre-incubation with 100 - 400  $\mu$ M D.U. psHA (dp 4) relative to 100 nM TIMP-3 w/o GAG is shown in (A) for LRP-1 cluster II (690 RU) and in (B) for LRP-1 cluster IV (380 RU) surfaces. Adapted from [R447] with modifications. One-way ANOVA: # ( $p < 0.05$ ), ## ( $p < 0.01$ ), ### ( $p < 0.001$ ) vs. TIMP-3 w/o GAG; \* ( $p < 0.05$ ), \*\*\* ( $p < 0.001$ ) vs. respective treatment.

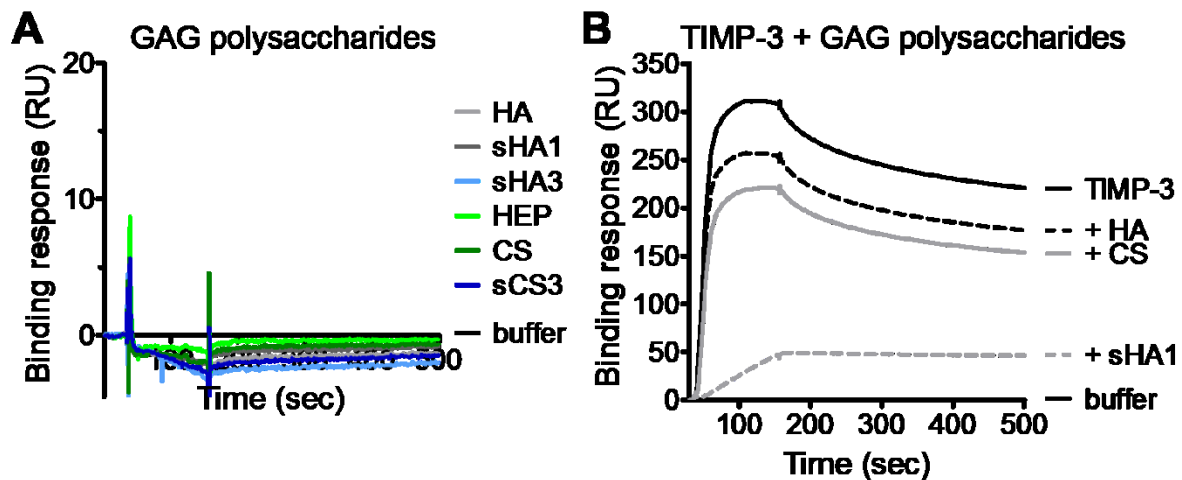


**Fig. 7.4 Interaction of solute GAGs with VEGFR-2.** Representative sensorgrams showing the binding response of 100  $\mu$ M D.U. GAGs dissolved in HBS-EP in the absence of 100 nM TIMP-3 (A) or in the presence of TIMP-3 (B) after injection over VEGFR-2 surfaces (124 RU).

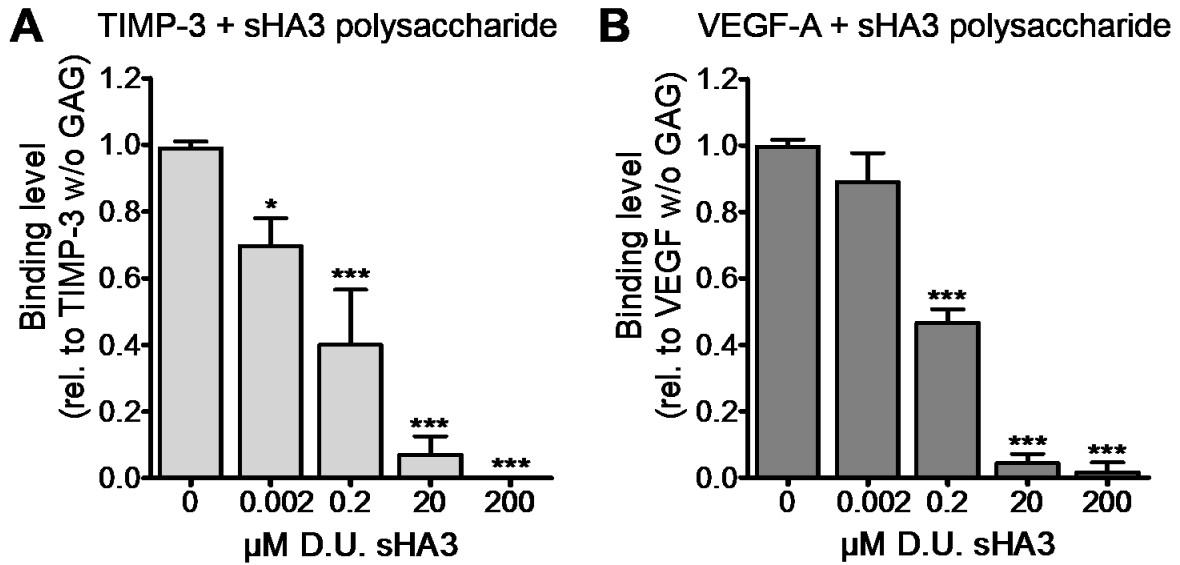


**Fig. 7.5 Influence of sHA3 polysaccharide concentrations on the TIMP-3/VEGFR-2 and VEGF-A/VEGFR-2 interaction.** Relative binding levels determined via SPR are displayed for 20 nM TIMP-3 (A) or VEGF-A (B) after pre-incubation with 0.002 - 200 μM D.U. sHA3 polysaccharides after injection over VEGFR-2 surfaces (63 RU). One-way ANOVA: \* ( $p < 0.05$ ), \*\*\* ( $p < 0.001$ ) vs. TIMP-3 or VEGF-A w/o sHA3. Adapted from [R453] with modifications.

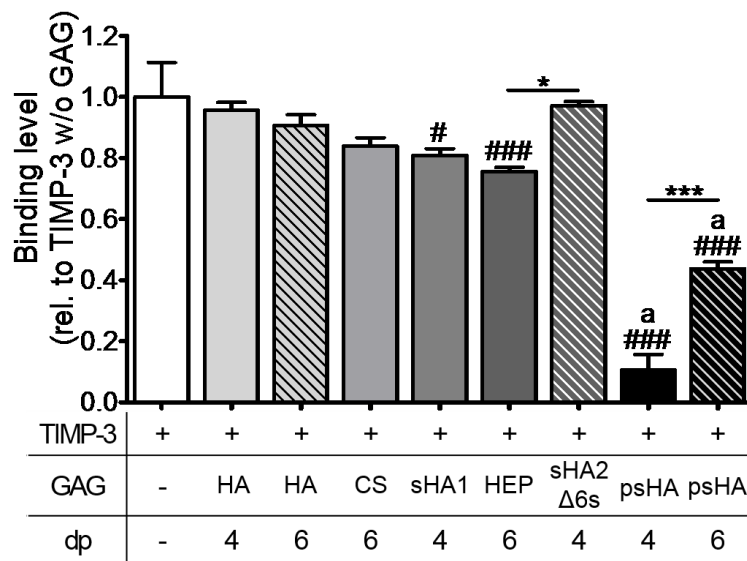


**Fig. 7.6 Effects of GAG oligosaccharides on the TIMP-3/VEGFR-2 interplay.** Relative binding levels are displayed for 20 nM TIMP-3 after pre-incubation with 40 μM D.U. GAG oligosaccharides after injection over VEGFR-2 surfaces (124 RU, 69 RU). One-way ANOVA: # ( $p < 0.05$ ), ### ( $p < 0.001$ ) vs. TIMP-3 w/o GAG; \* ( $p < 0.05$ ), \*\*\* ( $p < 0.001$ ) vs. respective treatment; a ( $p < 0.001$ ) vs. HA (dp 4, dp 6), CS (dp 6), sHA1 (dp 4), HEP (dp 6), sHA2Δ6s (dp 4). Adapted from [R453] with modifications.

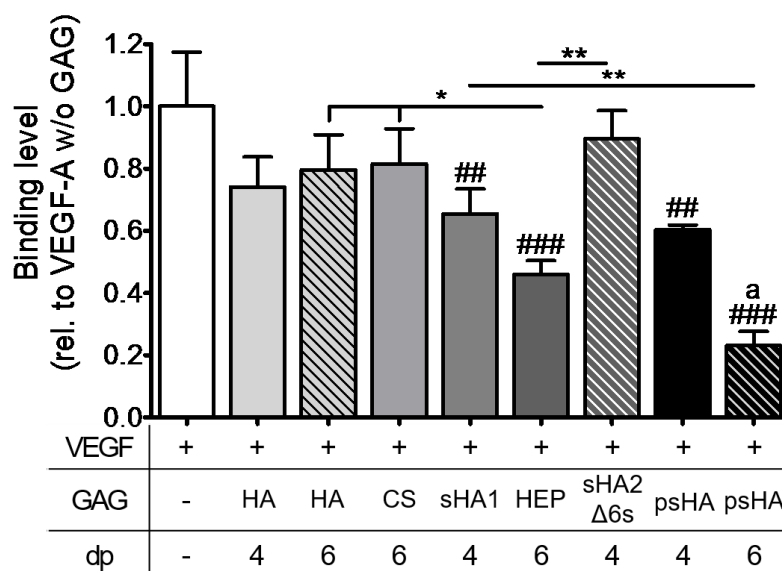


**Fig. 7.7 Effects of GAG oligosaccharides on the VEGF-A/VEGFR-2 interaction.** Relative binding levels are displayed for 20 nM VEGF-A after pre-incubation with 40 μM D.U. GAG oligosaccharides after injection over VEGFR-2 surfaces (53 RU, 69 RU). One-way ANOVA: ## ( $p < 0.01$ ), ### ( $p < 0.001$ ) vs. VEGF-A w/o GAG; \* ( $p < 0.05$ ), \*\* ( $p < 0.01$ ) vs. respective treatment; a ( $p < 0.001$ ) vs. HA (dp 4, dp 6), CS (dp 6), sHA2Δ6s (dp 4). Adapted from [R453] with modifications.

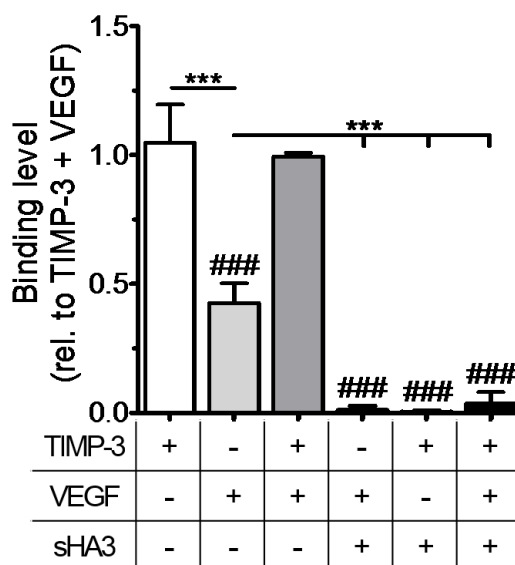


**Fig. 7.8 Effect of sHA3 on the VEGF-A and TIMP-3 competition for VEGFR-2 binding.** Relative SPR binding levels are displayed for 50 nM TIMP-3 and 1 nM VEGF-A after pre-incubation with 200 μM D.U. sHA3 polysaccharide after injection over immobilized VEGFR-2 (63 RU). One-way ANOVA: ### ( $p < 0.001$ ) vs. TIMP-3 + VEGF-A, \*\*\* ( $p < 0.001$ ) vs. respective treatment. Adapted from [R453] with modifications.

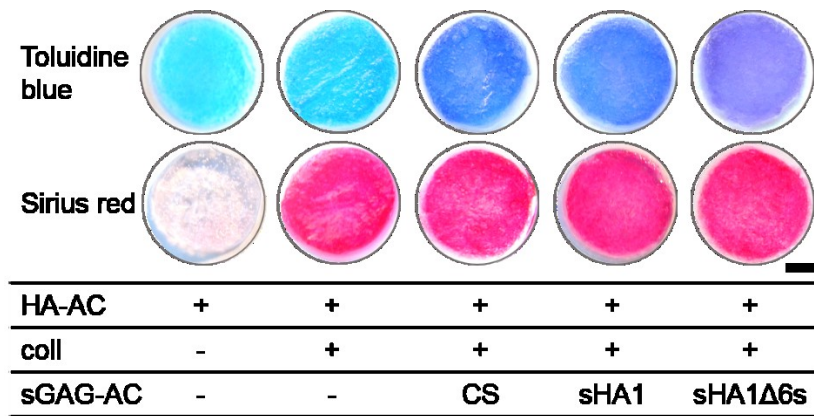


**Fig. 7.9 Visualization of sulfated GAGs and collagen in hydrogels.** Hydrogels were incubated with Toluidine blue or Sirius red to stain sGAGs (dark blue) or collagen (red). Adapted from [R475] with modifications.

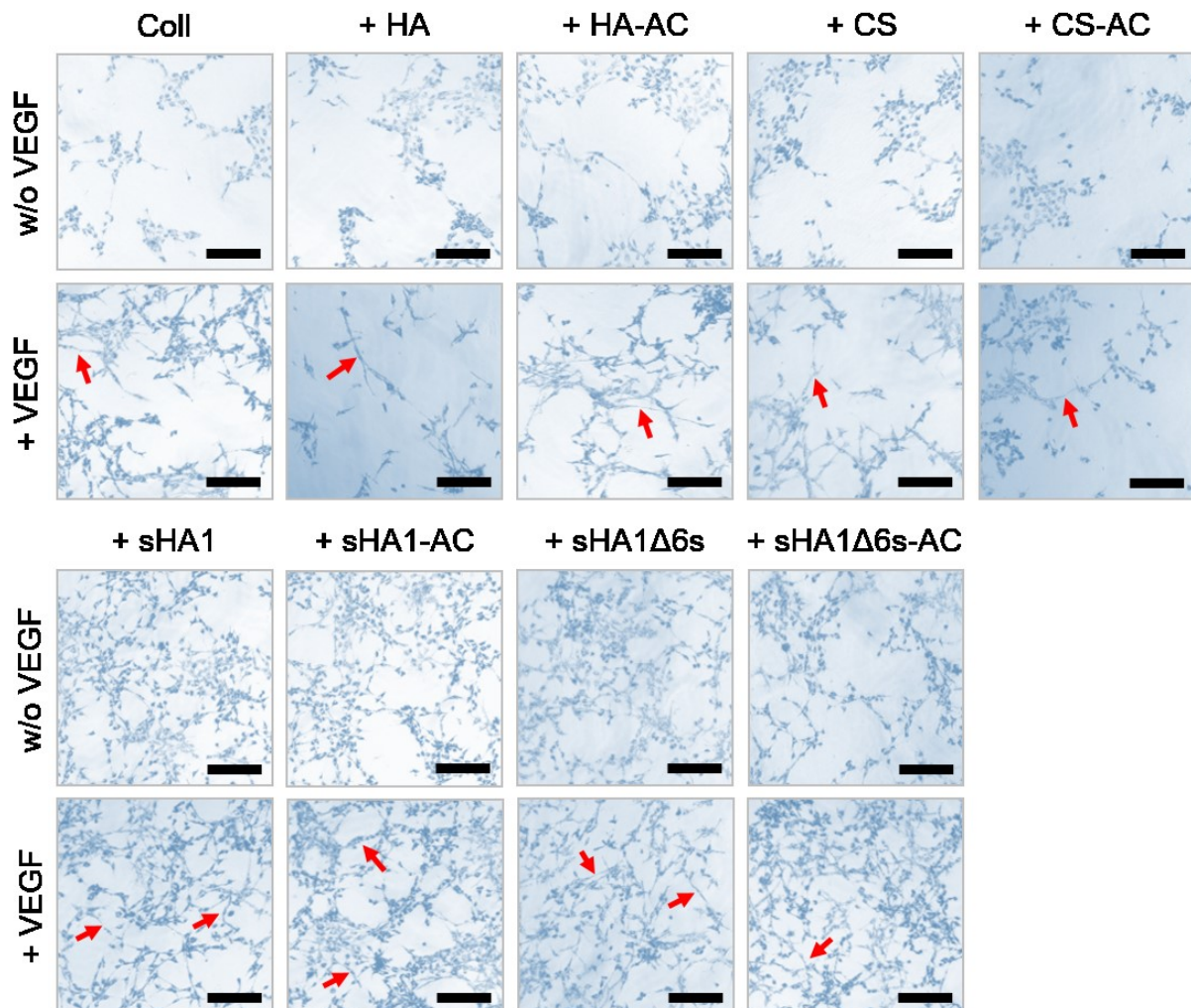


**Fig. 7.10 Influence of VEGF-A and solute GAGs on the tube formation of PAE/KDR cells.** Living cells after 72 hours of cultivation of initially 25000 PAE/KDR cells on collagen-coatings in the presence of 400  $\mu$ M D.U. GAG with or without 50 ng VEGF-A per sample under serum-free conditions were visualized by the incubation with MTT. Red arrows highlight some of the formed tubes. The scale bar represents 100  $\mu$ m.

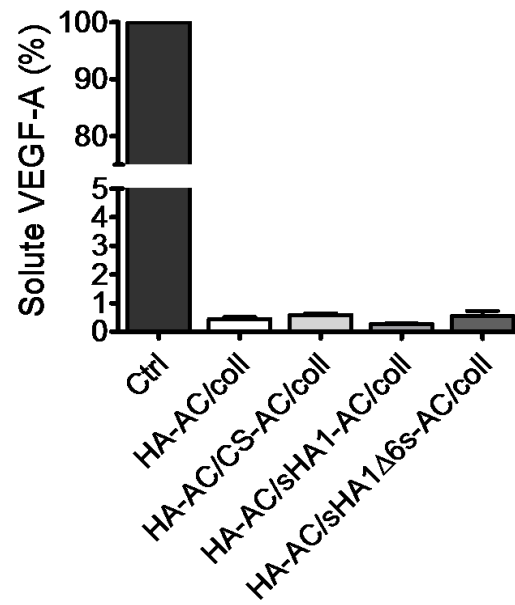


**Fig. 7.11 Solute VEGF-A after incubation of hydrogels with VEGF-A in cell culture media.** Hydrogels were incubated overnight with 50 ng VEGF-A and the amounts of solute VEGF-A in the supernatants were afterwards quantified via sandwich ELISA. A solution of VEGF-A in cell culture media, which was not incubated with hydrogels, served as control (Ctrl).

## LITERATURE

- [1] Sen CK, Gordillo GM, Roy S, Kirsner R, Lambert L, Hunt TK, et al. Human skin wounds: A major and snowballing threat to public health and the economy. *Wound Repair Regen* 2009;17:763–71.
- [2] Carter MJ. Economic evaluations of guideline-based or strategic interventions for the prevention or treatment of chronic wounds. *Appl Health Econ Health Policy* 2014;12:373–89.
- [3] Gottrup F. A specialized wound-healing center concept: Importance of a multidisciplinary department structure and surgical treatment facilities in the treatment of chronic wounds. *Am J Surg* 2004;187:19–20.
- [4] Hidalgo-Bastida LA, Cartmell SH. Mesenchymal Stem Cells, Osteoblasts and Extracellular Matrix Proteins: Enhancing Cell Adhesion and Differentiation for Bone Tissue Engineering. *Tissue Eng Part B Rev* 2010;16:405–12.
- [5] Frantz C, Stewart KM, Weaver VM. The extracellular matrix at a glance. *J Cell Sci* 2010;123:4195–200.
- [6] Ferrara N, Henzel WJ. Pituitary follicular cells secrete a novel heparin-binding growth factor specific for vascular endothelial cells. *Biochem Biophys Res Commun* 1989;161:851–8.
- [7] Yu WH, Yu SSC, Meng Q, Brew K, Woessner JF. TIMP-3 binds to sulfated glycosaminoglycans of the extracellular matrix. *J Biol Chem* 2000;275:31226–32.
- [8] Yu W, Woessner JF. Heparan Sulfate Proteoglycans as Extracellular Docking Molecules for Matrilysin (Matrix Metalloproteinase 7). *J Biol Chem* 2000;275:4183–91.
- [9R] Scharnweber D, Hübner L, Rother S, Hempel U, Anderegg U, Samsonov SA, et al. Glycosaminoglycan derivatives: promising candidates for the design of functional biomaterials. *J Mater Sci Mater Med* 2015;26:232.
- [10] Troeberg L, Lazenbatt C, Anower-E-Khuda MF, Freeman C, Federov O, Habuchi H, et al. Sulfated Glycosaminoglycans Control the Extracellular Trafficking and the Activity of the Metalloprotease Inhibitor TIMP-3. *Chem Biol* 2014;21:1300–9.
- [11] Teran M, Nugent MA. Synergistic Binding of Vascular Endothelial Growth Factor-A and Its Receptors to Heparin Selectively Modulates Complex Affinity. *J Biol Chem* 2015;290:16451–62.
- [12] Lu P, Weaver VM, Werb Z. The extracellular matrix: A dynamic niche in cancer progression. *J Cell Biol* 2012;196:395–406.
- [13] Harburger DS, Calderwood DA, Sci JC, Res B, Harburger DS, David A, et al. Integrin signalling at a glance. *J Cell Sci* 2009;122:159–63.
- [14] Humphries JD, Humphries MJ. Integrin ligands at a glance. *J Cell Sci* 2006;119:3901–3.
- [15] Xian X, Gopal S, Couchman JR. Syndecans as receptors and organizers of the extracellular matrix. *Cell Tissue Res* 2010;339:31–46.
- [16] Leitinger B, Hohenester E. Mammalian collagen receptors. *Matrix Biol* 2007;26:146–55.
- [17] Schmidt S, Friedl P. Interstitial cell migration: Integrin-dependent and alternative adhesion mechanisms. *Cell Tissue Res* 2010;339:83–92.
- [18] Bierbaum S, Scharnweber D. Artificial Extracellular Matrices to Functionalize Biomaterial Surfaces. vol. 2. Elsevier Ltd.; 2011.
- [19] Carter EM, Raggio CL. Genetic and orthopedic aspects of collagen disorders. *Curr Opin Pediatr* 2009;21:46–54.
- [20] Di Lullo GA, Sweeney SM, Körkkö J, Ala-Kokko L, San Antonio JD. Mapping the Ligand-binding Sites and Disease-associated Mutations on the Most Abundant Protein in the Human, Type I Collagen. *J Biol Chem* 2002;277:4223–31.
- [21] Myllyharju J. Intracellular post-translational modifications of collagens. *Top Curr Chem* 2005;247:115–47.
- [22] Gelse K, Pöschl E, Aigner T. Collagens - Structure, function, and biosynthesis. *Adv Drug Deliv Rev* 2003;55:1531–46.
- [23] Kadler K, Holmes D, Trotter J, Chapman J. Collagen fibril formation. *Biochem J* 1996;316:1–11.
- [24] Wood GC, Keech MK. The formation of fibrils from collagen solutions. 1. The effect of experimental conditions: kinetic and electron-microscope studies. *Biochem J* 1960;75:588–98.

- [25] Birk DE, Silver FH. Collagen fibrillogenesis in vitro: comparison of types I, II, and III. *Arch Biochem Biophys* 1984;235:178–85.
- [26] Corsi A, Xu T, Chen XD, Boyde A, Liang J, Mankani M, et al. Phenotypic effects of biglycan deficiency are linked to collagen fibril abnormalities, are synergized by decorin deficiency, and mimic Ehlers-Danlos-like changes in bone and other connective tissues. *J Bone Miner Res* 2002;17:1180–9.
- [27] Kalamajski S, Oldberg A. The role of small leucine-rich proteoglycans in collagen fibrillogenesis. *Matrix Biol* 2010;29:248–53.
- [28] Nomura Y. Structural change in decorin with skin aging. *Connect Tissue Res* 2006;47:249–55.
- [29] Xue M, Jackson CJ. Extracellular Matrix Reorganization During Wound Healing and Its Impact on Abnormal Scarring. *Adv Wound Care* 2015;4:119–36.
- [30] Bella J. Collagen structure: new tricks from a very old dog. *Biochem J* 2016;473:1001–25.
- [31] Alford AI, Kozloff KM, Hankenson KD. Extracellular matrix networks in bone remodeling. *Int J Biochem Cell Biol* 2015;65:20–31.
- [32] Krieg T, Aumailley M. The extracellular matrix of the dermis: Flexible structures with dynamic functions. *Exp Dermatol* 2011;20:689–95.
- [33] Srinivasan A, Sehgal PK. Characterization of biocompatible collagen fibers-a promising candidate for cardiac patch. *Tissue Eng - Part C Methods* 2010;16:895–903.
- [34] Mizuno K, Bächinger HP, Imamura Y, Hayashi T, Adachi E. Fragility of reconstituted type V collagen fibrils with the chain composition of  $\alpha 1(V)\alpha 2(V)\alpha 3(V)$  respective of the D-periodic banding pattern. *Connect Tissue Res* 2013;54:41–8.
- [35] Whitford D. *Proteins-Structure and Function*. Chichester: John Wiley & Sons, Inc; 2005.
- [36] Sweeney SM, Guy CA, Fields GB, San Antonio JD. Defining the domains of type I collagen involved in heparin- binding and endothelial tube formation. *Proc Natl Acad Sci U S A* 1998;95:7275–80.
- [37] Munakata H, Takagaki K, Majima M. Interaction between collagens and glycosaminoglycans investigated using a surface plasmon resonance biosensor. *Glycobiology* 1999;9:1023–7.
- [38] Singh P, Carraher C, Schwarzbauer JE. Assembly of fibronectin extracellular matrix. *Annu Rev Cell Dev Biol* 2010;26:397–419.
- [39] van Hinsbergh VW, Collen A, Koolwijk P. Role of fibrin matrix in angiogenesis. *Ann N Y Acad Sci* 2001;936:426–37.
- [40] Chen XD. Extracellular matrix provides an optimal niche for the maintenance and propagation of mesenchymal stem cells. *Birth Defects Res Part C - Embryo Today Rev* 2010;90:45–54.
- [41] To WS, Midwood KS. Plasma and cellular fibronectin: distinct and independent functions during tissue repair. *Fibrogenesis Tissue Repair* 2011;4:21.
- [42] Woods A, Longley RL, Tumova S, Couchman JR. Syndecan-4 binding to the high affinity heparin-binding domain of fibronectin drives focal adhesion formation in fibroblasts. *Arch Biochem Biophys* 2000;374:66–72.
- [43] Sharma A, Askari JA, Humphries MJ, Jones EY, Stuart DI. Crystal structure of a heparin- and integrin-binding segment of human fibronectin. *EMBO J* 1999;18:1468–79.
- [44] Chung CY, Erickson HP. Glycosaminoglycans modulate fibronectin matrix assembly and are essential for matrix incorporation of tenascin-C. *J Cell Sci* 1997;110:1413–9.
- [45] Järveläinen H, Sainio A, Koulu M, Wight TN, Penttinen R. Extracellular Matrix Molecules: Potential Targets in. *Pharmacol Rev* 2009;61:198–223.
- [46] Hardingham TE, Fosang AJ. Proteoglycans: many forms and many functions. *FASEB J* 1992;6:861–70.
- [47] Schaefer L, Schaefer RM. Proteoglycans: From structural compounds to signaling molecules. *Cell Tissue Res* 2010;339:237–46.
- [48] Xu D, Esko JD. Demystifying Heparan Sulfate-Protein Interactions. *Annu Rev Biochem* 2014;83:129–57.
- [49] Sasisekharan R, Raman R, Prabhakar V. Glycomics approach to structure-function relationships of glycosaminoglycans. *Annu Rev Biomed Eng* 2006;8:181–231.
- [50] Ernst S, Langer R, Cooney CL, Sasisekharan R. Enzymatic Degradation of Glycosaminoglycans. *Crit Rev Biochem Mol Biol* 1995;30:387–444.



- [51] Liu J, Shriver Z, Marshall Pope R, Thorp SC, Duncan MB, Copeland RJ, et al. Characterization of a heparan sulfate octasaccharide that binds to herpes simplex virus type 1 glycoprotein D. *J Biol Chem* 2002;277:33456–67.
- [52] Stanton H, Melrose J, Little CB, Fosang AJ. Proteoglycan degradation by the ADAMTS family of proteinases. *Biochim Biophys Acta - Mol Basis Dis* 2011;1812:1616–29.
- [53] Sugahara K, Kitagawa H. Recent advances in the study of the biosynthesis and functions of sulfated glycosaminoglycans. *Curr Opin Struct Biol* 2000;10:518–27.
- [54] Mikami T, Kitagawa H. Biosynthesis and function of chondroitin sulfate. *Biochim Biophys Acta* 2013;1830:4719–33.
- [55] Heng BC, Bezerra PP, Meng QR, Chin DW-L, Koh LB, Li H, et al. Adhesion, proliferation, and gene expression profile of human umbilical vein endothelial cells cultured on bilayered polyelectrolyte coatings composed of glycosaminoglycans. *Biointerphases* 2010;5:FA53-62.
- [56] Prince CW, Navia JM. Glycosaminoglycan alterations in rat bone due to growth and fluorosis. *J Nutr* 1983;113:1576–82.
- [57] Silbert JE, Sugumaran G. Biosynthesis of Chondroitin/Dermatan Sulfate. *IUBMB Life* 2002;54:177–86.
- [58] Avram S, Shaposhnikov S, Buiu C, Mernea M. Chondroitin Sulfate Proteoglycans: Structure-Function Relationship with Implication in Neural Development and Brain Disorders. *Biomed Res Int* 2014;2014:642798.
- [59] Hintze V, Moeller S, Schnabelrauch M, Bierbaum S, Viola M, Worch H, et al. Modifications of hyaluronan influence the interaction with human bone morphogenetic protein-4 (hBMP-4). *Biomacromolecules* 2009;10:3290–7.
- [60] Barkalow FJ, Schwarzbauer JE. Interactions between fibronectin and chondroitin sulfate are modulated by molecular context. *J Biol Chem* 1994;269:3957–62.
- [61] DeAngelis PL. Glycosaminoglycan polysaccharide biosynthesis and production: Today and tomorrow. *Appl Microbiol Biotechnol* 2012;94:295–305.
- [62] Toida T, Sakai S, Akiyama H, Linhardt RJ. Immunological activity of chondroitin sulfate. *Adv Pharmacol* 2006;53:403–15.
- [63] Trowbridge JM, Gallo RL. Dermatan sulfate: new functions from an old glycosaminoglycan. *Glycobiology* 2002;12:117R–25R.
- [64] Funderburgh JL. Keratan sulfate biosynthesis. *IUBMB Life* 2002;54:187–94.
- [65] Pomin VH, Piquet AA, Pereira MS, Mourão PAS. Residual keratan sulfate in chondroitin sulfate formulations for oral administration. *Carbohydr Polym* 2012;90:839–46.
- [66] Pomin VH. Keratan sulfate: An up-to-date review. *Int J Biol Macromol* 2015;72:282–9.
- [67] Quantock AJ, Young RD, Akama TO. Structural and biochemical aspects of keratan sulphate in the cornea. *Cell Mol Life Sci* 2010;67:891–906.
- [68] Sommarin Y, Wendel M, Shen Z, Hellman U, Heinegård D. Osteoadherin, a Cell-binding Keratan Sulfate Proteoglycan in Bone, Belongs to the Family of Leucine-rich Repeat Proteins of the Extracellular Matrix. *J Biol Chem* 1998;273:16723–9.
- [69] Nader HB, Chavante SF, Dos-Santos EA, Oliveira FW, De-Paiva JF, Jerônimo SMB, et al. Heparan sulfates and heparins: Similar compounds performing the same functions in vertebrates and invertebrates? *Brazilian J Med Biol Res* 1999;32:529–38.
- [70] Lindahl U, Kjellén L. Pathophysiology of heparan sulphate: Many diseases, few drugs. *J Intern Med* 2013;273:555–71.
- [71] Kolset SO, Pejler G. Serglycin: a structural and functional chameleon with wide impact on immune cells. *J Immunol* 2011;187:4927–33.
- [72] Capila I, Linhardt RJ. Heparin - Protein Interactions. *Angew Chemie - Int Ed* 2002;41:391–412.
- [73] Ori A, Wilkinson MC, Fernig DG. A systems biology approach for the investigation of the heparin/heparan sulfate interactome. *J Biol Chem* 2011;286:19892–904.
- [74] Kreuger J, Spillmann D, Li JP, Lindahl U. Interactions between heparan sulfate and proteins: The concept of specificity. *J Cell Biol* 2006;174:323–7.
- [75] Lindahl U, Bäckström G, Thunberg L, Leder IG. Evidence for a 3-O-sulfated d-glucosamine residue in the antithrombin-binding sequence of heparin. *Proc Natl Acad Sci U S A* 1980;77:6551–5.

- [76] Atha DH, Lormeau SJ, Petitou IM, Rosenberg RD, Choay J. Contribution of Monosaccharide Residues in Heparin Binding to Antithrombin III. *Biochemistry* 1985;24:6723–9.
- [77] Liu H, Zhang Z, Linhardt RJ, Liu H, Linhardt RJ. Lessons learned from the contamination of heparin. *Nat Prod Rep* 2009;26:313–21.
- [78] Linhardt RJ, Liu J. Synthetic heparin. *Curr Opin Pharmacol* 2012;12:217–9.
- [79] Prehm P. Hyaluronate is synthesized at plasma membranes. *Biochem J* 1984;220:597–600.
- [80] Kogan G, Šoltés L, Stern R, Gemeiner P. Hyaluronic acid: A natural biopolymer with a broad range of biomedical and industrial applications. *Biotechnol Lett* 2007;29:17–25.
- [81] Necas J, Bartosikova L, Brauner P, Kolar J. Hyaluronic acid (hyaluronan): A review. *Vet Med (Praha)* 2008;53:397–411.
- [82] Stern R, Asari AA, Sugahara KN. Hyaluronan fragments: An information-rich system. *Eur J Cell Biol* 2006;85:699–715.
- [83] Maytin E V. Hyaluronan: More than just a wrinkle filler. *Glycobiology* 2016;26:553–9.
- [84] Bellamy N, Campbell J, Robinson V, Gee T, Bourne R, Wells G. Viscosupplementation for the treatment of osteoarthritis of the knee. *Cochrane Database Syst Rev* 2006;19:CD005321.
- [85] Goldberg VM, Buckwalter JA. Hyaluronans in the treatment of osteoarthritis of the knee: Evidence for disease-modifying activity. *Osteoarthr Cartil* 2005;13:216–24.
- [86] Moseley R, Leaver M, Walker M, Waddington RJ, Parsons D, Chen WYJ, et al. Comparison of the antioxidant properties of HYAFF-11p75, AQUACEL and hyaluronan towards reactive oxygen species in vitro. *Biomaterials* 2002;23:2255–64.
- [87] Day AJ, Prestwich GD. Hyaluronan-binding proteins: Tying up the giant. *J Biol Chem* 2002;277:4585–8.
- [88] Goodison S, Urquidi V, Tarin D. CD44 cell adhesion molecules. *Mol Pathol* 1999;52:189–96.
- [89] Turley EA, Noble PW, Bourguignon LYW. Signaling properties of hyaluronan receptors. *J Biol Chem* 2002;277:4589–92.
- [90] Gendron C, Kashiwagi M, Ngee HL, Enghild JJ, Thøgersen IB, Hughes C, et al. Proteolytic activities of human ADAMTS-5: Comparative studies with ADAMTS-4. *J Biol Chem* 2007;282:18294–306.
- [91] Coutinho MF, Lacerda L, Alves S. Glycosaminoglycan storage disorders: A review. *Biochem Res Int* 2012;2012.
- [92] Calabro A, Midura R, Wang A, West L, Plaas A, Hascall VC. Fluorophore-assisted carbohydrate electrophoresis (FACE) of glycosaminoglycans. *Osteoarthr Cartil* 2001;9:S16–22.
- [93] Stern R, Jedrzejewski MJ. Hyaluronidases: Their genomics, structures, and mechanisms of action. *Chem Rev* 2006;106:818–39.
- [94] Lepperdinger G, Müllegger J, Kreil G. Hyal2 - Less active, but more versatile? *Matrix Biol* 2001;20:509–14.
- [95] Frost GI, Cso TB, Wong T, Stern R. Purification, Cloning, and Expression of Human Plasma Hyaluronidase 1. *Biochem Biophys Res Commun* 1997;236:10–5.
- [96] Watt F, Fujiwara H. Cell-Extracellular Matrix Interactions in Normal and Diseased Skin. *Cold Spring Harb Perspect Biol* 2011;3:1–15.
- [97] Timpl R. Structure and biological activities of basement membrane proteins. *Eur J Biochem* 1989;180:487–502.
- [98] Watt FM, Huck WTS. Role of the extracellular matrix in regulating stem cell fate. *Nat Rev Mol Cell Biol* 2013;14:467–73.
- [99] Carrino DA, Sorrell JM, Caplan AI. Age-related changes in the proteoglycans of human skin. *Arch Biochem Biophys* 2000;373:91–101.
- [100] Bernstein EF, Underhill CB, Hahn PJ, Brown DB, Uitto J. Chronic sun exposure alters both the content and distribution of dermal glycosaminoglycans. *Br J Dermatol* 1996;135:255–62.
- [101] Maccari F, Volpi N. Structural characterization of the skin glycosaminoglycans in patients with pseudoxanthoma elasticum. *Int J Dermatol* 2008;47:1024–7.
- [102] Juhlin L. Hyaluronan in skin. *J Intern Med* 1997;242:61–6.
- [103] Papakonstantinou E, Roth M, Karakiulakis G. Hyaluronic Acid: A Key Molecule in Skin Aging. *Dermatoendocrinol* 2012;4:253–8.
- [104] Salmon CR, Tomazela DM, Ruiz KGS, Foster BL, Paes Leme AF, Sallum EA, et al. Proteomic analysis of human dental cementum and alveolar bone. *J Proteomics* 2013;91:544–55.

- [105] Crockett JC1, Rogers MJ, Coxon FP, Hocking LJ HM. Bone remodelling at a glance. *J Cell Sci* 2011;124:991–8.
- [106] Velasco CR, Collic-Jouault S, Redini F, Heymann D, Padrines M. Proteoglycans on bone tumor development. *Drug Discov Today* 2010;15:553–60.
- [107] Ezzo JA. Putting the “Chemistry” Back into Archaeological Bone Chemistry Analysis: Modeling Potential Dietary Indicators. *J Anthropol Archaeol* 1994;13:1–34.
- [108] Koike T, Izumikawa T, Tamura JI, Kitagawa H. Chondroitin sulfate-E fine-tunes osteoblast differentiation via ERK1/2, Smad3 and Smad1/5/8 signaling by binding to N-cadherin and cadherin-11. *Biochem Biophys Res Commun* 2012;420:523–9.
- [109] Allen MR, Hock JM, Burr DB. Periosteum: Biology, regulation, and response to osteoporosis therapies. *Bone* 2004;35:1003–12.
- [110] Dallas SL, Prideaux M, Bonewald LF. The osteocyte: An endocrine cell . . . and more. *Endocr Rev* 2013;34:658–90.
- [111] Guo S, DiPietro LA. Factors Affecting Wound Healing. *J Dent Res* 2010;89:219–29.
- [112] Enoch S, Leaper DJ, Beldon P. Basic science of wound healing. *Surg* 2010;28:409–12.
- [113] Pakyari M, Farrokhi A. Critical Role of Transforming Growth Factor Beta in Different Phases of Wound Healing. *Adv Wound Care* 2013;2:215–24.
- [114] Kataoka H, Kono H, Patel Z, Rock KL. Evaluation of the Contribution of Multiple DAMPs and DAMP Receptors in Cell Death-Induced Sterile Inflammatory Responses. *PLoS One* 2014;9:e104741.
- [115] Zaja-Milatovic S, Richmond A. CXC chemokines and their receptors: A case for a significant biology role in cutaneous wound healing. *Histol Histopathol* 2008;23:1399–407.
- [116] Behm B, Babilas P, Landthaler M, Schreml S. Cytokines, chemokines and growth factors in wound healing. *J Eur Acad Dermatology Venereol* 2012;26:812–20.
- [117] Li J, Chen J, Kirsner R. Pathophysiology of acute wound healing. *Clin Dermatol* 2007;25:9–18.
- [118] Shirakata Y, Kimura R, Nanba D, Iwamoto R, Tokumaru S, Morimoto C, et al. Heparin-binding EGF-like growth factor accelerates keratinocyte migration and skin wound healing. *J Cell Sci* 2005;118:2363–70.
- [119] Qi JH, Ebrahim Q, Moore N, Murphy G, Claesson-Welsh L, Bond M, et al. A novel function for tissue inhibitor of metalloproteinases-3 (TIMP3): inhibition of angiogenesis by blockage of VEGF binding to VEGF receptor-2. *Nat Med* 2003;9:407–15.
- [120] Reinke JM, Sorg H. Wound repair and regeneration. *Eur Surg Res* 2012;49:35–43.
- [121] Betts DC, Müller R. Mechanical regulation of bone regeneration: theories, models, and experiments. *Front Endocrinol (Lausanne)* 2014;5:1–14.
- [122] Sánchez-Duffhues G, Hiepen C, Knaus P. Bone morphogenetic protein signaling in bone homeostasis. *Bone* 2015;80:43–59.
- [123] Feng X, McDonald JM. Disorders of bone remodeling. *Annu Rev Pathol* 2011;6:121–45.
- [124] Raggatt LJ, Partridge NC. Cellular and molecular mechanisms of bone remodeling. *J Biol Chem* 2010;285:25103–8.
- [125] Aguda AH, Panwar P, Du X, Nguyen NT, Brayer GD, Brömme D. Structural basis of collagen fiber degradation by cathepsin K. *Proc Natl Acad Sci U S A* 2014;111:17474–9.
- [126] Rachner TD, Khosla S, Hofbauer LC. Osteoporosis: Now and the future. *Lancet* 2011;377:1276–87.
- [127] Broughton G, Janis JE, Attinger CE. Wound Healing: An Overview. *Plast Reconstr Surg* 2006;June Suppl:1–32.
- [128] Rodriguez PG, Felix FN, Woodley DT, Shim EK. The role of oxygen in wound healing: A review of the literature. *Dermatologic Surg* 2008;34:1159–69.
- [129] Lynam EC, Xie Y, Dawson R, McGovern J, Upton Z, Wang X. Severe hypoxia and malnutrition collectively contribute to scar fibroblast inhibition and cell apoptosis. *Wound Repair Regen* 2015;23:664–71.
- [130] Edwards R, Harding KG. Bacteria and wound healing. *Curr Opin Infect Dis* 2004;17:91–6.
- [131] Menke NB, Ward KR, Witten TM, Bonchev DG, Diegelmann RF. Impaired wound healing. *Clin Dermatol* 2007;25:19–25.
- [132] Gosain A, DiPietro LA. Aging and Wound Healing. *World J Surg* 2004;28:321–6.

- [133] Swift ME, Burns AL, Gray KL, DiPietro LA. Age-related alterations in the inflammatory response to dermal injury. *J Invest Dermatol* 2001;117:1027–35.
- [134] Sadoun E, Reed MJ. Impaired angiogenesis in aging is associated with alterations in vessel density, matrix composition, inflammatory response, and growth factor expression. *J Histochem Cytochem* 2003;51:1119–30.
- [135] Plisko A, Gilchrest BA. Growth Factor Responsiveness of Cultured Human Fibroblasts Declines with Age. *J Gerontol* 1983;38:513–8.
- [136] Tashiro K, Shishido M, Fujimoto K, Hirota Y, Yo K, Gomi T, et al. Age-related disruption of autophagy in dermal fibroblasts modulates extracellular matrix components. *Biochem Biophys Res Commun* 2014;443:167–72.
- [137] Boskey A, Coleman R. Aging and Bone. *Crit Rev Oral Biol Med* 2010;89:1333–48.
- [138] IDF Diabetes Atlas. seventh ed. Brussel, Belgium: International Diabetes Federation; 2015.
- [139] Tamayo T, Rosenbauer J, Wild SH, Spijkerman AMW, Baan C, Forouhi NG, et al. Diabetes in Europe: An update. *Diabetes Res Clin Pract* 2014;103:206–17.
- [140] Goncalves I, Bengtsson E, Colhoun HM, Shore AC, Palombo C, Natali A, et al. Elevated plasma levels of MMP-12 are associated with atherosclerotic burden and symptomatic cardiovascular disease in subjects with type 2 diabetes. *Arterioscler Thromb Vasc Biol* 2015;35:1723–31.
- [141] Brem H, Tomic-Canic M. Cellular and molecular basis of wound healing in diabetes. *J Clin Invest* 2007;117:1219–22.
- [142] Tandara AA, Mustoe TA. Oxygen in Wound Healing - More than a Nutrient. *World J Surg* 2004;28:294–300.
- [143] Lerman OZ, Galiano RD, Armour M, Levine JP, Gurtner GC. Cellular Dysfunction in the Diabetic Fibroblast: Impairment in Migration, Vascular Endothelial Growth Factor Production, and Response to Hypoxia. *Am J Pathol* 2003;162:303–12.
- [144] Leslie WD, Rubin MR, Schwartz A V., Kanis JA. Type 2 diabetes and bone. *J Bone Miner Res* 2012;27:2231–7.
- [145] Sapna G, Gokul S, Bagri-Manjrekar K. Matrix metalloproteinases and periodontal diseases. *Oral Dis.* 2014;20:538-50.
- [146] Gibson D, Cullen B, Legerstee R, Harding K, Schultz G. MMPs Made Easy. *Wounds Int* 2009;1:1–6.
- [147] Nagase H, Visse R, Murphy G. Structure and function of matrix metalloproteinases and TIMPs. *Cardiovasc Res* 2006;69:562–73.
- [148] Overall CM. Molecular Determinants of Metalloproteinase Substrate Specificity: Matrix Metalloproteinase Substrate Binding Domains, Modules, and Exosites. *Mol Biotechnol* 2002;22:051–86.
- [149] Tocchi A, Parks WC. Functional interactions between matrix metalloproteinases and glycosaminoglycans. *FEBS J* 2013;280:2332–41.
- [150] Brinckerhoff CE, Matrisian LM. Matrix metalloproteinases: a tail of a frog that became a prince. *Nat Rev Mol Cell Biol* 2002;3:207–14.
- [151] Visse R, Nagase H. Matrix metalloproteinases and tissue inhibitors of metalloproteinases: Structure, function, and biochemistry. *Circ Res* 2003;92:827–39.
- [152] Murphy G, Nagase H. Reappraising metalloproteinases in rheumatoid arthritis and osteoarthritis: destruction or repair? *Nat Clin Pract Rheumatol* 2008;4:128–35.
- [153] Maskos K. Crystal structures of MMPs in complex with physiological and pharmacological inhibitors. *Biochimie* 2005;87:249–63.
- [154] Yamamoto K, Murphy G, Troeberg L. Extracellular regulation of metalloproteinases. *Matrix Biol* 2015;44–46:1–9.
- [155] Van den Steen PE, Y GO, Wormald MR, Dwek RA, Y PMR. Matrix remodelling enzymes , the protease cascade and glycosylation. *Biochim Biophys Acta* 2001;1528:61–73.
- [156] Bode W, Gomis-Rüth F-X, Stöckler W. Astacins, serralysins, snake venom and matrix metalloproteinases exhibit identical zinc-binding environments (HEXXHXXGXXH and Met-turn) and topologies and should be grouped into a common family , the “metzincins.” *FEBS J* 1993;331:134–40.
- [157] Hadler-Olsen E, Fadnes B, Sylte I, Uhlin-hansen L, Winberg JO. Regulation of matrix metalloproteinase activity in health and disease. *FEBS J* 2011;278:28–45.

- [158] van Wart HE, Birkedal-Hansen H. The cysteine switch: A principle of regulation of metalloproteinase activity with potential applicability to the entire matrix metalloproteinase gene family. *Proc Natl Acad Sci U S A* 1990;87:5578–82.
- [159] Sang QXA. Complex role of matrix metalloproteinases in angiogenesis. *Cell Res* 1998;8:171–7.
- [160] Pilcher BK, Dumin JA, Sudbeck BD, Krane SM, Welgus HG, Parks WC. The activity of collagenase-1 is required for keratinocyte migration on a type I collagen matrix. *J Cell Biol* 1997;137:1445–57.
- [161] Martins VL, Caley M, O'Toole EA. Matrix metalloproteinases and epidermal wound repair. *Cell Tissue Res* 2013;351:255–68.
- [162] Rohani MG, Parks WC. Matrix remodeling by MMPs during wound repair. *Matrix Biol* 2015;44–46:113–21.
- [163] Daniels JT, Cambrey AD, Occleston NL, Garrett Q, Tarnuzzer RW, Schultz GS, et al. Matrix metalloproteinase inhibition modulates fibroblast-mediated matrix contraction and collagen production in vitro. *Investig Ophthalmol Vis Sci* 2003;44:1104–10.
- [164] Ulrich D, Ulrich F, Unglaub F, Piatkowski A, Pallua N. Matrix metalloproteinases and tissue inhibitors of metalloproteinases in patients with different types of scars and keloids. *J Plast Reconstr Aesthet Surg* 2010;63:1015–21.
- [165] Hatori K, Sasano Y, Takahashi I, Kamakura S, Kagayama M, Sasaki K. Osteoblasts and osteocytes express MMP2 and -8 and TIMP1, -2, and -3 along with extracellular matrix molecules during appositional bone formation. *Anat Rec A Discov Mol Cell Evol Biol* 2004;277:262–71.
- [166] Goldberg GI, Wilhelm SM, Kronberger A, Bauer EA, Grant GA, Eisen Z. Human Fibroblast Collagenase. Complete primary structure and homology to an oncogene transformation-induced rat protein. *J Biol Chem* 1986;261:6600–5.
- [167] Hasty K, Pourmotabbed T, Goldberg GI, Thompson J, Spinella D, Stevens R, et al. Human neutrophil collagenase. A distinct gene product with homology to other matrix metalloproteinases. *J Biol Chem* 1990;265:11421–4.
- [168] Ortega N, Behonick DJ, Werb Z. Matrix remodeling during endochondral ossification. *Trends Cell Biol* 2004;14:86–93.
- [169] Murphy G, Allan JA, Willenbrock F, Cockett MI, Connell JPO, Docherty AJP. The Role of the C-terminal Domain in Collagenase and Stromelysin Specificity. *J Biol Chem* 1992;267:9612–8.
- [170] Ellsmere JC, Khanna RA, Michael LJ. Mechanical loading of bovine pericardium accelerates enzymatic degradation. *Biomaterials* 1999;20:1143–50.
- [171] Tonge TK, Ruberti JW, Nguyen TD. Micromechanical Modeling Study of Mechanical Inhibition of Enzymatic Degradation of Collagen Tissues. *Biophys J* 2015;109:2689–700.
- [172] Liu Y, Min D, Bolton T, Nubé V, Twigg SM, Yue DK, et al. Increased Matrix Metalloproteinase-9 Predicts Poor Wound Healing in Diabetic Foot Ulcers. *Diabetes Care* 2009;32:117–9.
- [173] Collier IE, Wilhelm SM, Eisen AZ, Marmer BL, Grant GA, Seltzer JL, et al. H-ras oncogene transformed human bronchial epithelial cells (TBE-1) secrete a single metalloproteinase capable of degrading basement membrane collagen. *J Biol Chem* 1988;263:6579–87.
- [174] Imai K, Okada Y. Purification of matrix metalloproteinases by column chromatography. *Nat Protoc* 2008;3:1111–24.
- [175] Winberg JO, Kolset SO, Berg E, Uhlin-Hansen L. Macrophages secrete matrix metalloproteinase 9 covalently linked to the core protein of chondroitin sulphate proteoglycans. *J Mol Biol* 2000;304:669–80.
- [176] Yu WH, Woessner JF. Heparin-enhanced zymographic detection of matrilysin and collagenases. *Anal Biochem* 2001;293:38–42.
- [177] Crabbe T, Ioannou C, Docherty AJP. Human progelatinase. *Eur J Biochem* 1993;218:431–8.
- [178] Crabbe T, Connell JPO, Smith BJ, Docherty AJP. Reciprocated Matrix Metalloproteinase Activation: A Process Performed by Interstitial Collagenase and Progelatinase A. *Biochemistry* 1994;33:14419–25.
- [179] Butler GS, Butler MJ, Atkinson SJ, Will H, Tamura T, Westrum SS Van, et al. The TIMP2 Membrane Type 1 Metalloproteinase “Receptor” Progelatinase A. *Biochemistry* 1998;273:871–80.

- [180] Wallon UM, Overall CM. The Hemopexin-Like Domain (C-Domain) of Human Gelatinase-A (Matrix Metalloproteinase-2) Requires Ca<sup>2+</sup> for Fibronectin and Heparin-Binding - Binding-Properties of Recombinant Gelatinase a C-Domain to Extracellular-Matrix and Basement-Membrane Components. *J Biol Chem* 1997;272:7473–81.
- [181] Theocharis AD, Gialeli C, Bouris P, Giannopoulou E, Skandalis SS, Aletras AJ, et al. Cell-matrix interactions: focus on proteoglycan-proteinase interplays and pharmacological targeting in cancer. *FEBS J* 2014;281:5023–42.
- [182] Iida J, Wilhelmson KL, Ng J, Lee P, Morrison C, Tam E, et al. Cell surface chondroitin sulfate glycosaminoglycan in melanoma: role in the activation of pro-MMP-2 (pro-gelatinase A). *Biochem J* 2007;403:553–63.
- [183] Murphy G. Tissue inhibitors of metalloproteinases. *Genome Biol* 2011;12:233.
- [184] Leivonen SK, Lazaridis K, Decock J, Chantry A, Edwards DR, Kähäri VM. TGF- $\beta$ -Elicited Induction of Tissue Inhibitor of Metalloproteinases (TIMP)-3 Expression in Fibroblasts Involves Complex Interplay between Smad3, p38 $\alpha$ , and ERK1/2. *PLoS One* 2013;8:e57474.
- [185] Becker A De, Van Hummelen P, Bakkus M, Vande Broek I, De Wever J, De Waele M, et al. Migration of culture-expanded human mesenchymal stem cells through bone marrow endothelium is regulated by matrix metalloproteinase-2 and tissue inhibitor of metalloproteinase-3. *Haematologica* 2007;92:440–9.
- [186] Huang Y, Song LX, Wu S, Fan F, Lopes-Virella MF. Oxidized LDL differentially regulates MMP-1 and TIMP-1 expression in vascular endothelial cells. *Atherosclerosis* 2001;156:119–25.
- [187] Amour A, Knight CG, Webster A, Slocombe PM, Stephens PE, Knäuper V, et al. The in vitro activity of ADAM-10 is inhibited by TIMP-1 and TIMP-3. *FEBS Lett* 2000;473:275–9.
- [188] Kashiwagi M, Tortorella M, Nagase H, Brew K. TIMP-3 Is a Potent Inhibitor of Aggrecanase 1 (ADAM-TS4) and Aggrecanase 2 (ADAM-TS5). *J Biol Chem* 2001;276:12501–4.
- [189] Loechel F, Fox JW, Murphy G, Albrechtsen R, Wewer UM. ADAM 12-S Cleaves IGFBP-3 and IGFBP-5 and Is Inhibited by TIMP-3. *Biochem Biophys Res Commun* 2000;278:511–5.
- [190] Ogata Y, Itoh Y, Nagase H. Steps involved in activation of the pro-matrix metalloproteinase 9 (progelatinase B)-tissue inhibitor of metalloproteinases-1 complex by 4-aminophenylmercuric acetate and proteinases. *J Biol Chem* 1995;270:18506–11.
- [191] Ward R V, Atkinson SJ, Reynolds JJ, Murphy G. Cell surface-mediated activation of progelatinase A: demonstration of the involvement of the C-terminal domain of progelatinase A in cell surface binding and activation of progelatinase A by primary fibroblasts. *Biochem J* 1994;304:263–9.
- [192] Morgunova E, Tuuttila A, Bergmann U, Tryggvason K, Huber R. Structural insight into the complex formation of latent matrix metalloproteinase 2 with tissue inhibitor of metalloproteinase 2. *Proc Natl Acad Sci U S A* 2002;99:7414–9.
- [193] Butler GS, Apte SS, Willenbrock F, Murphy G. Human Tissue Inhibitor of Metalloproteinases 3 Interacts with Both the N- and C-terminal Domains of Gelatinases A and B. *J Biol Chem* 1999;274:10846–51.
- [194] Ries C. Cytokine functions of TIMP-1. *Cell Mol Life Sci* 2014;71:659–72.
- [195] Qi JH, Anand-Apte B. Tissue inhibitor of metalloproteinase-3 (TIMP3) promotes endothelial apoptosis via a caspase-independent mechanism. *Apoptosis* 2015;20:523–34.
- [196] George SJ, Lloyd CT, Angelini GD, Newby AC, Baker AH. Inhibition of late vein graft neointima formation in human and porcine models by adenovirus-mediated overexpression of tissue inhibitor of metalloproteinase-3. *Circulation* 2000;101:296–304.
- [197] Sahebjam S, Khokha R, Mort JS. Increased collagen and aggrecan degradation with age in the joints of Timp3<sup>-/-</sup> mice. *Arthritis Rheum* 2007;56:905–9.
- [198] Cardellini M, Menghini R, Martelli E, Casagrande V, Marino A, Rizza S, et al. TIMP3 is reduced in atherosclerotic plaques from subjects with type 2 diabetes and increased by SirT1. *Diabetes* 2009;58:2396–401.
- [199] Menghini R, Uccioli L, Vainieri E, Pecchioli C, Casagrande V, Stoehr R, et al. Expression of tissue inhibitor of metalloprotease 3 is reduced in ischemic but not neuropathic ulcers from patients with type 2 diabetes mellitus. *Acta Diabetol* 2013;50:907–10.
- [200] Brew K, Nagase H. The tissue inhibitors of metalloproteinases (TIMPs): An ancient family with structural and functional diversity. *Biochim Biophys Acta - Mol Cell Res* 2010;1803:55–71.

- [201] Toricelli M, Melo FHM, Peres GB, Silva DCP, Jasiulionis MG. Timp1 interacts with beta-1 integrin and CD63 along melanoma genesis and confers anoikis resistance by activating PI3-K signaling pathway independently of Akt phosphorylation. *Mol Cancer* 2013;12:22.
- [202] Lee MH, Atkinson S, Murphy G. Identification of the Extracellular Matrix (ECM) binding motifs of tissue inhibitor of metalloproteinases (TIMP)-3 and effective transfer to TIMP-1. *J Biol Chem* 2007;282:6887–98.
- [203] Zhang F, Lee K, Linhardt R. SPR Biosensor Probing the Interactions between TIMP-3 and Heparin/GAGs. *Biosensors* 2015;5:500–12.
- [204] Goodwin AM. In vitro assays of angiogenesis for assessment of angiogenic and anti-angiogenic agents. *Microvasc Res* 2007;74:172–83.
- [205] Vigetti D, Viola M, Karousou E, Deleonibus S, Karamanou K, Luca G De, et al. Epigenetics in extracellular matrix remodeling and hyaluronan metabolism. *FEBS J* 2014;281:4980–92.
- [206] Arpino V, Brock M, Gill SE. The role of TIMPs in regulation of extracellular matrix proteolysis. *Matrix Biol* 2015;44–46:247–54.
- [207] Gill SE, Parks WC. Metalloproteinases and their inhibitors: Regulators of wound healing. *Int J Biochem Cell Biol* 2008;40:1334–47.
- [208] Vu TH, Werb Z. Matrix metalloproteinases: Effectors of development and normal physiology. *Genes Dev* 2000;14:2123–33.
- [209] Bonnans C, Chou J, Werb Z. Remodelling the extracellular matrix in development and disease. *Nat Rev Mol Cell Biol* 2014;15:786–801.
- [210] Wynn TA. Cellular and molecular mechanisms of fibrosis. *J Pathol* 2008:199–210.
- [211] Muñoz-Félix JM, González-Núñez M, Martínez-Salgado C, López-Novoa JM. TGF- $\beta$ /BMP proteins as therapeutic targets in renal fibrosis. Where have we arrived after 25 years of trials and tribulations? *Pharmacol Ther* 2015;156:44–58.
- [212] Bondeson J, Wainwright S, Hughes C, Caterson B. The regulation of the ADAMTS4 and ADAMTS5 aggrecanases in osteoarthritis: A review. *Clin Exp Rheumatol* 2008;26:139–45.
- [213] Demidova-Rice, Tatiana N. Hamblin MR, Herman IM. Acute and Impaired Wound Healing: Pathophysiology and Current Methods for Drug Delivery, Part 1: Normal and Chronic Wounds: Biology, Causes, and Approaches to Care. *Adv Ski Wound Care* 2012;25:304–14.
- [214] Eming S, Krieg T, Davidson JM. Inflammation in wound repair: Molecular and cellular mechanisms. *J Invest Dermatol* 2007;127:514–25.
- [215] Stojadinovic O, Brem H, Vouthounis C, Lee B, Fallon J, Stallcup M, et al. Molecular pathogenesis of chronic wounds: the role of beta-catenin and c-myc in the inhibition of epithelialization and wound healing. *Am J Pathol* 2005;167:59–69.
- [216] Hasan A, Murata H, Falabella A, Ochoa S, Zhou L, Badiavas E, et al. Dermal fibroblasts from venous ulcers are unresponsive to the action of transforming growth factor-beta 1. *J Dermatol Sci* 1997;16:59–66.
- [217] Kim BC, Kim HT, Park SH, Cha JS, Yufit T, Kim SJ, et al. Fibroblasts from chronic wounds show altered TGF- $\beta$ -signaling and decreased TGF- $\beta$  type II receptor expression. *J Cell Physiol* 2003;195:331–6.
- [218] Herz J, Strickland DK. LRP: a multifunctional scavenger and signaling receptor. *J Clin Invest* 2001;108:779–84.
- [219] Lillis AP, Duyn LB Van, Murphy-ullrich JE, Dudley K. The low density lipoprotein receptor-related protein 1: Unique tissue-specific functions revealed by selective gene knockout studies. *Physiol Rev* 2009;88:887–918.
- [220] Boucher P. LRP: Role in Vascular Wall Integrity and Protection from Atherosclerosis. *Science* 2003;300:329–32.
- [221] Springer TA. An Extracellular beta-Propeller Module Predicted in Lipoprotein and Scavenger Receptors, Tyrosine Kinases, Epidermal Growth Factor Precursor, and Extracellular Matrix Components. *J Mol Biol* 1998;283:837–62.
- [222] Davis CG, Goldstein JL, Südhof TC, Anderson RGW, Russell DW, Brown MS. Acid-dependent ligand dissociation and recycling of LDL receptor mediated by growth factor homology region. *Nature* 1987;326:760–5.

- [223] Mikhailenko I, Considine W, Argraves K, Loukinov D, Hyman BT, Strickland DK. Functional domains of the very low density lipoprotein receptor: molecular analysis of ligand binding and acid-dependent ligand dissociation mechanisms. *J Cell Sci* 1999;112:3269–81.
- [224] Rudenko G. Structure of the LDL Receptor Extracellular Domain at Endosomal pH. *Science* 2002;298:2353–8.
- [225] Basu SK, Goldstein JL, Anderson RGW, Brown MS. Monensin interrupts the recycling of low density lipoprotein receptors in human fibroblasts. *Cell* 1981;24:493–502.
- [226] Neels JG, van den Berg BMM, Lookene A, Olivecrona G, Pannekoek H, van Zonneveld A-J. The Second and Fourth Cluster of Class A Cysteine-rich Repeats of the Low Density Lipoprotein Receptor-related Protein Share Ligand-binding Properties. *J Biol Chem* 1999;274:31305–11.
- [227] Lazic A, Dolmer K, Strickland DK, Gettins PGW. Dissection of RAP-LRP interactions: Binding of RAP and RAP fragments to complement-like repeats 7 and 8 from ligand binding cluster II of LRP. *Arch Biochem Biophys* 2006;450:167–75.
- [228] Simonovic M, Dolmer K, Huang W, Strickland DK, Volz K, Gettins PGW. Calcium coordination and pH dependence of the calcium affinity of ligand-binding repeat CR7 from the LRP. Comparison with related domains from the LRP and the LDL receptor. *Biochemistry* 2001;40:15127–34.
- [229] Herz J, Hamann U, Rogne S, Myklebost O, Gausepohl H, Stanley KK. Surface location and high affinity for calcium of a 500-kd liver membrane protein closely related to the LDL-receptor suggest a physiological role as lipoprotein receptor. *EMBO J* 1988;7:4119–27.
- [230] Mahley RW, Huang Y. Atherogenic remnant lipoproteins: Role for proteoglycans in trapping, transferring, and internalizing. *J Clin Invest* 2007;117:94–8.
- [231] Zilberberg A, Yaniv A, Gazit A. The Low Density Lipoprotein Receptor-1, LRP1, Interacts with the Human Frizzled-1 (HFz1) and Down-regulates the Canonical Wnt Signaling Pathway. *J Biol Chem* 2004;279:17535–42.
- [232] Emonard H, Bellon G, De Diesbach P, Mettlen M, Hornebeck W, Courtoy PJ. Regulation of matrix metalloproteinase (MMP) activity by the low-density lipoprotein receptor-related protein (LRP). A new function for an “old friend.” *Biochimie* 2005;87:369–76.
- [233] Etique N, Verzeaux L, Dedieu S, Emonard H. Lrp-1: A checkpoint for the extracellular matrix proteolysis. *Biomed Res Int* 2013;2013.
- [234] Yamamoto K, Owen K, Parker AE, Scilabra SD, Dudhia J, Strickland DK, et al. Low density lipoprotein receptor-related protein 1 (LRP1)-mediated endocytic clearance of a disintegrin and metalloproteinase with thrombospondin motifs-4 (ADAMTS-4): Functional differences of non-catalytic domains of ADAMTS-4 and ADAMTS-5 in LRP1 binding. *J Biol Chem* 2014;289:6462–74.
- [235] Van den Steen PE, Van Aelst I, Hvidberg V, Piccard H, Fiten P, Jacobsen C, et al. The Hemopexin and O<sup>-</sup>-Glycosylated Domains Tune Gelatinase B/MMP-9 Bioavailability via Inhibition and Binding to Cargo Receptors. *J Biol Chem* 2006;281:18626–37.
- [236] Barmina OY, Walling HW, Fiocco GJ, Freije JMP, López-Otín C, Jeffrey JJ, et al. Collagenase-3 binds to a specific receptor and requires the low density lipoprotein receptor-related protein for internalization. *J Biol Chem* 1999;274:30087–93.
- [237] Yang Z, Strickland DK, Bornstein P. Extracellular Matrix Metalloproteinase 2 Levels are Regulated by the Low Density Lipoprotein-related Scavenger Receptor and Thrombospondin 2. *J Biol Chem* 2001;276:8403–8.
- [238] Scilabra SD, Troeberg L, Yamamoto K, Emonard H, Thøgersen I, Enghild JJ, et al. Differential regulation of extracellular tissue inhibitor of metalloproteinases-3 levels by cell membrane-bound and shed low density lipoprotein receptor-related protein 1. *J Biol Chem* 2013;288:332–42.
- [239] Brandan E, Retamal C, Cabello-Verrugio C, Marzolo M-P. The low density lipoprotein receptor-related protein functions as an endocytic receptor for decorin. *J Biol Chem* 2006;281:31562–71.
- [240] Flannery CR, Zeng W, Corcoran C, Collins-Racie LA, Chockalingam PS, Hebert T, et al. Autocatalytic cleavage of ADAMTS-4 (aggrecanase-1) reveals multiple glycosaminoglycan-binding sites. *J Biol Chem* 2002;277:42775–80.



- [241] Zeng W, Corcoran C, Collins-Racie LA, LaVallie ER, Morris EA, Flannery CR. Glycosaminoglycan-binding properties and aggrecanase activities of truncated ADAMTSs: Comparative analyses with ADAMTS-5, -9, -16 and -18. *Biochim Biophys Acta* 2006;1760:517–24.
- [242] Ruiz J, Kouivaskaia D, Migliorini M, Robinson S, Saenko EL, Gorlatova N, et al. The apoE isoform binding properties of the VLDL receptor reveal marked differences from LRP and the LDL receptor. *J Lipid Res* 2005;46:1721–31.
- [243] Futamura M, Dhanasekaran P, Handa T, Phillips MC, Lund-katz S, Saito H. Two-step Mechanism of Binding of Apolipoprotein E to Heparin. *J Biol Chem* 2005;280:5414–22.
- [244] Salicioni AM, Mizelle KS, Loukinova E, Mikhailenko I, Strickland DK, Gonias SL. The low density lipoprotein receptor-related protein mediates fibronectin catabolism and inhibits fibronectin accumulation on cell surfaces. *J Biol Chem* 2002;277:16160–6.
- [245] Vogel S, Arnoldini S, Möller S, Schnabelrauch M, Hempel U. Sulfated hyaluronan alters fibronectin matrix assembly and promotes osteogenic differentiation of human bone marrow stromal cells. *Sci Rep* 2016;6:36418.
- [246] Yamamoto K, Okano H, Miyagawa W, Visse R, Shitomi Y, Santamaria S, et al. MMP-13 is constitutively produced in human chondrocytes and co-endocytosed with ADAMTS-5 and TIMP-3 by the endocytic receptor LRP1. *Matrix Biol* 2016:1–17.
- [247] Munesh S, Yoshitomi Y, Kusano Y, Koyama Y, Nishiyama A, Nakanishi H, et al. A novel function of syndecan-2, suppression of matrix metalloproteinase-2 activation, which causes suppression of metastasis. *J Biol Chem* 2007;282:28164–74.
- [248] Liu Q, Huang SS, Huang JS. Function of the Type V Transforming Growth Factor beta Receptor in Transforming Growth Factor beta-induced Growth Inhibition of Mink Lung Epithelial Cells. *J Biol Chem* 1997;272:18891–5.
- [249] Ling TY, Chen CL, Huang YH, Liu IH, Huang SS, Huang JS. Identification and characterization of the acidic pH binding sites for growth regulatory ligands of low density lipoprotein receptor-related protein-1. *J Biol Chem* 2004;279:38736–48.
- [250] Lyon M, Rushton G, Gallagher JT. The Interaction of the Transforming Growth Factor-betas with Heparin / Heparan Sulfate Is Isoform-specific. *J Biol Chem* 1997;272:18000–6.
- [251] McCaffrey TA, Falcone DJ, Du B. Transforming growth factor- $\beta$ 1 is a heparin-binding protein: Identification of putative heparin-binding regions and isolation of heparins with varying affinity for TGF- $\beta$ 1. *J Cell Physiol* 1992;152:430–40.
- [252] Lee J, Wee S, Gunaratne J, Chua RJE, Smith RAA, Ling L, et al. Structural determinants of heparin – transforming growth factor- $\beta$  1 interactions and their effects on signaling. *Glycobiology* 2015;25:1491–504.
- [253] Hintze V, Miron A, Moeller S, Schnabelrauch M, Wiesmann H-PP, Worch H, et al. Sulfated hyaluronan and chondroitin sulfate derivatives interact differently with human transforming growth factor- $\beta$ 1 (TGF- $\beta$ 1). *Acta Biomater* 2012;8:2144–52.
- [254] Godyna S, Liau G, Popa I, Stefansson S, Argraves WS. Identification of the low density lipoprotein receptor-related protein (LRP) as an endocytic receptor for thrombospondin-1. *J Cell Biol* 1995;129:1403–10.
- [255] Herndon ME, Stipp CS, Lander AD. Interactions of neural glycosaminoglycans and proteoglycans with protein ligands: Assessment of selectivity, heterogeneity and the participation of core proteins in binding. *Glycobiology* 1999;9:143–55.
- [256] Wang S, Herndon ME, Ranganathan S, Godyna S, Lawler J, Argraves WS, et al. Internalization but not binding of thrombospondin-1 to low density lipoprotein receptor-related protein-1 requires heparan sulfate proteoglycans. *J Cell Biochem* 2004;91:766–76.
- [257] Ramdin L, Perks B, Sheron N, Shute JK. Regulation of interleukin-8 binding and function by heparin and alpha2- macroglobulin. *Clin Exp Allergy* 1998;28:616–24.
- [258] Manning HB, Nickdel MB, Yamamoto K, Lagarto JL, Kelly DJ, Talbot CB, et al. Detection of cartilage matrix degradation by auto fluorescence lifetime. *Matrix Biol* 2013;32:32–8.
- [259] Adams RH, Alitalo K. Molecular regulation of angiogenesis and lymphangiogenesis. *Nat Rev Mol Cell Biol* 2007;8:464–78.
- [260] Swift MR, Weinstein BM. Arterial – Venous Specification During Development. *Circ Res* 2009;104:573–9.

- [261] Slaughter B V, Fisher OZ. Hydrogels in Regenerative Medicine. *Adv Mater* 2009;21:3307–29.
- [262] Dejana E. Endothelial cell-cell junctions: happy together. *Nat Rev Mol Cell Biol* 2004;5:261–70.
- [263] Risau W. Mechanisms of angiogenesis. *Nature* 1997;386:671–4.
- [264] Hanahan D. Signaling Vascular Morphogenesis and Maintenance. *Science* 1997;277:48–50.
- [265] Moyon D, Pardanaud L, Yuan L, Bréant C, Eichmann A. Plasticity of endothelial cells during arterial-venous differentiation in the avian embryo. *Development* 2001;128:3359–70.
- [266] Villa N, Walker L, Lindsell CE, Gasson J, Iruela-Arispe ML, Weinmaster G. Vascular expression of Notch pathway receptors and ligands is restricted to arterial vessels. *Mech Dev* 2001;108:161–4.
- [267] Wang HU, Chen ZF, Anderson DJ. Molecular distinction and angiogenic interaction between embryonic arteries and veins revealed by ephrin-B2 and its receptor Eph-B4. *Cell* 1998;93:741–53.
- [268] Belotti D, Foglieni C, Resovi A, Giavazzi R, Taraboletti G. Targeting angiogenesis with compounds from the extracellular matrix. *Int J Biochem Cell Biol* 2011;43:1674–85.
- [269] Neve A, Cantatore FP, Maruotti N, Corrado A, Ribatti D. Extracellular Matrix Modulates Angiogenesis in Physiological and Pathological Conditions. *Biomed Res Int* 2014;2014:1–10.
- [270] Martino MM, Brkic S, Bovo E, Burger M, Schaefer DJ, Wolff T, et al. Extracellular Matrix and Growth Factor Engineering for Controlled Angiogenesis in Regenerative Medicine. *Front Bioeng Biotechnol* 2015;3:1–8.
- [271] Kusumbe AP, Ramasamy SK, Adams RH. Coupling of angiogenesis and osteogenesis by a specific vessel subtype in bone. *Nature* 2014;507:323–8.
- [272] Chim SM, Tickner J, Chow ST, Kuek V, Guo B, Zhang G, et al. Angiogenic factors in bone local environment. *Cytokine Growth Factor Rev* 2013;24:297–310.
- [273] Kiselyov A, Balakin K V, Tkachenko SE. VEGF/VEGFR signalling as a target for inhibiting angiogenesis. *Expert Opin Investig Drugs* 2007;16:83–107.
- [274] Ferrara N, Gerber H, LeCouter J. The biology of VEGF and its receptors. *Nat Med* 2003;9:669–76.
- [275] Shibuya M. Differential roles of vascular endothelial growth factor receptor-1 and receptor-2 in angiogenesis. *J Biochem Mol Biol* 2006;39:469–78.
- [276] Lodomery MR, Harper SJ, Bates DO. Alternative splicing in angiogenesis: The vascular endothelial growth factor paradigm. *Cancer Lett* 2007;249:133–42.
- [277] Hilmi C, Guyot M, Pagès G. VEGF spliced variants: Possible role of anti-angiogenesis therapy. *J Nucleic Acids* 2012;2012.
- [278] Danastas K, Combes V, Lindsay LA, Grau GER, Thompson MB, Murphy CR. VEGF111: New insights in tissue invasion. *Front Physiol* 2015;6:1–5.
- [279] Park JE, Keller G-A, Ferrara N. The vascular endothelial growth factor (VEGF) isoforms: differential deposition into the subepithelial extracellular matrix and bioactivity of extracellular matrix-bound VEGF. *Mol Biol Cell* 1993;4:1317–26.
- [280] Houck KA, Leung DW, Rowland AM, Winer J, Ferrara N. Dual regulation of vascular endothelial growth factor bioavailability by genetic and proteolytic mechanisms. *J Biol Chem* 1992;267:26031–7.
- [281] Shibuya M. VEGF-VEGFR signals in health and disease. *Biomol Ther* 2014;22:1–9.
- [282] Bellomo D, Headrick JP, Silins GU, Paterson CA, Thomas PS, Gartside M, et al. Mice Lacking the Vascular Endothelial Growth Factor-B Gene (*Vegfb*) Have Smaller Hearts, Dysfunctional Coronary Vasculature, and Impaired Recovery From Cardiac Ischemia. *Circ Res* 2000;86:e29–35.
- [283] Bry M, Kivelä R, Holopainen T, Anisimov A, Tammela T, Soronen J, et al. Vascular endothelial growth factor-B acts as a coronary growth factor in transgenic rats without inducing angiogenesis, vascular leak, or inflammation. *Circulation* 2010;122:1725–33.
- [284] Alitalo K, Carmeliet P. Molecular mechanisms of lymphangiogenesis in health and disease. *Cancer Cell* 2002;1:219–27.
- [285] Ferrara N, Carver-Moore K, Chen H, Dowd M, Lu L, O’Shea KS, et al. Heterozygous embryonic lethality induced by targeted inactivation of the VEGF gene. *Nature* 1996;380:439–42.

- [286] Carmeliet P, Ferreira V, Breier G, Pollefeyt S, Kieckens L, Gertsenstein M, et al. Abnormal blood vessel development and lethality in embryos lacking a single VEGF allele. *Nature* 1996;380:435–9.
- [287] Terman BI, Dougher-vermazan M, Carrion ME, Dimitrov D, Armellino DC, Gospodarowicz D, et al. Identification of the KDR tyrosine kinase as a receptor for vascular endothelial cell growth factor. *Biochem Biophys Res Commun* 1992;187.
- [288] Waltenberger J, Claesson-Welsh L, Siegbahn A, Shibuya M, Heldin CH. Different signal transduction properties of KDR and Flt1, two receptors for vascular endothelial growth factor. *J Biol Chem* 1994;269:26988–95.
- [289] Shalaby F, Rossant J, Yamaguchi TP, Gertsenstein M, Wu X-F, Vreitman ML, et al. Failure of blood-island formation and vasculogenesis in Flk-1-deficient mice. *Nature* 1995;376:62–6.
- [290] Shibuya M. Vascular endothelial growth factor (VEGF)-Receptor2: its biological functions, major signaling pathway, and specific ligand VEGF-E. *Endothel J Endothel Cell Res* 2006;13:63–9.
- [291] Matsumoto T, Bohman S, Dixelius J, Berge T, Dimberg A, Magnusson P, et al. VEGF receptor-2 Y951 signaling and a role for the adapter molecule TSAd in tumor angiogenesis. *EMBO J* 2005;24:2342–53.
- [292] Shibuya M, Claesson-Welsh L. Signal transduction by VEGF receptors in regulation of angiogenesis and lymphangiogenesis. *Exp Cell Res* 2006;312:549–60.
- [293] Soker S, Fidder H, Neufeld G, Klagsbrun M. Characterization of novel vascular endothelial growth factor (VEGF) receptors on tumor cells that bind VEGF165 via its exon 7- encoded domain. *J Biol Chem* 1996;271:5761–7.
- [294] Hurwitz H, Fehrenbacher L, Novotny W, Cartwright T, Hainsworth J, Heim W, et al. Bevacizumab plus irinotecan, fluorouracil, and leucovorin for metastatic colorectal cancer. *N Engl J Med* 2004;350:2335–42.
- [295] Qi JH, Ebrahim Q, Ali M, Cutler A, Bell B, Prayson N, et al. Tissue inhibitor of metalloproteinases-3 peptides inhibit angiogenesis and choroidal neovascularization in mice. *PLoS One* 2013;8:e55667.
- [296] Ebrahim Q, Qi JH, Sugimoto M, Ali M, Sears JE, Cutler A, et al. Increased neovascularization in mice lacking tissue inhibitor of metalloproteinases-3. *Investig Ophthalmol Vis Sci* 2011;52:6117–23.
- [297] Bates DO, Pritchard Jones RO. The Role of Vascular Endothelial Growth Factor in Wound Healing. *Int J Low Extrem Wounds* 2003;2:107–20.
- [298] Krilleke D, Ng Y-SE, Shima DT. The heparin-binding domain confers diverse functions of VEGF-A in development and disease: a structure-function study. *Biochem Soc Trans* 2009;37:1201–6.
- [299] Vempati P, Popel AS, Mac Gabhann F. Formation of VEGF isoform-specific spatial distributions governing angiogenesis: computational analysis. *BMC Syst Biol* 2011;5:59.
- [300] Cochran S, Li C, Fairweather JK, Kett WC, Coombe DR, Ferro V. Probing the interactions of phosphosulfomannans with angiogenic growth factors by surface plasmon resonance. *J Med Chem* 2003;46:4601–8.
- [301] Chung AS, Ferrara N. Developmental and pathological angiogenesis. *Annu Rev Cell Dev Biol* 2011;27:563–84.
- [302] Gitay-Goren H, Cohen T, Tessler S, Soker S, Gengrinovitch S, Rockwell P, et al. Selective Binding of VEGF121 to One of the Three Vascular Endothelial Growth Factor Receptors of Vascular Endothelial Cells. *J Biol Chem* 1996;271:5519–23.
- [303] Jonca F, Ortega N, Gleizes PE, Bertrand N, Plouet J. Cell release of bioactive fibroblast growth factor 2 by exon 6- encoded sequence of vascular endothelial growth factor. *J Biol Chem* 1997;272:24203–9.
- [304] Gitay-Goren H, Soker S, Vlodaysky I, Neufeld G. The binding of vascular endothelial growth factor to its receptors is dependent on cell surface-associated heparin- like molecules. *J Biol Chem* 1992;267:6093–8.
- [305] Vander Kooi CW, Jusino MA, Perman B, Neau DB, Bellamy HD, Leahy DJ. Structural basis for ligand and heparin binding to neuropilin B domains. *Proc Natl Acad Sci U S A* 2007;104:6152–7.

- [306] Gengrinovitch S, Berman B, David G, Witte L, Neufeld G, Ron D. Glypican-1 Is a VEGF165 Binding Proteoglycan That Acts as an Extracellular Chaperone for VEGF 165. *J Biol Chem* 1999;274:10816–22.
- [307] Robinson CJ, Stringer SE. The splice variants of vascular endothelial growth factor (VEGF) and their receptors. *J Cell Sci* 2001;114:853–65.
- [308] Ashikari-Hada S, Habuchi H, Kariya Y, Kimata K. Heparin Regulates Vascular Endothelial Growth Factor 165 -dependent Mitogenic Activity, Tube Formation, and Its Receptor Phosphorylation of Human Endothelial Cells. *J Biol Chem* 2005;280:31508–15.
- [309] Tessler S, Rockwell P, Hicklin D, Cohen T, Levi BZ, Witte L, et al. Heparin modulates the interaction of VEGF165 with soluble and cell associated flk-1 receptors. *J Biol Chem* 1994;269:12456–61.
- [310] Terman B, Khandke L, MD-V, Maglione D, Lassam NJ, Gospodarowicz D, et al. VEGF receptor subtypes KDR and FLT1 show different sensitivities to heparin and placenta growth factor. *Growth Factors* 1994;11:187–95.
- [311] Cohen T, Gitay-Goren H, Sharon R, Shibuya M, Halaban R, Levi B, et al. VEGF121, a vascular endothelial growth factor (VEGF) isoform lacking heparin binding ability, requires cell-surface heparan sulfates for efficient binding to the VEGF receptors of human melanoma cells. *J Biol Chem* 1995;270:11322–6.
- [312] Brydone AS, Meek D, Maclaine S. Bone grafting, orthopaedic biomaterials, and the clinical need for bone engineering. *Proc Inst Mech Eng H* 2010;224:1329–43.
- [313] Shevchenko R V, James SL, James SE. A review of tissue-engineered skin bioconstructs available for skin reconstruction. *J R Soc Interface* 2010;7:229–58.
- [314] Papini R. Management of burn injuries of various depths. *BMJ* 2004;329:158–60.
- [315] Salbach-Hirsch J, Samsonov SA, Hintze V, Hofbauer C, Picke A, Rauner M, et al. Structural and functional insights into sclerostin-glycosaminoglycan interactions in bone. *Biomaterials* 2015;67:335–45.
- [R316] Rother S, Salbach-Hirsch J, Möller S, Seemann T, Schnabelrauch M, Hofbauer LC, et al. Bioinspired Collagen/Glycosaminoglycan-based Cellular Microenvironments for Tuning Osteoclastogenesis. *ACS Appl Mater Interfaces* 2015;7:23787–97.
- [317] O'Brien FJ. Biomaterials & scaffolds for tissue engineering. *Mater Today* 2011;14:88–95.
- [318] Williams DF. On the mechanisms of biocompatibility. *Biomaterials* 2008;29:2941–53.
- [319] Chan BP, Leong KW. Scaffolding in tissue engineering: General approaches and tissue-specific considerations. *Eur Spine J* 2008;17:467–79.
- [320] Engler AJ, Sen S, Sweeney HL, Discher DE. Matrix Elasticity Directs Stem Cell Lineage Specification. *Cell* 2006;126:677–89.
- [321] Babensee JE, Anderson JM, McIntire LV, Mikos AG. Host response to tissue engineered devices. *Drug Del Rev* 1998;33:111–39.
- [322] Hutmacher DWD. Scaffolds in tissue engineering bone and cartilage. *Biomaterials* 2000;21:2529–43.
- [323] Kim Y, Ko H, Kwon IK, Shin K. Extracellular Matrix Revisited: Roles in Tissue Engineering. *Int Neurourol J* 2016;Supplement:S23–9.
- [324] Williams DF. On the nature of biomaterials. *Biomaterials* 2009;30:5897–909.
- [325] Hollister SJ. Scaffold engineering: a bridge to where? *Biofabrication* 2009;1:12001.
- [326] Dai Z, Ronholm J, Tian Y, Sethi B, Cao X. Sterilization techniques for biodegradable scaffolds in tissue engineering applications. *J Tissue Eng* 2016;7:1–13.
- [327] Burdick JA, Prestwich GD. Hyaluronic Acid Hydrogels for Biomedical Applications. *Adv Mater* 2011;23:H41–56.
- [328] Yue K, Trujillo-de Santiago G, Alvarez MM, Tamayol A, Annabi N, Khademhosseini A. Synthesis, properties, and biomedical applications of gelatin methacryloyl (GelMA) hydrogels. *Biomaterials* 2015;73:254–71.
- [329] Chattopadhyay S, Raines RT. Review collagen-based biomaterials for wound healing. *Biopolymers* 2014;101:821–33.
- [330] Lima RS, Peruzzo DC, Napimoga MH, Saba-Chujfi E, Dos Santos-Pereira SA, Martinez EF. Evaluation of the biological behavior of mucograft® in human gingival fibroblasts: An in vitro study. *Braz Dent J* 2015;26:602–6.

- [331] Renner JN, Cherry KM, Su RSC, Liu JC. Characterization of resilin-based materials for tissue engineering applications. *Biomacromolecules* 2012;13:3678–85.
- [332] Wang Y, Kim HJ, Vunjak-Novakovic G, Kaplan DL. Stem cell-based tissue engineering with silk biomaterials. *Biomaterials* 2006;27:6064–82.
- [333] Damadzadeh B, Jabari H, Skrifvars M, Airola K, Moritz N, Vallittu PK. Effect of ceramic filler content on the mechanical and thermal behaviour of poly-l-lactic acid and poly-l-lactic-co-glycolic acid composites for medical applications. *J Mater Sci Mater Med* 2010;21:2523–31.
- [334] Friess W, Schlapp M. Sterilization of gentamicin containing collagen/PLGA microparticle composites. *Eur J Pharm Biopharm* 2006;63:176–87.
- [335] Kim S-S, Sun Park M, Jeon O, Yong Choi C, Kim B-S. Poly(lactide-co-glycolide)/hydroxyapatite composite scaffolds for bone tissue engineering. *Biomaterials* 2006;27:1399–409.
- [336] Bracaglia LG, Fisher JP. Extracellular Matrix-Based Biohybrid Materials for Engineering Compliant, Matrix-Dense Tissues. *Adv Healthc Mater* 2015;4:2475–87.
- [337] Lasprilla AJR, Martinez GAR, Lunelli BH, Jardini AL, Maciel R. Poly-lactic acid synthesis for application in biomedical devices — A review. *Biotechnol Adv* 2012;30:321–8.
- [338] Polat T, Wong CH. Anomeric reactivity-based one-pot synthesis of heparin-like oligosaccharides. *J Am Chem Soc* 2007;129:12795–800.
- [339] Seeberger PH. The logic of automated glycan assembly. *Acc Chem Res* 2015;48:1450–63.
- [340] Maruyama T, Toida T, Imanari T. Conformational changes and anticoagulant activity of chondroitin sulfate following its O -sulfonation 1. *Carbohydr Res* 1998;306:35–43.
- [341] Walenga JM, Jeske WP, Samama MM, Frapaise FX, Bick RL, Fareed J. Fondaparinux: a synthetic heparin pentasaccharide as a new antithrombotic agent. *Expert Opin Investig Drugs* 2002;11:397–407.
- [342] Zulueta MML, Lin SY, Hu YP, Hung SC. Synthetic heparin and heparan sulfate oligosaccharides and their protein interactions. *Curr Opin Chem Biol* 2013;17:1023–9.
- [343] Grombe R, Gouzy MF, Maitz MF, Freudenberg U, Zschoche S, Simon F, et al. Sulfated glycopolymer thin films - Preparation, characterization, and biological activity. *Macromol Biosci* 2007;7:195–200.
- [344] Neville GA, Rochon P, Rej RN, Perlin AS. Characterization and differentiation of some complex dextran sulfate preparations of medicinal interest. *J Pharm Sci* 1991;80:239–44.
- [345] Drozd NN, Logvinova YS, Torlopov MA, Udoratina E V. Effect of Sulfation and Molecular Weight on Anticoagulant Activity of Dextran. *Bull Exp Biol Med* 2017;162:462–5.
- [346] Berger J, Reist M, Mayer JM, Felt O, Peppas NA, Gurny R. Structure and interactions in covalently and ionically crosslinked chitosan hydrogels for biomedical applications. *Eur J Pharm Biopharm* 2004;57:19–34.
- [347] Salbach J, Rachner TD, Rauner M, Hempel U, Anderegg U, Franz S, et al. Regenerative potential of glycosaminoglycans for skin and bone. *J Mol Med* 2012;90:625–35.
- [348] Magnani A, Albanese A, Lamponi S, Barbucci R. Blood-interaction performance of differently sulphated hyaluronic acids. *Thromb Res* 1996;81:383–95.
- [349] Magnani A, Lamponi S, Rappuoli R, Barbucci R. Sulphated Hyaluronic Acids: a Chemical and Biological Characterisation. *Polym Int* 1998;46:225–40.
- [350] Hempel U, Hintze V, Möller S, Schnabelrauch M, Scharnweber D, Dieter P. Artificial extracellular matrices composed of collagen i and sulfated hyaluronan with adsorbed transforming growth factor  $\beta$ 1 promote collagen synthesis of human mesenchymal stromal cells. *Acta Biomater* 2012;8:659–66.
- [351] Van der Smissen A, Samsonov S, Hintze V, Scharnweber D, Moeller S, Schnabelrauch M, et al. Artificial extracellular matrix composed of collagen I and highly sulfated hyaluronan interferes with TGF $\beta$ (1) signaling and prevents TGF $\beta$ (1)-induced myofibroblast differentiation. *Acta Biomater* 2013;9:7775–86.
- [352] Hempel U, Möller S, Noack C, Hintze V, Scharnweber D, Schnabelrauch M, et al. Sulfated hyaluronan/collagen I matrices enhance the osteogenic differentiation of human mesenchymal stromal cells in vitro even in the absence of dexamethasone. *Acta Biomater* 2012;8:4064–72.

- [353] Kliemt S, Lange C, Otto W, Hintze V, Möller S, von Bergen M, et al. Sulfated Hyaluronan Containing Collagen Matrices Enhance Cell-Matrix-Interaction, Endocytosis, and Osteogenic Differentiation of Human Mesenchymal Stromal Cells. *J Proteome Res* 2013;12:378–89.
- [354] Salbach-Hirsch J, Ziegler N, Thiele S, Moeller S, Schnabelrauch M, Hintze V, et al. Sulfated glycosaminoglycans support osteoblast functions and concurrently suppress osteoclasts. *J Cell Biochem* 2014;115:1101–11.
- [355] Salbach J, Kliemt S, Rauner M, Rachner TD, Goettsch C, Kalkhof S, et al. The effect of the degree of sulfation of glycosaminoglycans on osteoclast function and signaling pathways. *Biomaterials* 2012;33:8418–29.
- [356] Tsourdi E, Salbach-hirsch J, Rauner M, Rachner TD, Moller S, Schnabelrauch M, et al. Glycosaminoglycans and their sulfate derivatives differentially regulate the viability and gene expression of osteocyte-like cell lines. *J Bioact Compat Polym* 2014;29:474–85.
- [357] Kajahn J, Franz S, Rueckert E, Forstreuter I, Hintze V, Moeller S, et al. Artificial extracellular matrices composed of collagen I and high sulfated hyaluronan modulate monocyte to macrophage differentiation under conditions of sterile inflammation. *Biomatter* 2012;2:226–36.
- [358] Franz S, Allenstein F, Kajahn J, Forstreuter I, Hintze V, Möller S, et al. Artificial extracellular matrices composed of collagen i and high-sulfated hyaluronan promote phenotypic and functional modulation of human pro-inflammatory M1 macrophages. *Acta Biomater* 2013;9:5621–9.
- [359R] Miron A, Rother S, Huebner L, Hempel U, Käßler I, Moeller S, et al. Sulfated Hyaluronan Influences the Formation of Artificial Extracellular Matrices and the Adhesion of Osteogenic Cells. *Macromol Biosci* 2014;14:1783–94.
- [360] Tømmeraas K, Melander C. Kinetics of hyaluronan hydrolysis in acidic solution at various pH values. *Biomacromolecules* 2008;9:1535–40.
- [361] Bienkowski MJ, Conrad HE. Structural characterization of the oligosaccharides formed by depolymerization of heparin with nitrous acid. *J Biol Chem* 1985;260:356–65.
- [362] Hassan MS, Mileva MM, Dweck HS, Rosenfeld L. Nitric oxide products degrade chondroitin sulfates. *Nitric Oxide* 1998;2:360–5.
- [363] Prieto JG, Pulido MM, Zapico J, Molina AJ, Gimeno M, Coronel P, et al. Comparative study of hyaluronic derivatives: Rheological behaviour, mechanical and chemical degradation. *Int J Biol Macromol* 2005;35:63–9.
- [364] Lowry KM, Beavers EM. Thermal stability of sodium hyaluronate in aqueous solution. *J Biomed Mater Res* 1994;28:1239–44.
- [365] Becher J, Möller S, Schnabelrauch M. Phase transfer-catalyzed synthesis of highly acrylated hyaluronan. *Carbohydr Polym* 2013;93:438–41.
- [366] Duan J, Kasper DL. Oxidative depolymerization of polysaccharides by reactive oxygen/nitrogen species. *Glycobiology* 2011;21:401–9.
- [367] Xiao Z, Zhao W, Yang B, Zhang Z, Guan H, Linhardt RJ. Heparinase 1 selectivity for the 3,6-di-O-sulfo-2-deoxy-2-sulfamido- $\alpha$ -D-glucopyranose (1,4) 2-O-sulfo- $\alpha$ -L-idopyranosyluronic acid (GlcNS3S6S-IdoA2S) linkages. *Glycobiology* 2011;21:13–22.
- [368] Lemmnitzer K, Schiller J, Becher J, Möller S, Schnabelrauch M. Improvement of the digestibility of sulfated hyaluronans by bovine testicular hyaluronidase: A UV spectroscopic and mass spectrometric study. *Biomed Res Int* 2014;2014.
- [369] Schiller J, Becher J, Möller S, Nimptsch K, Riemer T, Schnabelrauch M. Synthesis and Characterization of Chemically Modified Hyaluronan and Chondroitin Sulfate. *Mini Rev Org Chem* 2010;7:290–9.
- [370] Casu B, Naggi A, Torri G. Chemical derivatization as a strategy to study structure-activity relationships of glycosaminoglycans. *Semin Thromb Hemost* 2002;28:335–42.
- [371] Barbucci R, Leone G, Chiumiento A, Di Cocco ME, D’Orazio G, Gianferri R, et al. Low- and high-resolution nuclear magnetic resonance (NMR) characterisation of hyaluronan-based native and sulfated hydrogels. *Carbohydr Res* 2006;341:1848–58.
- [372] Matsuo M, Takano R, Kamei-Hayashi K, Hara S. A novel regioselective desulfation of polysaccharide sulfates: specific 6-O-desulfation with N,O-bis(trimethylsilyl)acetamide. *Carbohydr Res* 1993;241:209–15.

- [373] Du Y, Taga A, Suzuki S, Liu W, Honda S. Effect of structure modification of chondroitin sulfate C on its enantioselectivity to basic drugs in capillary electrophoresis. *J Chromatogr A* 2002;947:287–99.
- [374] Crescenzi V, Francescangeli A, Renier D, Bellini D. New cross-linked and sulfated derivatives of partially deacetylated hyaluronan: Synthesis and preliminary characterization. *Biopolymers* 2002;64:86–94.
- [375] Babasola O, Rees-Milton KJ, Bebe S, Wang J, Anastassiades TP. Chemically modified N-acetylated hyaluronan fragments modulate proinflammatory cytokine production by stimulated human macrophages. *J Biol Chem* 2014;289:24779–91.
- [376] Lin F, Lian G, Zhou Y. Synthesis of Fondaparinux: Modular synthesis investigation for heparin synthesis. *Carbohydr Res* 2013;371:32–9.
- [377] Werz DB, Ranzinger R, Herget S, Adibekian A, von der Lieth C-W, Seeberger PH. Exploring the structural diversity of mammalian carbohydrates (“glycospace”) by statistical databank analysis. *ACS Chem Biol* 2007;2:685–91.
- [378] Chang CH, Lico LS, Huang TY, Lin SY, Chang CL, Arco SD, et al. Synthesis of the heparin-based anticoagulant drug fondaparinux. *Angew Chemie - Int Ed* 2014;53:9876–9.
- [379] Zhu J, Marchant RE. Design properties of hydrogel tissue-engineering scaffolds. *Expert Rev Med Devices* 2011;8:607–26.
- [380] Prè ED, Conti G, Sbarbati A. Hyaluronic Acid (HA) Scaffolds and Multipotent Stromal Cells (MSCs) in Regenerative Medicine. *Stem Cell Rev Reports* 2016.
- [381] Tsurkan M V., Chwalek K, Prokoph S, Zieris A, Levental KR, Freudenberg U, et al. Defined polymer-peptide conjugates to form cell-instructive starpeg-heparin matrices in situ. *Adv Mater* 2013;25:2606–10.
- [382] Loth T, Hennig R, Kascholke C, Hötzel R, Hacker MC. Reactive and stimuli-responsive maleic anhydride containing macromers - Multi-functional cross-linkers and building blocks for hydrogel fabrication. *React Funct Polym* 2013;73:1480–92.
- [383] DeForest CA, Polizzotti BD, Anseth KS. Sequential click reactions for synthesizing and patterning three-dimensional cell microenvironments. *Nat Mater* 2009;8:659–64.
- [384] Burdick JA, Chung C, Jia X, Randolph MA, Langer R. Controlled Degradation and Mechanical Behavior of Photopolymerized Hyaluronic Acid Networks. *Biomacromolecules* 2005;6:386–91.
- [385] Möller S, Weisser J, Bischoff S, Schnabelrauch M. Dextran and hyaluronan methacrylate based hydrogels as matrices for soft tissue reconstruction. *Biomol Eng* 2007;24:496–504.
- [386] Shu XZ, Liu Y, Luo Y, Roberts MC, Prestwich GD. Disulfide cross-linked hyaluronan hydrogels. *Biomacromolecules* 2002;3:1304–11.
- [387] Creuzet C, Kadi S, Rinaudo M, Auzély-Velty R. New associative systems based on alkylated hyaluronic acid. Synthesis and aqueous solution properties. *Polymer* 2006;47:2706–13.
- [388] Qin X-H, Gruber P, Markovic M, Plochberger B, Klotzsch E, Stampfl J, et al. Enzymatic synthesis of hyaluronic acid vinyl esters for two-photon microfabrication of biocompatible and biodegradable hydrogel constructs. *Polym Chem* 2014;5:6523–33.
- [389] Shin H, Jo S, Mikos AG. Biomimetic materials for tissue engineering. *Biomaterials* 2003;24:4353–64.
- [390] Bryant SJ, Anseth KS. Controlling the spatial distribution of ECM components in degradable PEG hydrogels for tissue engineering cartilage. *J Biomed Mater Res A* 2003;64:70–9.
- [391] Kraehenbuehl TP, Zammaretti P, Van der Vlies AJ, Schoenmakers RG, Lutolf MP, Jaconi ME, et al. Three-dimensional extracellular matrix-directed cardioprogenitor differentiation: Systematic modulation of a synthetic cell-responsive PEG-hydrogel. *Biomaterials* 2008;29:2757–66.
- [392] Hersel U, Dahmen C, Kessler H. RGD modified polymers: Biomaterials for stimulated cell adhesion and beyond. *Biomaterials* 2003;24:4385–415.
- [393] Wojtowicz AM, Shekaran A, Oest ME, Dupont KM, Templeman KL, Hutmacher DW, et al. Coating of Biomaterial Scaffolds with the Collagen-mimetic Peptide GFOGER for Bone Defect Repair. *Biomaterials* 2010;31:2574–82.
- [394] Kisiel M, Martino MM, Ventura M, Hubbell JA, Hilborn J, Ossipov DA. Improving the osteogenic potential of BMP-2 with hyaluronic acid hydrogel modified with integrin-specific fibronectin fragment. *Biomaterials* 2013;34:704–12.

- [395] Bhakta G, Rai B, Lim ZXH, Hui JH, Stein GS, van Wijnen AJ, et al. Hyaluronic acid-based hydrogels functionalized with heparin that support controlled release of bioactive BMP-2. *Biomaterials* 2012;33:6113–22.
- [396] Li L, Qian Y, Jiang C, Lv Y, Liu W, Zhong L, et al. The use of hyaluronan to regulate protein adsorption and cell infiltration in nanofibrous scaffolds. *Biomaterials* 2012;33:3428–45.
- [397] De Colli M, Massimi M, Barbeta A, Di Rosario BL, Nardecchia S, Conti Devirgiliis L, et al. A biomimetic porous hydrogel of gelatin and glycosaminoglycans cross-linked with transglutaminase and its application in the culture of hepatocytes. *Biomed Mater* 2012;7:55005.
- [398] Kim TG, Chung HJ, Park TG. Macroporous and nanofibrous hyaluronic acid/collagen hybrid scaffold fabricated by concurrent electrospinning and deposition/leaching of salt particles. *Acta Biomater* 2008;4:1611–9.
- [399] Zhu C, Fan D, Wang Y. Human-like collagen/hyaluronic acid 3D scaffolds for vascular tissue engineering. *Mater Sci Eng C* 2014;34:393–401.
- [400] Purcell BP, Kim IL, Chuo V, Guinen T, Dorsey SM, Burdick JA. Incorporation of Sulfated Hyaluronic Acid Macromers into Degradable Hydrogel Scaffolds for Sustained Molecule Delivery. *Biomater Sci* 2014;2:693–702.
- [401] Feng Q, Lin S, Zhang K, Dong C, Wu T, Huang H, et al. Sulfated hyaluronic acid hydrogels with retarded degradation and enhanced growth factor retention promote hMSC chondrogenesis and articular cartilage integrity with reduced hypertrophy. *Acta Biomater* 2017;53:329–42.
- [402] Köhling, S., Künze, G., Lemmnitzer, K., Bermudez, M., Wolber, G., Schiller, J., Huster, D., Rademann J. Chemoenzymatic synthesis of spin-labeled, sulfated tetrahyaluronan for elucidation of its complex with interleukin-10. *Chemistry* 2016;22:5563–74.
- [403] Kunze R, Rösler M, Möller S, Schnabelrauch M, Riemer T, Hempel U, et al. Sulfated hyaluronan derivatives reduce the proliferation rate of primary rat calvarial osteoblasts. *Glycoconj J* 2010;27:151–8.
- [404] Becher J, Möller S, Weiss D, Schiller J, Schnabelrauch M. Synthesis of new regioselectively sulfated hyaluronans for biomedical application. *Macromol Symp* 2010;296:446–52.
- [405] Schulz MC, Korn P, Stadlinger B, Range U, Möller S, Becher J, et al. Coating with artificial matrices from collagen and sulfated hyaluronan influences the osseointegration of dental implants. *J Mater Sci Mater Med* 2014;25:247–58.
- [406] van der Smissen A, Hintze V, Scharnweber D, Moeller S, Schnabelrauch M, Majok A, et al. Growth promoting substrates for human dermal fibroblasts provided by artificial extracellular matrices composed of collagen I and sulfated glycosaminoglycans. *Biomaterials* 2011;32:8938–46.
- [407] Hintze V, Miron A, Möller S, Schnabelrauch M, Heinemann S, Worch H, et al. Artificial extracellular matrices of collagen and sulphated hyaluronan enhance the differentiation of human mesenchymal stem cells in the presence of dexamethasone. *J Tissue Eng Regen Med* 2014;8:314–24.
- [408] Williams BR, Gelman RA, Poppke DC, Piez KA. Collagen fibril formation. Optimal in vitro conditions and preliminary kinetic results. *J Biol Chem* 1978;253:6578–85.
- [409] Satoh A, Kojima K, Koyama T, Ogawa H, Matsumoto I. Immobilization of saccharides and peptides on 96-well microtiter plates coated with methyl vinyl ether-maleic anhydride copolymer. *Anal Biochem* 1998;260:96–102.
- [410] Skarja GA, Brown AL, Ho RK, May MH, Sefton M V. The effect of a hydroxamic acid-containing polymer on active matrix metalloproteinases. *Biomaterials* 2009;30:1890–7.
- [411] Myszka DG. Improving biosensor analysis. *J Mol Recognit* 1999;12:279–84.
- [412] Junqueira LCU, Bignolas G, Brentani RR. Picrosirius staining plus polarization microscopy, a specific method for collagen detection in tissue sections. *Histochem J* 1979;11:447–55.
- [413] Terry DE, Chopra RK, Ovenden J, Anastassiades TP. Differential use of Alcian blue and toluidine blue dyes for the quantification and isolation of anionic glycoconjugates from cell cultures: application to proteoglycans and a high-molecular-weight glycoprotein synthesized by articular chondrocytes. *Anal Biochem* 2000;285:211–9.
- [414] Volpi N, Maccari F, Emilia R. Detection of submicrogram quantities of glycosaminoglycans on agarose gels by sequential staining with toluidine blue and Stains-All. *Electrophoresis* 2002;23:4060–6.



- [415] Lowry OH, Rosebrough NJ, Farr AL, Randall RJ. Protein measurement with the Folin phenol reagent. *J Biol Chem* 1951;193:265–75.
- [416] Farndale RW, Buttle DJ, Barrett AJ. Improved quantitation and discrimination of sulphated glycosaminoglycans by use of dimethylmethylene blue. *Biochim Biophys Acta* 1986;883:173–7.
- [417] Muckenschnabel I, Bernhardt G, Spruss T, Dietl B, Buschauer A. Quantitation of hyaluronidases by the Morgan-Elson reaction: Comparison of the enzyme activities in the plasma of tumor patients and healthy volunteers. *Cancer Lett* 1998;131:13–20.
- [418] Elson LA, Morgan WJ. A colorimetric method for the determination of glucosamine and chondrosamine. *Biochem J* 1933;27:1824–8.
- [419] Balazs EA, Berntsen KO, Karossa J, Swann DA. An automated method for the determination of hexosamines. *Anal Biochem* 1965;12:559–64.
- [420] van der Harst MR, Brama PAJ, van de Lest CHA, Kiers GH, DeGroot J, van Weeren PR. An integral biochemical analysis of the main constituents of articular cartilage, subchondral and trabecular bone. *Osteoarthr Cartil* 2004;12:752–61.
- [421] Volpi N, Maccari F, Titze J. Simultaneous detection of submicrogram quantities of hyaluronic acid and dermatan sulfate on agarose-gel by sequential staining with toluidine blue and Stains-All. *J Chromatogr B Anal Technol Biomed Life Sci* 2005;820:131–5.
- [422] Chang KH, Liao H-TT, Chen J-PP. Preparation and characterization of gelatin/hyaluronic acid cryogels for adipose tissue engineering: In vitro and in vivo studies. *Acta Biomater* 2013;9:9012–26.
- [423] Waltenberger J, Claesson-Welsh L, Siegbahn A, Shibuya M. Different Signal Transduction Properties of KDR and Flt1, Two Receptors for Vascular Endothelial Growth Factor. *J Biol Chem*. 1994;269:26988–95.
- [424] Favier B, Alam A, Barron P, Bonnin J, Laboudie P, Fons P, et al. Neuropilin-2 interacts with VEGFR-2 and VEGFR-3 and promotes human endothelial cell survival and migration. *Blood* 2006;108:1243–51.
- [425] Tomasz M, Palom Y. The mitomycin bioreductive antitumor agents: Cross-linking and alkylation of DNA as the molecular basis of their activity. *Pharmacol Ther* 1997;76:73–87.
- [426] Holló Z, Homolya L, Davis CW, Sarkadi B. Calcein accumulation as a fluorometric functional assay of the multidrug transporter. *Biochim Acta* 1994;1191:384–8.
- [427] Hess R, Jaeschke A, Neubert H, Hintze V, Moeller S, Schnabelrauch M, et al. Synergistic effect of defined artificial extracellular matrices and pulsed electric fields on osteogenic differentiation of human MSCs. *Biomaterials* 2012;33:8975–85.
- [428] Peschel D, Zhang K, Aggarwal N, Brendler E, Fischer S, Groth T. Synthesis of novel celluloses derivatives and investigation of their mitogenic activity in the presence and absence of FGF2. *Acta Biomater* 2010;6:2116–25.
- [429] Weiss CO, Varadhan R, Puhan MA, Vickers A, Bandeen-roche K, Boyd CM, et al. Multimorbidity and Evidence Generation. *J Gen Intern Med* 2014;29:653–60.
- [430] Lobmann R, Ambrosch A, Schultz G, Waldmann K, Schiweck S, Lehnert H. Expression of matrix-metalloproteinases and their inhibitors in the wounds of diabetic and non-diabetic patients. *Diabetologia* 2002;45:1011–6.
- [R431] Rother S, Samsonov SA, Hofmann T, Blaszkiewicz J, Köhling S, Moeller S, et al. Structural and functional insights into the interaction of sulfated glycosaminoglycans with tissue inhibitor of metalloproteinase-3 - A possible regulatory role on extracellular matrix homeostasis. *Acta Biomater* 2016;45:143–54.
- [432] Lee KB, Nam DH, Nuhn JAM, Wang J, Schneider IC, Ge X. Direct expression of active human tissue inhibitors of metalloproteinases by periplasmic secretion in *Escherichia coli*. *Microb Cell Fact* 2017;16:73.
- [433] Nagase H, Woessner JF, Nagase H, Woessner JF. Matrix Metalloproteinases. *J Biol Chem* 1999;274:21491–4.
- [434] Murphy G. Tissue inhibitors of metalloproteinases. *Genom Biol* 2011;12:233.
- [435] Satoh T, Nishiyama K, Nagahata M, Teramoto A, Abe K. The research on physiological property of functionalized hyaluronan: Interaction between sulfated hyaluronan and plasma proteins. *Polym Adv Technol* 2004;15:720–5.

- [436] Hintze V, Samsonov SA, Anselmi M, Moeller S, Becher J, Schnabelrauch M, et al. Sulfated Glycosaminoglycans Exploit the Conformational Plasticity of Bone Morphogenetic Protein-2 (BMP-2) and Alter the Interaction Profile with Its Receptor. *Biomacromolecules* 2014;15:3083–92.
- [437] Robinson DE, Buttle DJ, Short RD, McArthur SL, Steele D a., Whittle JD. Glycosaminoglycan (GAG) binding surfaces for characterizing GAG-protein interactions. *Biomaterials* 2012;33:1007–16.
- [438] Boschetti E, Girot P, Secheresse JP, Saint Blancard J. Study of the molecular interaction between lysozyme and heparin and application in affinity chromatography. *J Chromatogr* 1981;210:469–75.
- [439] Zou S, Magura CE, Hurley WL. Heparin-binding properties of lactoferrin and lysozyme. *Comp Biochem Physiol* 1992;103B:889–95.
- [440] Wetter LR, Deutsch HF. Immunological studies on egg white proteins. IV. Immunochemical and physical studies of lysozyme. *J Biol Chem* 1951;192:237–42.
- [441] Canfield RE. The Amino Acid Sequence of Egg White Lysozyme The Amino Acid Sequence of Egg White Lysozyme. *J Biol Chem* 1963;228:2698–707.
- [442] Ferrara N, Houck K, Jakeman L, Leung DW. Molecular and biological properties of the vascular endothelial growth factor family of proteins. *Endocr Rev* 1992;13:18–32.
- [443] Anderson SM, Chen TT, Iruela-arisppe ML, Segura T. The phosphorylation of vascular endothelial growth factor receptor-2 (VEGFR-2) by engineered surfaces with electrostatically or covalently immobilized VEGF. *Biomaterials* 2009;30:4618–28.
- [444] Ono K, Hattori H, Takeshita S. Structural features in heparin that interact with VEGF 165 and modulate its biological activity. *Glycobiology* 1999;9:705–11.
- [445] Wong ME, Hollinger JO, Pinero GJ. Integrated processes responsible for soft tissue healing. *Oral Surg Oral Med Oral Pathol Oral Radiol Endod* 1996;82:475–92.
- [446] Willnow TE, Orthn K, Herzsl J. Molecular dissection of ligand binding sites on the low density lipoprotein receptor-related protein. *J Biol Chem* 1994;269:15827–32.
- [R447] Rother S, Samsonov SA, Hempel U, Vogel S, Möller S, Blaszkiewicz J, et al. Sulfated hyaluronan alters the interaction profile of TIMP-3 with the endocytic receptor LRP-1 cluster II and IV and increases the extracellular TIMP-3 level of human bone marrow stromal cells. *Biomacromolecules* 2016;17:3252–61.
- [448] Godyna S, Liao G, Popa I, Stefansson S, Argraves WS. Identification of the low density lipoprotein receptor-related protein (LRP) as an endocytic receptor for thrombospondin-1. *J Cell Biol* 1995;129:1403–10.
- [449] Mikhailenko I, Krylov D, Argraves KM, Roberts DD, Liao G, Strickland DK. Cellular internalization and degradation of thrombospondin-1 is mediated by the amino-terminal heparin binding domain (HBD). High affinity interaction of dimeric HBD with the low density lipoprotein receptor-related protein. *J Biol Chem* 1997;272:6784–91.
- [450] Schmidt JR, Kliemt S, Preissler C, Moeller S, von Bergen M, Hempel U, et al. Osteoblast-released Matrix Vesicles, Regulation of Activity and Composition by Sulfated and Non-sulfated Glycosaminoglycans. *Mol Cell Proteomics* 2016;15:558–72.
- [451] Millauer B, Witzigmann-voos S, Schnürch H, Martinez R, Møller NP, Risau W, et al. High affinity VEGF binding and developmental expression suggest Flk-1 as a major regulator of vasculogenesis and angiogenesis. *Cell* 1993;72:835–46.
- [452] Quinn TP, Peters KG, De Vries C, Ferrara N, Williams LT, Vries CDE, et al. Fetal liver kinase 1 is a receptor for vascular endothelial growth factor and is selectively expressed in vascular endothelium. *Proc Natl Acad Sci U S A* 1993;90:7533–7.
- [R453] Rother S, Samsonov SA, Moeller S, Schnabelrauch M, Rademann J, Blaszkiewicz J, et al. Sulfated Hyaluronan Alters Endothelial Cell Activation *in Vitro* by Controlling the Biological Activity of the Angiogenic Factors Vascular Endothelial Growth Factor-A and Tissue Inhibitor of Metalloproteinase-3. *ACS Appl Mater Interfaces* 2017;9:9539–50.
- [454] Krilleke D, DeErkenez A, Schubert W, Giri I, Robinson GS, Ng YS, et al. Molecular mapping and functional characterization of the VEGF164 heparin-binding domain. *J Biol Chem* 2007;282:28045–56.

- [455] Cole CL, Hansen SU, Baráth M, Rushton G, Gardiner JM, Avizienyte E, et al. Synthetic heparan sulfate oligosaccharides inhibit endothelial cell functions essential for angiogenesis. *PLoS One* 2010;5:e11644.
- [456] Di Benedetto M, Starzec A, Vassy R, Perret G-Y, Crépin M. Distinct heparin binding sites on VEGF165 and its receptors revealed by their interaction with a non sulfated glycoaminoglycan (NaPaC). *Biochim Biophys Acta* 2008;1780:723–32.
- [457] Hintze V, Samsonov SA, Anselmi M, Moeller S, Becher J, Schnabelrauch M, et al. Sulfated Glycosaminoglycans Exploit the Conformational Plasticity of Bone Morphogenetic Protein - 2 (BMP-2) and Alter the Interaction Profile with Its Receptor. *Biomacromolecules* 2014;15:3083–92.
- [458] Mulder PPMFA, Molema G, Koster S, van der Linden HJ, Verpoorte E. Behaviour of Human Umbilical Vein Endothelial Cells (HUVEC) Cultivated in Microfluidic channels. *2006 Int Conf Microtechnologies Med Biol* 2006;67657:155–7.
- [459] Freudenberg U, Zieris A, Chwalek K, Tsurkan M V, Maitz MF, Atallah P, et al. Heparin desulfation modulates VEGF release and angiogenesis in diabetic wounds. *J Control Release* 2015;220:79–88.
- [460] Hamilton JL, Nagao M, Levine BR, Chen D, Olsen BR, Im H. Targeting VEGF and Its Receptors for the Treatment of Osteoarthritis and Associated Pain. *J Bone Miner Res* 2016;31:911–24.
- [461] Bierbaum S, Douglas T, Hanke T, Scharnweber D, Tippelt S, Monsees TK, et al. Collageneous matrix coatings on titanium implants modified with decorin and chondroitin sulfate: Characterization and influence on osteoblastic cells. *J Biomed Mater Res - Part A* 2006;77:551–62.
- [462] Douglas T, Heinemann S, Mietrach C, Hempel U, Bierbaum S, Scharnweber D, et al. Interactions of collagen types I and II with chondroitin sulfates A-C and their effect on osteoblast adhesion. *Biomacromolecules* 2007;8:1085–92.
- [463] Tian H, Li C, Liu W, Li J, Li G. The influence of chondroitin 4-sulfate on the reconstitution of collagen fibrils in vitro. *Colloids Surfaces B Biointerfaces* 2013;105:259–66.
- [464] Rammelt S, Illert T, Bierbaum S, Scharnweber D, Zwipp H, Schneiders W. Coating of titanium implants with collagen, RGD peptide and chondroitin sulfate. *Biomaterials* 2006;27:5561–71.
- [465] Chapman JA, Tzaphlidou M, Meeks KM, Kadler KE. The collagen fibril - a model system studying the staining and fixation. *Electron Microsc Rev* 1990;3:143–82.
- [466] Obrink B. The influence of glycosaminoglycans on the formation of fibers from monomeric tropocollagen in vitro. *Eur J Biochem* 1973;34:129–37.
- [467] Stamov D, Grimmer M, Salchert K, Pompe T, Werner C. Heparin intercalation into reconstituted collagen I fibrils: Impact on growth kinetics and morphology. *Biomaterials* 2008;29:1–14.
- [468] Stuart K, Panitch A. Influence of chondroitin sulfate on collagen gel structure and mechanical properties at physiologically relevant levels. *Biopolymers* 2008;89:841–51.
- [469] Shi L, Ermis R, Garcia A, Telgenhoff D, Aust D. Degradation of human collagen isoforms by *Clostridium collagenase* and the effects of degradation products on cell migration. *Int Wound J* 2010;7:87–95.
- [470] Scozzafava A, Supuran CT. Protease inhibitors: Synthesis of L-alanine hydroxamate sulfonylated derivatives as inhibitors of *Clostridium histolyticum* collagenase. *Bioorg Med Chem Lett* 2000;10:499–502.
- [471] Bond MD, Vanwart HE. Characterization of the Individual Collagenases From *Clostridium-Histolyticum*. *Biochemistry* 1984;23:3085–91.
- [472] Guo Y, Yuan T, Xiao Z, Tang P, Xiao Y, Fan Y, et al. Hydrogels of collagen/chondroitin sulfate/hyaluronan interpenetrating polymer network for cartilage tissue engineering. *J Mater Sci Mater Med* 2012;23:2267–79.
- [473] Cai S, Liu Y, Zheng Shu X, Prestwich GD. Injectable glycosaminoglycan hydrogels for controlled release of human basic fibroblast growth factor. *Biomaterials* 2005;26:6054–67.
- [474] Segura T, Anderson BC, Chung PH, Webber RE, Shull KR, Shea LD. Crosslinked hyaluronic acid hydrogels: A strategy to functionalize and pattern. *Biomaterials* 2005;26:359–71.
- [R475] Rother S, Galiazzo VD, Kilian D, Fiebig KM, Becher J, Moeller S, et al. Hyaluronan/collagen hydrogels with sulfated hyaluronan for improved repair of vascularized tissue tune the binding of proteins and promote endothelial cell growth. *Macromol Biosci* 2017;accepted:1–13.

- [476] Servaty R, Schiller J, Binder H, Arnold K. Hydration of polymeric components of cartilage - an infrared spectroscopic study on hyaluronic acid and chondroitin sulfate. *Int J Biol Macromol* 2001;28:121–7.
- [477] Hu X, Li D, Zhou F, Gao C. Biological hydrogel synthesized from hyaluronic acid, gelatin and chondroitin sulfate by click chemistry. *Acta Biomater* 2011;7:1618–26.
- [478] Maksimenko A V., Schechilina Y V., Tischenko EG. Role of the Glycosaminoglycan Microenvironment of Hyaluronidase in Regulation of Its Endoglycosidase Activity. *Biochem* 2003;68:862–8.
- [479] Suzuki A, Toyoda H, Toida T, Imanari T. Preparation and inhibitory activity on hyaluronidase of fully O-sulfated hyaluro-oligosaccharides. *Glycobiology* 2001;11:57–64.
- [480] Shen B, Shimmom S, Smith MM, Ghosh P. Biosensor analysis of the molecular interactions of pentosan polysulfate and of sulfated glycosaminoglycans with immobilized elastase, hyaluronidase and lysozyme using surface plasmon resonance (SPR) technology. *J Pharm Biomed Anal* 2003;31:83–93.
- [481] Ossipov D A., Piskounova S, Varghese OP, Hilborn J. Functionalization of hyaluronic acid with chemoselective groups via a disulfide-based protection strategy for in situ formation of mechanically stable hydrogels. *Biomacromolecules* 2010;11:2247–54.
- [482] Peattie RA, Pike DB, Yu B, Cai S, Shu XZ, Prestwich GD, et al. Effect of Gelatin on Heparin Regulation of Cytokine Release from Hyaluronan-Based Hydrogels. *Drug Deliv* 2008;15:389–97.
- [483] Potente M, Gerhardt H, Carmeliet P. Basic and therapeutic aspects of angiogenesis. *Cell* 2011;146:873–87.
- [484] Lokeshwar VB, Lida N, Bourguignon LYW. The cell adhesion molecule, GP116, is a new CD44 variant (ex14/v10) involved in hyaluronic acid binding and endothelial cell proliferation. *J Biol Chem* 1996;271:23853–64.
- [485] Kleinheinz J, Jung S, Wermker K, Fischer C, Joos U. Release kinetics of VEGF165 from a collagen matrix and structural matrix changes in a circulation model. *Head Face Med* 2010;6:17.
- [486] Barrientos S, Brem H, Stojadinovic O, Tomic-Canic M. Clinical application of growth factors and cytokines in wound healing. *Wound Repair Regen* 2014;22:569–78.
- [487] Lauer G, Sollberg S, Cole M, Flamme I, Stürzebecher J, Mann K, et al. Expression and proteolysis of vascular endothelial growth factor is increased in chronic wounds. *J Invest Dermatol* 2000;115:12–8.
- [488] Bao P, Kodra A, Tomic-Canic M, Golinko MS, Ehrlich HP, Brem H. The Role of Vascular Endothelial Growth Factor in Wound Healing. *J Surg Res* 2009;153:347–58.
- [489] Hanjaya-Putra D, Yee J, Ceci D, Truitt R, Yee D, Gerecht S. Vascular endothelial growth factor and substrate mechanics regulate in vitro tubulogenesis of endothelial progenitor cells. *J Cell Mol Med* 2010;14:2436–47.
- [490] Saunders RL, Hammer DA. Assembly of human umbilical vein endothelial cells on compliant hydrogels. *Cell Mol Bioeng* 2010;3:60–7.
- [491] Acevedo-Acevedo S, Crone WC. Substrate stiffness effect and chromosome missegregation in hIPS cells. *J Negat Results Biomed* 2015;14:22.

**PERMISSIONS TO REUSE DATA FOR THESIS/DISSERTATION**

Data from [R316]: Reprinted (adapted) with permission from Rother S, Salbach-Hirsch J, Möller S, Seemann T, Schnabelrauch M, Hofbauer LC, et al. Bioinspired Collagen/Glycosaminoglycan-based Cellular Microenvironments for Tuning Osteoclastogenesis. *ACS Appl Mater Interfaces* 2015;7:23787–97. Copyright 2015 American Chemical Society.

Data from [R447]: Reprinted (adapted) with permission from Rother S, Samsonov SA, Hempel U, Vogel S, Möller S, Blaszkiewicz J, et al. Sulfated hyaluronan alters the interaction profile of TIMP-3 with the endocytic receptor LRP-1 cluster II and IV and increases the extracellular TIMP-3 level of human bone marrow stromal cells. *Biomacromolecules* 2016;17:3252–61. Copyright 2016 American Chemical Society.

Data from [R453]: Reprinted (adapted) with permission from Rother S, Samsonov SA, Moeller S, Schnabelrauch M, Rademann J, Blaszkiewicz J, et al. Sulfated Hyaluronan Alters Endothelial Cell Activation in Vitro by Controlling the Biological Activity of the Angiogenic Factors Vascular Endothelial Growth Factor-A and Tissue Inhibitor of Metalloproteinase-3. *ACS Appl Mater Interfaces* 2017;9:9539–50. Copyright 2017 American Chemical Society.

Data from [R475]: Reprinted (adapted) with permission from Rother S, Galiazzo VD, Kilian D, Fiebig KM, Becher J, Moeller S, et al. Hyaluronan/collagen hydrogels with sulfated hyaluronan for improved repair of vascularized tissue tune the binding of proteins and promote endothelial cell growth. *Macromol Biosci* 2017. Copyright 2017 John Wiley and Sons.

## LIST OF PUBLICATIONS

1. A. Miron, **S. Rother**, L. Huebner, U. Hempel, I. Käppler, S. Moeller, M. Schnabelrauch, D. Scharnweber, V. Hintze: Sulfated hyaluronan influences the formation of artificial extracellular matrices and the adhesion of osteogenic cells. *Macromol Biosci.* 2014; 14(12):1783-94. (Impact factor 2014: 3.851)
2. D. Scharnweber, L. Hübner, **S. Rother**, U. Hempel, U. Anderegg, S. A. Samsonov, M. T. Pisabarro, L. Hofbauer, M. Schnabelrauch, S. Franz, J. Simon, V. Hintze. Glycosaminoglycan derivatives: promising candidates for the design of functional biomaterials. *J Mater Sci Mater Med.* 2015;26(9):232. (Impact factor 2015: 2.272)
3. **S. Rother**, J. Salbach-Hirsch, S. Möller, T. Seemann, M. Schnabelrauch, L. Hofbauer, V. Hintze, D. Scharnweber. Bioinspired collagen/glycosaminoglycan-based cellular microenvironments for tuning osteoclastogenesis. *ACS Appl Mater Interfaces.* 2015; 7(42):23787-97. (Impact factor 2015: 7.145)\*
4. A. K. Picke, J. Salbach-Hirsch, V. Hintze, **S. Rother**, M. Rauner, C. Kascholke, S. Möller, R. Bernhardt, S. Rammelt, M. Schnabelrauch, M. Schulz-Siegmund, M. C. Hacker, D. Scharnweber, C. Hofbauer, L. C. Hofbauer. Sulfated hyaluronan improves bone regeneration of diabetic rats by scavenging sclerostin and enhancing osteoblast function. *Biomaterials.* 2016; 96:11-23. (Impact factor 2016: 8.402)
5. **S. Rother**, S. A. Samsonov, T. Hofmann, J. Blaszkiwicz, S. Köhling, S. Moeller, M. Schnabelrauch, J. Rademann, S. Kalkhof, M. von Bergen, M. T. Pisabarro, D. Scharnweber, V. Hintze. Structural and functional insights into the interaction of sulfated glycosaminoglycans with tissue inhibitor of metalloproteinase-3 – a possible regulatory role on extracellular matrix homeostasis. *Acta Biomater.* 2016; 45:143-154. (Impact factor 2016: 6.319)\*
6. **S. Rother**, S. A. Samsonov, U. Hempel, S. Vogel, S. Moeller, J. Blaszkiwicz, S. Köhling, M. Schnabelrauch, J. Rademann, M. T. Pisabarro, V. Hintze, D. Scharnweber. Sulfated hyaluronan alters the interaction profile of TIMP-3 with the endocytic receptor LRP-1 cluster II and IV and increases the extracellular TIMP-3 level of human bone marrow stromal cells. *Biomacromolecules.* 2016; 17(10):3252-3261. (Impact factor 2015: 5.583)\*
7. W. Metzger, **S. Rother**, T. Pohlemann, S. Möller, M. Schnabelrauch, V. Hintze, D. Scharnweber. Evaluation of cell-surface interaction using a 3D spheroid cell culture model on artificial extracellular matrices. *Mater Sci Eng C Mater Biol Appl.* 2017; 73:310-318. (Impact factor 2015: 3.420)
8. **S. Rother**, S. A. Samsonov, S. Moeller, M. Schnabelrauch, J. Rademann, J. Blaszkiwicz, S. Köhling, J. Waltenberger, M. T. Pisabarro, D. Scharnweber, V. Hintze. Sulfate hyaluronan alters endothelial cell activation in vitro by controlling the biological activity of the angiogenic factors vascular endothelial growth factor-A and tissue inhibitor of metalloproteinase-3. *ACS Appl Mater Interfaces.* 2017; 9(11):9539-9550. (Impact factor 2015: 7.145)\*
9. L. Koehler, S. A. Samsonov, **S. Rother**, S. Vogel, S. Köhling, S. Moeller, M. Schnabelrauch, J. Rademann, U. Hempel, M. T. Pisabarro, D. Scharnweber, V. Hintze. Sulfated hyaluronan derivatives modulate TGF- $\beta$ 1:receptor complex formation: possible consequences for TGF- $\beta$ 1 signaling. *Sci Rep.* 2017; 7(1):1210. (Impact factor 2015: 5.228)
10. S. Bhowmick, **S. Rother**, H. Zimmermann, P. S. Lee, S. Moeller, M. Schnabelrauch, V. Koul, R. Jordan, V. Hintze, D. Scharnweber. Biomimetic electrospun scaffolds from main extracellular matrix components for skin tissue engineering application – The role of chondroitin sulfate and sulfated hyaluronan. *Mater Sci Eng C Mater Biol Appl.* 2017; 79:15-22. (Impact factor 2015: 3.420)

11. **S. Rother**, V. D. Galiazzo, D. Kilian, K. M. Fiebig, J. Becher, S. Möller, U. Hempel, M. Schnabelrauch, J. Waltenberger, D. Scharnweber, V. Hintze. Hyaluronan/collagen hydrogels with sulfated hyaluronan for improved repair of vascularized tissue tune the binding of proteins and promote endothelial cell growth. *Macromol. Biosci.* 2017; doi: 10.1002/mabi.201700154. [Epub ahead of print] (Impact factor 2016: 3.680)\*
12. S. Bhowmick, **S. Rother**, H. Zimmermann, P. S. Lee, S. Moeller, M. Schnabelrauch, V. Koul, R. Jordan, V. Hintze, D. Scharnweber. Reciprocal influence of hMSCs / HaCaT cultivated on electrospun scaffolds. *J Mater Sci Mater Med.* 2017; accepted (Impact factor 2016: 2.325)

\*The highlighted articles contain already published parts of this thesis.

### PRESENTATIONS AT CONFERENCES, PAPER IN CONFERENCE PROCEEDINGS

1. J. Salbach-Hirsch, J. Kraemer, L. Huebner, **S. Rother**, M. Rauner, S. Samsonov, M.T. Pisabarro, S. Moeller, M. Schnabelrauch, D. Scharnweber, L.C. Hofbauer, V. Hintze: Sulfated hyaluronan promotes osteoclastogenesis through interference with OPG and RANKL/OPG complex formation, Annual Conference of the German Society of Biomaterials (DGBM), Erlangen, 26.-28.09.2013 (Poster)
2. **S. Rother**, V. Hintze, D. Scharnweber: Engineering biofunctional matrices composed of collagen, glycosaminoglycan derivatives and proteoglycan analogs for improved tissue regeneration, 4. Dresdner Werkstoffsymposium, Dresden, 18 - 19 November 2013 (Oral presentation and poster)
3. L. Huebner, A. van der Smissen, S. Samsonov, **S. Rother**, S. Moeller, M. Schnabelrauch, M. T. Pisabarro, D. Scharnweber, U. Anderegg, V. Hintze: Impaired TGF- $\beta$ 1 signalling due to altered receptor complex formation in the presence of sulfated hyaluronan derivatives, Gordon Research Conference Biointerface Science 2014, Lucca (Barga), Italien, 15.06.-20.06.2014 (Poster)
4. V. Hintze, A. van der Smissen, S. Samsonov, L. Huebner, **S. Rother**, D. Scharnweber, S. Moeller, M. Schnabelrauch, M. T. Pisabarro, U. Anderegg: Sulfated hyaluronan derivatives interfere with TGF- $\beta$ 1 signalling, ESB 2014, Liverpool, 31.08.-03.09.2014 (Oral presentation V. Hintze)
5. **S. Rother**, S.Thönes, J. Salbach-Hirsch, S. Moeller, M. Schnabelrauch, U. Anderegg, L. C. Hofbauer, V. Hintze, D. Scharnweber: Design of multi-component artificial extracellular matrices and their effects on cells relevant to wound healing, 26th European Conference on Biomaterials, Liverpool, 31.08.-03.09.2014 (Oral presentation and poster)
6. **S. Rother**, S.Thönes, J. Salbach-Hirsch, S. Moeller, M. Schnabelrauch, U. Anderegg, L. C. Hofbauer, V. Hintze, D. Scharnweber: Multi-Component Artificial Extracellular Matrices Influence Cells Relevant to Wound Healing, Annual Conference of the German Society of Biomaterials (DGBM), Dresden, 06.11.-08.11.2014 (Oral presentation and poster)
7. L. Huebner, A. van der Smissen, S. Samsonov, **S. Rother**, S. Moeller, M. Schnabelrauch, M. T. Pisabarro, D. Scharnweber, U. Anderegg, V. Hintze: Sulfated hyaluronan derivatives impair TGF- $\beta$ 1 signalling due to altered receptor complex formation, Annual Conference of the German Society of Biomaterials (DGBM), Dresden, 06.11.-08.11.2014 (Poster)
8. **S. Rother**, J. Salbach-Hirsch, S. Moeller, M. Schnabelrauch, L. C. Hofbauer, V. Hintze and D. Scharnweber: Multi-component artificial extracellular matrices for the regulation of osteoclast differentiation, International Symposium Interface Biology of Implants, Warnemünde, 06.05.-08.05.2015 (Poster)

9. L. Huebner, S. Samsonov, **S. Rother**, S. Moeller, M. Schnabelrauch, M. T. Pisabarro, D. Scharnweber, V. Hintze: Interaction of sulfated hyaluronan with TGF- $\beta$ 1 alters receptor complex formation and impairs growth factor signaling, International Symposium Interface Biology of Implants, Warnemünde, 06.05.-08.05.2015 (Poster)
10. **S. Rother**, A. Hoehnel, S. Moeller, M. Schnabelrauch, T. Henle, V. Hintze and D. Scharnweber: Sulfated glycosaminoglycans alter the activity of matrix metalloproteinases (MMPs), ISHAS HA 2015 Conference, Florenz, 07.06.-11.06.2015 (Poster)
11. V. Hintze, A. van der Smissen, S. Samsonov, L. Huebner, **S. Rother**, D. Scharnweber, S. Moeller, M. Schnabelrauch, M. T. Pisabarro, U. Anderegg: Collagen-based artificial extracellular matrices (aECM): a promising therapeutic option for fibrosis intervention, ISHAS HA 2015 Conference, Florenz, 07.06.-11.06.2015 (Oral presentation V. Hintze and poster)
12. S. A. Samsonov, A. van der Smissen, L. Huebner, **S. Rother**, S. Moeller, M. Schnabelrauch, V. Hintze, D. Scharnweber, U. Anderegg, M. T. Pisabarro: Elucidation of molecular mechanisms behind sulfated hyaluronan and TGF- $\beta$ 1 interactions by in silico and experimental approaches, Beilstein Glyco-Bioinformatics Symposium 2015, Potsdam, 22.06.-26.06.2015 (Oral presentation S. A. Samsonov and poster)
13. D. Scharnweber, L. Huebner, **S. Rother**, U. Anderegg, S. Samsonov, M. T. Pisabarro, L. Hofbauer, M. Schnabelrauch, S. Franz, J. Simon, V. Hintze: Glycosaminoglycan Derivatives – Promising Candidates for the Design of Functional Biomaterials, 27th European Conference on Biomaterials, Krakow, 30.08.-03.09.2015 (Keynote lecture D. Scharnweber)
14. S. Bhowmick, **S. Rother**, V. Hintze, S. Moeller, M. Schnabelrauch, V. Koul, D. Scharnweber: Electrospun Nanofibrous Scaffolds Composed of Gelatin and Sulfated Hyaluronan for Wound Healing Applications, European Burns Association Congress, Hannover, 16.09.-19.09. 2015 (Oral presentation S. Bhowmick)
15. V. Hintze, L. Huebner, **S. Rother**, S. A. Samsonov, S. Moeller, M. Schnabelrauch, D. Scharnweber, M. T. Pisabarro: SPR binding analysis of multi component systems: sulfated hyaluronan alters the complex formation of growth factors with their receptors, Biacore<sup>TM</sup> user meeting, Berlin, 01.10.-02.10.2015 (Oral presentation V. Hintze)
16. S. Bhowmick, **S. Rother**, S. Moeller, M. Schnabelrauch, V. Koul, D. Scharnweber: Gelatin / Sulfated Hyaluronan / Chondroitin Sulfate Tri-copolymer Electrospun Scaffold Promotes Epithelial Differentiation of Human Mesenchymal Stem Cells (hMSCs) on Keratinocytes-hMSCs Contact Co-culture, BiTerm 2016 conference, New Delhi, India, 15.04.-17.04.2016 (Oral presentation S. Bhowmick)
17. **S. Rother**, S.A. Samsonov, T. Hofmann, U. Hempel, J. Blaszkiewicz, J. Rademann, S. Moeller, M. Schnabelrauch, S. Kalkof, M. von Bergen, M.T. Pisabarro, D. Scharnweber, V. Hintze: Functional und structural insights into TIMP-3- glycosaminoglycan interactions - implications for the design of functional biomaterials improving chronic wound treatment, 10th World Biomaterials Congress, Montreal, Canada, 17.05.-22.05.2016 (Poster)
18. S. Thönes, **S. Rother**, V. Galiazzo, J. Becher, D. Scharnweber, M. Schnabelrauch, V. Hintze, U. Anderegg: Hyaluronan-collagen hydrogels support growth of human fibroblasts and are applicable to experimental skin wounds, 10th World Biomaterials Congress, Montreal, Canada, 17.05.-22.05.2016 (Poster)
19. S. Köhling, G. Künze, **S. Rother**, K. Lemnitzer, J. Blaszkiewicz, V. Hintze, S. Kalkhof, D. Scharnweber, D. Huster, J. Schiller, J. Rademann: Biomolecular interactions of defined sulfated oligo-hyaluronane probes: Toward a rational optimization of GAG-based biomaterials, 10th World Biomaterials Congress, Montreal, Canada, 17.05.-22.05.2016 (Poster)



20. L. Koehler, **S. Rother**, S. Moeller, M. Schnabelrauch, V. Hintze, D. Scharnweber: Sulfated glycosamino-glycan derivatives affect the bioactivity of angiogenic growth factors, 10th World Biomaterials Congress, Montreal, Canada, 17.05.-22.05.2016 (Poster)
21. **S. Rother**, S.A. Samsonov, T. Hofmann, U. Hempel, J. Blaszkiewicz, S. Köhling, J. Rademann, S. Moeller, M. Schnabelrauch, S. Kalkhof, M. von Bergen, M.T. Pisabarro, D. Scharnweber and V. Hintze: Functional und structural insights into TIMP-3- GAG interactions - implications for the design of functional biomaterials, Frontiers in Biomaterials Science: 2. International Symposium of the Transregio 67, Leipzig, 24.06.-25.06.2016 (Oral presentation)
22. V. Hintze, L. Köhler, **S. Rother**, U. Hempel, U. Anderegg, S. A. Samsonov, M. T. Pisabarro, L. Hofbauer, M. Schnabelrauch, S. Franz, J. Simon, D. Scharnweber: Artificial extracellular matrices based on collagen and glycosaminoglycan derivatives – promising candidates for the design of functional biomaterials, 6th Freiberg Collagen Symposium, Freiberg, 14.09.-15.09.2016 (Keynote lecture V. Hintze)
23. **S. Rother**, S.A. Samsonov, T. Hofmann, U. Hempel, J. Blaszkiewicz, S. Köhling, J. Rademann, S. Moeller, M. Schnabelrauch, S. Kalkhof, M. von Bergen, M.T. Pisabarro, D. Scharnweber and V. Hintze: Functional und structural insights into TIMP-3- glycosaminoglycan interactions - implications for the design of functional biomaterials for chronic wound healing, 6th Freiberg Collagen Symposium, Freiberg, 14.09.-15.09.2016 (Oral presentation)
24. D. Scharnweber, L. Huebner, **S. Rother**, U. Anderegg, S. Samsonov, M. T. Pisabarro, L. Hofbauer, M. Schnabelrauch, S. Franz, J. Simon, V. Hintze: Glycosaminoglycan Derivatives – Promising Candidates for the Design of Functional Biomaterials, 6th International Congress on Biotechnologies for Spinal Surgery, Berlin, 26.04.-28.04.2017 (Oral presentation)
25. P. S. Lee, R. Hess, **S. Rother**, R. Bernhardt, H. Eckert, M. Bobeth, A. Lode, G. Cuniberti, M. Gelinsky, D. Scharnweber: Bone tissue engineering: A proof-of-concept to derive physiological relevant tailor-made bone constructs *in vitro*, European Chapter Meeting of the Tissue Engineering and Regenerative Medicine International Society 2017 (TERMIS), Davos, Switzerland, 26.-30.06.2017 (Poster P. S. Lee)
26. **S. Rother**, S.A. Samsonov, T. Hofmann, U. Hempel, S. Vogel, J. Rademann, S. Moeller, M. Schnabelrauch, S. Kalkhof, M. von Bergen, M.T. Pisabarro, D. Scharnweber and V. Hintze: Interaction of tissue inhibitor of metalloproteinase-3 with sulfated hyaluronan - implications for the treatment of pathologic tissue degradation, 19th European Carbohydrate Symposium (EUROCARB), Barcelona, Spain, 02.07.-06.07.2017 (Poster)

## ACKNOWLEDGEMENT

The work for this thesis was supported, encouraged and impacted by a number of very special people, to whom I would like to express my gratitude.

First and foremost, I would like to thank Prof. Dr. Dieter Scharnweber (Max Bergmann Center of Biomaterials, Institute of Materials Science, TU Dresden) for giving me the opportunity to work on that fascinating topic for my PhD thesis. He supported my work in manifold ways by his trust he has placed in me, his mixture of encouraging and challenging me that mainly guided my scientific and personal development and his inexhaustible feedback throughout my research. His open mindedness for new ideas allowed me to strongly extend my research especially regarding the investigations concerning TIMP-3.

I am also very thankful to Prof. Dr. Thomas Henle (Institute of food chemistry, TU Dresden) for his strong and steady support over the last years, when I started as a student assistant in his group during my 5<sup>th</sup> semester, then joined his group again for my diploma studies, where I realized that research is what I want to do, followed by his willingness to supervise this work.

I would like to particularly point out Dr. habil. Vera Hintze, for introducing me into the field of matrix engineering, supporting me and sharing her knowledge. I have enjoyed the time we spent together on scientific discussions and conferences.

Particular thanks go to Aline Katzschner and Heike Zimmermann for their excellent technical assistance and for making me feel like a lab family member directly from the very beginning. I would like to thank my diploma and master students Karen M. Fiebig, Vanessa Galiazzo, Vera Krönert, Andrea Höhnel and Daria Glushkina as well as my lab rotation students David Killian and Anastasia Moraiti for their dedicated participation, which helped to advance main and sub projects. Additional thanks go to the students David Werner, Reneé Unbehau and Juliane Moritz for their work on related subtopics as well as to Anna Jäschke for my personal “science cat”. Furthermore, I warmly thank Linda Köhler, Sina Rößler, Poh Soo Lee and Benjamin Kruppke for their support, helpful advices and for all the fun we had together in the lab, the office and during leisure activities.

I also wish to express my appreciations to all members of the Transregio 67, especially to Dr. Stephanie Möller, Dr. Sergey A. Samsonov, Dr. Juliane Salbach-Hirsch, Sarah Vogel, Dr. Ute Hempel, Dr. M. Teresa Pisabarro, Prof. Dr. Lorenz Hofbauer, Dr. Matthias Schnabelrauch, Prof. Dr. Jörg Rademann, Joanna Blaszkiewics, Sebastian Köhling, Prof. Dr. Stefan Kalkhof, Prof. Dr. Martin von Bergen for their fruitful and productive collaboration. I would like to thank further external collaborators as Prof. Dr. Johannes Waltenberger, Dr. Wolfgang Metzger and Dr. Sirsendu Bhowmick.

I really appreciate the linguistic skills of Dr. Susanne Bierbaum, who helped me by reading the draft version of this thesis. I would like to thank Dr. Cornelia Wolf-Brandstetter for being the

first food chemist working in the group of Prof. Dr. Scharnweber mainly determining his good impression for food chemists and Marita Keil for her administrative assistance. For the friendly and scientific atmosphere, I also thank Dr. Thomas Hanke and all members as well as the holder of the chair for biomaterials Prof. Dr. Hans-Peter Wiesmann. Moreover, I would also like to thank my former supervisor Dr. Michael Hellwig for always supporting me throughout my scientific “evolution”.

Special thanks go to the graduate academy of the Transregio 67 and of the TU Dresden. I am grateful to the Deutsche Forschungsgemeinschaft (DFG) for financial support of the SFB Transregio 67, which enabled the realization of this research.

In addition, I have to thank my family, especially my little sister Lisa, for all their love and support during my whole life.

Last but not least, I would like to thank my lovely husband Stephan for his continuous support in tackling any challenges in my daily life, his stoic patience and his never-ending humor. This work would not be possible without him.

**DECLARATION**

Die vorliegende Arbeit wurde in der Gruppe Biomaterial-Entwicklung am Max-Bergmann-Zentrum für Biomaterialien Dresden in Kooperation mit der Professur für Lebensmittelchemie der Technischen Universität Dresden unter Anleitung von Prof. Dr. Dieter Scharnweber und Prof. Dr. Thomas Henle angefertigt.

Hiermit versichere ich, dass ich die vorliegende Arbeit ohne unzulässige Hilfe Dritter und ohne Benutzung anderer als der angegebenen Hilfsmittel angefertigt habe; die aus fremden Quellen direkt oder indirekt übernommenen Gedanken sind als solche kenntlich gemacht. Die Arbeit wurde bisher weder im Inland noch im Ausland in gleicher oder ähnlicher Form einer anderen Prüfungsbehörde vorgelegt.

Ich erkenne die Promotionsordnung der Fakultät Mathematik und Naturwissenschaften der Technischen Universität Dresden vom 23.02.2011 zuletzt geändert am 15.06.2011 und 18.06.2014 in allen Teilen an. Weiterhin versichere ich, dass bisher kein erfolgloses früheres Promotionsverfahren stattgefunden hat.

Ort, Datum

Unterschrift